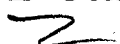


A study of the organic and inorganic  
geochemistry of sulphur in shales

Simon Patrick Dean  


Submitted in accordance with the requirements for  
the degree of Doctor of Philosophy

The University of Leeds  
Department of Earth Sciences  
September, 1994

The candidate confirms that the work submitted is his own and that appropriate credit has  
been given where reference has been made to the work of others.

# Abstract

The formation, evolution and weathering of sulphur bearing compounds within shales have been investigated using range of samples from the Carboniferous (Bowland Shales and Caton Shales) and the Jurassic (Jet Rock).

Experimental methodologies have been developed and modified where necessary, to enable both the concentrations and isotopic composition of sulphur compounds in shales to be determined.

The Caton Shales contain a mixture of authigenic (range 3.1 to 15.3ppm) and detrital (range 0 to 9.99ppm) uranium. The precipitation of authigenic uranium was partly controlled by organic carbon. Preferential absorption of uranium by phosphate produced authigenic uranium enrichment within a horizon containing phosphate pellets. Palaeoenvironmental conditions at the time of deposition of the Caton Shales were determined using a variety of parameters which indicate oxic bottom water conditions. The C/S ratio (mean 0.69) is lower than expected because there has been significant loss of organic carbon and a small loss of pyrite sulphur.

The septarian concretions of the Caton Shales have had a complex history. The carbonate cements evolved from a heavy (-1.5‰ PDB) to a light (-14.5‰ PDB) oxygen composition and a light (-29‰ PDB) to a heavy (-7‰ PDB) carbon composition. Initial formation of the concretion matrix took place early during diagenesis, close to the sediment water interface. Overpressuring of the sediment resulted in the formation of cracks which were filled by cements derived from a mixture of meteoric water and sulphate reduction. Regional tectonic activity initiated a later generation of cracks which were filled by three distinct generations of carbonate cements. The last cementation phase was accompanied by hydrocarbon migration. The use of  $K_{\alpha}$  X - ray maps of large areas of diagenetic cement provide a rapid method of obtaining geochemical data.

The Jet Rock shows a positive correlation between reactive iron and organic carbon and DOP is independent of organic carbon indicating significant syngenetic pyrite formation. High TOC concentrations (>8%) are found around the Whalestone concretions where different diagenetic conditions prevailed. Samples with TOC<8% contain framboidal pyrite with  $\delta^{34}\text{S}$  in the range -30 to

-22‰. At higher TOC the pyrite is produced with a closed sulphate supply ( $\delta^{34}\text{S}$  -24‰ to -20‰). Organo-sulphur compounds (OSC) are present within the solvent soluble organic matter (dominated by dibenzothiophenes). The organically bound sulphur ( $\delta^{34}\text{S}$  -14.0‰ to 3.6‰) is isotopically heavier than the framboidal generation of pyrite within the Jet Rock, but isotopically similar to the massive pyrite ( $\delta^{34}\text{S}$  -12.8‰) ascribed to be a later generation of pyrite.

A model is presented to describe the isotopic evolution of sulphur in the Jet Rock. A first generation of framboidal pyrite formed during open system sulphate reduction. Massive pyrite and OSC then formed contemporaneously during closed system sulphate reduction, creating isotopically heavy compounds.

Shale samples are prone to weathering. Visual inspection of the surface of shale prior to collection will not necessarily ensure a fresh sample. Weathering affects samples to depths greater than 1m in well consolidated shale outcrops. Geochemical data obtained from surface samples should be treated with caution. Weathered shales contain more soluble iron than fresh samples. This has obvious implications for the DOP parameter. Reactive iron values will be falsely high, thus lowering the measured DOP of the sample. Organic matter is lost from shales during diagenesis by a variety of processes. Weathering also reduces the organic matter content of shales. Rock Eval results show significant loss of S1 yields. Hydrocarbon exploration data is susceptible to error if the analysis is performed on weathered source rocks.

Soluble sulphate and elemental sulphur may be present in apparently fresh shales. They are probably derived from the oxidation of organo-sulphur compounds and pyrite respectively. The use of  $\delta^{18}\text{O}$  measurements on soluble sulphate enables the source of the oxygen to be established. For the shales studied, the oxygen is comprised of a mixture of atmospheric oxygen and water derived oxygen. Oxygen values which are isotopically similar to atmospheric oxygen can be produced during equilibration reactions of pore waters at elevated temperatures.

# Acknowledgements

I would like to thank my supervisors Rob Raiswell and Simon Bottrell in Leeds and Andy Carr from British Gas for their help, advice and encouragement throughout this project. This project was funded by a NERC-CASE studentship in conjunction with British Gas.

Thanks must also go to many people at various institutions around the country. At British Gas (LRS), Phil Highton is thanked for his help with petrographic analysis of kerogens and Mike Cocksedge for his time spent looking for dibenzothiophene by GC-MS; Andy Gize (Manchester) for discussion over the elusive dibenzothiophenes and for finding some; Jim Marshall for enabling me to use Liverpool's carbonate carbon and oxygen isotope analysis facilities.

Technical support from the Department of Earth Sciences in Leeds was given by Alan Grey, Tom Oddy, Keith Reid and Keith Cowling. Special thanks must go to Dave Hatfield for all his help in the lab.

Within the Department at Leeds, additional help from the following is gratefully acknowledged: Geoff Lloyd for SEM guidance and Eric Condliffe for driving lessons on the probe; Frank Buckley for his help and advice on many wet chemistry issues and together with Joan Rooke, for help with AA and ICP analysis; Dave Banks for fluid inclusion analysis; Richard Collier for useful discussions on the regional geology of the Bowland Basin and Paul Wignall for most things to do with shales.

I would also like to acknowledge Andy Barker, Hesham Al-Biatty, Quentin Fisher, Randolph Haggerty, Anwyn Hughes, Marcus Leosson, James Maynard, Ros and Steve Pike and Carolyn Young for making life entertaining at Leeds.

I would finally like to thank Alison and the rest of my family for their support during my years as a perpetual student.



# Contents

<b>Abstract</b>	<b>i</b>
<b>Acknowledgements</b>	<b>iii</b>
<b>Contents</b>	<b>iv</b>
<b>List of Tables</b>	<b>x</b>
<b>List of Figures</b>	<b>xiii</b>
<b>List of Plates</b>	<b>xvi</b>
<b>List of Symbols and Abbreviations</b>	<b>xvii</b>

## **Chapter 1 - Introduction**

1.0	Introduction	1
1.1	Aims of the thesis	2
1.2	Laboratory work	3
1.3	Thesis layout	3

## **Chapter 2 - Previous studies: organic and inorganic geochemistry of mud rocks**

2.0	Introduction	5
2.1	Black shale deposition	5
2.2	Diagenesis	6
	2.2.1 Organic matter preservation	6
	2.2.2 Oxic respiration	8
	2.2.3 Denitrification	10
	2.2.4 Manganese and iron reduction	10
	2.2.5 Sulphate reduction	11
	2.2.6 Methane oxidation	11
	2.2.7 Methane Production	11
2.3	Sedimentary pyrite formation	12
	2.3.1 The role of organic matter	12
	2.3.2 The role of sulphate availability	13
	2.3.3 The role of iron mineralogy	15
	2.3.4 The role of sulphide availability	17
2.4	Iron sulphides	17

2.5	Carbon-iron-sulphur relationships in sediments	19
	2.5.1 Carbon/sulphur ratios	19
	2.5.2 Degree of pyritisation	24
2.6	Stable isotopes	25
	2.6.1 Equilibrium fractionation	27
	2.6.2 Kinetic fractionation	27
	2.6.3 Nomenclature	28
	2.6.4 Carbonate carbon	28
	2.6.5 Organic carbon	28
	2.6.6 Carbonate oxygen	31
	2.6.7 Sulphate oxygen	31
	2.6.8 Sulphur	32
2.7	Radiogenic isotopes	35
2.8	Organic geochemistry	36
	2.8.1 Organic composition of living materials	36
	2.8.2 Isomers in organic geochemistry	38
2.9	Bitumen	38
	2.9.1 Normal alkanes	39
	2.9.2 Branched alkanes	39
	2.9.3 Hopanes	42
	2.9.4 Steranes	47
2.10	Kerogen	47
	2.10.1 Origin of kerogen	51
	2.10.2 Types of kerogen	53
2.11	Maturity indicators	57
2.12	Organically bound sulphur	57

### Chapter 3 - Analytical methodology

3.0	Introduction	62
3.1	Preparation of samples for geochemical analysis	62
3.2	Carbon analysis	63
	3.2.1 Operation of the Carlo Erba	63
	3.2.2 Organic Carbon Determination	65
	3.2.2.1 Ashing	65
	3.2.2.2 Carbonate Dissolution	65
	3.2.2.3 Whole Rock Pyrolysis	65
3.3	Bitumen Extraction	68
3.4	Liquid Chromatography	71

3.5	Gas Chromatography	71
	3.5.1 Gas Chromatography - Mass Spectrometry	71
	3.5.2 Gas Chromatography - Atomic Emission Detection	75
3.6	Kerogen Isolation	75
3.7	Stable Isotope Analysis	75
	3.7.1 Organic Carbon	75
	3.7.2 Carbonate Oxygen and Carbon	76
	3.7.3 Sulphur	77
	3.7.3.1 Pyrite	77
	3.7.3.2 Elemental	80
	3.7.3.3 Sulphate	80
	3.7.3.4 Organic	82
3.8	Sulphur Analysis	83
	3.8.1 Operation of the Carlo Erba	83
	3.8.2 Total Sulphur and Organic Sulphur	83
	3.8.3 Elemental Sulphur	83
	3.8.4 Sulphate Sulphur	85
	3.8.5 Pyrite Sulphur	85
3.9	Acid Soluble Iron	91
3.10	X-ray Analysis	94
	3.10.1 X-ray Diffraction	94
	3.10.2 X-ray Fluorescence	96
3.11	Electron Microscopy	96
	3.11.1 Scanning Electron Microscope	96
	3.11.2 Electron Microprobe	96

## **Chapter 4 - Geochemistry of the Caton Shales**

4.0	Introduction	97
4.1	Geographical Location	97
4.2	Geological Setting	99
4.3	Burial history of the shales	99
4.4	Caton Shales	102
4.5	Geochemistry of the sequence	105
	4.5.1 Radioactive characterisation of the Caton Shales	105
	4.5.1.1 Ganister	105
	4.5.1.2 Shale	108
	4.5.2 Carbon, Iron, Sulphur relationships	111
	4.5.3 Organic matter within the Caton Shales	118

4.5.3.1	Kerogen	118
4.5.3.2	Bitumen	118
4.5.3.3	Organic Carbon Isotopes	125
4.6	Origins of Carbonate Concretions	129
4.6.1	Timing and growth of the concretions	130
4.6.1.1	Porosity	130
4.6.1.2	Depth	132
4.6.1.3	Duration	132
4.6.1.4	Temperature	134
4.6.1.5	Shape	134
4.6.1.6	Sedimentology	135
4.7	Septa Formation	135
4.7.1	Septarian concretions from the Caton Shales	135
4.8	Geochemistry of the Concretion cements	136
4.8.1	Stable isotopes	136
4.8.1.1	Concretion matrix	140
4.8.1.2	Early septarian concretions	141
4.8.1.3	Late septarian cements	143
4.8.2	Cation Chemistry	143
4.8.2.1	Calcium	148
4.8.2.2	Manganese	148
4.8.2.3	Iron	148
4.8.2.4	Magnesium	150
4.9	Authigenesis and evolution of the concretions	150
4.9.1	Stage 1 - Concretion formation	150
4.9.2	Stage 2 - Initial septarian crack formation	150
4.9.3	Stage 3 - Cementation of the septarian cracks	152
4.9.4	Stage 4 - Late septarian crack formation	152
4.9.5	Stage 5 - Cementation of the late septa	152
4.10	Conclusions	153

## Chapter 5 - Geochemistry of the Jet Rock

5.0	Introduction	154
5.1	Geological setting	154
5.2	The Jet Rock	156
5.3	Samples	157
5.4	Gamma ray Spectrometry	161
5.5	Carbon, Iron and Sulphur relationships	161

5.6	Organic Matter	170
	5.6.1 Kerogen	170
	5.6.2 Bitumen	170
	5.6.3 Biological markers	176
5.7	Organo-Sulphur compounds	186
5.8	Sulphur Isotopes	192
5.9	A model for the formation of organo-sulphur compounds	198
5.10	The geochemistry of the Cannon Ball Doggers and their host sediment	200
	5.10.1 Origin of the Cannon Ball Doggers	200
	5.10.2 Organic Carbon	202
	5.10.3 Carbonate carbon and oxygen	203
	5.10.4 Sulphur isotopes and bulk geochemistry	203
	5.10.5 Clay mineral reactions	208
5.11	Conclusions	211

## Chapter 6 - The weathering of mudrocks

6.0	Introduction	213
6.1	Sulphate in Shales	213
6.2	Oxidation of reduced sulphur	214
	6.2.1 Inorganic sulphur	214
	6.2.2 Organic sulphur	217
6.3	Oxidation mechanisms	217
6.4	Oxygen isotope systematics	219
6.5	In situ weathering of shales	223
	6.5.1 Iron	223
	6.5.2 Organic matter	227
	6.5.3 Sulphur	231
	6.5.3.1 Sulphate in Jurassic shales	231
	6.5.3.2 Isotopic composition of sulphate in the Jet Rock	234
	6.5.3.3 Sulphate in Carboniferous shales	239
	6.5.3.4 Isotopic composition of sulphate from Carboniferous shales	242
	6.5.3.5 Sulphate	245
	6.5.3.6 Elemental Sulphur	250
6.6	Conclusions	251

## **Chapter 7 - General conclusions and suggestions for future work**

7.0	Introduction	252
7.1	Analytical methods	252
7.2	Geochemistry of the Caton Shales	252
7.3	Formation of Septarian concretions	253
7.4	Geochemistry of the Jet Rock	254
7.5	Weathering of shales	255
7.6	Concluding remarks	256

## **Appendix - Statistical methods**

A.1	Linear correlation analysis	257
A.2	Least squares estimate	257
A.3	Coefficient of linear regression	257
A.4	Coefficient of determination	258
A.5	Significance of linear correlation coefficient	258
A.6	Confidence limits	258

# List of Tables

2.1	The relationship between bottom water conditions and oxygen levels within sediment	7
2.2	Principle microbially mediated reactions during diagenesis	9
2.3	Rate constants and half lives for sedimentary iron minerals with respect to their sulphidation	16
2.4	DOP as a palaeoenvironmental indicator	16
2.5	Stable isotopes of oxygen, carbon and sulphur	26
2.6	Fractionation resulting from the oxidation of sulphides	26
2.7	Composition of biological material	37
2.8	Average elemental composition of principle constituents of living organic matter	38
2.9	Main sources of n-alkanes	40
2.10	Organic parameters used as thermal maturity indicators for hydrocarbon source rocks	49
2.11	Kerogen type nomenclature	56
3.1	Comparison of the contamination introduced to shale samples during different methods of crushing	64
3.2	Reproducibility of carbon analyses using the Carlo Erba	64
3.3	Comparison of the different methods used to determine organic carbon	67
3.4	Soxhlet extraction of bitumen over different lengths of time	70
3.5	Reproducibility of soxhlet extraction	70
3.6	Diagnostic ions studied by GC-MS	74
3.7	Reproducibility of Cp-1 samples relative to different aliquots of reference gas	74
3.8	Duplicate measurements of $\delta^{34}\text{S}$	79
3.9	Reproducibility of $\text{SO}_2$ preparation for $\delta^{34}\text{S}$ isotopic analysis	79
3.10	Reproducibility of sulphur measurements using the Carlo Erba	84
3.11	Recovery of elemental sulphur from a rock matrix	84
3.12	Recovery of pyrite	89
3.13	Change in the relative concentration of iron extracted with boiling time	89
3.14	Reproducibility of iron extraction	95

4.1	Radiogeochemical data of the Caton Shales	106
4.2	Distribution of U, Th and K in clay minerals	109
4.3	Distribution of U, Th and K within the Caton Shales	109
4.4	Summary of organic geochemical data from the Caton Shales	112
4.5	Summary of the inorganic geochemistry of the Caton Shales (second set of samples)	116
4.6	Summary of the Rock Eval data from the Caton Shales (second set of samples)	117
4.7	Relative proportions of the maceral groups	119
4.8	Maturity parameters determined optically	119
4.9	Average chemical composition of soluble organic fractions extracted from the Caton Shales	121
4.10	Relative proportions of the fractions making up the bitumens	121
4.11	Molecular parameters determined by GC and GC-MS	124
4.12	$\delta^{13}\text{C}$ for bitumens and concretion 'oil'	128
4.13	Mineral abundance in carbonate free residue of concretion matrix	131
4.14	Molecular migration distances and flow velocities for a muddy sediment	131
4.15	$\delta^{18}\text{O}$ and $\delta^{13}\text{C}$ for carbonate cements from the concretions	139
4.16	Isotope and geochemical composition of cements from the concretions	142
4.17	Probe traverse analysis (Fe, Mg, Mn and Ca)	146
5.1	Location of the Jet Rock samples	160
5.2	Gamma Ray log of the Jet Rock	162
5.3	Carbon, Iron, Sulphur geochemical summary	166
5.4	Rock Eval data from the Jet Rock	173
5.5	Summary of the transformation ratios for organic carbon	175
5.6	Relative proportions of the fractions from bitumens extracted	178
5.7a	Elemental composition of the bitumen	179
5.7b	Elemental composition of the asphaltene fraction	180
5.7c	Elemental composition of the aliphatic fraction	181
5.7d	Elemental composition of the aromatic fraction	182
5.7e	Elemental composition of the polar fraction	183
5.8	Summary of biomarker ratios	185



5.9	Sulphur isotope data for the Jet Rock	193
5.10	Rate constants and their half lives for iron bearing minerals	201
5.11	Porosity estimates for the Cannon Ball Dogger host sediments	205
5.12	Summary of the chemical analyses of the carbonate free residues of the Cannon Ball Doggers and host sediment	206
5.13	$\delta^{34}\text{S}$ of pyrite from the Cannon Ball Doggers	207
5.14	Mineralogy of the Jet Rock	209
6.1	Summary of fractionation factors for the water-sulphate system	222
6.2	Oxidation of sulphite and oxygen incorporation	222
6.3	Iron extractions on fresh and weathered samples	224
6.4	Cumulative iron extracted from fresh and weathered samples	224
6.5	Depth of samples taken from the Caton Shales	228
6.6	Summary of Rock Eval data for weathered Carboniferous shales	228
6.7	Bitumen extracted from the Caton Shales	230
6.8	Loss of carbon due to thermal maturation	230
6.9	Summary of thermal maturities for samples taken during this study	232
6.10	Average band energies for a range of carbon and sulphur bonds	232
6.11	Summary of the sulphur-bearing compounds in the Jet Rock	233
6.12	$\delta^{34}\text{S}$ for sulphur-bearing compounds in the Jet Rock	236
6.13	$\delta^{18}\text{O}$ and $\delta^{34}\text{S}$ values for sulphate extracted from Carboniferous shales	243
6.14	$\delta^{34}\text{S}$ for sulphur compounds found in shales	243
A.1	Correlation coefficients	260
A.2	Values of t	261

# List of Figures

2.1	Depth profile of FOAM sediment showing the concentration of dissolved sulphate, pyrite sulphur, elemental sulphur and the rate of sulphate reduction	14
2.2	Dissolved pore water sulphide in FOAM sediment	14
2.3	Diagrammatic representation of the overall process of sedimentary pyrite formation	18
2.4	C/S plot for modern fresh water and marine sediments	20
2.5	Theoretical plots of C/S and DOP for euxinic sediments	22
2.6	Plot of C/S versus vitrinite reflectance for normal marine shales	23
2.7	Changes in $\delta^{34}\text{S}$ of reactant and product during closed system sulphate reduction	29
2.8	Isotopic variation of $\delta^{13}\text{C}$ in organic and inorganic compounds	30
2.9	Variation in $\delta^{34}\text{S}$ throughout the Phanerozoic	34
2.10	Isoprenoids found in modern and ancient sediments	41
2.11	Transformation of chlorophyll into pristane and phytane	43
2.12	Pr/nC17 and Ph/nC18 as palaeoenvironmental indicators	44
2.13	Structure of hopanes and steranes	45
2.14	Demethylation of hopanes	46
2.15	Relationship between sterol composition and depositional environment	48
2.16	Maturity related isomerism of sterols	50
2.17	Organic matter transformations during burial	52
2.18	van Krevelen diagram	54
2.19	Structure of Type I, II and III kerogens	55
2.20	Formation of organic sulphur compounds	59
2.21	Structures of organic sulphur compounds	60
2.22	Functionality of organically bound sulphur	61
3.1	Comparison of the methods in determining organic carbon	66
3.2	Soxhlet extraction apparatus	69
3.3	Liquid column chromatography apparatus	72
3.4	Organic carbon solvent extraction scheme	73
3.5	Sulphur dioxide conversion procedure	78
3.6	Sulphide reaction tube	79

3.7	Sulphate reaction tube	79
3.8	Copper acetate bridge complex	79
3.9	Apparatus to determine reduced sulphur	87
3.10	Recovery of pyrite	88
3.11	Pyrite digestion as evidenced by XRF	90
3.12	Relationships between iron concentrations and absorbance	92
3.13	Mineral matrix effects on iron absorbance	93
3.14	Extractable iron relative to boiling times	93
4.1	Simplified geological map of the region around Lowgill	98
4.2	Generalised sedimentary sequence of the Lower Carboniferous sediments in the Craven Basin	100
4.3	Thermal history of the basin from AFTA data	101
4.4	Sedimentary log of the Caton Shales	103
4.5	Spatial distribution of concretions	104
4.6	Log of U, Th and K distribution	107
4.7	Relationship between Th and K	110
4.8	Relationship between authigenic uranium and organic carbon	110
4.9	C/S relationship for the Caton Shales	113
4.10	Relationship between DOP and organic carbon for the Caton Shales	113
4.11	Model values for C/S ratios	114
4.12	van Krevelen type diagram of Rock Eval data for Caton Shales	120
4.13	Thermal maturity of the Caton Shales	120
4.14	GC trace for extracted shale	122
4.15	GC-MS trace for extracted shale	123
4.16	GC trace for concretion 'oil'	126
4.17	GC-MS trace for concretion 'oil'	127
4.18	Principle septarian crack orientation horizontal to bedding	137
4.19	Trend in isotope evolution in septarian cements	138
4.20	Relationship between $\delta^{18}\text{O}$ and $\delta^{13}\text{C}$ for a subset of 20 samples	144
4.21	Change in Mn/Fe ratio with $\delta^{18}\text{O}$	149
4.22	Change in Mn/Fe ratio with $\delta^{13}\text{C}$	149
4.23	Change in Mg/Fe ratio with $\delta^{18}\text{O}$	151
4.24	Change in Mg/Fe ratio with $\delta^{13}\text{C}$	151

5.1	Stratigraphy of the Lower Jurassic on the Yorkshire coast	155
5.2	Location map of Port Mulgrave	158
5.3	Sedimentary log of the Jet Rock at Port Mulgrave	159
5.4	Relationship between uranium and organic carbon	163
5.5	Relationship between sulphur, reactive iron and DOP with organic carbon	165
5.6	Relationship between pyrite sulphur, DOP and organic carbon with reactive iron	169
5.7	Cross plot of $\delta^{34}\text{S}$ pyrite and organic carbon	171
5.8	Constituents of the kerogen isolated from PM1 and PM2	172
5.9	van Krevelen type plot (HI and OI)	174
5.10	Estimated $R_0$ from a van Krevelen type plot	174
5.11	Extractable organic matter as a function of TOC	177
5.12	Hetero-atom plot of the organic fractions of the Jet Rock	184
5.13	GC traces for the aliphatic fractions of PM1, PM8 and PM17	187
5.14	Pr/nC17 and Ph/nC18 cross plot	188
5.15	GC AED trace showing dibenzothiophene in the Jet Rock	189
5.16	Incorporation of sulphur into organic matter	191
5.17	Relationship between $\delta^{34}\text{S}$ and sulphur concentration from bitumens extracted from the Jet Rock	195
5.18	Relationship between oxygen index and $\delta^{34}\text{S}$ of the bitumen	196
5.19	Variation of $\delta^{34}\text{S}$ of the bitumen and kerogen with pyrite sulphur	197
5.20	Summary of the sulphur incorporation model	199
6.1	Oxidation pathways of reduced sulphur	215
6.2	Distribution of $\delta^{18}\text{O}$ within geological samples	220
6.3	The relationship between $\delta^{18}\text{O}$ in water and sulphate	220
6.4	Relationship between soluble sulphate and pyrite sulphur concentrations	226
6.5	Concentration of sulphate as a function of organic carbon	226
6.6	Sulphate concentrations in weathered and fresh samples from the Jet Rock	235
6.7	Distribution of the isotopic composition of sulphur-bearing compounds in the Jet Rock	235
6.8	Relationship between sulphate concentration and $\delta^{34}\text{S}$ of the sulphur in fresh and weathered samples	238
6.9	$\delta^{34}\text{S}$ in weathered and fresh samples from the Jet Rock	238

6.10	Variation of $\delta^{18}\text{O}$ and sulphate concentration for the Jet Rock	240
6.11	$\delta^{18}\text{O}$ in weathered and fresh samples from the Jet Rock	240
6.12	Variation of $\delta^{18}\text{O}$ and $\delta^{34}\text{S}$ in sulphate extracted from fresh and weathered samples of the Jet Rock	241
6.13	Variation of $\delta^{18}\text{O}$ and sulphate concentration for Carboniferous shales	241
6.14	Relationship between $\delta^{18}\text{O}$ and sulphate concentrations for the shale samples investigated in this study	244
6.15	$\delta^{18}\text{O}$ and $\delta^{34}\text{S}$ for Carboniferous samples	246
6.16	Distribution of $\delta^{34}\text{S}$ isotopic values for shale samples	248
6.17	Relationship between sulphate and organic S isotopic composition	249

## List of Plates

4.1	$K\alpha$ X-ray maps of magnesium, calcium and iron together with a back-scattered electron micrograph of a septarian crack	145
-----	---	-----

# List of Symbols and Abbreviations

A	ampere		
AA	atomic absorption		
AFTA	apatite fission track analysis		
atm	atmospheric pressure		
aq	aqueous		
DCM	dichloromethane		
DOP	degree of pyritisation		
EDTA	ethylene-diamine-tetra-acetic acid		
FID	flame ionising detector		
FPD	flame photometric detector		
GC	gas chromatography		
GC-MS	gas chromatography - mass spectrometry		
GC - AED	gas chromatography - atomic emission detection		
ICP-AES	inductively coupled plasma-emission spectrometry		
J	joule		
K	Kelvin		
LOM	level of oraganic metamorphism		
M	molarity		
mol.	number of moles		
OBS	organically bound sulphur		
ppm	parts per million		
SEM	scanning electron microscopy		
TOC	total organic carbon		
TSR	thermochemical sulphate reduction		
XRD	X-ray diffraction		
XRF	X-ray fluorescence		
a	fractionation factor	$\sigma_{n-1}$	standard deviation
$\delta$	del	%	percent
$K_{sp}$	solubility product	‰	permil
m/e	mass to charge ratio		<u>Prefix</u>
x	sediment depth	n	nano 10 <sup>-9</sup>
$\omega$	mean sedimentation rate	$\mu$	micro 10 <sup>-6</sup>
°C	degree Celcius	m	milli 10 <sup>-3</sup>
~	approximately equal	c	centi 10 <sup>-2</sup>
$\nu$	vibrational frequency of a molecule	k	kilo 10 <sup>3</sup>

Bring me sulphur, old nurse, that cleanses all  
pollution and bring me fire, that I may purify the  
house with sulphur.

Homer, *Odyssey*, Book 22, p481.

# Chapter 1

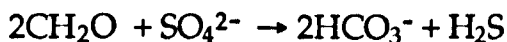
## Introduction

### 1.0 Introduction

Sulphur, the sixteenth element in order of abundance, occupies about 0.005 mass percent of the earth's crust and is widely distributed in nature. It exists in five common oxidation states:

-2	sulphides, H <sub>2</sub> S, organosulphur compounds etc.
-1	disulphides (pyrite)
0	elemental sulphur
+4	SO <sub>2</sub>
+6	SO <sub>4</sub> <sup>2-</sup>

Pyrite, FeS<sub>2</sub>, is the most common sulphur bearing mineral found within sediments. The formation of pyrite has been intensively studied (e.g. Berner 1970, Goldhaber and Kaplan 1974, Goldhaber et al 1977, Berner 1982, Berner 1984, Raiswell and Berner 1985, Canfield 1989). In marine systems, the concentration of dissolved sulphur is in the order of 28mmol (usually in the form of SO<sub>4</sub><sup>2-</sup>). Bacteria such as *Desulphovibrio* are dominant in anaerobic environments, and their primary metabolic pathway involves the reduction of sulphate, liberating hydrogen sulphide as a by-product. Organic matter acts as a reducing agent in the reaction.



Sulphate reducing bacteria account for the greatest loss of organic matter within the anoxic zone of the sediment column (Berner 1985).

Most oil and gas accumulations contain low concentrations of sulphur (<1.0%). Living organisms assimilate sulphur into organic compounds. The concentration of these compounds within the total biomass cannot always account for the sulphur found in hydrocarbon reserves.

Recent studies suggest that reduced sulphur species can become incorporated into organic matter within sediments during diagenesis (e.g. Mango 1983, François 1987, Vairavamurthy and Mopper 1987, Sinninghe Damsté *et al.* 1989a,b,c, Kohnen *et al.* 1991a,b, Raiswell *et al.* 1993a,b).



Hydrocarbons which contain significant amounts of hydrogen sulphide are termed "sour". The exploitation of such hydrocarbon reserves and their subsequent combustion has led to environmental problems such as acid rain. With increasing environmental awareness, stricter legislation is being enforced to limit such emissions, the most predominant being oxides of sulphur. Therefore, the cost of desulphurisation has to be taken into account when evaluating the economic potential of a hydrocarbon deposit.

## 1.1 Aims of the Thesis

Studies by workers such as Canfield *et al.* (1992) have begun to investigate the relative importance of iron mineralogy in the rate of formation of pyrite. However, the rate at which organic compounds compete with iron bearing minerals for hydrogen sulphide is poorly understood. Raiswell *et al.* (1993a) have used an isotopic approach to the problem. Despite this recent work, there is a significant gap in our understanding of this process.

This thesis aims to provide a greater insight into the formation, evolution and weathering of sulphur bearing compounds found within mud rocks. A range of samples have been collected from the Carboniferous and Jurassic and analysed by a combination of isotopic, organic and inorganic techniques.

Specifically, the aims of this thesis are to:

- a) use organic and inorganic parameters to identify the palaeoenvironmental conditions at the time of deposition and the nature of the organic material at the time of deposition
- b) identify the sulphur bearing species in mud rocks
- c) determine possible formation pathways for sulphur compounds using a detailed molecular and isotopic approach
- d) determine the relative time of formation of sulphur compounds
- e) investigate the effects of weathering on sulphur species in mud rocks

- f) identify the nature and source of the oxidant in the weathering process

## **1.2 Laboratory Work**

The majority of analysis was performed at Leeds University in the Department of Earth Sciences. Isotopic analysis of carbonate cements were performed by the author at Liverpool University. Sulphate oxygen analysis was performed courtesy of Brian Robinson at the Institute of Geological and Nuclear Sciences, Lower Hutt, New Zealand.

GC and GC-MS analysis of organic samples were performed in British Gas laboratories (LRS) by the author and at Manchester University by Andy Gize. GC-AED was performed on a small number of samples at the Energy and Environment Centre at the University of North Dakota, USA by Peter Louie.

Details of analytical methodology are given in Chapter 3.

## **1.3 Thesis Layout**

In Chapter 2, an overview of current literature is presented. The diagenesis of mud rocks is reviewed with specific emphasis on the sulphur species taking part in the reactions resulting in the formation of pyrite, elemental sulphur and organically bound sulphur compounds. The palaeoenvironmental conditions are also discussed.

The methodology of laboratory techniques used in this thesis is discussed in Chapter 3.

Chapter 4 presents a study of Carboniferous shales and carbonate concretions from the flanks of the Bowland Basin. A detailed geochemical comparison of host sediment and cements within the concretion matrix enables an evolutionary sequence to be established for the Caton Shales

An organic and inorganic geochemical study of the Jet Rock (Upper Lias, Lower Jurassic) is given in Chapter 5. Sulphur isotope studies provide information on the relative formation of organic sulphur compounds and diagenetically formed pyrite.

In Chapter 6, the weathering of sulphur species is considered. Data from the Caton Shales, the Jet Rock and the Bowland Shales are compared and contrasted. Use of sulphate sulphur and sulphate oxygen isotope analysis indicates the nature of oxidation of organic and inorganic sulphur.

The conclusions from this study are presented in Chapter 7 together with a discussion and suggestions for future work.

# Chapter 2

## Previous Studies: Organic and inorganic geochemistry of mudrocks

### 2.0 Introduction

This chapter presents a selective review of the inorganic and organic geochemistry of mud rocks. Major subjects include: organic rich shale deposition, bacterial reactions during diagenesis, pyrite formation and organic matter composition, degradation and transformation.

### 2.1 Black shale deposition

Argillaceous organic-rich marine rocks are collectively known as black shales (e.g. Wignall, 1991). The accumulation of organic carbon in marine environments has traditionally been thought to be promoted by bottom water anoxia. Wignall and Maynard (1993) have reviewed the proposed mechanisms for the deposition of organic rich mudrocks and this is further discussed by Canfield (1989b) and extensively discussed by Wignall (1994).

There are currently two differing models for the formation of black shales. The mineralisation of organic carbon is slower under anoxic conditions than in oxic. Therefore, organic rich shales accumulate in areas of anoxia as a result of enhanced preservation. Wignall (1991) has proposed an expanding oxygen restricted 'puddle' model, such that subsidence and a subsequent sea-level rise together with a decreased sediment supply led to the expansion of the oxygen restricted puddle, resulting in the deposition of black shales resting on unconformities or basal transgressive lags.

Middleburg (1991) and Coveney *et al.* (1991) have suggested similar models based on the accumulation of black shales associated with zones of high productivity. Pedersen and Calvert (1990) suggest that it is the rate of primary production of organic matter and not water column anoxia which controls the

accumulation of organic rich sediment. Such primary production (dominated by plankton) is dependant upon a nutrient supply in the eutrophic zone of the oceans. This in turn is governed by the vertical stability of the water column (Ryther, 1963). Concentrations of dissolved oxygen in bottom waters are very low in areas of high productivity as a result of a high organic carbon flux into the sediment and a correspondingly high uptake of oxygen. The resulting low levels of oxygen increase the preservation potential of the organic matter deposited in the sediment.

Sedimentation rates may also play an important role in organic matter preservation. Sedimentation rates are generally high in areas of high productivity and very low in stratified sedimentary basins. After indepth comparisons between the two models, (the preservation model and the productivity model) Wignall (1994) suggests that the preservation model is "more generally applicable to black shale deposition".

Tyson and Pearson (1991) have proposed a terminology relating the bottom water conditions (within 1m of the sediment water interface) and the oxygen levels within the sediment. These are summarised in Table 2.1.

## 2.2 Diagenesis

Diagenesis, i.e. the low temperature physical and chemical processes altering a sediment prior to lithification, is dominated by microbial activity. The microbes (both aerobic and anaerobic) metabolise organic matter with varying oxidising agents to produce  $\text{CO}_2$ ,  $\text{CH}_4$ ,  $\text{NH}_3$  and  $\text{H}_2\text{S}$ . Such reactions deplete the levels of oxygen in the sediment.

### 2.2.1 Organic matter preservation

Studies on the degradation of organic matter in oxic and anoxic environments have been reviewed by Henrichs and Reeburgh (1987) and more recently by Canfield (1989b), Wignall (1994) and references therein. There appears to be little significant difference in the rate at which organic matter is metabolised by microbes in oxic and anoxic environments. Aerobic bacteria are able to metabolise more complex organic material, therefore in anaerobic conditions,

**Table 2.1**

Oxygen ml/l	Oxygenation Regime		Physiological Regime
	Facies	Biofacies	
8.0 - 2.0	Oxic	Aerobic	Normoxic
2.0 - 0.2 2.0 - 1.0 1.0 - 0.5 0.5 - 0.2	Dysoxic moderate severe extreme	Dysaerobic	Hypoxic
0.2 - 0.0	Suboxic	Quasi anaerobic	
0.0 (H <sub>2</sub> S)	Anoxic	Euxinic	Anoxic

Terminology relating the bottom water conditions and the oxygen levels within the sediment (after Tyson and Pearson, 1991).

the less readily metabolisable organic compounds are broken down more slowly than would be the case in oxic environments.

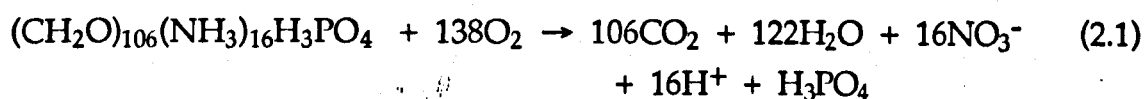
Sulphate reduction and oxic respiration have been found to oxidise equal amounts of organic carbon in nearshore sediments (Jørgensen, 1982; Canfield, 1987). At low sedimentation rates (e.g. characteristic of deep sea deposits) oxic respiration is the dominant reaction. Canfield (1987) found that between 100 and 1,000 times more carbon was oxidised by oxic respiration than sulphate reduction in such conditions. In euxinic environments sulphate reduction oxidises approximately the same amount of organic carbon as would be oxidised by both processes in a normal marine sediment (at a similar depositional rate).

The oxidation of organic carbon in sediments only ceases when the supply of oxidant is cut off. Further degradation of labile organic matter takes place via fermentation reactions. Canfield (1987) showed consistent findings in that almost as much organic carbon is oxidised by sulphate reduction in euxinic sediments as is oxidised by the sum of sulphate reduction and oxic respiration in normal marine sediments with similar depositional rates.

Canfield and Raiswell (1991b) have reviewed the decomposition reactions of organic matter in oxic and anoxic environments. They can be broken down into a series of reactions of decreasing thermodynamic favourability as the oxidising agent changes from dissolved oxygen to fermentation reactions. These reactions are summarised in Table 2.2.

### 2.2.2 Oxic Respiration

Aerobic organisms utilise dissolved oxygen to metabolise organic matter within the aerobic region of the sediment. Assuming a Redfield-type organic matter composition with a C/N/P ratio of 106/16/1 (Redfield, 1942), the reaction can be expressed as:



This reaction has been shown to remove large quantities of organic matter from the sediment (e.g. Menzel, 1974; Berner 1980; Wilson *et al.* 1985 ). With

Table 2.2

Environment	Diagenetic Zone	Schematic Equation	$\Delta G^{\circ}(\text{kJmol}^{-1} \text{ of CH}_2\text{O})$	$\delta^{13}\text{C}_{\text{CO}_2}$
Oxic	Aerobic Oxidation	$\text{CH}_2\text{O} + \text{O}_2 \rightarrow \text{CO}_2 + \text{H}_2\text{O}$	-475	
Sub-oxic	Nitrate Reduction/ Denitrification	$5\text{CH}_2\text{O} + 4\text{NO}_3^- \rightarrow 4\text{HCO}_3^- + 3\text{H}_2\text{O} + 2\text{N}_2 + \text{CO}_2$	-448	-25 to -28 ‰
	Mn Reduction	$\text{CH}_2\text{O} + 2\text{MnO}_2 + 3\text{CO}_2 + \text{H}_2\text{O} \rightarrow 2\text{Mn}^{2+} + 4\text{HCO}_3^- + \text{CO}_2 + \text{H}_2\text{O}$	-349	
	Fe Reduction	$\text{CH}_2\text{O} + 4\text{Fe}(\text{OH})_3 + 7\text{CO}_2 \rightarrow 4\text{Fe}^{2+} + 8\text{HCO}_3^- + 3\text{H}_2\text{O}$	-114	
Anoxic	Sulphate Reduction	$2\text{CH}_2\text{O} + \text{SO}_4^{2-} \rightarrow 2\text{HCO}_3^- + \text{H}_2\text{S}$	-77	-28 ‰
	Methanogenesis	$2\text{CH}_2\text{O} \rightarrow \text{CH}_4 + \text{CO}_2$	-58	
	(Decarboxylation)	$\text{RCO}_2\text{H} \rightarrow \text{CO}_2 + \text{RH}$		-20 ‰

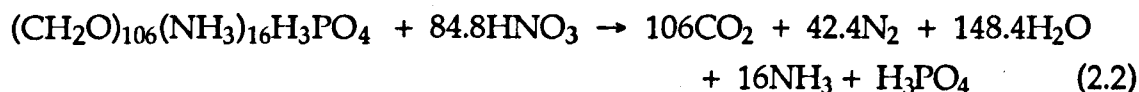
Diagenetic chemical reactions moderated by micro-organisms and the associated palaeoenvironmental conditions.



increasing sedimentation rates, there is an increase in the organic matter preservation. Although there is an increased clastic 'dilution factor', organic matter spends less time in the oxygenated region of the sediment thus decreasing the amount of time available for oxidative degradation and benthic grazing.

### 2.2.3 Denitrification

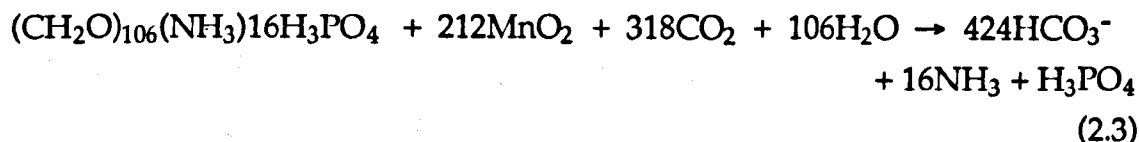
As the levels of oxygen decrease due to diffusion limited processes, nitrate reduction becomes a more dominant reaction.



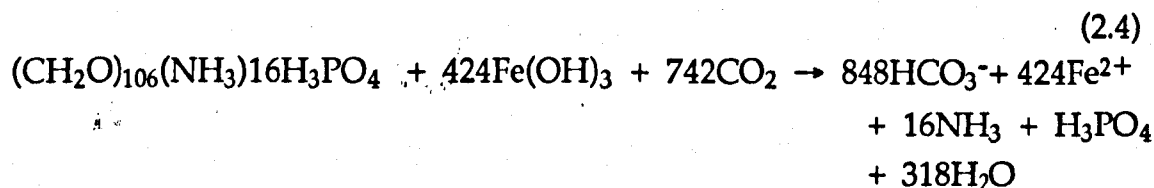
There are low levels of nitrate in marine systems (~1000 times less than sulphate (Berner, 1980)) which suggest this reaction may be of little significance. However, it has been reported as accounting for the oxidation of over 10% of organic matter in some sediments (Henrichs and Reeburgh, 1987 and Jørgensen, 1983). This may be the result of nitrate becoming regenerated in overlying oxic layers, therefore acting as an "electron shunt" which would facilitate redox reactions.

### 2.2.4 Manganese and Iron Reduction

Anaerobic bacteria utilise manganese (IV) and iron (III) compounds as oxidising agents. Such oxidation of organic matter using metal oxides can be represented by :

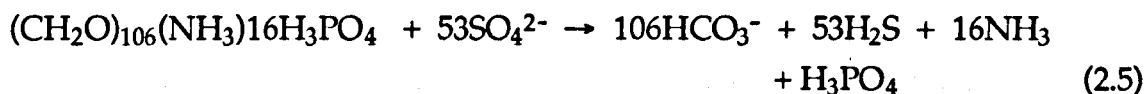


and



## 2.2.5 Sulphate Reduction

In anaerobic conditions *Desulfovibrio* bacteria reduce sea water sulphate to hydrogen sulphide. Goldhaber and Kaplan (1974) showed that sulphate-reducing bacteria cannot readily metabolise macromolecular sedimentary organic matter. Therefore other fermentative bacteria must be involved to break down organic matter into a form more readily utilised by the sulphate reducers. The overall process can be represented as:



Recent work (Coleman et al., 1993) has shown that some species of sulphate reducing bacteria are capable of reducing Fe(III) directly when sulphate becomes depleted.

## 2.2.6 Methane Oxidation

Fermentation reactions produce methane. In environments where sedimentation rates are slow, this methane may diffuse up into the zone of sulphate reduction and become an important reducing agent (e.g. Iversen and Jørgensen 1985, Alperin *et al.*, 1988).



Aerobic and suboxic bacteria also utilise methane in their metabolic reactions. However in this case methane acts as the reducing agent in the reaction:



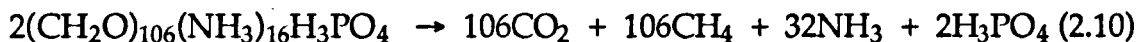
## 2.2.7 Methane Production

Methanogenesis or methane formed microbiologically from the breakdown of organic matter can be regarded as a two step process:





The overall reaction can be represented as one of organic matter disproportionation:



## 2.3 Sedimentary pyrite formation

Pyrite occurs ubiquitously in marine argillaceous rocks (Ronov, 1976; Berner, 1982) which contains organic matter and will therefore develop anoxic, sulphate reducing conditions (Berner and Raiswell, 1983). Many studies have investigated the formation of pyrite in natural systems (e.g. Berner, 1970, 1984; Goldhaber and Kaplan, 1974; Jørgensen, 1977; Howarth and Jørgensen, 1984; Raiswell and Berner, 1985; Fisher and Hudson, 1987) and experimental systems (Berner 1964, 1967, 1970; Rickard 1974, 1975, 1989a, 1989b; Pyzik and Sommer, 1981).

Dissolved sulphate is microbially reduced by organic matter to produce  $\text{H}_2\text{S}$  (Equation 2.5). Under oxic conditions, oxygen enters the sediment by molecular diffusion or by physical mixing (caused by wave and current stirring or bioturbational activity). The oxygen is consumed by aerobic bacteria during their metabolism of organic matter. Thus anaerobic conditions develop below the layer of oxic respiration. Here pyrite forms via the reaction of  $\text{H}_2\text{S}$  with iron minerals (Berner, 1970, 1984; Canfield and Raiswell, 1991a).

The rate at which pyrite can form is controlled by the amount and nature of organic matter, the availability of dissolved sulphate and the nature of the iron minerals within the sediment.

### 2.3.1 The role of organic matter

Sulphate reduction is a complex multi-step process involving the initial depolymerisation of sedimentary organic compounds by fermentative microorganisms into simple organic compounds which are used by sulphate reducing bacteria (Jørgensen, 1982; Berner, 1984). The organic matter acts as a

reducing agent to convert sulphate into hydrogen sulphide and also provides the energy source for the reaction.

Westrich (1983) and Westrich and Berner (1984) have shown experimentally that organic matter can be limiting in pyrite formation. Phytoplankton were added to a sediment which was known to have a low rate of sulphate reduction. The rate of sulphate reduction was found to be directly proportional to the amount of organic matter added to the sediment and that the nature of the organic matter directly affected the rate of sulphate reduction compared with fresh plankton.

Concentrations of refractory organic matter such as humic substances, build up in sediments as a result of preferential degradation of labile organic compounds (Bada and Lee, 1977) and sulphate reducing bacteria are less readily able to utilise the residual organic matter. Marine organic matter, dominated by algae, is more easily degraded by bacteria than terrestrially derived organic matter comprising of resistant lignins, resins and waxes (Goldhaber and Kaplan, 1974).

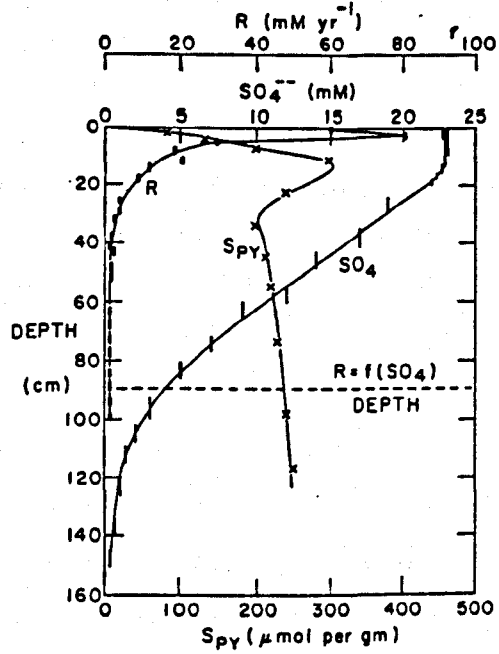
### 2.3.2 The role of sulphate availability

The amount of sulphate in the sediment is controlled by ionic diffusion to a depth of about 1m (Goldhaber *et al.*, 1977) and bioturbational mixing in the upper 20cm or so of the sediment. Although the mixing process increases sulphate concentrations, oxygen is brought into the sediment and H<sub>2</sub>S diffuses out. Bioturbation thus leads to oxidation of pyrite and the loss of hydrogen sulphide from the system.

The profile shown by Berner (1984) (Figure 2.1) is typical of sulphate concentrations in modern sediments. A constant concentration of sulphate marks the zone of intense bioturbation. This region has the fastest rate of sulphate reduction and is where the majority of pyrite is formed. As conditions become permanently anoxic, the rate of sulphate reduction decreases markedly, limited by the supply of labile organic matter. However, pyrite formation does continue in the presence of H<sub>2</sub>S and reactive iron minerals.

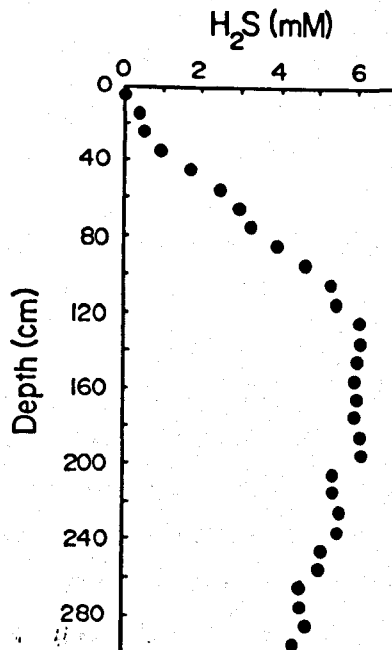
The rate of sulphate reduction in marine sediments is controlled by physical factors such as temperature and more importantly by the nature of the

Figure 2.1



Depth profile of FOAM sediment showing the concentration of dissolved sulphate, pyrite sulphur, elemental sulphur and the rate of sulphate reduction. After Berner, 1984.

Figure 2.2



Dissolved pore water sulphide in FOAM sediment. After Canfield, 1992.

reducing agent, i.e. the organic matter substrate (Westrich and Berner, 1984). Sulphate concentrations only affect the rate of sulphate reduction when concentrations fall below 3mmol (Boudreau and Westrich, 1984). The typical sea water sulphate concentration is in the order of 28mmol, thus sulphate concentrations only affect the rate of sulphate reduction when rates are already low due to the oxidation of most of the reactive organic matter. Sulphate in marine environments is usually not thought to be a limiting factor in pyrite formation (Berner, 1970, 1984).

### 2.3.3 The role of iron

Detrital iron minerals are a common component of terrigenous and marine sediments. In environments dominated by carbonates, the formation of pyrite is often limited by the availability of iron minerals, e.g. Berner (1972).

Sediment pore waters either dominated by iron or sulphide are typically close to saturation with respect to mackinawite (Canfield and Raiswell, 1991a). The nature of the iron bearing minerals is an important control on the rate of pyrite formation (Canfield, 1989a; Canfield *et al.*, 1992). Reactive iron minerals may be defined as that fraction of iron in marine sediments which can potentially react with sulphide (Berner, 1970; Goldhaber and Kaplan, 1974; Jørgensen, 1977; Raiswell and Berner, 1985; Canfield, 1989a; Raiswell *et al.*, 1993a). Canfield (1989a) has shown that iron oxide and oxyhydroxide phases play a dominant role in early diagenetic pyrite formation and hence make up the bulk of the reactive iron minerals.

The rate constants and half lives for the reactions of a range of iron bearing minerals with a 1mmol dissolved sulphide solution are shown in Table 2.3 (after Canfield *et al.*, 1992). Clearly the iron oxides dominate early diagenesis and react with rapidly with H<sub>2</sub>S, keeping the pore water sulphide concentrations low. Sulphide concentrations will increase as the poorly reactive iron silicates become the dominant iron bearing phase because these phases remove the H<sub>2</sub>S more slowly than it can be added. As can be seen from Table 2.3, the amount of pyrite formed is a function not only of organic carbon, sulphate and iron but also on the contact time of H<sub>2</sub>S with iron minerals. The contact time with dissolved sulphide  $x/\omega$  (where  $x$  is the sediment depth and  $\omega$  is the mean sedimentation rate) can vary from 50 years e.g. Schem Harbour to at least 10<sup>6</sup> years e.g. Peru Trench (Raiswell *et al.*, 1993a).

**Table 2.3**

Iron Mineral	Rate Constant (Yr <sup>-1</sup> )	Half-Life
Ferrihydrite	2200	2.8 hours
Lepidocrocite	> 85	< 3 days
Goethite	22	11.5 days
Haematite	12	31 days
Magnetite (uncoated)	$6.6 \times 10^{-3}$	105 years
'Reactive' Silicates	$3 \times 10^{-3}$	230 years
Sheet silicates	$8.2 \times 10^{-6}$	84,000 years
Ilmenite, Garnets, Augite, Amphibole.	$\ll 8.2 \times 10^{-6}$	$\gg 84,000$ years

Rate constants and half-lives of sedimentary iron minerals with respect to their sulphidation (from Canfield et al., 1992).

**Table 2.4**

Environment	Bottom water conditions	DOP
Aerobic	fully oxygenated bottom waters significant benthic activity	<0.42
Restricted	low bottom water oxygen restricted benthic fauna	0.46-0.75
Inhospitable	H <sub>2</sub> S bearing or very low oxygen levels no benthic activity	>0.75

Degree of pyritisation (DOP) used as a palaeoenvironmental indicator.

### 2.3.4 The role of sulphide availability

Canfield and Raiswell (1991a) have noted that some sediments with rapid sulphate reduction rates (tens to hundreds of mmol per litre per year), may have high concentrations of dissolved sulphide but in other examples (e.g. Mississippi Delta) there is no accumulation of dissolved sulphide. In the latter case it is thought that sulphide concentrations are buffered at low levels by the rapid reaction of fine grained iron oxide/oxyhydroxide minerals with dissolved sulphide. The concentration of sulphide builds up in pore waters only when all the most 'reactive iron minerals' have been depleted leaving the much less reactive iron silicates in the sediment (which will not have the same buffering capacity).

The amount of hydrogen sulphide available for pyrite formation at any one time is determined by the balance between the rate of production and the rate of removal. Initially the rate of production is the limiting factor i.e. the rate of sulphate reduction. In general, as the depth of burial increases, the concentration of  $H_2S$  in the sediment rises up to a maximum. This is the case at the FOAM site as shown in Figure 2.2 (Canfield *et al.* 1992). The concentration of  $H_2S$  gradually decreases as the removal processes predominate over the production.

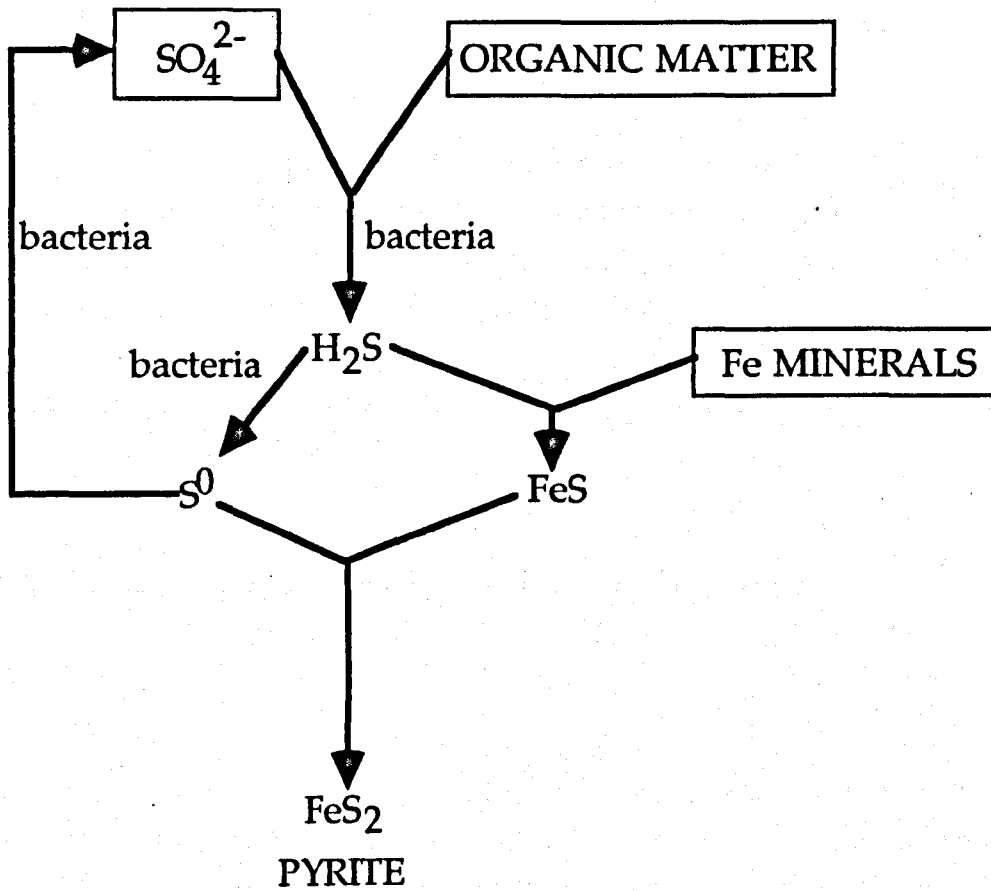
Berner and Westrich (1985) considered the removal of  $H_2S$  from sediments. It was suggested that when hydrogen sulphide can no longer be removed from the sediment by fixation as pyrite, it may be then lost from the sediment via oxidation reactions with molecular oxygen (mixed into the sediment by benthic activity). In addition to oxidation, physical mechanisms were also proposed for the escape of  $H_2S$  from the sediment. Bubbles of gas (methane) migrating upwards through the sediment may strip  $H_2S$  out of the system. Conduits produced by benthos increase the amount of  $H_2S$  which can easily escape from the sediment.

## 2.4 Iron sulphides

Once  $H_2S$  has been formed, it reacts with iron bearing minerals to form iron sulphide (Figure 2.3). Pyrite is rarely the initial mineral formed which is commonly mackinawite or greigite.



Figure 2.3



Diagrammatic representation of the overall process of sedimentary pyrite formation.  
After Berner, 1972.

Mackinawite has a variable composition ranging from  $\text{FeS}_{0.9}$  to  $\text{FeS}_{0.95}$  (Goldhaber and Kaplan, 1974). It forms by the reaction of  $\text{Fe}^{2+}$  with  $\text{H}_2\text{S}$  at near neutral pH (Berner, 1970). Rickard (1989a, b) has shown that hydrotroilite ( $\text{FeS}_n\text{H}_2\text{O}$ ) forms initially and subsequently decomposes to mackinawite over a period of hours.

Greigite ( $\text{Fe}_3\text{S}_4$ ) is thought to form from the oxidation of mackinawite (Goldhaber and Kaplan, 1974). The transformation of greigite into pyrite is associated with the formation of framboidal pyrite (Al Biatty, 1990; Sweeney and Kaplan 1990; Canfield and Raiswell, 1991a).

Marcasite and pyrrhotite formation are thought to be very rare during sediment diagenesis (Canfield and Raiswell, 1991a).

## 2.5 C-S-Fe relationships in sediments

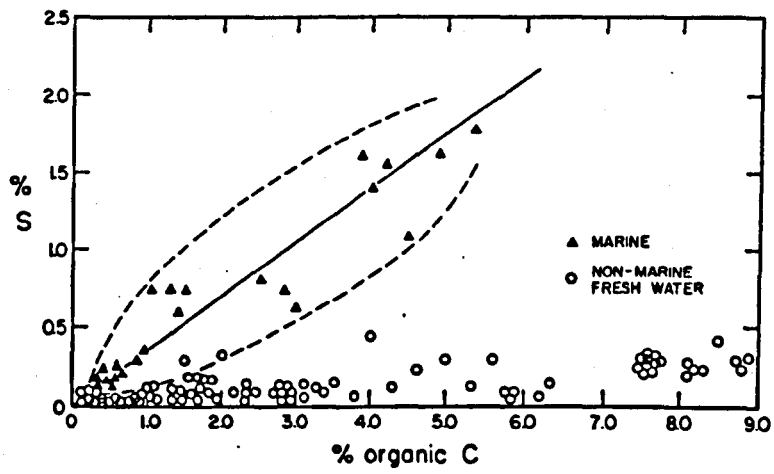
### 2.5.1 C/S ratios

In normal marine sediments, pyrite formation is usually limited by organic matter. In fresh water sediments, sulphate concentrations are low enough (less than 1/200 sea water) to limit the formation of pyrite. Thus there is much less diagenetic pyrite formed in fresh water than in marine organic rich sediments (Berner and Raiswell, 1983). Berner and Raiswell (1984) have used this argument to construct a method to distinguish fresh water from marine sediments.

A plot of organic carbon against pyritic sulphur for normal marine sediments, i.e. sediments deposited under normally oxygenated marine conditions (Figure 2.4) produces a positive linear correlation with an intercept at zero (Berner, 1970; Berner and Raiswell 1983, 1984; Berner 1984). This correlation shows the control of pyrite formation by organic carbon limitation. An approximately constant proportion of organic carbon is used to form pyrite, therefore at high levels of organic carbon there are large amounts of pyrite. The average carbon (C) / sulphur (S) weight ratio for recent normal marine sediments is  $2.8 \pm 1.5$  (Berner 1982).

The C/S ratio is much lower for fresh water sediments since the concentration of dissolved sulphate is much lower than in marine environments. The region

Figure 2.4



C/S plot for modern fresh water and marine sediments.  
After Berner and Raiswell, 1983.

where sulphate reduction takes place is much closer to the sediment/water interface and is confined to a shallow depth (in the order of a few centimetres). Therefore there is very little pyrite formed and the correlation between carbon and sulphur is poor (Figure 2.4).

In euxinic environments, where the bottom waters contain significant concentrations of  $H_2S$ , pyrite can form within the water column, i.e. syngenetically and independently of organic carbon (Figure 2.5). At low concentrations of organic carbon, high concentrations of pyrite would be expected in such conditions. The C/S plot for euxinic environment will therefore have a positive intercept on the sulphur axis (Figure 2.5), indicating the presence of syngenetic pyrite. In euxinic environments, the amount of pyrite formed is limited by reactive iron minerals. The C/S plot will therefore reflect the relationship between carbon and iron, as all the reactive iron minerals will become pyritised.

Temperature has been recognised as the dominant factor in determining post diagenetic organic matter loss from sediments during burial (Raiswell and Berner, 1987). The average C/S ratio for ancient sediments (Devonian to Tertiary) has been found to be  $1.8 \pm 0.5$  (Raiswell and Berner, 1987). This ratio is lower than the value for modern sediments and is thought to be a thermal maturity effect. Assuming a constant initial mean C/S ratio for normal marine shales since the Devonian, Raiswell and Berner (1987) have shown a decrease in C/S with increasing thermal maturity (measured by vitrinite reflectance) (Figure 2.6). Thus the original C/S ratio can be estimated if the sediment maturity is known.

Pre-Devonian C/S ratios are very low  $0.5 \pm 0.1$  (Raiswell and Berner, 1986). Such low values cannot be explained by thermal maturation effects alone and it has been argued that the appearance of vascular land plants during the Devonian resulted in an increased input of refractory organic carbon into sedimentary basins. This has the net effect of reducing the efficiency of pyrite formation (Raiswell and Berner, 1986).

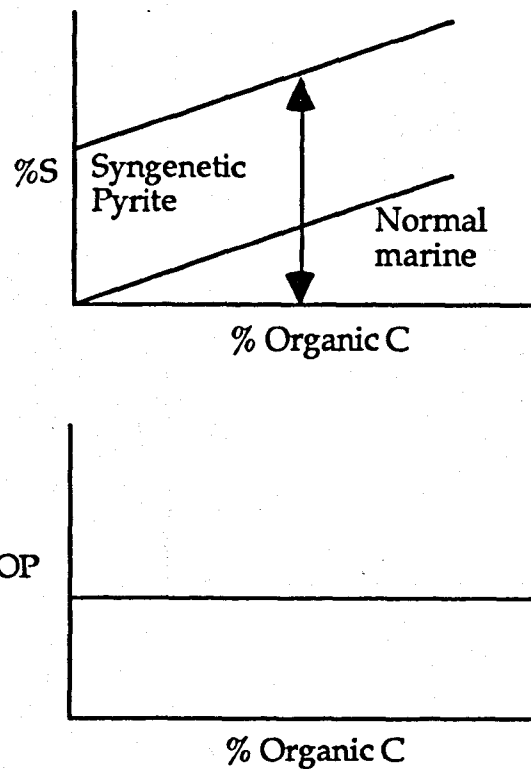
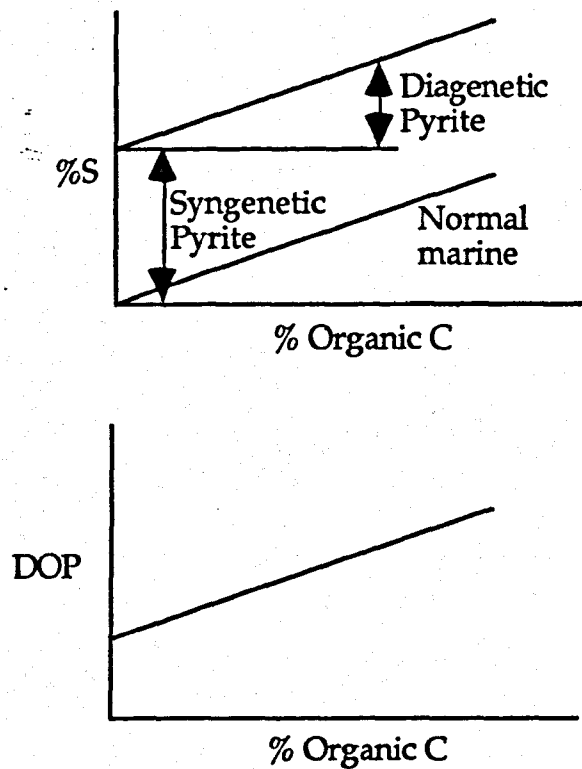
Raiswell and Berner (1987) have however noted several limitations of the C/S method as a palaeoenvironmental indicator:

1. Sediments must contain faunal or other evidence for deposition under normal marine conditions.

Figure 2.5

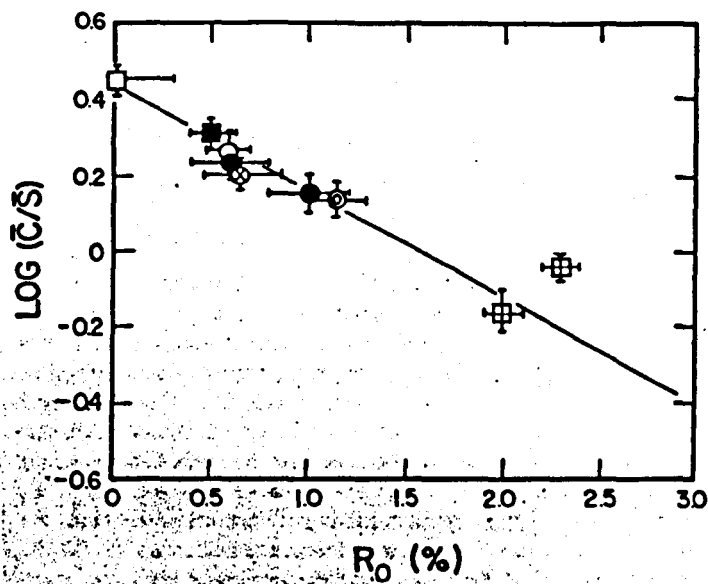
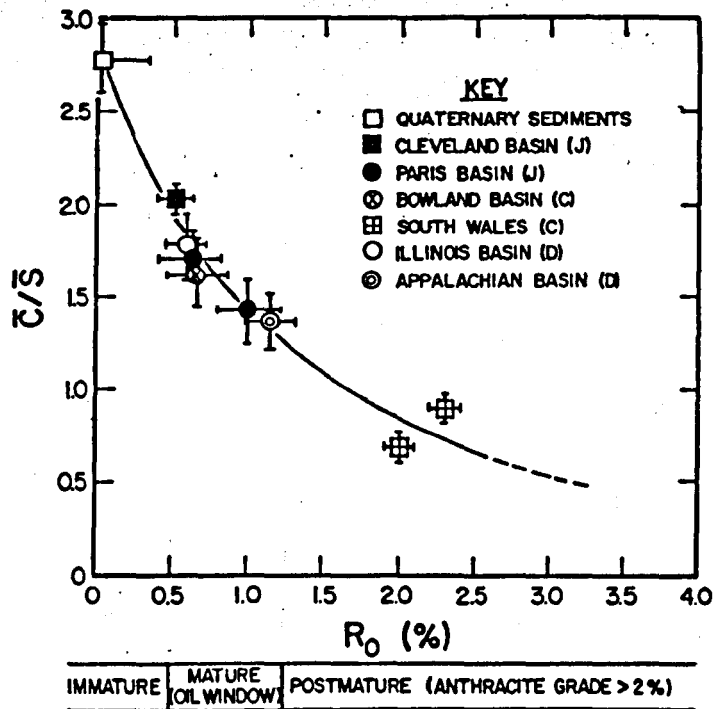
Euxinic Sediment

Iron Limited Sediment



Theoretical plots of C/S and DOP for euxinic sediments.

Figure 2.6



Plot of C/S versus vitrinite reflectance for normal marine shales.

2. Appreciable organic carbon must be present. Sediments low in organic carbon undergo such limited sulphate reduction and pyrite formation that they may contain significant proportions of non-pyrite sulphur.
3. Fresh outcrop or drill core material must be used to avoid the loss of pyrite sulphur by modern weathering.
4. Sediments should not be high in  $\text{CaCO}_3$  or biogenic silica such that iron availability would have been the limiting factor for pyrite formation.
5. No additions or losses of sulphide sulphur should have occurred prior to, and during maturation.
6. Evaporites or any rocks containing appreciable sulphate minerals should be avoided.
7. Sediments older than the Devonian should not be used because their initial C/S ratios may have been lower.

### 2.5.2 Degree of pyritisation

Berner (1970) defined the degree of pyritisation, DOP as:

$$\text{DOP} = \frac{\text{Pyritic iron}}{\text{Reactive iron}}$$

Reactive iron is the sum of the pyritic iron and the residual iron potentially reactive towards  $\text{H}_2\text{S}$ . Use of the DOP parameter enables the effects of variable reactive iron concentrations in euxinic environments to be removed. By considering the relationships between DOP and organic carbon, the C/S plots of euxinic sediments can be reinterpreted.

If all the reactive iron in a euxinic sediment has become pyritised during syngenetic formation, then iron is the limiting factor for pyrite formation. This will result in a constant DOP with increasing organic carbon content (Figure 2.5). In sediments where both diagenetic and syngenetic pyrite have formed then the degree of pyritisation will be positively correlated to organic carbon. This correlation is due to the addition of carbon limited diagenetic pyrite to syngenetic pyrite. Some euxinic sediments, e.g. Posidonia Shale, show evidence of no dependence of organic carbon on detrital iron. In such an environment the C/S plot will show constant high sulphur concentrations independent of organic carbon. The degree of pyritisation would also be independent of organic carbon.

Raiswell *et al.* (1988) have used DOP as a palaeoenvironmental indicator defining three types of environment (Table 2.4). A DOP value of 0.45 separates aerobic from restricted bottom waters. Environments with inhospitable bottom waters were found to have a degree of pyritisation in the range 0.55 to 0.93. There is some overlap between inhospitable and restricted bottom waters but a DOP 0.75 separates over 90% of the data.

Recent work (Canfield *et al.*, 1992; Raiswell *et al.*, 1994) suggests that DOP values are modified by iron mineral reactivity and exposure time to dissolved sulphide. Canfield *et al.* (1992) show that values of DOP cannot be used to demonstrate uniquely iron or sulphur limitation in pyrite formation. Low values of DOP would suggest that sulphide is limiting in pyrite formation. However, a situation can be envisaged where once the iron oxides (except magnetite) and oxyhydroxides have become pyritised, the remaining iron minerals are slow to react. Hydrogen sulphide will be lost from the sediment by diffusion as the rate of production greatly exceeds the rate of reaction with the remaining iron minerals. A situation where iron has become the limiting factor has now been established. Thus, pyrite formation will depend on the relative rates of sulphate reduction compared to rates of sulphide reaction with iron minerals of which DOP does not give any information.

Raiswell *et al.* (1994) have related values of the estimated half-lives of iron minerals (with respect to their sulphidation) to DOP. They conclude that DOP should be expressed with respect to rapidly reacting (half-lives <3.5 years) and slowly reacting (half-lives >84,000 years) iron pools established by preferential iron extraction techniques.

## 2.6 Stable isotopes

Elements with low atomic masses which have stable isotopes with a large proportional difference in mass, may show isotopic fractionation resulting from chemical processes within the geosphere. Oxygen, carbon and sulphur have such isotopes as shown in Table 2.5.

Fractionation of stable isotopes is a consequence of thermodynamic properties of isotopically different molecules. Hoefs (1980) and Thode (1991) describe the fractionation and the properties of 'isotopic molecules'. Isotopic fractionation may be divided into two main processes, equilibrium and kinetic fractionation.



**Table 2.5**

Element	Stable Isotopes and relative abundance	Isotopes Measured	Standard
O	$^{16}\text{O}$ $^{17}\text{O}$ $^{18}\text{O}$ 99.756 : 0.039 : 0.205	$^{16}\text{O}$ $^{18}\text{O}$	SMOW Standard Marine Ocean Water (or PDB)
C	$^{12}\text{C}$ $^{13}\text{C}$ 98.89 : 1.11	$^{12}\text{C}$ $^{13}\text{C}$	PDB Pee Dee Belemnite
S	$^{32}\text{S}$ $^{33}\text{S}$ $^{34}\text{S}$ $^{35}\text{S}$ 95.02 : 0.75 : 4.21 : 0.02	$^{32}\text{S}$ $^{34}\text{S}$	CDT Canon Diablo Troilite

Stable isotopes of oxygen, carbon and sulphur.

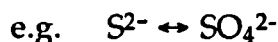
**Table 2.6**

Oxidising Agent	Fractionation	Reference
Sulphate	0 to -3.7‰	Orr(1974); Husain and Krouse (1979)
Oxygen	-5‰	Fry <i>et al.</i> (1986)
Aerobic bacteria	0 to +2‰	Fry <i>et al.</i> (1986)
Anaerobic bacteria	0 to -18 (?) ‰	Fry <i>et al.</i> (1986)

Fractionation resulting from the oxidation of sulphides to form elemental sulphur grouped by oxidising agent.

### 2.6.1 Equilibrium Fractionation

Lighter isotopes are more stable in a reduced form. Thus, when isotopic equilibrium is established between compounds of different oxidation states, light isotopes are preferentially fractionated into the more reduced species, and the heavier isotopes into the oxidised species,



At equilibrium, the  $S^{2-}$  will be  $^{32}S$  enriched and the  $SO_4^{2-}$  will be  $^{34}S$  enriched.

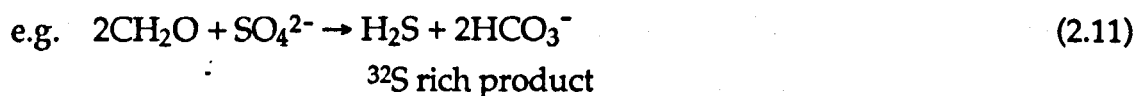
Electron transfer reactions rarely proceed with more than two electrons being transferred in any one step. Clearly a change from, for example, 2- in  $S^{2-}$  to +6 in  $SO_4^{2-}$  which would require the transfer of 8 electrons, will require several steps. In practice intermediates will play an important role in the overall fractionation. Since pH and Eh may affect the concentration of intermediate species, equilibrium may not always be established.

### 2.6.2 Kinetic Fractionation

The vibrational frequency of a molecule ( $\nu$ ) is a measure of the strength of the bonding within that molecule, such that

$$\nu \propto \text{mass}^{-1/2}$$

Thus, the lighter isotopes will have weaker bonds and therefore they will react faster.



This kinetic fractionation is unidirectional and is independent of oxidation or reduction.

Other physical processes in which a mass difference is important (e.g. diffusion due to temperature or concentration gradients, evaporation, melting and crystallisation) may also lead to fractionation.

### 2.6.3 Nomenclature

The separation between two isotopes of an element is expressed in terms of  $\alpha$ , the fractionation factor, defined as:

$$\alpha = \frac{R_A}{R_B}$$

where  $R_A$  is the ratio of heavy to light isotopes in phase A and,  $R_B$  is the ratio of heavy to light isotopes in phase B.

An alternative way of expressing fractionation is in terms of a measure relative to an arbitrary standard (Table 2.5) as  $\delta$  notation.

$$\delta_{\text{heavy}} \text{‰} = \left[ \frac{R_{\text{sample}} - R_{\text{standard}}}{R_{\text{standard}}} \right] \times 1000$$

Figure 2.7 shows how the components of a system change in  $\delta$  values during a reaction.

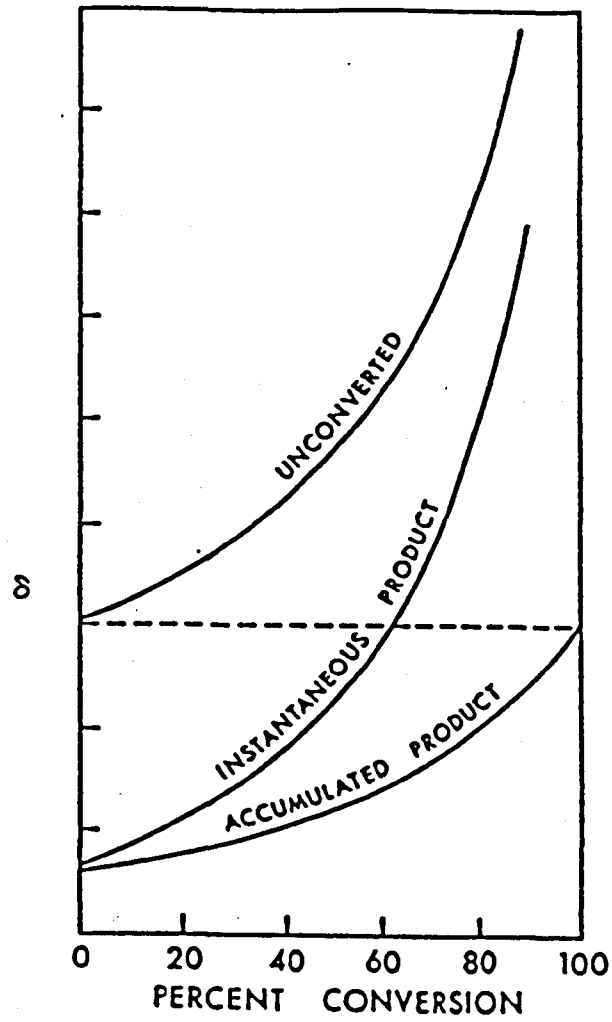
### 2.6.4 Carbonate Carbon

The common product of all microbially mediated diagenetic reactions is inorganic carbon as  $\text{CO}_2$  or  $\text{HCO}_3^-$ . Many studies (Curtis, 1977; Irwin et al., 1977; Coleman and Raiswell, 1981 and Scotchman, 1991b) have attempted to link the isotopic composition of the inorganic carbon species (preserved as biogenic carbonates) formed during microbially mediated organic matter oxidation to precursor source organic material. Table 2.2 and Figure 2.8 show the fractionation and isotopic composition of carbon associated with these processes.

### 2.6.5 Organic Carbon

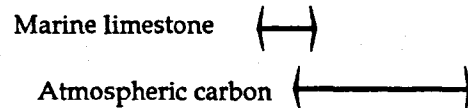
An extensive review of stable carbon isotopes (Feux, 1977) summarises the main features of the origin and migration of hydrocarbons in relation to their  $\delta^{13}\text{C}$  values. Ranges of the  $\delta^{13}\text{C}$  values of organic materials are shown in Figure 2.8. The  $\delta^{13}\text{C}$  of bitumen and kerogen lies within a similar range to the

Figure 2.7

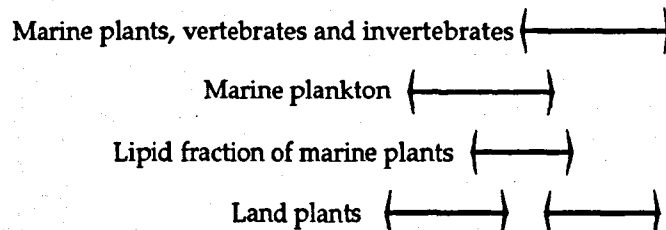


Changes in  $\delta^{34}\text{S}$  of reactant and product during closed system sulphate reduction.

### Inorganic carbon



### Carbon in living organisms



### Hydrocarbon source materials

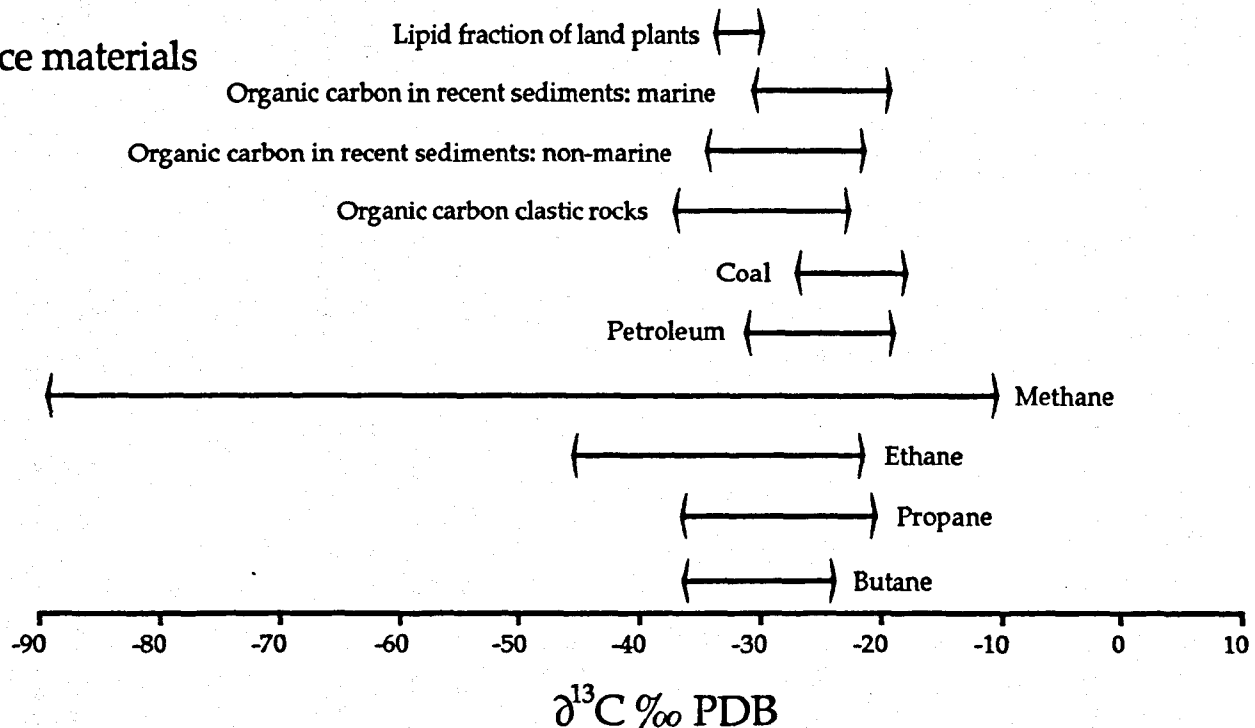


Figure 2.8

Isotopic variation in  $\delta^{13}\text{C}$  in organic and inorganic compounds. After Miles, 1989.

precursor source material, indicating that little net fractionation is caused by diagenetic and subsequent maturation and migration processes. Thus stable carbon isotopes may be useful in identifying oil-source correlations and migration effects where different sources are involved.

### 2.6.6 Carbonate Oxygen

Oxygen isotope ratios can be used as geothermometers. For low temperature systems, i.e. those within the diagenetic regime, there is an approximate relationship between temperature (T) and the fractionation factor ( $\alpha$ ) such that:

$$\ln \alpha \propto \frac{1}{T^2}$$

From this relationship, Clayton *et al.* (1966) used experimental data to derive an empirical relationship between calcite and water (the reservoirs of oxygen) expressed as:

$$10^3 \ln \alpha = [2.78(10^6 T^{-2})] - 2.89.$$

But,

$$10^3 \ln \alpha = \delta_A - \delta_B = \Delta_{A-B}.$$

This equation can be readily used to estimate the temperature of formation of calcite, given the isotopic composition of the cement and the formation water. The composition of the formation water is not always known directly as values may be changed by interactions with the sediment.

### 2.6.7 Sulphate Oxygen

The  $\delta^{18}\text{O}$  value of marine sulphate ions is +9.7‰ (Feux, 1977). Given the fractionation factor for isotope exchange between water and sulphate oxygen is 1.024 (Urey, 1947) or 1.0311 (Lloyd, 1968), it is evident that the oxygen is not in isotopic equilibrium. The oxygen incorporated into sulphate is lighter than the reservoir composition of oxygen, i.e. sulphate oxygen is enriched in  $^{16}\text{O}$ . Sulphate oxygen isotopes are considered in more detail in Chapter 6 where weathering is discussed.

## 2.6.8 Sulphur

Isotopic fractionation of sulphur during sulphate reduction arises due to biogenic fractionation induced by *Desulphovibrio* bacteria, as reviewed by Chambers and Trudinger (1978).

The fractionation factors in modern sediments are typically in the range of 1.030 to 1.050 (Chambers and Trudinger, 1978), but Goldhaber and Kaplan (1980) have reported values in the order of 1.060. Experimental values generally have a lower range, higher values are observed in sediments. Kaplan and Rittenburg (1964) have shown that the fractionation of sulphur depends on many factors including the rate of reduction, the nature and availability of organic matter, temperature and the size of the sulphate reservoir. However Chambers et al., (1976) suggested that no significant changes in fractionation occurred over the temperature range 35-55°C.

The supply of sulphate from the reservoir has an effect on the isotopic composition of the product and reservoir composition. In an open system,  $^{32}\text{S}$  is preferentially consumed resulting in a consistently light product. If the system should become closed, the re-supply of light sulphur is prevented and  $\text{H}_2\text{S}$  produced by sulphate reduction will become progressively heavier. Thus the  $\delta^{34}\text{S}$  of pyrite, for example, formed from bacterially derived  $\text{H}_2\text{S}$  may exceed the  $\delta^{34}\text{S}$  of the initial reservoir value of the sulphate (Hallberg, 1985; Thode, 1991).

Abiological sulphate reduction (thermogenic sulphate reduction, TSR), i.e. the direct reduction of sulphate by organic matter, also leads to a kinetic sulphur isotope effect. The fractionation of sulphur during TSR has been shown to be temperature dependant (Harrison and Thode, 1957; Husain and Krouse, 1978; Kiyosu, 1980; Kiyosu and Krouse, 1990). In the diagenetic temperature range, fractionation is in the order of 20‰, at 100°C it is 15‰ and above 200°C the fractionation is 10‰ (further decreasing with temperature). Kiyosu and Krouse (1990) have defined a kinetic sulphur isotope fractionation equation for TSR:

$$10^3 (\alpha - 1) = 3.32 \times 10^6 / T^2 - 4.91$$

However Orr (1982) shows that during the TSR in oils at temperatures between 80-120°C there is negligible net isotope fractionation. This is probably

due to the available sulphate being consumed completely and no kinetic isotope fractionation being preserved. Thermogenic sulphate reduction is characterised by isotopically heavy organo-sulphur compound formation (Powell and Macqueen, 1984).

The thermal decomposition of organo-sulphur compounds results in the release of H<sub>2</sub>S. The kinetic sulphur isotope fractionation is negligible, usually less than 2‰ (e.g. Krouse *et al.*, 1987); therefore the H<sub>2</sub>S released by thermal maturation will be isotopically similar to that of the source organic matter.

During the oxidation of sulphides into elemental sulphur, there is, in general, thought to be little or no fractionation. However some authors have reported significant fractionations between +2 and -5‰ (Table 2.6) depending on the oxidising agent used. Elemental sulphur produced by sulphide oxidation will therefore usually have an isotopic composition resembling that of the precursor sulphide.

It must be noted that if sulphate is the oxidising agent of sulphides, there will be an equilibrium effect in addition to any kinetic isotope effect. This will produce elemental sulphur with an isotopic signature dominated by the parent sulphide.

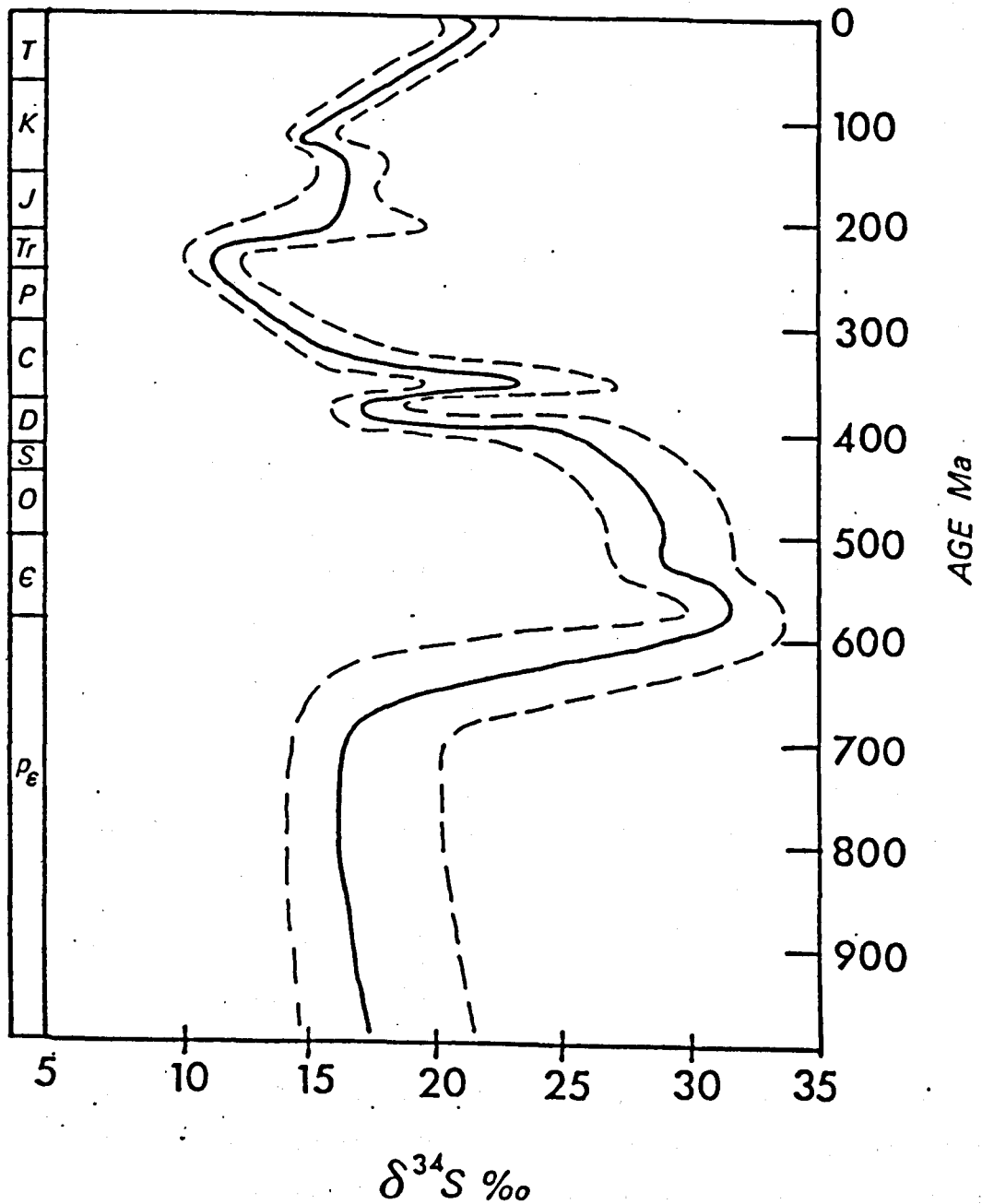
The isotopic exchange between H<sub>2</sub>S and S<sup>0</sup> has been experimentally determined by Tudge and Thode (1950) to be about +3‰ between 0 and 25°C, becoming almost zero at temperatures above 80°C. Such reactions are thought to occur when the two species are in prolonged contact and become more significant when the sulphur is in a reactive state e.g. liquid or dissolved in hydrocarbons and/or H<sub>2</sub>S.

The formation of sulphate either by oxidation of elemental sulphur (microbially or abiologically) or directly from sulphides has a very small associated isotopic fractionation (Nakai and Jensen, 1964; Claypool *et al.*, 1980; Fry *et al.*, 1986). Therefore sulphate derived from oxidative processes would have a sulphur isotope composition similar to the precursor reduced species.

Marine dissolved sulphate (with a concentration of ~28 mmol) is the dominant reservoir for sulphate available for sulphate reduction. The δ<sup>34</sup>S value for sulphur in modern marine waters is constant within narrow limits of +20.11 ± 0.4‰ (Rees *et al.*, 1978). This value has varied over geological time (Figure



Figure 2.9



Variation in  $\delta^{34}\text{S}$  composition of marine sulphate minerals throughout the Phanerozoic.  
After Haggerty, 1993.

2.9) as recorded by the isotopic compositions of evaporitic sulphates (Claypool *et al.*, 1980).

Sulphur bound to organic compounds occurs in kerogens, bitumens and crude oils (e.g. Krouse, 1977). The measured  $\delta^{34}\text{S}$  of an organic fraction is an averaged value of all the  $\delta^{34}\text{S}$  values for each organically bound sulphur atom in different chemical environments. Organosulphur compounds may occur as a result of primary assimilated sulphur or may have formed during later incorporation via sulphurising agents e.g.  $\text{H}_2\text{S}$ ,  $\text{HS}^-$ ,  $\text{H}_2\text{S}_n^{\text{x-}}$  and  $\text{S}^0$ .

Oil evolving from kerogen has almost the same sulphur isotopic composition as the source kerogen (Krouse, 1977) making  $\delta^{34}\text{S}$  measurements useful in source rock to oil correlation.

Bacterial sulphate reduction may lead to either enriched  $\delta^{34}\text{S}$  or depleted  $\delta^{34}\text{S}$  ratios. Bacteria may decompose sulphur bearing compounds, preferentially processing the  $^{32}\text{S}$ , thus enriching the residual compounds in  $^{34}\text{S}$ . Conversely organic sulphur compounds may be formed by bacteria. Enrichment or depletion of the  $\delta^{34}\text{S}$  values of the organo-sulphur compounds will depend on the isotopic composition of the dissolved sulphate, the microbial growth rate and the types of bacteria (Manowitz, 1990).

Thermogenic sulphate reduction is characterised by isotopically heavy organosulphur compound formation (Powell and Macqueen, 1984).

## 2.7 Radiogenic Isotopes

The Uranium-238, thorium-230 and potassium-40 decay series all have radioisotopes which can be measured by gamma ray spectrometry ( $^{40}\text{K}$  gamma rays;  $^{214}\text{Bi}$  gamma rays from the uranium series;  $^{208}\text{Tl}$  gamma rays from the Th series). It was first recognised by Adams and Weaver (1958) that marine shales are more radioactive than non-marine shales. Marine shales contain more uranium than shales deposited in non-marine environments (Bloxam and Thomas, 1969).

Primary uranium bearing minerals are oxidised to the uranyl ion ( $\text{UO}_2^{2+}$ ) which is relatively mobile in acidic solutions (and in neutral and alkaline environments where  $\text{CO}_3^{2-}$  is present; Langmuir, 1978). The uranium is later

fixed in sediments under reducing conditions as  $\text{UO}_2$  or an oxyhydroxide of  $\text{UO}_2$ .

Adams and Weaver (1958) used the redox chemistry of uranium as a palaeoenvironmental indicator to estimate bottom water anoxia. Thorium is relatively immobile relative to uranium, thus the ratio of the two elements will provide a measure of the bottom water oxygenation.

The crustal abundance of thorium and uranium were found to have a ratio of 3.5 (Adams *et al.*, 1959). A Th/U ratio of the detrital clay fraction in a study by Myers and Wignall (1987) is in the range 3 to 5. For organic rich mudrocks Myers and Wignall (1987) have used this ratio to estimate the authigenic uranium where:

$$U_{\text{authigenic}} = U_{\text{total}} - \frac{\text{Th}_{\text{total}}}{3}$$

assuming that all the Th is contained in the detrital component of the sediment.

## 2.8 Organic Geochemistry

Organic matter deposited in sediments is derived from biological material. Once an organism has died, the constituents (proteins, carbohydrates, lipids and lignin) will start to decompose. The amount and composition of the organic matter which is preserved in the sediment depends on the nature and extent of degradation of the primary material.

With increasing burial, continued physical and (bio)chemical reactions alter the nature of the organic matter. The temperature will increase, conditions will become more anhydrous and microbial activity will diminish. The organic compounds can be arbitrarily divided into two components; kerogen and bitumen. The bitumen fraction is soluble in common organic solvents and the kerogen is the insoluble residue.

### 2.8.1 Organic composition of living material

Living organisms fall into one of two categories, either terrestrial or aquatic. Terrestrial organic matter is derived from land plants and in general, higher

**Table 2.7**

Material	% Composition			
	Lipids	Proteins	Lignins	Carbohydrates
Phytoplankton	11	23	0	66
Zooplankton	10	60	0	22
Bacteria	20	60	0	20
Sphagnum moss	2	10	2	54
Sedge	3	12	5	47
Oak leaves	5	6	37	52
Lycopod spores	50	8	0	42

Average composition of a selection of biological material (Tissot and Welte, 1974)

**Table 2.8**

Material	% Weight				
	C	H	O	S	N
Carbohydrates	44	6	50	-	-
Lignin	63	5	32	0.1	0.3
Proteins	53	7	22	1	17
Lipids	76	12	12	-	-

The average elemental composition of the principal constituents of living organic matter (Tissot and Welte, 1974).

plants are rich in lignins and low in lipids. However seeds, pollen and leaf waxes contain large quantities of lipids (Table 2.7 and Table 2.8).

### 2.8.2 Isomers in organic geochemistry

Organic compounds must be regarded as three dimensional structures. As such the relative positions of atoms or functional groups about a particular carbon atom may affect the chemistry of the whole compound. When there are several different structures which can be produced from a given molecular formula, each structure is known as an isomer.

Structural isomerism arises where there is a positional difference of one of constituent groups, e.g. n-propanol and iso-propanol. If four different functional groups are arranged about a carbon atom, then there is the potential for optical isomerism. The carbon atom is known as the chiral centre. Some compounds with chiral centres are able to rotate polarised light. The Cahn-Ingold-Prelog system is used to indicate the absolute configuration of the groups around a chiral carbon. R is assigned to a compound which produces a clockwise rotation of polarised light and L for an anticlockwise rotation.

Geometrical isomerism is a form of optical isomerism. In a molecule with double bonds (strictly pi-bonds), groups are not free to rotate about the double bond. Groups at the same side of the double bond are known as cis and groups on opposite sides trans. Another way of writing this form is to use  $\alpha$  and  $\beta$  notation. In two dimensions  $\alpha$  can be regarded as projecting into the plane of the paper and  $\beta$  out of the paper. Thus  $\alpha\alpha$  and  $\beta\beta$  are cis isomers and  $\alpha\beta$  and  $\beta\alpha$  are trans isomers.

## 2.9 Bitumen

Within the bitumen fraction, individual compounds can be identified which closely resemble compounds (or large fragments of compounds) found in natural products. Such compounds are known as geochemical fossils or biomarkers (Seifert and Moldowan, 1981). For example, porphyrins and the isoprenoids pristane and phytane are thought to derive from the chlorophyll molecule (Treibs, 1934 and Blumer *et al.* (1964). The carbon skeleton of

biomarkers remains unchanged during diagenesis, however, functional groups may be altered or lost with carbon-carbon bonds being broken or formed.

Four main groups of organic compounds were studied during this work; the alkanes, hopanes, steranes and organo-sulphur compounds.

### 2.9.1 Normal Alkanes

Normal (or n-) alkanes comprise of straight chains of carbon atoms either saturated or unsaturated (containing carbon-carbon double or triple bonds). Brassell *et al.* (1980) summarises the main sources of n-alkanes as shown in Table 2.9. The n-alkanes derived from terrestrial higher plants show a strong predominance of the odd carbon numbers to the even carbon numbers. Bray and Evans (1961) developed the Carbon Preference Index (CPI) as a measure of the odd/even predominance of the n-alkanes in the range from C<sub>24</sub> to C<sub>34</sub>.

$$\text{Where, } \text{CPI} = \frac{1}{2} \left[ \frac{\text{C}_{25} + \text{C}_{27} + \text{C}_{29} + \text{C}_{31} + \text{C}_{33}}{\text{C}_{24} + \text{C}_{26} + \text{C}_{28} + \text{C}_{30} + \text{C}_{32}} + \frac{\text{C}_{25} + \text{C}_{27} + \text{C}_{29} + \text{C}_{31} + \text{C}_{33}}{\text{C}_{26} + \text{C}_{28} + \text{C}_{30} + \text{C}_{32} + \text{C}_{34}} \right]$$

As the maturity increases, the CPI decreases until the amounts of odd and even alkanes becomes equal (CPI=1). The CPI may also be affected by bacterial activity (Tissot and Welte, 1984) which preferentially degrades the odd numbered alkanes. Hence the CPI can be used as a maturity parameter (Table 2.10). Welte and Walples (1973) have identified some sequences where there is a dominance of even alkanes in areas of terrestrial input. They suggest that because of prevalent anaerobic conditions, reduction reactions are of more importance than decarboxylation reactions, hence the end products may have an additional carbon atom. Clearly care must be taken when applying the CPI as a maturation parameter.

### 2.9.2 Branched alkanes

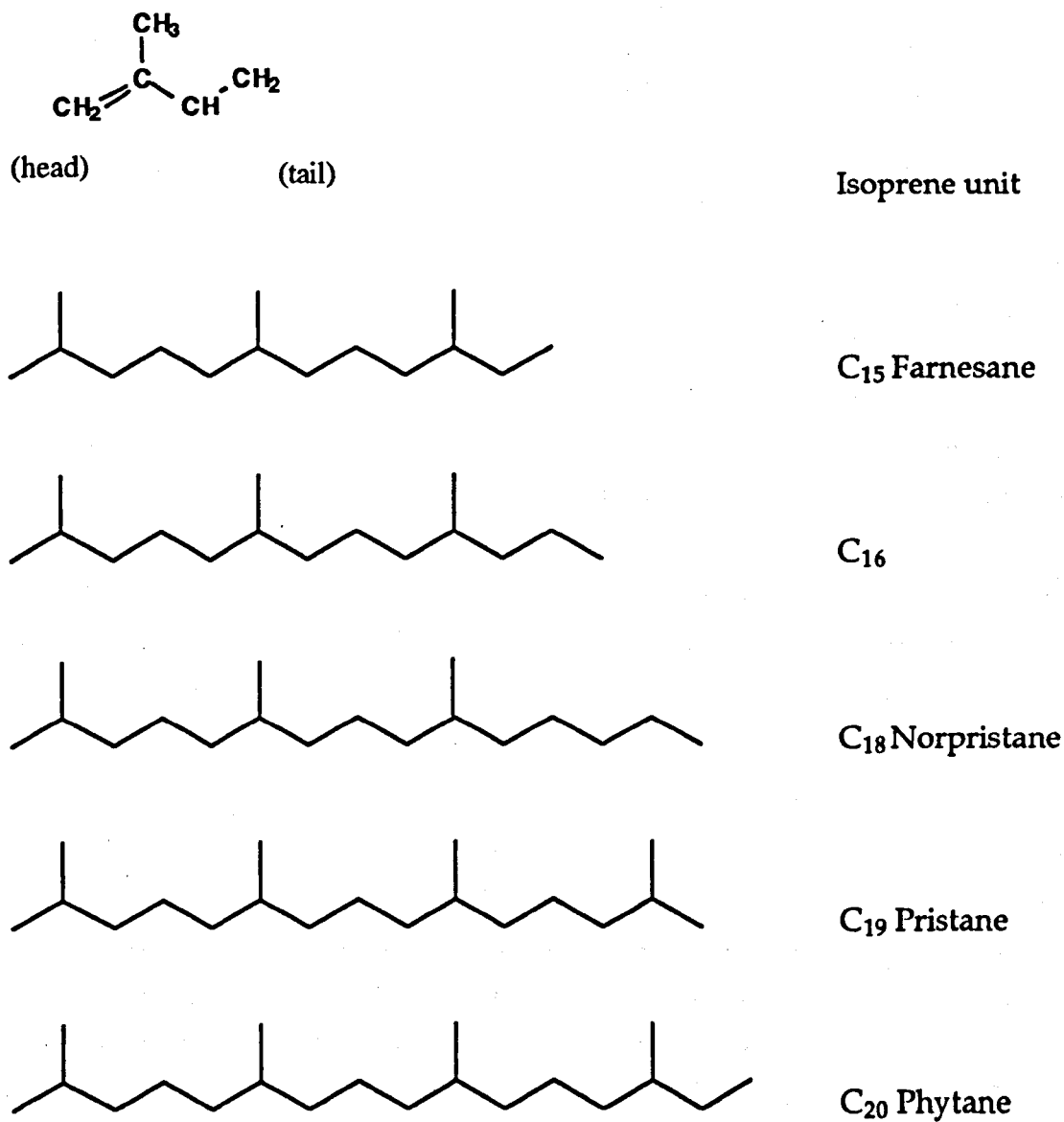
The most common type of branched alkanes in ancient sediments are generally, the regular alicyclic isoprenoids (Figure 2.10), which contain chains of the isoprene unit (Figure 2.10) linked 'head to tail' (Tissot and Welte, 1984). The most common source of pristane (Pr) and phytane (Ph) is thought to be via phytol derived from the side chain of the chlorophyll molecule. The relative

**Table 2.9**

Source	Carbon number range	Dominant carbon number
Bacteria	14 → 29	17, 25, 26
Fungi	25 → 29	29
Algae	13 → 26	17, 23 → 29
Land Plants	15 → 37	27, 29, 31

The main sources of n-alkanes from living material.  
After Brassel *et al.* (1978).

Figure 2.10



Dominant molecules of regular isoprenoids found in ancient sediments.



amount of pristane and phytane formed is thought to be controlled by the redox conditions at the time of deposition and early diagenesis (Didyk *et al.*, 1978). Figure 2.11 summarises the transformation of chlorophyll derived phytol into pristane and phytane. In oxic conditions, phytol undergoes decarboxylation reactions (with the loss of 1 carbon atom) to form pristane whereas in reducing conditions phytol is reduced to phytane.

However, more recent work by ten Haven *et al.* (1987) and ten Haven and Rullkötter (1988) suggests alternative sources for pristane and phytane, e.g. tocopherol (algal) and zooplankton form pristane and archaeobacteria form phytane. The Pr/Ph ratio has also been found to change due to maturation effects (increasing with maturation).

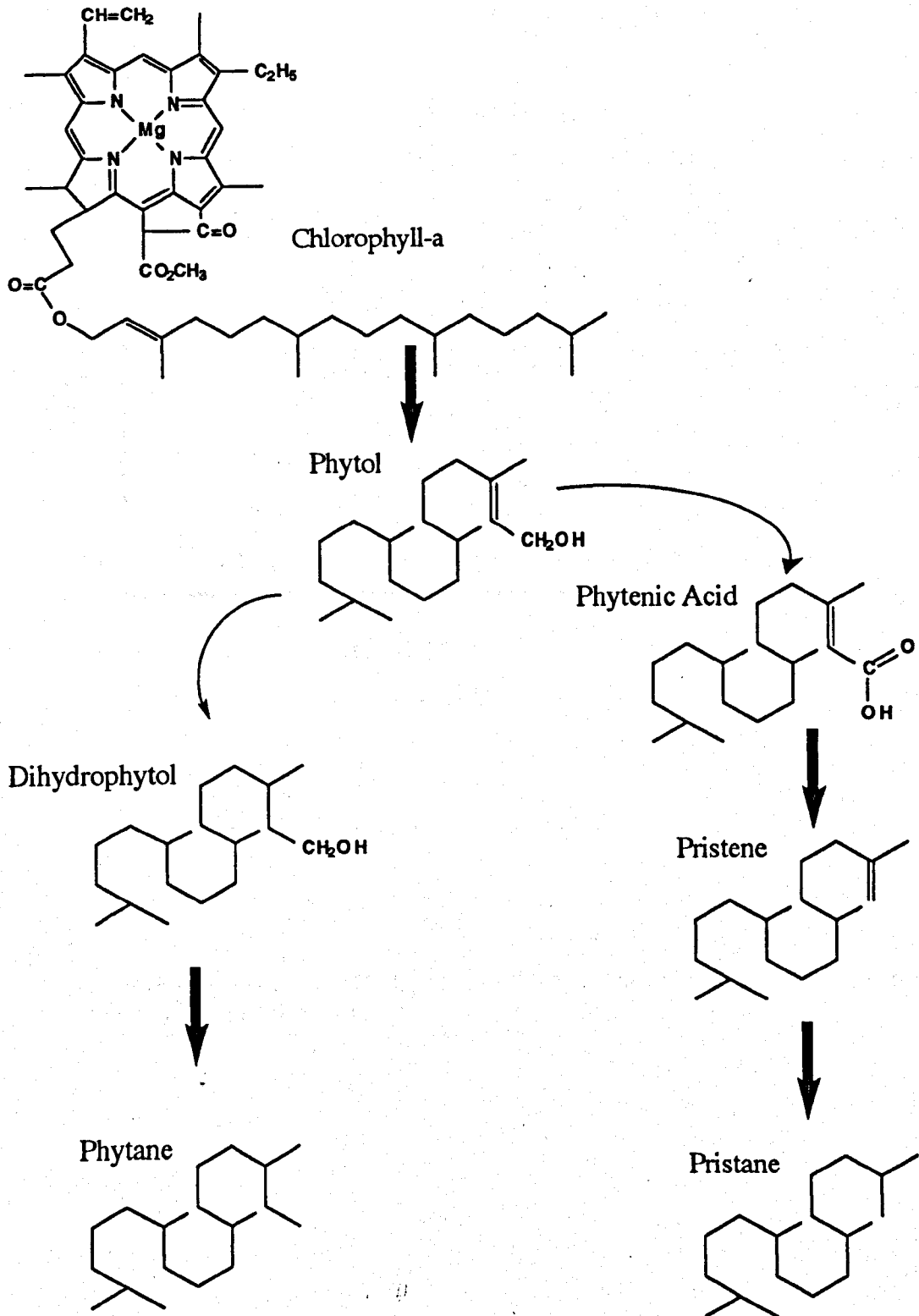
N-alkanes are more readily metabolisable and are therefore more prone to biodegradation. A plot of Pr against n-C17 will indicate the Eh conditions during early diagenesis and the maturity of the sediment (Leythaeuser and Schwarzkopf, 1986). By incorporating the ratio Ph/n-C18 (Figure 2.12) the environment of deposition may be established given the limitations of using alkane biomarkers.

### 2.9.3 Hopanes

The hopanes (members of the C<sub>27</sub> to C<sub>35</sub> group of compounds) are thought to be principally derived from bacteria (Ousisson, 1979). In immature sediments, the hopanes have a 17 $\beta$ (H),21 $\beta$ (H) configuration. With increased maturity, isomerism to the 17 $\alpha$ (H),21 $\beta$ (H) and the 17 $\beta$ (H),21 $\alpha$ (H) occurs. Hopanes with carbon numbers >C<sub>31</sub>, are thought to have an S:R ratio of 60:40 (the ratio of the S and R optical isomers, Seifert and Moldowan, 1980). With increasing maturity, the biologically imposed 22R configuration is replaced by the 22S configuration. The diagnostic ion for hopanes is m/z=191 (Figure 2.13).

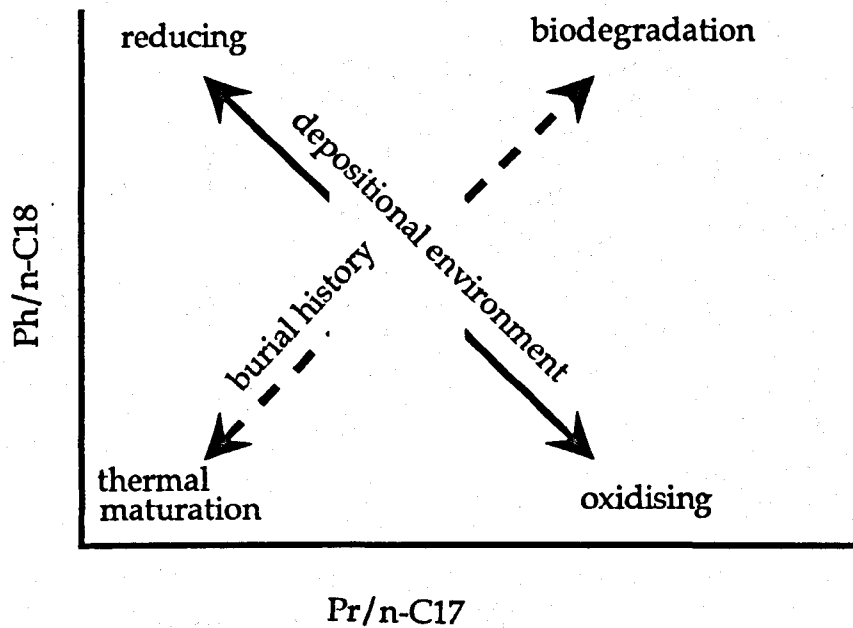
In biodegraded oils, the C<sub>25</sub> carbon attached to the C<sub>10</sub> carbon is removed (Figure 2.14). Thus the presence of demethylated hopanes indicate the intense biodegradation of the hopanes (Volkman *et al.*, 1983).

Figure 2.11



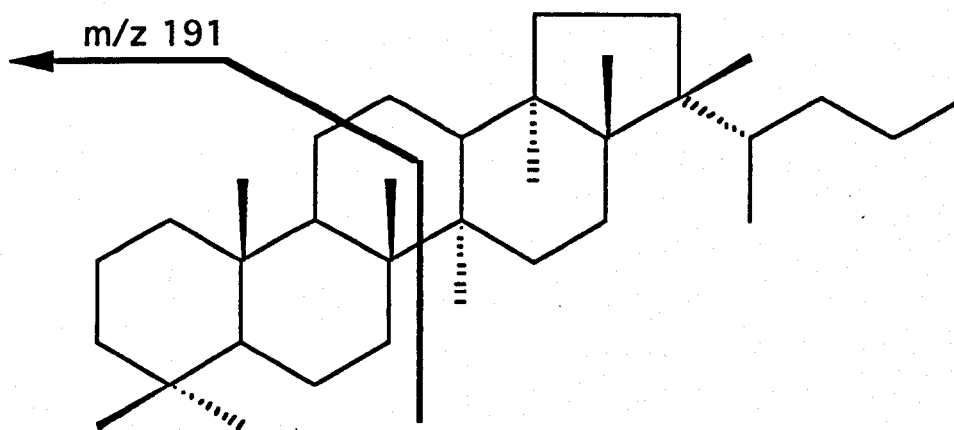
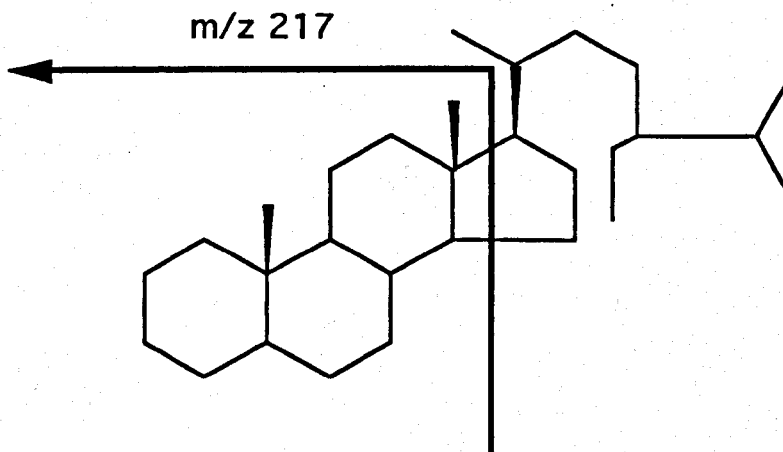
The transformation of chlorophyll derived phytol into pristane ( $\text{C}_{19}$ ) and phytane ( $\text{C}_{20}$ ).

Figure 2.12



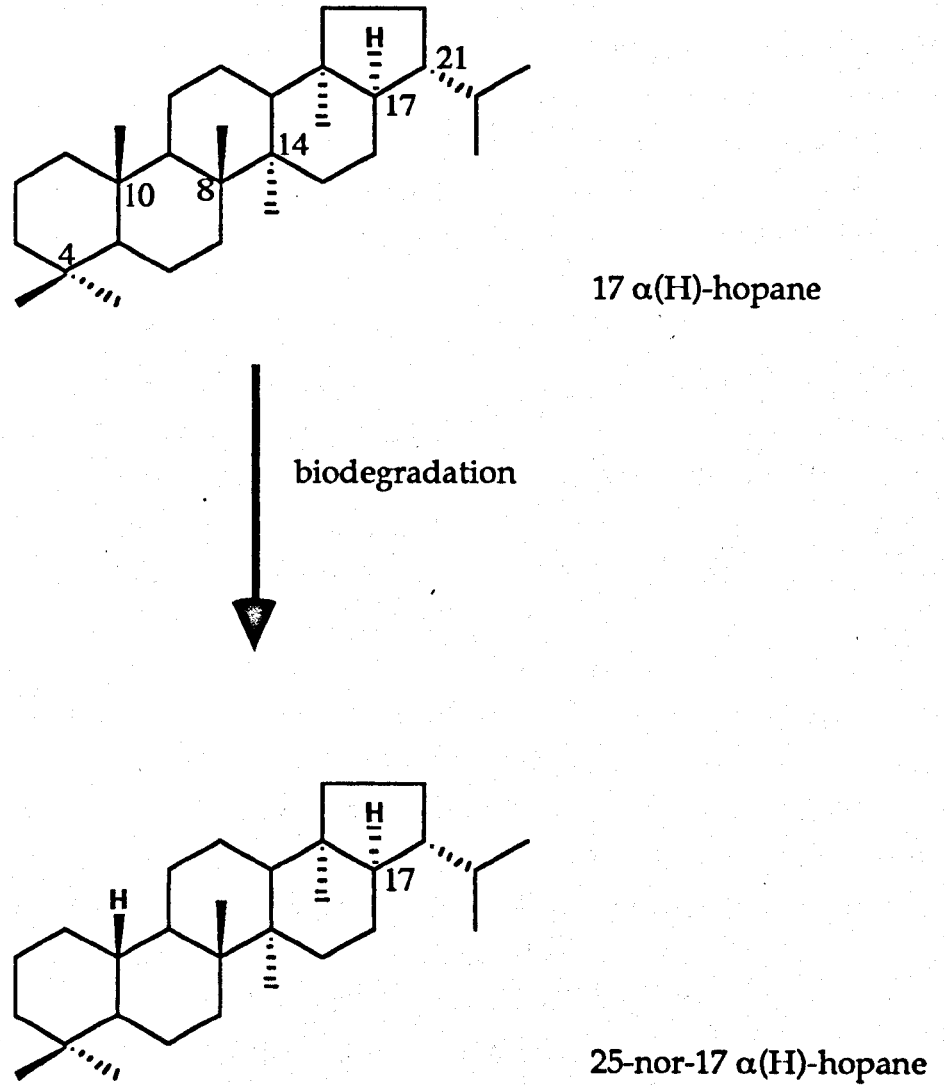
Pristane/heptadecane against phytane/octadecane used as a maturation and palaeoenvironmental indicator.

Figure 2.13

Hopane/MoretaneRegular Sterane

Structure of hopane and sterane biomarkers with their dominant  $m/z$  fragments.

Figure 2.14



Demethylation of 17  $\alpha$ (H)-hopane by biodegradation.

### 2.9.4 Steranes

Steranes are not found in any living biological material, however the precursor materials i.e. sterols, stenols, stanols, stannones and stenones, occur widely in living material, although they are rarely found in young sediments. Steranes are derived from sterols via sterenes and steradienes, e.g. Mackenzie (1984) and de Leeuw and Baas (1986). Steranes are comprised of six isoprene units which have been polymerised and have undergone cyclisation (Tissot and Welte, 1984).

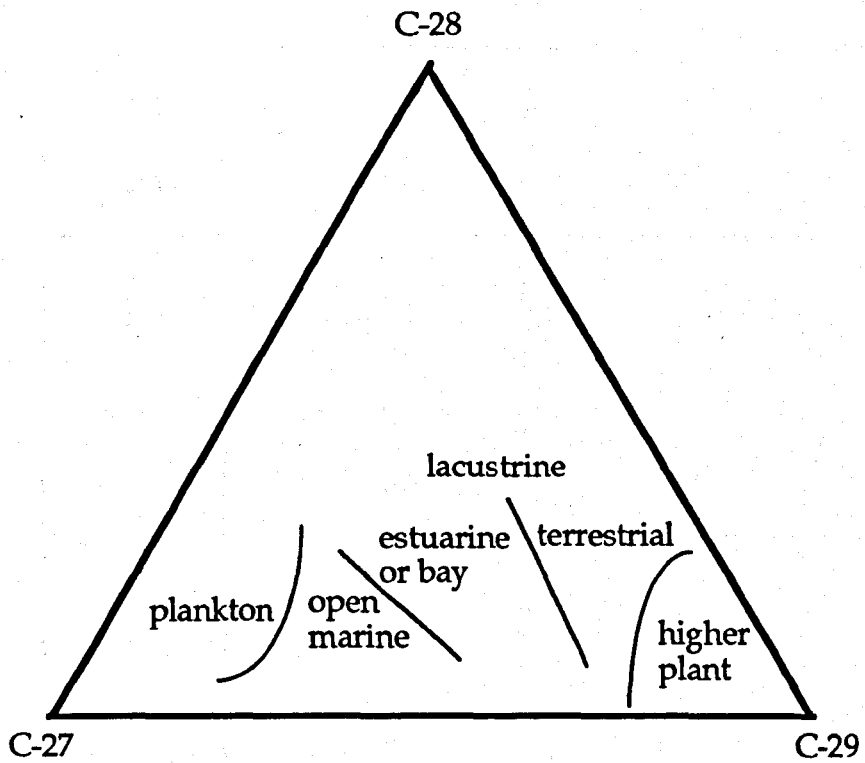
Huang and Meinschein (1979) used the ratios of the C<sub>27</sub>, C<sub>28</sub> and C<sub>29</sub> sterols as a palaeoenvironmental indicator (Figure 2.15). C<sub>27</sub> sterols are most abundant in marine organic matter. Higher land plants are dominated by C<sub>29</sub> sterols. The C<sub>30</sub> sterols are found only in marine organic matter. However studies by Volkman (1986) and Grantham and Wakefield (1988) have shown C<sub>29</sub> sterols derived from some marine organisms.

Sterols have 8 $\beta$ (H),9 $\alpha$ (H),10 $\beta$ (H),14 $\alpha$ (H),17 $\alpha$ (H) 20R stereochemistry. With increasing maturity, changes occur at the 5, 13, 17 and 20 positions (Mackenzie *et al.*, 1982). At equilibrium, there is a mixture of both the 5 $\alpha$ (H),14 $\alpha$ (H),17 $\alpha$ (H) 20S and 20R isomers and the 5 $\alpha$ (H),14 $\beta$ (H),17 $\beta$ (H) 20S and 20R isomers in a ratio of 1:1:3:3 (Mackenzie, 1984) (Figure 2.16). The maturity parameters based on Steranes are summarised in Table 2.10. Biodegradation removes C<sub>20</sub>R compounds faster than the C<sub>20</sub>S analogues, with the C<sub>27</sub> being removed faster than the C<sub>28</sub> or the C<sub>29</sub> steranes (Mackenzie *et al.*, 1982).

## 2.10 Kerogen

Kerogen, the organic fraction of a sediment which is insoluble in both common organic solvents and mineral acids (Durand, 1980), is the most abundant form of organic carbon in the crust of the earth. Humins, the precursor of kerogen contains a significant hydrolysable fraction which decreases with increasing burial.

Figure 2.15



Relationship between sterol composition and depositional environment.

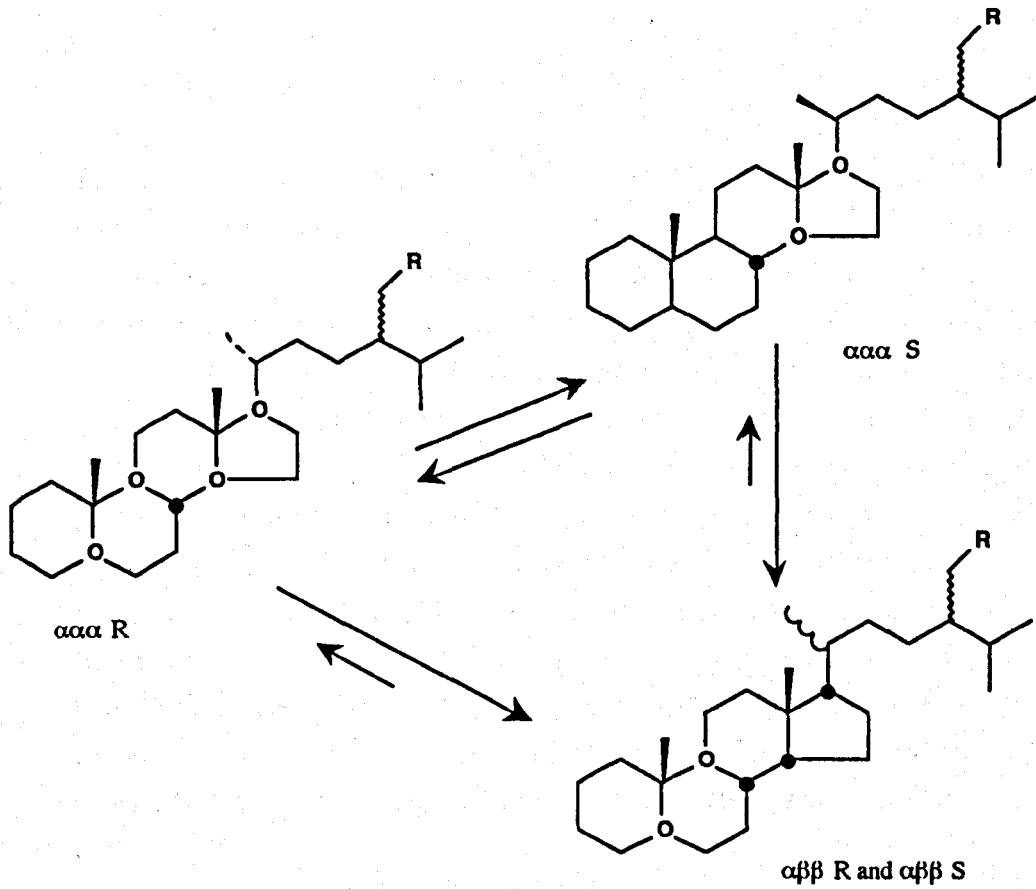
Table 2.10

MATURITY	Vitrinite Reflectance % R <sub>o</sub>	Spore Colour Index (SCI)	Carbon Preference Index (CPI)	T max (°C)		H/C ratio		Biomarker Ratios	
				Kerogen I	Type II	Kerogen I	Type II	Hopane 22S/22R	Sterane 20S/20R
Immature	<0.5	1.0-3.5	>1.5	<435 ± 10	<427 ±10	1.6	1.2	0.4	0.25
Early mature	0.5 - 0.65	3.5 - 5.0	1.5 - 1.2	435 - 444 ± 10	427 - 435 ± 10	1.6 - 1.45	1.2 - 1.1	0.4 - 0.6	0.25-0.35
Peak mature	0.65 - 0.9	5.0 - 7.0	1.2 - 1.0	444 - 455 ± 10	435 - 442 ± 10	1.45 - 1.0	1.1 - 0.9	> 0.6	0.35 - 0.5
Late mature	0.9 - 1.3	7.0 - 8.5	1.0	>455	>442	1.0 - 0.8	0.9 - 0.8	-	>0.5
Post mature	>1.3	8.5 - 10	1.0	-	-	0.8 - 0.5	0.8 - 0.5	-	-

A comparison of maturity parameters for oil prone source rocks.



Figure 2.16



The maturity related isomerisation of 5 $\alpha$ (H), 14 $\alpha$ (H), 17 $\alpha$ (H) 20R C<sub>29</sub> sterane.  
After Mackenzie, 1984.

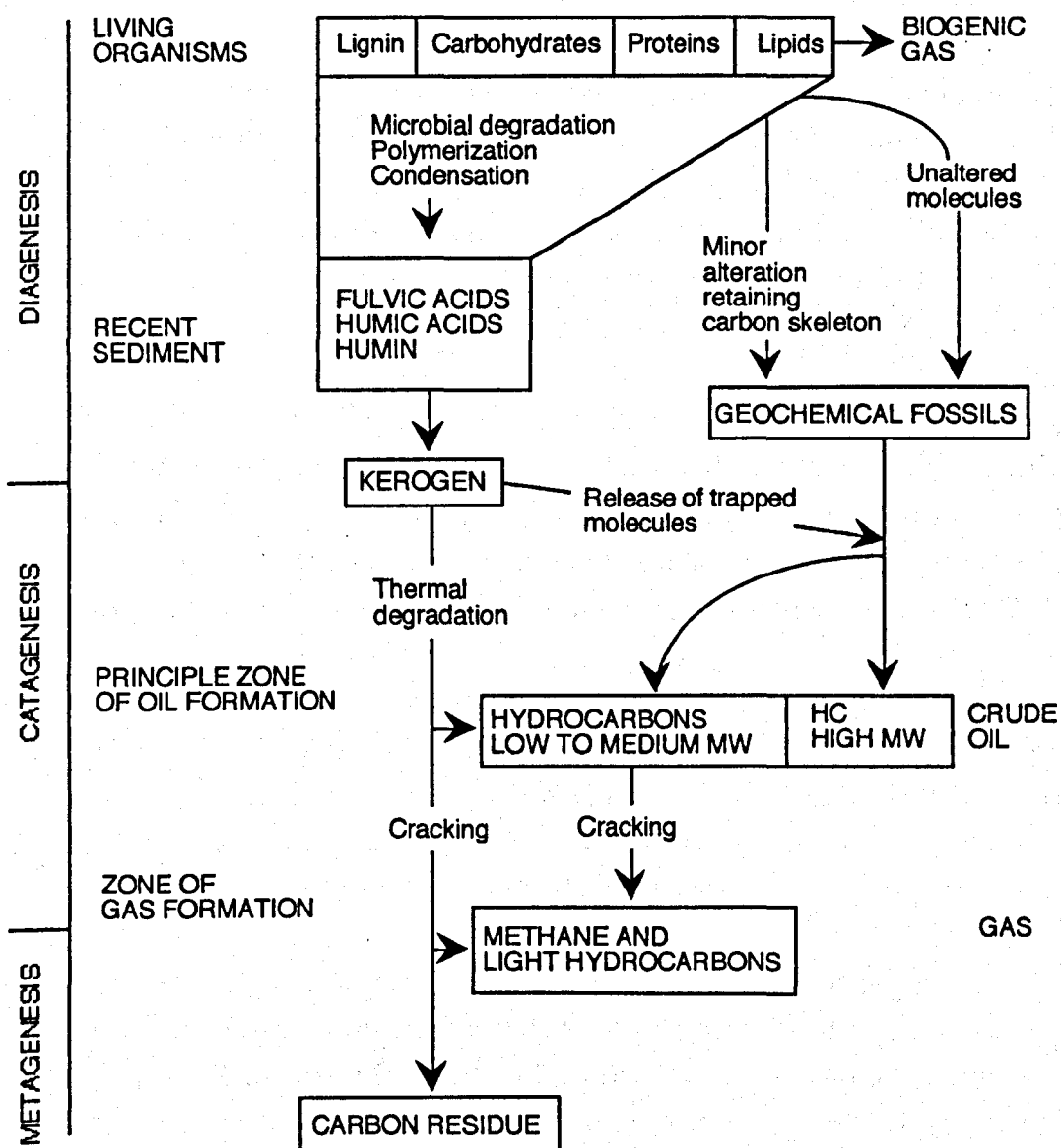
### 2.10.1 Origin of kerogen

Organic matter deposited in environments which have a high sedimentation rate and are anoxic will have the greatest potential for preservation. This sedimentary organic matter undergoes a series of chemical and physical changes to form kerogen and hydrocarbon products. This takes place in three steps; diagenesis, catagenesis and metagenesis (Figure 2.17).

The mechanisms of formation of kerogen from precursor sedimentary organic matter are uncertain. Huc (1980) has proposed a mechanism by which the biological macropolymers are broken down into lower molecular weight components, possibly their monomers (phenols, amino acids etc.). These functionalised units then recombine to form random structures linked via heteroatomic and carbon-carbon bonds. An alternative hypothesis for the formation of kerogen is summarised by Tegelaar (1989), who suggests that kerogen results from the selective preservation of resistant biomacromolecules. Largeau *et al.* (1984,1986) and Nip *et al.* (1986, 1989) have observed such highly resistant insoluble and non-hydrolysable macromolecular structures in a variety of organisms. It seems likely that both microbial depolymerisation of biopolymeric material (followed by polymerisation to create geopolymeric kerogen) and selective preservation of resistant biomacromolecules may be involved in kerogen formation.

The resulting immature kerogen has a three dimensional macromolecular structure made up of 2-4 sub-parallel aromatic sheets consisting of about 10 aromatic rings and short alkyl chains (Tissot and Welte, 1984). As kerogen becomes buried, the spacing between the aromatic sheets decreases and structural organisation increases (Behar and Vandenbroucke, 1986). Low molecular weight compounds may become trapped within the kerogen structure (Yen, 1974). Behar and Vandenbroucke (1986, 1988) have studied the thermal maturation of various types of kerogen with respect to their structure. However, as Rullkötter and Michaelis (1990) have noted, some of the structural interpretation inferred by Behar and Vandenbroucke (1986, 1988) is unsupported by analytical data and should therefore be treated with care.

Figure 2.17



Organic matter transformations during burial.

### 2.10.2 Types of kerogen

The chemical composition of kerogens will vary depending upon their origin. Welte (1969) and Durand *et al.* (1972) applied the chemical studies of coals by van Krevelen (1961) to characterise the thermal evolution of the kerogens. Atomic ratios of H/C and O/C plotted as a van Krevelen diagram (Figure 2.18) show the three main kerogen types. On increasing maturation, the H/C and O/C ratios decrease until eventually all kerogen types become graphitic with no further hydrocarbon generating potential (Figure 2.19). This change is ascribed mainly to the elevated temperatures associated with increasing burial depths (Katz, 1983).

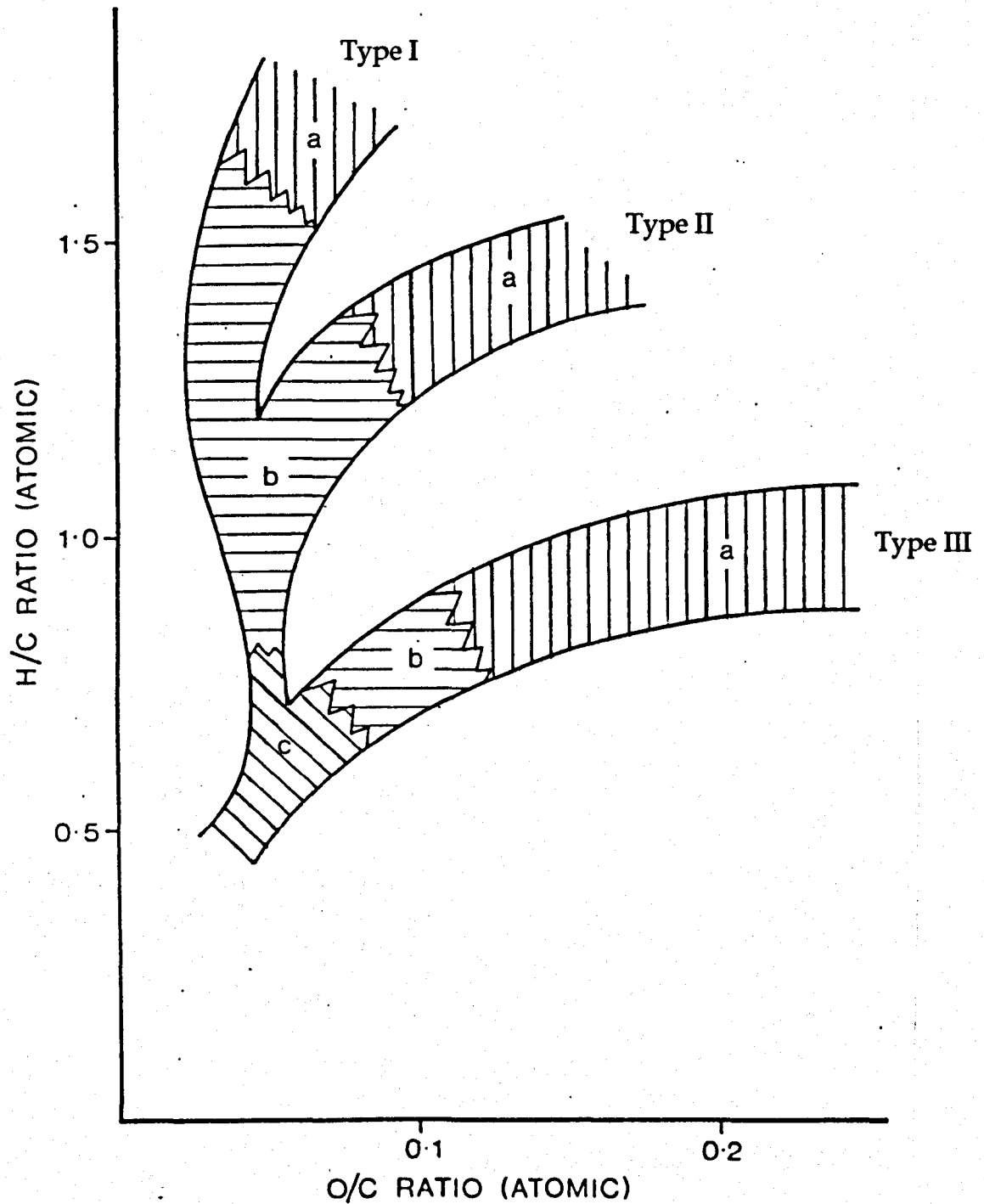
Type I kerogens (Figure 2.19) are initially hydrogen rich and oxygen poor being dominated by aliphatic compounds with n-alkanes more abundant than cyclic alkanes. Type I kerogens are principally derived from algal material (Derenne *et al.*, 1988). Microbiological attack on sedimentary organic matter also yields Type I kerogen. It is the chemical equivalent of alganite (Table 2.11).

Type II kerogens (Figure 19) are the most common kerogen type (Tissot and Welte, 1984). They are also hydrogen rich and are relatively oxygen poor, with fewer linear aliphatic compounds and more alicyclic and naphthenic compounds (Miles, 1989). Type II kerogens are formed from marine derived organic matter, typically phytoplankton and bacteria.

Type III kerogens (Figure 19) have low H/C ratios and generally high O/C ratios and are dominated by polyaromatic nuclei derived from higher plant material. The aromatic nature of this type of kerogen reduces the oil generating potential but it will generate gas at the appropriate maturity.

In addition to the three principle kerogen types, a fourth type of kerogen has been defined. It has characteristically high O/C ratios and extremely low H/C ratios. Aromatic nuclei dominate the structure with an almost complete absence of an aliphatic component (Zilm *et al.*, 1981). Type IV kerogen is formed from highly oxidised or reworked organic matter (Cope, 1980).

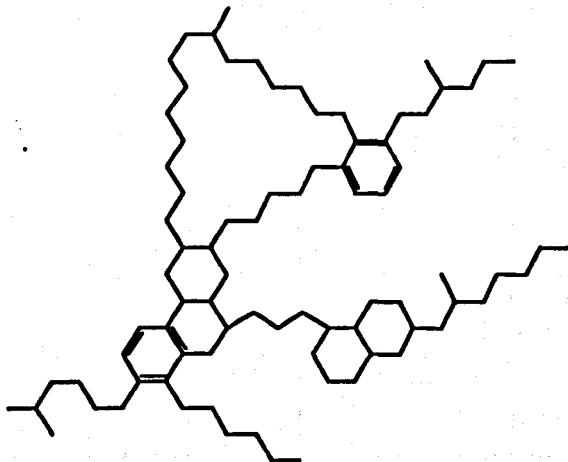
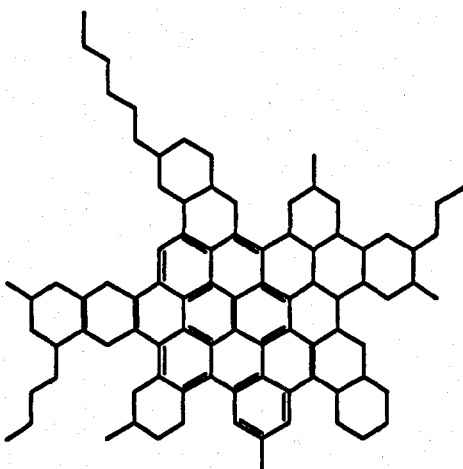
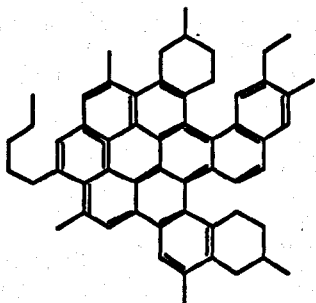
Figure 2.18



- a.  $\text{CO}_2$ ;  $\text{H}_2\text{O}$ , heavy heteroatomic compounds
- b. OIL
- c. GAS

Van Krevelen diagram showing kerogen types based on their O/C and H/C ratios and their principle products during thermal evolution.  
After Tissot and Welte, 1984.

Figure 2.19

Type I KerogenType II KerogenType III Kerogen

Structure of Type I, II and III Kerogens.

**Table 2.11**

Algal	Liptinite or	Alganite	Sapropel Bituminite Resinite Amorphite L	Algal sapropel	Type I Kerogen
Herbaceous stem	Exinite	Sporinite Cutinite Suberinite Liptodendrite		Amorphous	Waxy sapropel
Woody	Vitrinite	Vitrinite  Amorphinite V	Telinite Vitrodetrinite Collinite		Humic
Coaly	Inertinite	Inertinite	Semifusinite Fusinite Pyrofusinite Inertodendrinite Macrinite Micrinite	Humic	Type IV Kerogen

Correlation of kerogen type nomenclature.  
After Miles, 1989.

## 2.11 Maturity indicators

Organic matter changes in its physical and chemical properties during diagenesis, catagenesis and metagenesis, hence careful examination of the kerogen and hydrocarbons (bitumen, oil and gas), may allow the level of maturity to be determined. The Level of Organic Metamorphism (LOM; Hood *et al.*, 1975) can be derived by comparing various techniques for thermal maturity measurement.

Maturity indicators can be divided into two broad categories; those which measure physical properties such as fluorescence and reflectance of light, and those which use chemical analyses (H/C and O/C) of bulk phases together with more detailed analyses of individual compounds or classes of compounds e.g. CPI, Pr/n-C<sub>17</sub> and sterane ratios. Tissot and Welte (1978) summarise these techniques. A comparison of the parameters used in this study is given in Table 2.10.

## 2.12 Organically Bound Sulphur

Sinninghe Damsté and DeLeeuw (1989) have reviewed the structure and geochemical significance of organically bound sulphur (OBS) in the geosphere. A more specific review (Sinninghe Damsté and DeLeeuw, 1992) of organically bound sulphur in coal summarises the present state of understanding of OBS.

The organic sulphur content of kerogen (the dominant form of organic matter in sediments and sedimentary rocks) varies with type and evolution (Durand and Monin, 1980); Tissot and Welte, 1984). Kerogen Types I and III are generally low in OBS whilst Type II kerogen in marine sediments contains the highest amount of sulphur. A sub classification of Type II-S has been proposed by Orr (1986) for kerogens having an atomic S/C ratio of greater than 0.04. The high sulphur contents of marine derived kerogen and the structures of the OSC (which are very different from those biosynthesised sulphur compounds) cannot be explained simply by the assimilation of sulphur into amino acids either photosynthetically or chemosynthetically (Goldhaber and Kaplan, 1974).

Hydrogen sulphide (formed as a result of microbially mediated sulphate reduction) or partially oxidised products (polysulphides and elemental sulphur)



have been suggested to form organically bound sulphur compounds (Nissenbaum and Kaplan, 1972; Gransch and Posthuma, 1974; Dinur *et al.*, 1980; Aizenshtat *et al.*, 1983; Tissot and Welte, 1984; François, 1987; Vairavamurthy and Mopper, 1987; Sinninghe Damsté *et al.*, 1989a,c; Kohnen *et al.*, 1989; Suzuki and Philp, 1990; Kohnen *et al.*, 1990; Kohnen *et al.*, 1991a,b; Sinninghe Damsté, and Rijpstra, 1993).

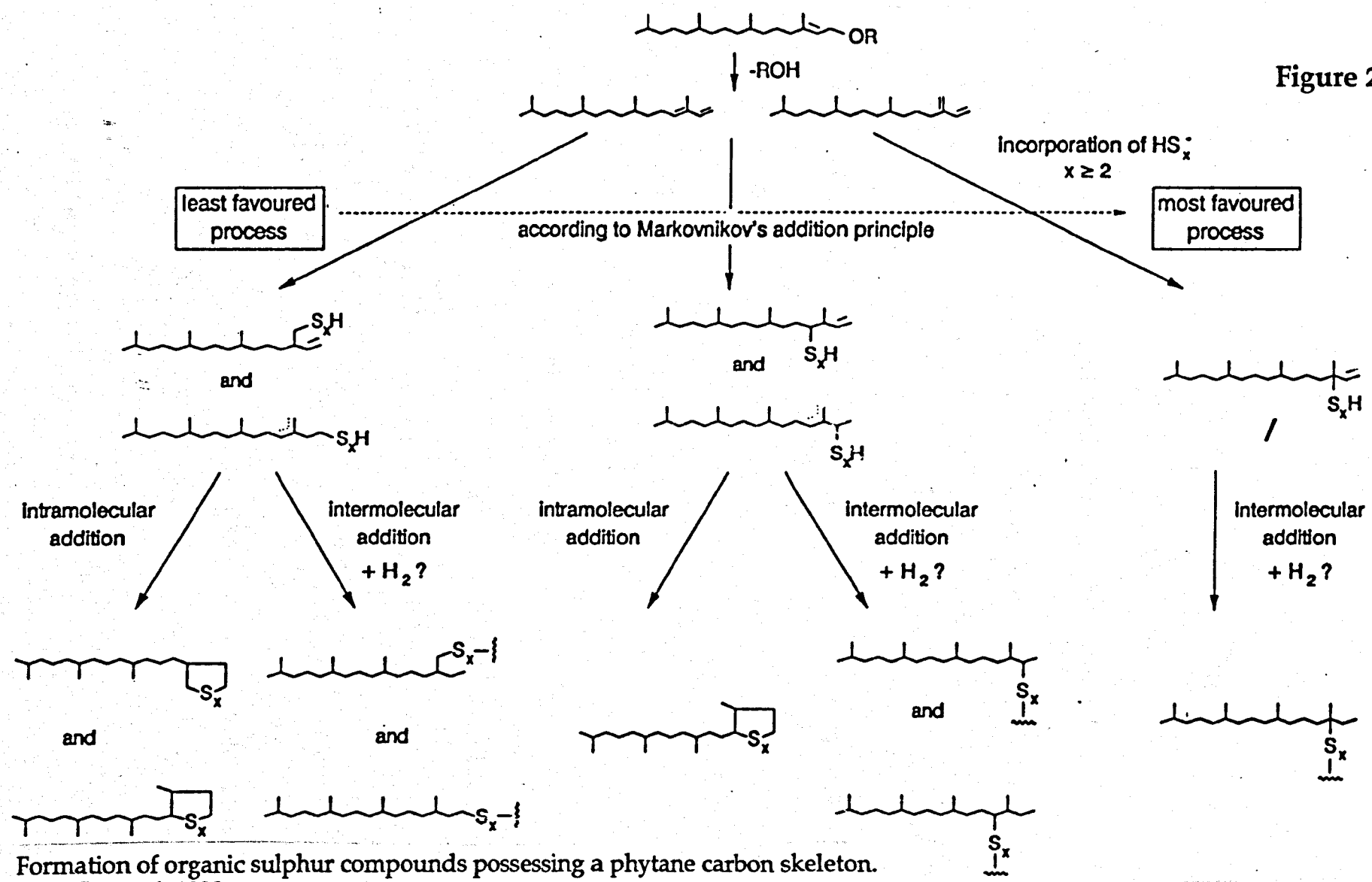
The relative timing of the incorporation of sulphur into organic compounds is not well understood and forms part of this study (Chapter 5). Berner (1984) suggests that iron competes successfully with organic matter as a sink for sulphur and thus the concentrations of sulphate and reactive iron are thought to be limiting factors in the formation of OBS in sediments (Sinninghe Damsté *et al.*, 1989a; Tuttle *et al.*, 1990).

Experimental studies (e.g. Martin and Hodgson, 1973; Casagrande *et al.*, 1979; Mango, 1983; LaLonde *et al.*, 1987; de Graaf *et al.*, 1992 ) have demonstrated possible reaction mechanisms for OSC formation via reaction with H<sub>2</sub>S, polysulphides or elemental sulphur. The occurrence of highly branched isoprenoid sulphur compounds (Kohnen *et al.*, 1990) can be accounted for by the incorporation of reduced or partially reduced sulphur into unsaturated alkenes during early diagenesis.

A general model for the incorporation of sulphur into high molecular weight compounds has been proposed by Sinninghe Damsté *et al.* (1989a). The incorporation of sulphur into organic precursors with double bonds (or other reactive functional groups) will lead to the formation of sulphur rich high molecular weight substances and OSC (Figure 2.20). Precursors with conjugated double bonds in a favourable position for nucleophilic addition to form intermediate thiols may yield low molecular weight OSC.

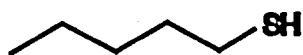
Organo-sulphur compounds can be classified by their structures e.g. Sinninghe Damsté and De Leeuw (1992), as shown in Figure 2.21. They may also be grouped by their functionality (Figure 2.22). Detailed studies of OSC in crude oils, bitumens and kerogens have been made by many authors including Sinninghe Damsté *et al.*, (1987, 1989a, 1990); Payzant *et al.* (1988), and George and Gorbaty (1989).

Figure 2.20

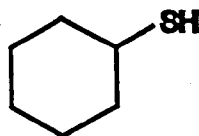


Formation of organic sulphur compounds possessing a phytane carbon skeleton.  
 After Damsté, 1989.

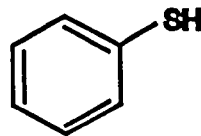
Figure 2.21

Thiols (Mercaptans)

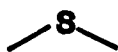
1-pentanethiol



cyclohexanethiol



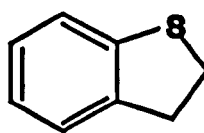
benzenethiol

Sulfides (Thiaalkanes / cycloalkanes)

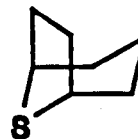
2-thiapropane



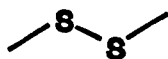
thiacyclopentane



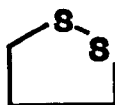
1-thiaindan



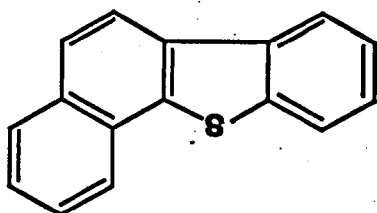
8-thiabicyclo[3,2,1]octane

Disulfides

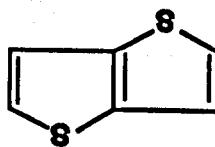
2,3-dithiabutane



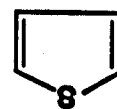
1,2-dithiacyclopentane

Thiophenes and Condensed Thiophenes

thiophene



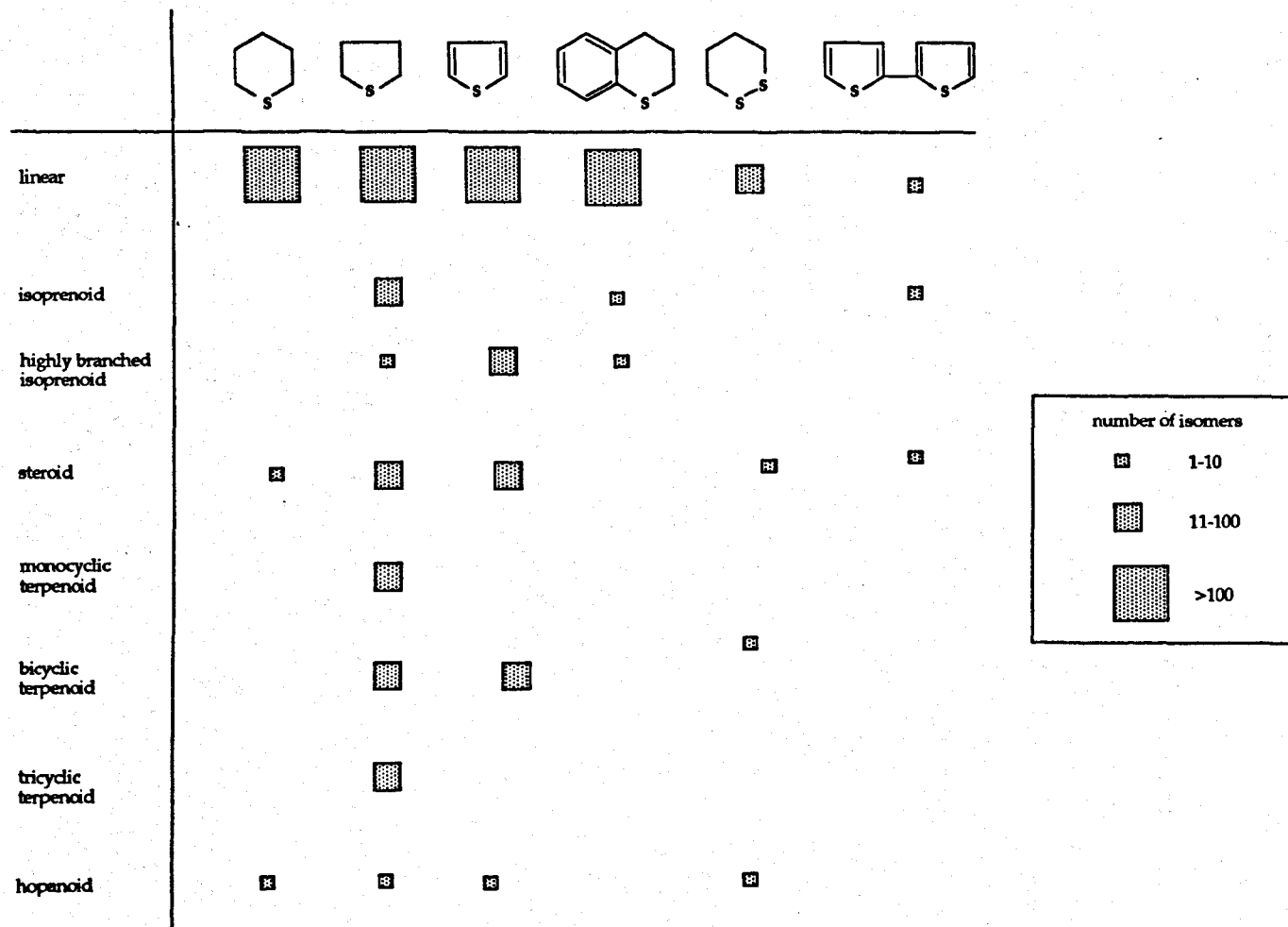
thieno[3,2,b]thiophene



9-thia-1,2-benzofluorene

Structures of organic sulphur compounds.

Figure 2.22



Classification of organically bound sulphur compounds based on their functionality.

# Chapter Three

## Geochemical Methodology

### 3.0 Introduction

Inorganic and organic parameters have been measured in this study using a variety of analytical procedures. Sulphur and carbon contents of whole rock samples and chemically separated fractions of the samples were determined by gas chromatography using a Carlo Erba 1106 Elemental Analyser. Reduced sulphur was determined using a modified method of Raiswell *et al.* (1988) and acid soluble iron using the acid leaching method of Berner (1970).

Stable isotope measurements were performed using a VG SIRA 10 mass spectrometer for sulphur and organic carbon and a SIRA 12 mass spectrometer for carbonate carbon and oxygen. Molecular studies on organic compounds were undertaken using GC and GC-MS techniques after chemical preparation. Uranium, thorium and potassium were measured in situ in the field using a GR-256 Exploranium gamma-ray spectrometer. Electron microscopy was used to image and analyse qualitatively (SEM) and quantitatively (electron microprobe) polished specimens. The above methods are described in more detail below.

### 3.1 Preparation of samples for geochemical analysis

Care was taken to collect fresh rock samples. However, any surface weathering found on the samples was removed prior to crushing. The surface of the samples was washed with distilled water and dried overnight by evaporation. About 1kg of the sample was crushed in a jaw crusher, and then in a steel pestle and mortar, to reduce the rock fragments to < 2mm in diameter. A tungsten carbide "tema" swing mill was used to crush 60g portions of the rock fragments to under 250 mesh. The tema was not left on for more than 3 seconds at any one time to prevent excessive heating of the sample. The crushed samples were stored in clean glass jars with aluminium foil under the caps. All equipment was carefully cleaned after crushing each sample in order

to prevent cross contamination. Table 3.1 shows the contamination produced by crushing pure quartz, and analysing the powder by XRF.

## 3.2 Carbon Analysis

All carbon analyses were performed using a Carlo Erba 1106 Elemental Analyser unless otherwise stated. The alternative was a Leco CHN 600 carbon analyser which was used to determine organic carbon contents directly.

The analysis involved the determination of organic carbon (bitumen CHN and kerogen CHN), inorganic carbon and total carbon. Maynard (1991) and Al-Biatty (1990) have described in detail the principles and methodology involved using the Carlo Erba 1106 Elemental Analyser.

### 3.2.1 Operation of the Carlo Erba 1106 Elemental Analyser

Weighed samples (1-2 mg) contained in tin containers are combusted in a quartz reaction tube at 1030°C, flushed with a constant flow of helium. When the sample is introduced into the reaction tube, the helium flow is enriched with oxygen to produce flash combustion. The resulting gases are passed over Cr<sub>2</sub>O<sub>3</sub> to ensure quantitative combustion, before being passed over copper at 650°C (to eliminate excess oxygen and oxides of nitrogen) prior to the introduction of the gases into the chromatographic column. Separation of the sample gases is achieved by eluting the three component mixture on a chromatographic column held at a temperature of 100°C and packed with Porapak QS. The yields of N<sub>2</sub>, CO<sub>2</sub> and H<sub>2</sub>O are measured by a thermal conductivity detector. Compositions of unknown samples are measured by calibrating the machine with a standard of known composition. Acetanilide was used as a CHN standard (%C=71.09, %H=10.36, %N=6.71).

In addition to acetanilide, an internal standard (SCW10, a typical grey shale) was run throughout the study period. The results give an indication of the reproducibility of carbon analyses. The results are shown in Table 3.2. The reproducibility is shown to be good. An average analytical error for the determination of carbon using the Carlo Erba is 0.16%.

**Table 3.1**

Method	Minor	Trace
by hand in steel mortar	Fe	Cu, Al, Mg, Ca, Cr, Mn, Ti, Ni
tema (tungsten carbide barrel)	W, Fe	B, Al, Mg, Ca, Cu, Mn, Ti

Contamination by the different processes of crushing quartz.

**Table 3.2**

Sample	R/S	SCW10
number of analyses	10	10
%C max.	1.78	11.79
%C min.	1.28	11.33
%C mean	1.57	11.52
standard deviation ( $\sigma_{n-1}$ )	0.16	0.16

Reproducibility of carbon analyses of shale samples using the Carlo Erba elemental analyser.

The reproducibility is shown to be good. An average analytical error for the the determination of carbon using the Carlo Erba is 0.16%.

### 3.2.2 Organic Carbon Determination

Organic carbon was determined using three methods. Each method will be discussed in turn within the following sections.

#### 3.2.2.1 Ashing

This method described by Krom and Berner (1983) utilises the fact that organic matter can be removed by ashing small amounts of samples in a muffle furnace at 450°C for 12 hours. By measuring the total carbon and the carbon remaining in the sample after ashing, (using the Carlo Erba as described by Maynard, 1991) the weight percent organic carbon can be calculated as the difference between the two. Dolomite would start to dissociate at these temperatures, however none of the samples analysed was thought to contain significant amounts. Figure 3.1 shows a comparison of the methods used for the determination of organic carbon.

#### 3.2.2.2 Carbonate Dissolution

Carbonate was removed from the sample using a 25 times excess hydrochloric acid (10% v/v) and allowing the reaction at least 12 hours for completion. The weight loss was noted and the organic carbon content was calculated using the expression:

$$\text{wt \% Organic C} = \text{wt \% C residue} \times \left( 1 - \frac{\text{wt loss}}{\text{original mass of sample}} \right)$$

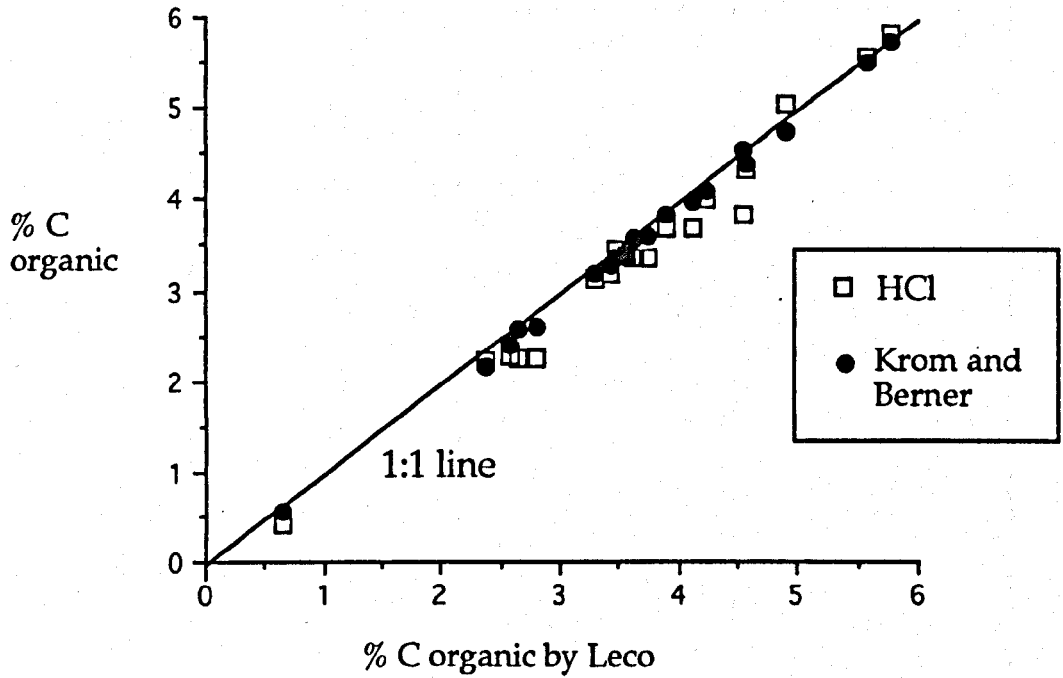
Figure 3.1 shows a comparison of the methods used for the determination organic carbon.

#### 3.2.2.3 Whole Rock Pyrolysis

A Leco CHN 600 carbon analyser was used to determine total organic carbon contents of some samples. These analyses were performed courtesy of British Gas plc.



Figure 3.1



Relationship between the three different methods used in the determination of organic carbon. The HCl and Krom and Berner methods give slightly lower values than using the Leco, but this is not significant at the 95% level.

**Table 3.3**

Sample	% C organic		
	HCl	Leco	Krom and Berner
DK 36	3.70	4.12	3.98
DK 35	5.83	5.77	5.74
DK 34	3.36	3.73	3.61
DK 33	4.32	4.57	4.40
DK 32	3.68	3.90	3.83
DK 31	5.04	4.91	4.75
DK 30A	0.41	0.66	0.55
DK 30	2.26	2.65	2.58
DK 29	3.13	3.28	3.18
DK 28A	4.02	4.23	4.09
DK 28	3.84	4.55	4.55
DK 27	3.36	3.62	3.58
DK 26	3.20	3.42	3.27
DK 25	3.40	3.55	3.36
DK 24	2.25	2.79	2.61
DK 23	2.28	2.58	2.40
DK 22A	2.23	2.37	2.18
DK 22	5.57	5.58	5.49
DK 21	3.44	3.48	3.38

Comparison of different organic carbon determinations on a shale sample.

A Leco THA-200 was used to pyrolyse whole rock samples. A small amount (<1 mg) of rock powder was heated in a crucible at 100°C. The volatile hydrocarbons driven off were recorded (S0) using a flame ionising detector (FID). The temperature was then increased to 300°C, and the yield of hydrocarbons generated was measured (S1) by FID. Finally the temperature was increased to 550°C to volatilise solid organic compounds e.g. kerogens, and the yield measured (S2). The temperature at which the maximum rate of hydrocarbon evolution occurs is recorded as the  $T_{\max}$  temperature. These analyses were performed courtesy of British Gas plc.

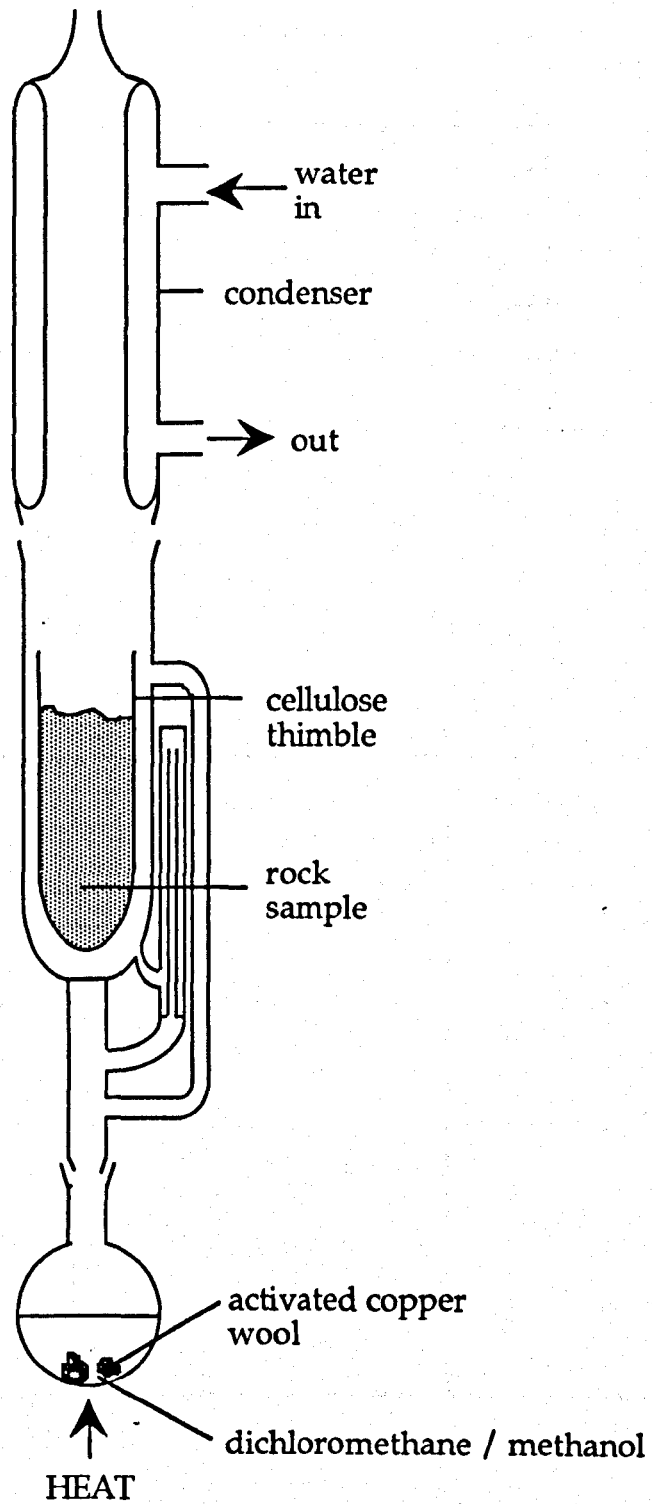
Figure 3.1 and Table 3.3 show a comparison of the methods used to determine organic carbon. Both the HCl and the ashing method of Krom and Berner (1983) show slightly lower values of organic carbon contents with off-sets of -0.42% and -0.17% respectively. Given that the Leco method involves only one step in handling the sample, the experimental error will be minimal relative to the other two methods. As the HCl and ashing methods use the Carlo Erba to determine the carbon content of the sample after suitable chemical work up procedures, the discrepancy between the two sets of data is brought about by error in the work up procedure. The method of Krom and Berner (1983) has fewer manipulative steps than the HCl method, accounting for the greater proximity to the values obtained by Leco analysis. The coefficients of determination ( $r^2$ ) being 0.998 and 0.977 respectively, relative to the Leco analysis.

### 3.3 Bitumen extractions

Soluble organic compounds (bitumen) were separated from crushed rock samples by soxhlet extraction (Figure 3.2). The times of extraction and solvent systems used are shown in Table 3.4. Typically, about 50 g of rock powder was extracted for 24 hours using about 180ml of the DCM / methanol azeotrope. The bitumen was concentrated by rotary evaporation and stored in glass sample vials in a solution of dichloromethane and kept in a refrigerator at ~5°C away from daylight.

The dichloromethane methanol azeotrope (93:7) was found to be the most efficient solvent with an extraction time of 24 hours (Table 3.4). The reproducibility of the soxhlet extraction technique was established by splitting an homogenised sample into four aliquots and extracting them (Table 3.5).

Figure 3.2



Soxhlet apparatus used to solvent extract rock powders.

**Table 3.4**

Extraction Time (hours)		12	24	48	72
Bitumen Extracted (mg/g) (sample PM 16)	DCM	15.69	16.21	15.94	16.07
	DCM/methanol (93:7)	16.93	17.28	17.46	17.39

Soxhlet extraction of bitumen over different lengths of time.

**Table 3.5**

Sample weight (g)	Extract (mg)	Extractability (mg/g)
48.743	0.866	17.28
53.285	0.923	17.32
42.942	0.792	18.45
46.731	0.818	17.50
mean	0.850	17.64
standard deviation ( $\sigma_{n-1}$ )	0.058	0.550

Reproducibility of soxhlet extraction

From these results, it can be seen that the extraction procedure shows good reproducibility.

### 3.4 Liquid Column Chromatography

The bitumen samples were evaporated to dryness on a rotary evaporator before being separated into asphaltene (n-pentane insolubles) and maltene fractions by precipitation with n-pentane. The asphaltenes were then filtered off using sintered glass frits. The maltene fractions (asphaltene free bitumen) were further fractionated into an aliphatic, an aromatic and a polar fraction on activated silica-alumina columns (Figure 3.3). The maltenes were adsorbed onto a minimum of activated alumina and introduced onto the column already washed with n-pentane. The column was then eluted sequentially with a solution of n-pentane, dichloromethane and finally methanol or tetrahydrofuran. The elutants were collected and the volumes reduced by rotary evaporation prior to storage in glass sample tubes. These were kept out of daylight, in a cool place. Figure 3.4 summarises the separation procedure.

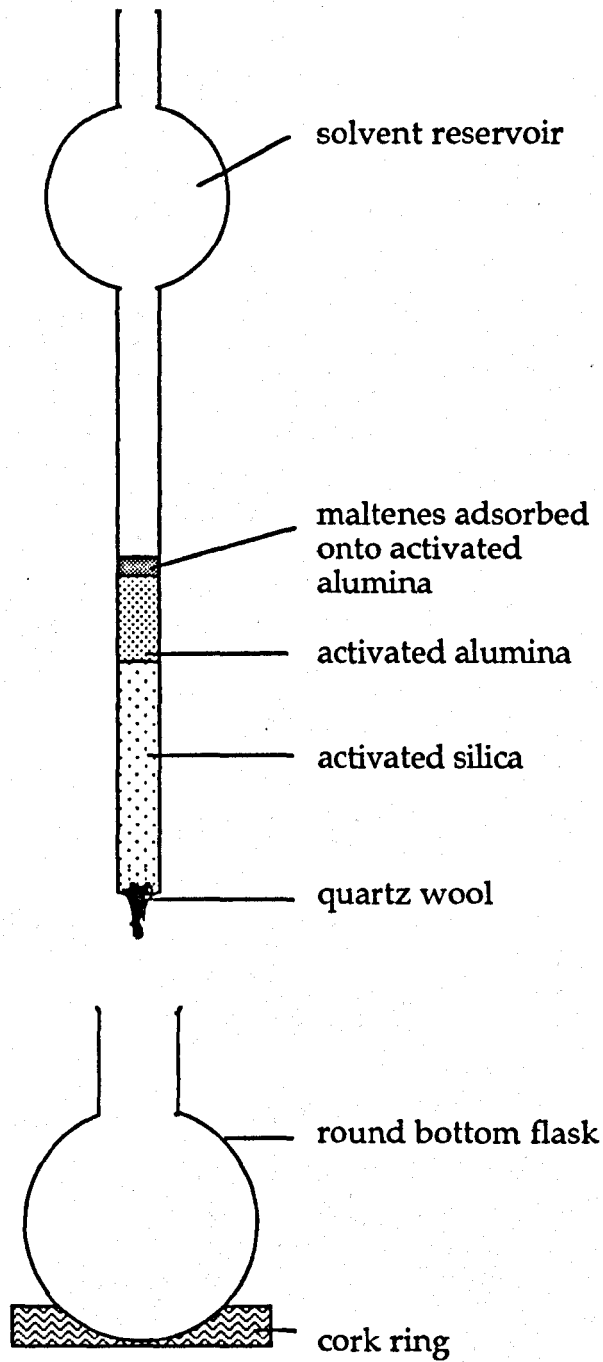
### 3.5 Gas Chromatography

GC analyses of samples were performed on a Varian 3400 capillary gas chromatograph fitted with an autosampler and integrator. This was run with a flame ionisation detector or, in the case of organo sulphur compound classification, with a dual flame ionisation detector/flame photometric detector (FID-FPD). The column used was a 25m 0.22mm i.d. fused silica column coated with a cross banded non-polar phase (CP Sil 50). A temperature program of 50°C for the first minute and 5°C per minute thereafter up to 320°C was used.

#### 3.5.1 Gas Chromatography - Mass Spectrometry

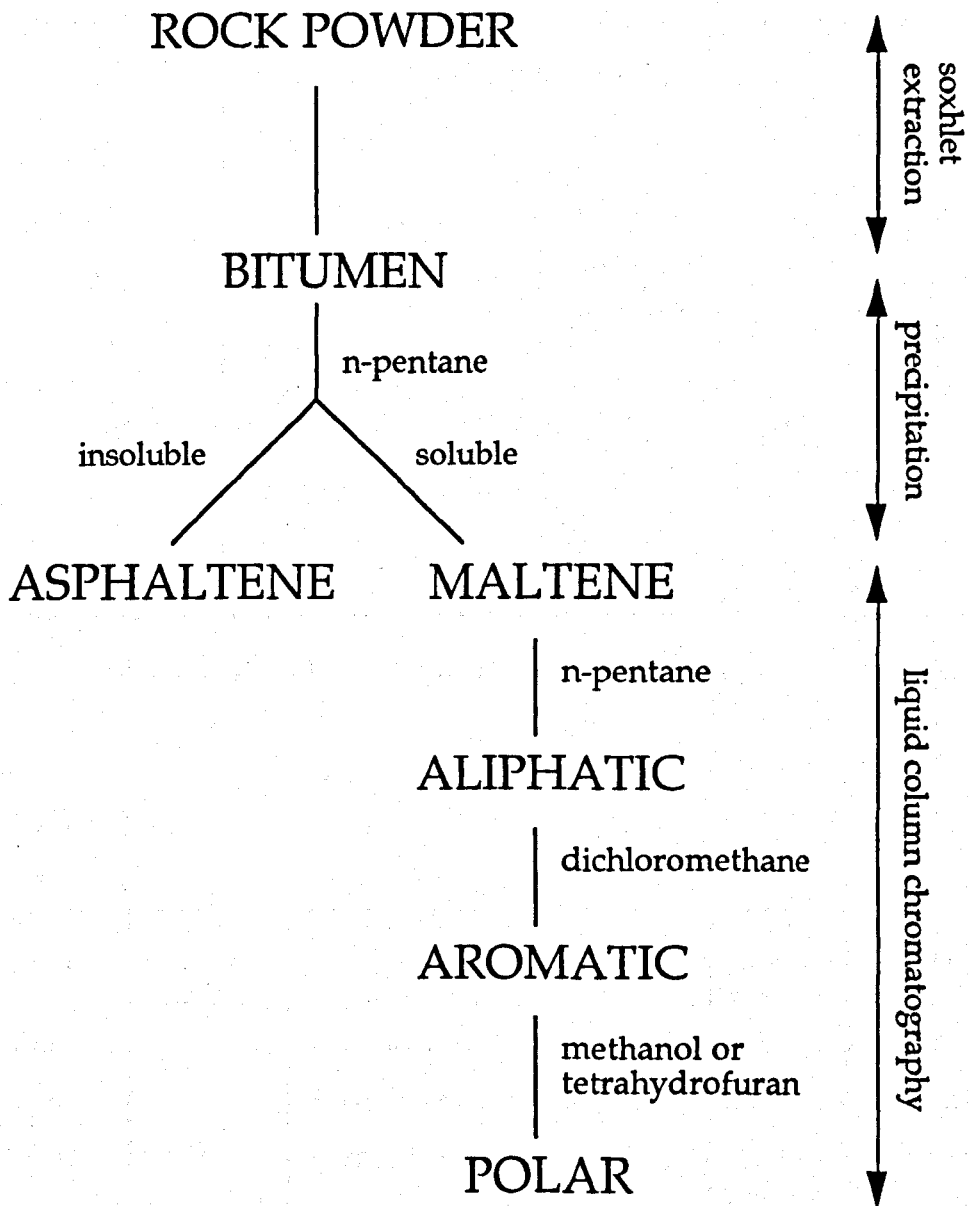
A Varian 3400 capillary gas chromatograph as described in section 3.5 was used in conjunction with a Finnegan TSQ 70 triple sector quadrupole instrument. The TSQ was set to monitor the prespecified ionic mass equivalents (m/e) in accordance with those expected to form from the fragmentation of biological marker compounds. Table 3.6 shows the mass/charge fragments selected during this study.

Figure 3.3



Column and packing used to fractionate maltenes into aliphatic, aromatic and polar fractions by column chromatography.

Figure 3.4



Solvent extraction scheme.



Table 3.6

m/e	Class of compound
177	moretanes and demethylated hopanes
191	triterpanes
217	steranes
218	regular steranes 14 $\beta$ (H) 17 $\beta$ (H)
231	methyl steranes
259	rearranged steranes
184	dibenzothiophene
198	methyl benzothiophene

Diagnostic ions used to detect different classes of organic compounds in GC-MS analysis.

Table 3.7

Ref Gas	No. of samples	$\delta^{66}\text{S}$ in ‰	mean ‰	ssdm ‰
41	3	-11.808, -11.864, -11.972	-11.88	0.014
42	4	-12.476, -12.553, -12.578, -12.408	-12.50	0.016
44	4	-12.587, -12.488, -12.495, -12.334	-12.48	0.033
46	2	-12.057, -12.182	-12.12	0.008
56	2	-12.244, -12.362	-12.30	0.007
	$\Sigma$ 15			$\Sigma$ 0.078

Reproducibility of Cp-1 samples relative to different aliquots of reference gas.

$$S_{\text{pooled}} = \sqrt{\frac{0.078}{(15-5)}} = 0.088 \text{ ‰}$$

### 3.5.2 Gas Chromatography - Atomic Emission Detection

A Hewlett-Packard Series II gas chromatograph interfaced with a Hewlett-Packard atomic emission detector and equipped with an HP7673 autosampler was used for detailed sulphur compound analyses. Wavelengths used to monitor sulphur and carbon were 181.037nm and 193.030nm respectively. Extracts were analysed using 1  $\mu$ L injections at a split ratio of 1:60 into a wide bore (25m x 0.32mm i.d., 0.17 $\mu$ m film thickness) HP-5 column. The injector port temperature was 300°C, and a packed liner was used. All samples were injected at an oven temperature of 60°C, held for 2 minutes, followed by a temperature ramp at 5°C min<sup>-1</sup> to 320°C and held for 5 minutes.

### 3.6 Kerogen Isolation

Kerogen (insoluble organic matter) was isolated from the bitumen free residue after soxhlet extraction. The pyrite was removed from the sample using a modified method as described by Riley *et al.* (1990) by boiling with nitric acid (2M) for 1 hour.

The silicate matrix was removed from the residue by reaction with hydrofluoric acid, which was cautiously added in excess to the samples and heated to dryness on a steam bath in Pt crucibles. A further aliquot of HF was added and the process repeated. AlCl<sub>3</sub> (10%) was added to complex any unreacted HF and to convert fluorides into chlorides which could be removed by washing with distilled water.

### 3.7 Stable isotope analysis

#### 3.7.1. Stable Carbon Isotope Analysis of Organic Compounds

Organic compounds, either fractions of extracted bitumen, bitumen or kerogen were isolated as described earlier. Samples containing 1-2 mg of organic carbon were loaded into 6 mm o.d. silica tubes (9 mm o.d. for kerogen samples) having first been left in a muffle furnace at 500°C for at least 8 hours to drive off any organic carbon contaminants.

Copper (II) oxide, having first been left in a muffle furnace for 12 hours at 500°C to remove any organic matter, was added in excess. Silver and copper wires were added in order to remove any oxides of sulphur or nitrogen which may form during the oxidation of the organic matter by the copper (II) oxide. The sample tubes were evacuated, sealed and heated to 850°C for 12 hours. The CO<sub>2</sub> was purified in a vacuum line. After cooling, a n-pentane trap at -130°C was used to purify the CO<sub>2</sub> by distillation, prior to collecting.

Samples of carbon dioxide were analysed using a VG Isogas SIRA 10 triple collecting mass spectrometer. Samples and standards used: National Bureau of Standards (NBS) Oil Number 22 and Australian National University (ANU) Sucrose (TRW, 1981). The data were corrected using the procedures of Craig (1957).

### 3.7.2 Stable Oxygen and Carbon Isotope Analysis of Carbonates

Samples of carbonate were drilled out by hand using a dental drill and tungsten carbide tipped drill bits. The samples were then rinsed with dichloromethane to remove any bitumen or other major organic carbon surface contaminants. After drying, the samples were stored in a desiccator prior to analysis.

Between 3 and 5 mg of sample was ashed in a Bio-Rad E2000 Plasma Asher for 4 hours. This removed any residual organic matter. The ashed carbonate samples were reacted with 2ml orthophosphoric acid under high vacuum (usually  $< 5 \times 10^{-5}$  atm). The reaction temperature was maintained by immersing the reaction vessels in a thermostatically controlled water bath (calcite at 25°C and dolomite at 50°C). On completion of the reaction (typically 18 hours) the CO<sub>2</sub> gas produced was purified by trapping H<sub>3</sub>PO<sub>4</sub> and water vapour in an acetone trap at -87°C, before collecting the sample.

Samples of carbon dioxide were analysed using an automated VG Isogas SIRA 12 triple collecting mass spectrometer. Samples and internal standards (U3) were run against an internal reference gas.  $\delta^{13}\text{C}$  and  $\delta^{18}\text{O}$  values were calculated assuming fractionation factors of 1.01025 for calcite liberating CO<sub>2</sub> with reaction of phosphoric acid (Craig, 1957) and 1.01011 for CO<sub>2</sub> liberated from dolomite at 50°C with phosphoric acid (Deines, 1980).

### 3.7.3 Stable Sulphur Isotope Analysis

Geological samples often contain sulphur in low concentrations. It is therefore necessary to concentrate the sulphur into a form which can be readily converted into sulphur dioxide prior to analysis by mass spectrometry. Figure 3.5 summarises the conversions performed during this study.

The reproducibility of the standard preparation technique was estimated by analysing the variation of  $\delta^{66}\text{S}$  values for the Cp-1 standard, measured against each batch of reference gas (Table 3.7). A pooled estimate of the standard deviation was calculated using the sum of the squares of deviations from the mean as described in the Appendix 1. The error on the mass spectrometer has been estimated to be in the order of  $\pm 0.005\%$  on  $\delta^{66}\text{S}$  by performing replicate analysis of the same gas sample (Bottrell, pers. comm.).

Duplicate pairs of a series of samples were analysed to check on the reproducibility of producing  $\text{SO}_2$  (Table 3.8). The duplicates, with the exception of one pair are all within the error of  $\pm 0.2\%$ .

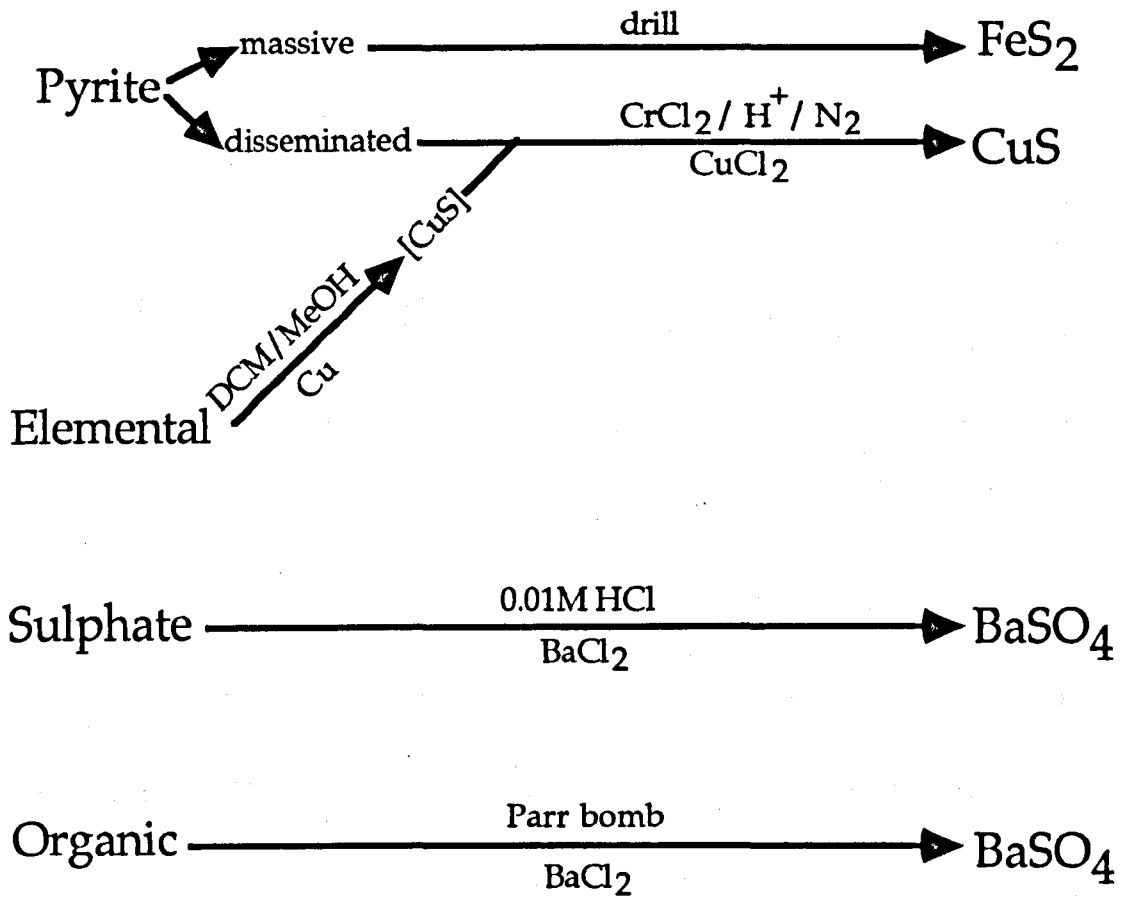
#### 3.7.3.1 Pyrite

Massive pyrite samples were drilled out by hand using a dental drill and tungsten carbide tipped drill bits. Disseminated pyrite sulphur was reduced and reprecipitated as  $\text{CuS}$  during the pyrite sulphur determination process as described later.

The method of Robinson and Kusakabe (1975) was used to determine the sulphur isotopic composition of sulphide samples. Between 3 and 7mg of sulphur was mixed with 200mg of  $\text{Cu}_2\text{O}$  in an agate pestle and mortar and packed into quartz tubing (Figure 3.6). The sample was outgassed to a background pressure of  $2 \times 10^{-5}$  bars, then reacted at a temperature of  $1080^\circ\text{C}$  for 15 minutes. Water was trapped in a methylated spirits trap at  $-80^\circ\text{C}$  and carbon dioxide was removed by distillation from an n-pentane trap at  $-130^\circ\text{C}$ . The purified sulphur dioxide samples were collected in airtight sample tubes prior to analysis.

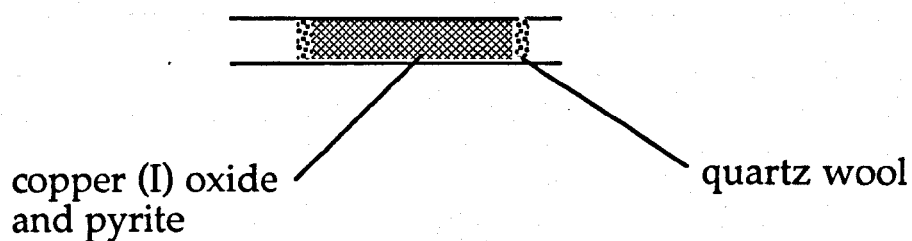
Samples of  $\text{SO}_2$  were analysed using a VG Isogas SIRA 10 gas source mass spectrometer. Samples and internal standards (British Geological Survey chalcopyrite Cp-1) were run against an internal reference gas.  $\delta^{34}\text{S}$  values were

Figure 3.5



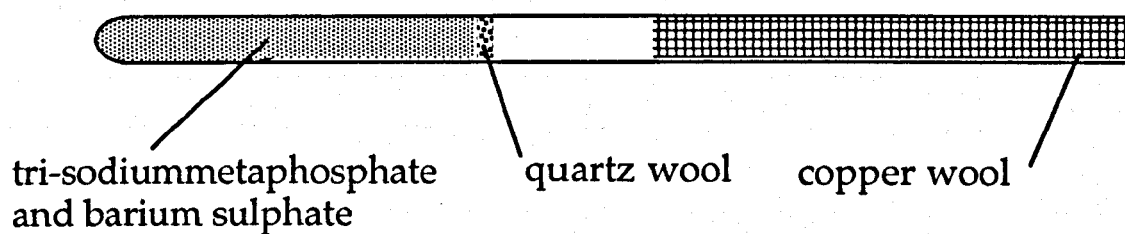
Summary of conversion procedures to convert geological samples into a form which can be converted into sulphur dioxide prior to mass spectrometry.

Figure 3.6



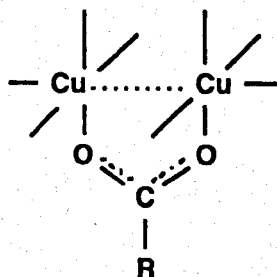
Sulphide reaction tube.

Figure 3.7



Sulphate reaction tube.

Figure 3.8



Copper acetate bridge complex stabilising copper in the Cu(I) oxidation state.

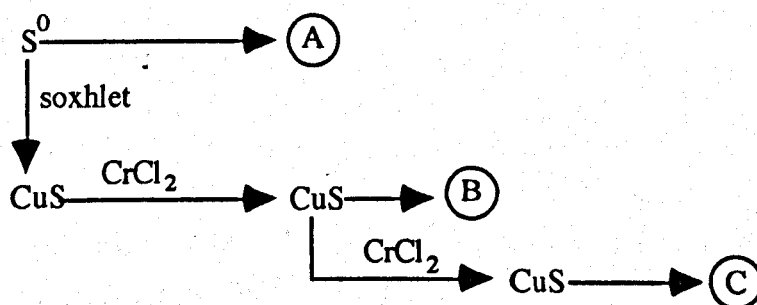
Table 3.8

Duplicate pair (‰)		mean (‰)	deviation from mean (‰)
-21.77	-21.51	-21.64	0.13
-24.13	-24.44	-24.13	0.16
-21.72	-21.67	-21.70	0.03
-22.82	-23.01	-22.92	0.09
-24.46	-25.33	-24.90	0.44

Duplicate pairs of a series of samples were analysed to check on the reproducibility of producing  $\text{SO}_2$ . The duplicates, with the exception of one pair are all within the error of  $\pm 0.2\text{‰}$ .

Table 3.9

Sample			
	A	B	C
	-8.099	-8.792	-8.522
	-8.251	-8.811	-8.425
		-8.639	-8.578
		-9.005*	-8.863
mean	-8.175	-8.637	-8.597
$\sigma_{n-1}$	0.107	0.382	0.188



Reproducibility of  $\text{SO}_2$  preparation for  $\delta^{34}\text{S}$  isotopic analysis.

$\delta^{34}\text{S}$  values for samples which have been sequentially extracted and reprecipitated (\* sample frozen in by mass spectrometer - probable error in measurement, therefore value was rejected).

calculated using standard correction procedures (e.g. Craig, 1957 and Coleman, 1980).

### 3.7.3.2 Elemental Sulphur

Elemental sulphur is isolated by addition of activated copper wool to the receiving flask during the soxhlet extraction of samples. The resulting copper wool coated with CuS was converted into a concentrated copper (II) sulphide precipitate by the method used to determine pyrite sulphur. The copper (II) sulphide is also treated in the same way to produce sulphur dioxide, before analysing the gas on a VG SIRA 10 mass spectrometer.

Simple tests were performed on CuS precipitates to check for isotopic fractionation of sulphur. The isotopic composition of sulphur in pyrite was analysed by direct conversion to SO<sub>2</sub> using Cu<sub>2</sub>O and also by converting the pyritic sulphur to CuS by CrCl<sub>2</sub> reduction prior to conversion to SO<sub>2</sub>. The results in Table 3.8 show a fractionation of about 0.5‰.

Standardised elemental sulphur was added to a sulphur free shale matrix and extracted as described in section 3.8.5. The copper sulphide precipitated onto the activated copper wool was concentrated as CuS using chromous chloride and reprecipitating CuS. As a further test, the copper sulphide precipitate formed during chromous chloride attack was reprecipitated during a subsequent digestion procedure in chromous chloride.

The results (Table 3.9) indicate a systematic enrichment of <sup>32</sup>S upon the initial formation of copper sulphide, with no further fractionation associated with the reprecipitation of CuS.

### 3.7.3.3 Sulphate

Acid soluble sulphate was leached out of samples using a 0.01M solution of Analar HCl. The sulphate was reprecipitated from a warm solution (~70°C) as barium sulphate by adding excess 10% BaCl<sub>2</sub> (aq.). Care was taken to prevent the pH falling below 2.5pH, thus preventing oxygen exchange between water and sulphate.



Between 10 and 20mg of the dried  $\text{BaSO}_4$  was intimately mixed with a flux of tri-sodiummetaphosphate and packed into quartz tubes (Figure 3.7). A copper wool plug was inserted into the end of the reaction tube to aid in the conversion of  $\text{SO}_3$  to  $\text{SO}_2$ . The sulphur dioxide produced on heating at a temperature of  $950^\circ\text{C}$  with a background pressure of better than  $2 \times 10^{-5}$  mbars was purified as described earlier.

### 3.7.3.4 Organically bound sulphur

To convert organic sulphur into  $\text{SO}_2$  prior to isotopic analysis, the organic carbon must first be removed. This was achieved by oxidation-combustion in a 300ml Parr bomb and the sulphur, as sulphatic sulphur, precipitated as barium sulphate, following a modified method reported by the ASTM (D 129-64).

Organic samples (bitumen, kerogen, asphaltene, maltene, aliphatic, aromatic or polar) were transferred into nickel crucibles, the combined weight of sample and solvent (tetrahydrofuran or ethanol) being less than 1g. In the case of kerogen samples, a few drops of ethanol were added to aid initiation of combustion.

The samples were combusted in a 300ml Parr oxygen bomb with an atmosphere of 30atm  $\text{O}_2$ . After cooling (at least 10 minutes) the bomb was vented slowly and the internal surfaces washed out with distilled water. Bromine water (10ml, 1%) was added to the washings and the solution was covered and heated at  $\sim 80^\circ\text{C}$  for 1 hour. The covers were removed and heating was continued until all the  $\text{Br}_2$  vapour had disappeared. Organic acids and iron are removed by the addition of ammonia (10ml, 10%) and the precipitates filtered off. The filtrate is acidified with hydrochloric acid (10ml, 10%) and the sulphate then precipitated as  $\text{BaSO}_4$  on the addition of barium chloride (25ml, 10%).  $\text{SO}_2$  is prepared from the precipitated  $\text{BaSO}_4$  as described in section 3.7.3.3.

## 3.8 Sulphur Analysis

### 3.8.1 Operation of the Carlo Erba 1106 Elemental Analyser

Weighed samples (1-2 mg) and  $V_2O_5$  (~1 mg) contained in tin containers are combusted in a quartz reaction tube at  $1010^\circ\text{C}$ , flushed with a constant flow of helium. When the sample is introduced into the reaction tube, the helium flow is enriched with oxygen to produce flash combustion. The resulting gases are passed over  $WO_3$  to ensure quantitative combustion, before being passed over copper at  $650^\circ\text{C}$  to eliminate excess oxygen and to convert the  $SO_2$  and  $SO_3$  into  $SO_2$  via  $CuSO_4$ . The reaction gases pass through a water trap filled with anhydrous magnesium perchlorate before eluting the mixture of gases on a chromatographic column held at a temperature of  $80^\circ\text{C}$  and packed with Porapack QS. The yield of  $SO_2$  is measured by a thermal conductivity detector. Compositions of unknown samples are measured by calibrating the machine with a standard of known composition. Sulphanilamide was used as a sulphur standard (%C=41.84, %H=4.86, %S=18.62).

As in the case for carbon analyses, an internal standard (SCW 10) was analysed over the entire period of research. The results are shown in Table 3.10.

### 3.8.2 Total sulphur and organic sulphur

Total sulphur and organically bound sulphur were quantified using the Carlo Erba 1106 Elemental Analyser as described by Maynard (1991) and Al-Biatty (1990).

### 3.8.3 Elemental sulphur

Elemental sulphur was determined by introducing activated copper wool into the soxhlet apparatus (Figure 3.2). The dissolved elemental sulphur reacts with the copper as shown in Equation 3.1



The amount of copper sulphide produced was determined using the same procedure used to establish the amount of pyrite within a sample as described

**Table 3.10**

Sample	SCW 10	R/S
number of analyses	10	10
%S max.	2.83	2.40
%S min.	2.21	2.30
%S mean	2.68	2.34
standard deviation	0.19	0.04

Reproducibility of sulphur analyses for an internal standard (SCW 10) and the laboratory standard (R/S).

**Table 3.11**

mass of S added / g	mass of S recovered / g	% recovered
0.2680	0.2678	99.94
0.2122	0.2103	99.12
0.1230	0.1206	98.05
0.0974	0.0976	100.21
0.0566	0.0561	99.17
0.0206	0.0207	100.46
		mean 99.49
		$\sigma_{n-1}$ 0.89

Recovery of elemental sulphur from a rock matrix.

later, and hence the concentration of elemental sulphur can be calculated. The recovery of elemental sulphur was found to be excellent. Aliquots of elemental sulphur were added to an homogenised sulphur free mud rock matrix. The rock/sulphur mixture was soxhlet extracted using DCM/methanol (93:7) and elemental sulphur was trapped using Cu wool. The recovery is shown in Table 3.10.

### 3.8.4 Sulphate sulphur

The amount of sulphate within a sample was determined gravimetrically using barium chloride to precipitate the sulphate. Acid soluble sulphate was leached out of samples using a 0.01M solution of HCl. The sulphate was reprecipitated (Equation 3.2) from a warm solution ( $\sim 70^{\circ}\text{C}$ ) as barium sulphate by adding excess  $\text{BaCl}_2$  (10% ).



### 3.8.5 Pyrite Sulphur

Pyrite can be regarded as ferrous iron ( $\text{Fe}^{\text{II}}$ ) combined with a disulphide species ( $[\text{S-S}]^{2-}$ ). The sulphur in the -1 oxidation state can be further reduced to the -2 oxidation state by the addition  $\text{Cr}^{2+}$  (Equation 3.3). Chromous chloride has been shown to be a selective reducing agent for reduced sulphur species (Canfield *et al.* 1986). However tests have shown (this study and Canfield *et al.* 1986) that only  $\sim 87\%$  of elemental sulphur will react. This is thought to be due to the hydrophobic nature of elemental sulphur preventing complete reaction.

Chromous chloride (1M in 10% HCl) was freshly prepared before use by activating a Jones Reductor (packed with amalgamated zinc) with 10% HCl and passing chromic chloride (2M in 10% HCl) through. The resulting chromous chloride was stored in air tight containers under an atmosphere of nitrogen.



The evolved hydrogen sulphide was trapped under an atmosphere of nitrogen in a copper (II) solution, in the form of CuS. Copper was chosen as a suitable metal as the solubility product of CuS is low and any unreacted copper can readily be established by the titration with EDTA. H<sub>2</sub>S is a weak electrolyte, ionising as:



$$[\text{H}^+]^2 [\text{S}^{2-}]$$

which obeys the law of mass action,  $K = \frac{[\text{H}^+]^2 [\text{S}^{2-}]}{[\text{H}_2\text{S}]} = K_{sp} / (\text{mol. l}^{-1})$ .

$$[\text{H}_2\text{S}]$$

K is very low ( $K_{sp} \text{ CuS} = 6.3 \times 10^{-36} \text{ mol.l}^{-1}$ ), therefore, at any time during dissociation [S<sup>2-</sup>] will be low. If [H<sup>+</sup>] is low, to maintain the value of K, [S<sup>2-</sup>] is reduced by H<sub>2</sub>S formation.

Copper sulphate was originally chosen to precipitate the H<sub>2</sub>S as CuS because it is relatively inexpensive and has a high solubility product. Subsequently the acetate salt was chosen to replace sulphate, to avoid any possible sulphur isotopic contamination from the CuSO<sub>4</sub>. However, this has occasionally given unreliable and non reproducible results.

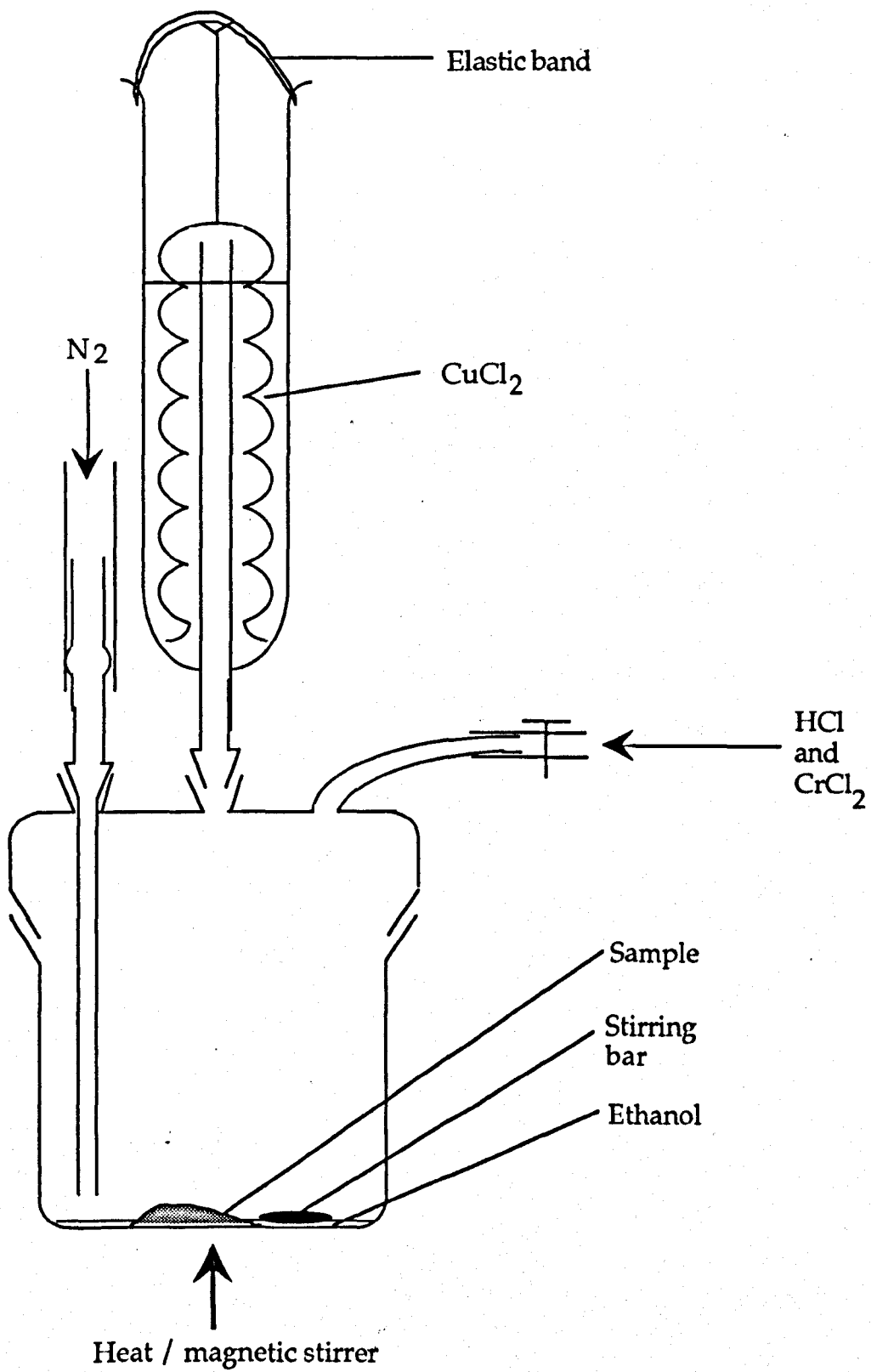
In aqueous systems, Cu<sup>+</sup> is unstable and disproportionates into Cu<sup>2+</sup> and Cu<sup>0</sup>, i.e. it undergoes self oxidation-reduction (Pourbaix, 1960).



The overall equilibrium can be shifted by adding anions which precipitate insoluble Cu<sup>I</sup> compounds or by adding a more stable complexing agent. The acetate group is a pi electron accepting ligand, and two copper ions can be bridged by an acetate group thus stabilising the Cu<sup>I</sup> state (Figure 3.8).

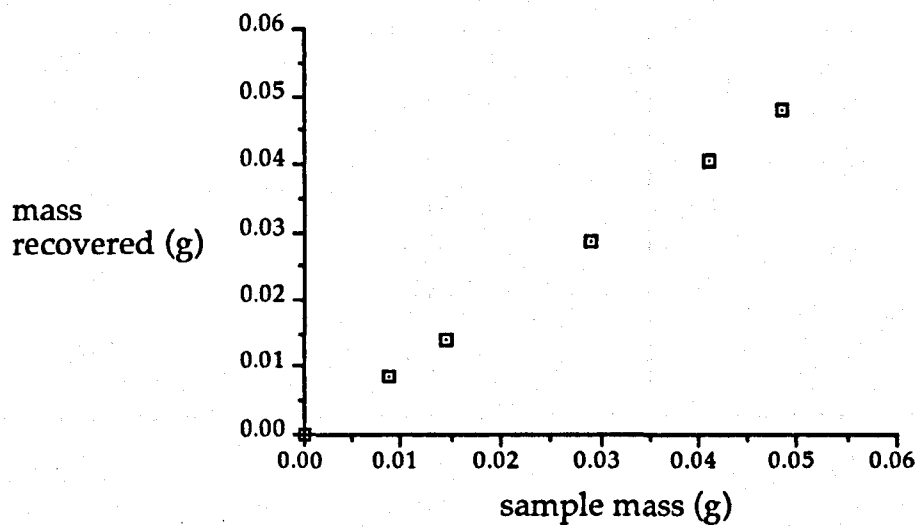
The precipitate then consists of Cu<sub>2</sub>S and CuS. Back titration of the unused Cu is used to measure the copper precipitated, which is assumed to be CuS. Errors therefore result if Cu<sub>2</sub>S is significant. Copper chloride was used in place of copper acetate to yield precise and accurate analyses of standard compounds via the following scheme.

Figure 3.9



Apparatus used to determine reduced sulphur.

Figure 3.10



The recovery of pyrite using the chromous chloride extraction technique.

**Table 3.12**

sample mass / g	mass of pyrite recovered	% recovery
0.000	0.000(0)	undefined
0.009	0.088(2)	98.02
0.014	0.013(9)	99.10
0.029	0.028(7)	98.38
0.041	0.040(4)	98.64
0.048	0.047(5)	98.99

Recovery of pyrite as determined using the chromous chloride extraction technique.

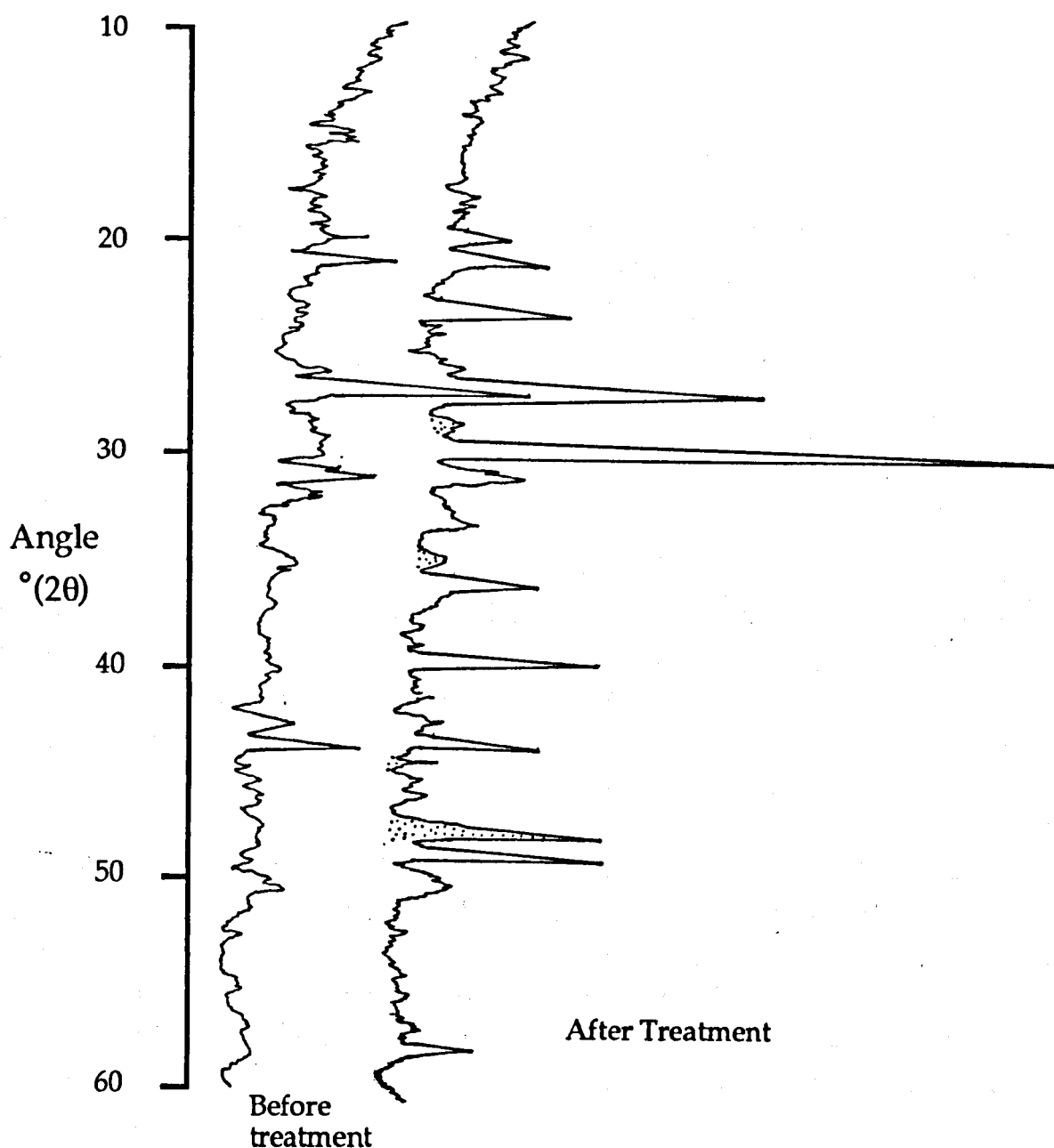
**Table 3.13**

Pre Boil (minutes)	Boil (minutes)	wt% Fe
0	1.0	1.31
0.5	1.0	1.20
0.5	1.5	1.42
0.5	2.0	1.90
0.5	3.0	2.02
1.0	1.0	1.40
1.0	1.5	1.71
1.0	2.0	1.99
1.0	3.0	2.08

Change in the concentration of iron extracted by concentrated hydrochloric acid as boiling times vary.

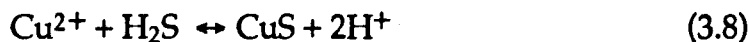


Figure 3.11



XRD pattern of sample PM16 before and after treatment with chromous chloride.

The shaded peaks are those produced by pyrite. Loss of other major peaks after treatment is ascribed to calcite dissolution from the sample. The scan speed was set at two degrees per minute.



The apparatus used is shown in Figure 3.9. The recovery of pyrite using this method is illustrated in Figure 3.10 and Table 3.12.

X-ray diffraction was performed on a whole rock sample PM14 prior to and after extraction by chromous chloride (Figure 3.11). The trace clearly shows the substantial reduction in the peaks produced by pyrite after reaction with chromous chloride.

### 3.9 Acid soluble iron

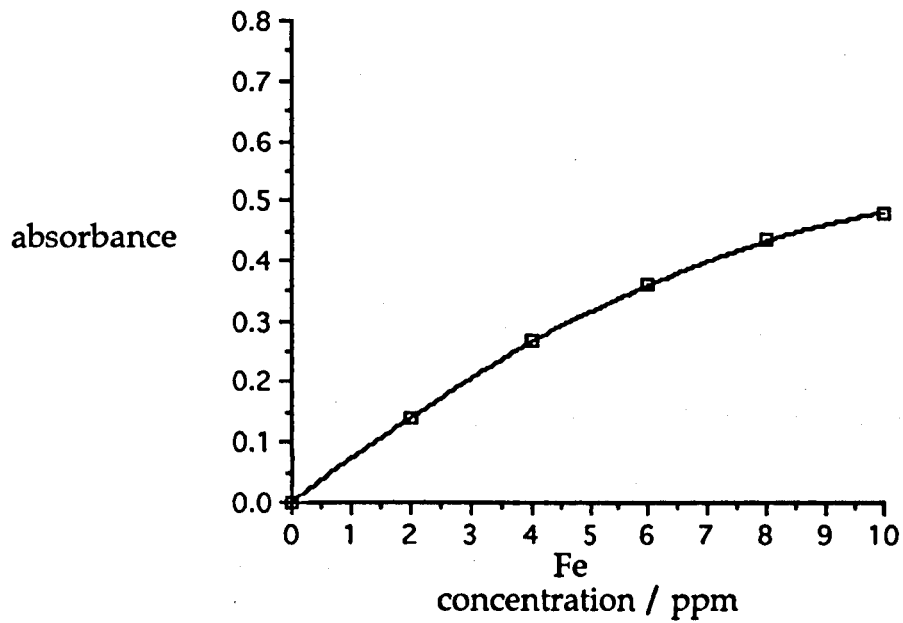
Hydrochloric acid (5ml, 12M) was quickly added to about 100mg of homogenised rock powder in a test tube. The acid was brought to the boil over 1 minute and then boiled for a further minute. The reaction was quenched with distilled water and transferred to a volumetric flask. The flask was made up to volume and shaken to mix the solution prior to filtration and analysis by atomic absorption spectrophotometry.

Standards were initially made containing 0, 2, 4, 6, 8 and 10ppm Fe with the same matrix of HCl as the samples. However, there appeared to be appreciable deviation from the linear correlation of concentration and absorbance (Beer Lambert Law) above concentrations exceeding 5ppm (Figure 3.12). 5ppm Fe was adopted as a working threshold value. Samples containing concentrations greater than this value were diluted accordingly to fit in the chosen range of between 0 and 5ppm Fe.

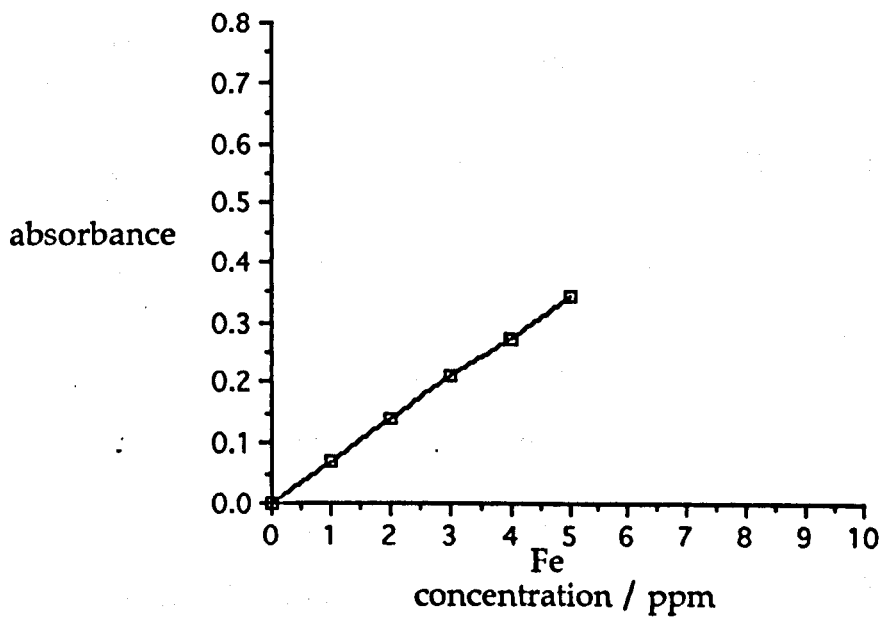
Mineral matrix effects were also considered. Standard additions of 0, 1, 2, 3, and 4 ppm Fe were added to aliquots of the extracted PM16 sample. The results are shown on Figure 3.13. There is good correlation between absorbance and concentration with no apparent effect from the inorganic mineral matrix.

The duration of both the pre-boil and boiling times was crucial in determining the amount of iron extracted from the samples (Table 3.13 and Figure 3.14).

Figure 3.12

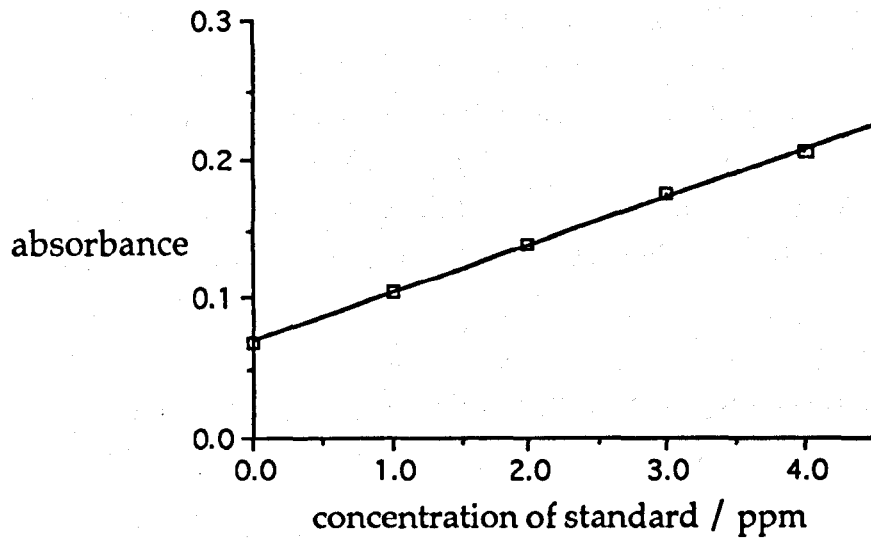


Non-linear relationship of concentration and absorbance for concentrations greater than 5ppm iron.



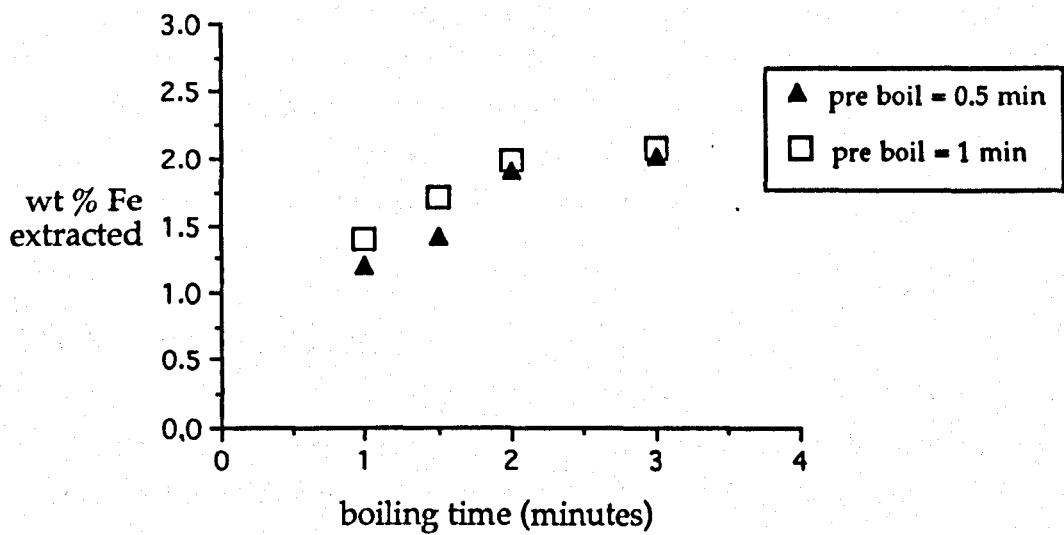
Linear relationship of concentration and absorbance for concentrations less than 5ppm iron.

Figure 3.13



Mineral matrix effects on iron absorbance.

Figure 3.14



Extractable iron relative to boiling times in hydrochloric acid.

The oxyhydroxides and some oxides react very quickly with the HCl, but with prolonged attack, minerals such as chlorite start to break down, as shown by Raiswell *et al.* (1994). For the reactive iron values to be used in the calculation of the degree of pyritisation parameter (DOP= pyrite Fe/{pyrite Fe + HCl extricable Fe}), values must be used with the same extraction procedure. In this study, the procedure quoted by Berner (1970) was adopted i.e. 1 minute pre-boil and 1 minute boiling of ~0.1g of the sample with HCl (5ml, 12N). A comparison of different extraction procedures is given in Leventhal and Taylor (1990).

The reproducibility of this method was found to be very good, providing that the boiling times were carefully adhered to, as shown by the results in Table 3.6.

A spectrophotometric method of determining iron was also attempted. This used 1,10-orthophenanthroline to complex with iron (II), to produce the orange-red complex  $[\text{Fe}(\text{Phen})_3]^{2+}$ . Hydroxylamine hydrochloride (10% aq) was used as a reducing agent to maintain iron in the +2 oxidation state. The maximum absorbance of the solutions was measured using a Philips UV-Vis spectrophotometer at a wavelength of 508 nm.

This method was found to be unsatisfactory as precision was worse than 5%. It is thought that organic matter within the samples creates interference with the complex formation and also absorbs light to a small extent in this region of the spectrum. Therefore the determination of iron was only performed using the atomic absorption technique described earlier.

## 3.10 X-ray Analysis

X-ray diffraction and X-ray fluorescence were used to determine the compositions of whole rock powders and mineral separates.

### 3.10.1 X-ray Diffraction (XRD)

X-ray diffraction analyses were performed on randomly oriented samples using a Philips PW 1840 unit with 35kV Cu  $k_{\alpha}$  radiation and PC-APD software. The samples were produced by smearing dense suspensions in acetone onto

**Table 3.14**

Sample	wt% Fe
PM 16	1.39
PM 16	1.38
PM 16	1.40
PM 16	1.42
PM 16	1.39
mean	1.40
$\sigma_{n-1}$	0.01

Reproducibility of the concentrated hydrochloric acid iron extraction technique.

glass slides and allowing the solvent to evaporate off. The rate of change of the incident angle was 1° per minute.

### **3.10.2 X-ray Fluorescence (XRF)**

Major element analysis was performed by X-ray fluorescence on a Philips BW 1400 XRF spectrometer. Samples were fused with LiBO<sub>4</sub> and the resulting glass cast to form a disc. A detailed description of this method is given by Padfield and Gray (1971).

## **3.11 Electron Microscopy**

### **3.11.1 Scanning Electron Microscope (SEM)**

Lloyd (1987) gives a good review of back scattered electron microscope techniques and sample preparations. A Camscan Series 4 SEM with an energy dispersive x-ray spectrometer spot analysis system was used during this study. In most cases a working distance of 21 mm and an accelerating voltage of 25kV was used to image polished samples with a conductive carbon coat.

### **3.11.2 Electron Microprobe**

A cameca SX-50 fitted with three wavelength dispersive spectrometers and a Link 10/55S energy dispersive system was used to perform electron microprobe analyses. The quoted error on the quantitative results is accurate to one decimal place. Typical running conditions were: accelerating voltage 15kV; count times 30 seconds; beam current 10nA.

The microprobe was also used to generate large scale  $k_{\alpha}$  X-ray maps of the cements within the septarian concretions studied.

## Chapter 4

# The Geochemistry of the Caton Shales

### 4.0 Introduction

This chapter presents an investigation into the diagenesis of a mud rich sequence from the Arnsbergian (Namurian) of Northern England. A section of the Lower Caton Shales was subjected to petrographic, geochemical and isotopic investigations with the aims of (i) clarifying the burial and diagenetic history; (ii) investigating the effects of weathering on a mud rich sequence.

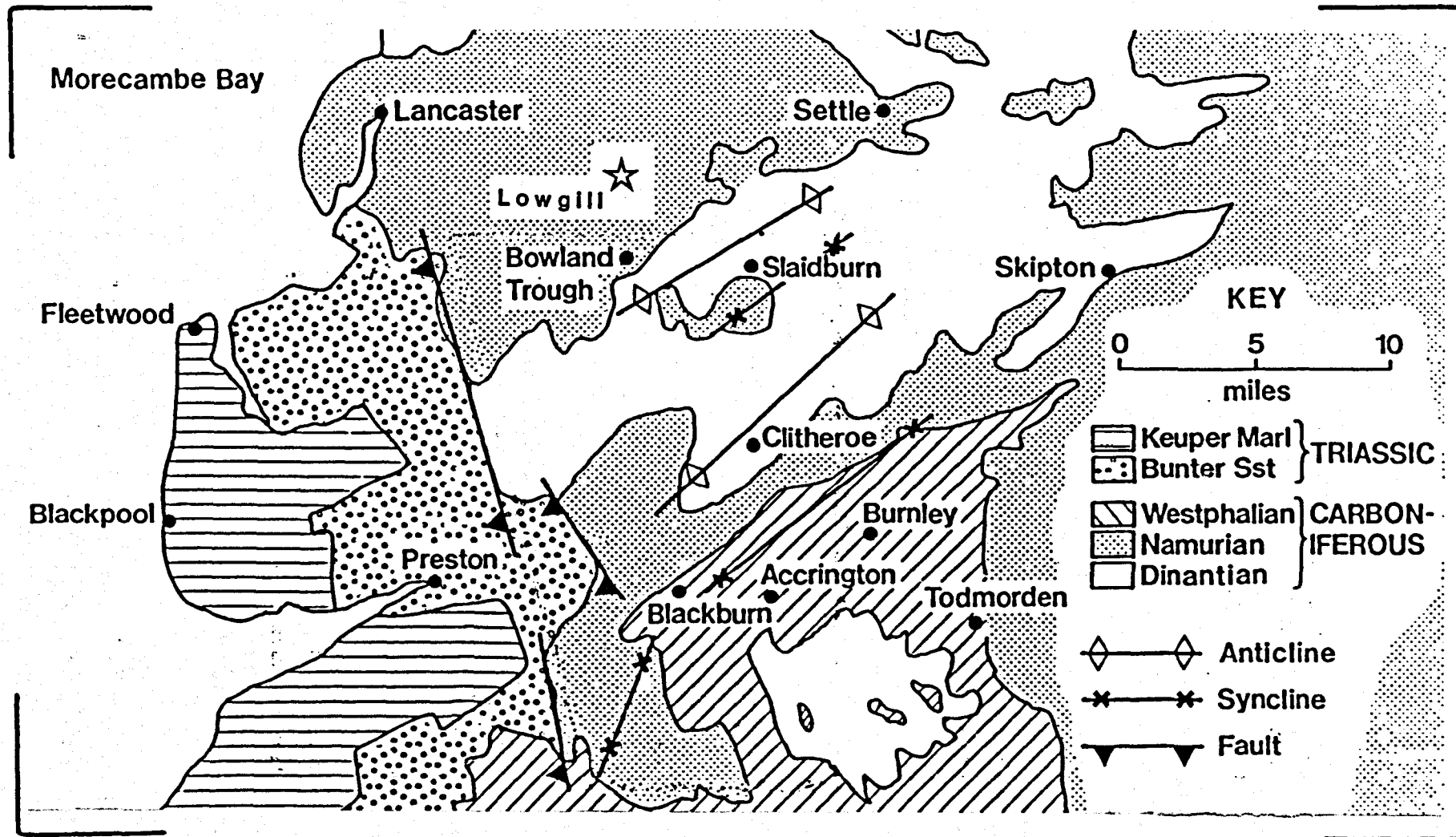
Septarian concretions form two dominant horizons in the 10m section chosen for study. Two generations of fracturing has taken place. An early calcite cement fills the first generation of septa and a later more complex cement fills the second. The central cavities of the concretions contain a dark brown bituminous material which post-dates the initial formation of the concretion matrix. The presence of hydrocarbon fluid inclusions in the latest generation of carbonate cement indicates migration of organic rich fluids at some time in the past, contemporaneous with late stage cementation. A detailed comparative study of the organic matter within the shale sequence and that found within the concretions was undertaken to establish the origin of the concretion hosted bitumen.

### 4.1 Geographical Location

Samples were collected from a stream section on the bank of a tributary of the River Hindburn near the village of Low Gill (GR. 3648 4638), 24km west of Settle. About 30m of gently dipping strata was exposed with a heavily weathered surface. Figure 4.1 shows a simplified geological map locating the region.



Figure 4.1



Simplified geological map of the region around Lowgill.

## 4.2 Geological Setting

The evolution of the Bowland Basin has been discussed by Gawthorpe (1987b). It forms one of the small sedimentary basins making up part of the Central Province of Northern England (Collinson, 1988), and is separated from the more slowly subsiding Askrigg Block to the north by the Craven Fault system. The Bowland Basin is a NE-SW trending sedimentary basin bounded by two main land masses, the Askrigg/Bowland High to the N and NW and the Central Pennine High to the SE. The control of sedimentation was dominated by the underlying structural units of the pre-Carboniferous.

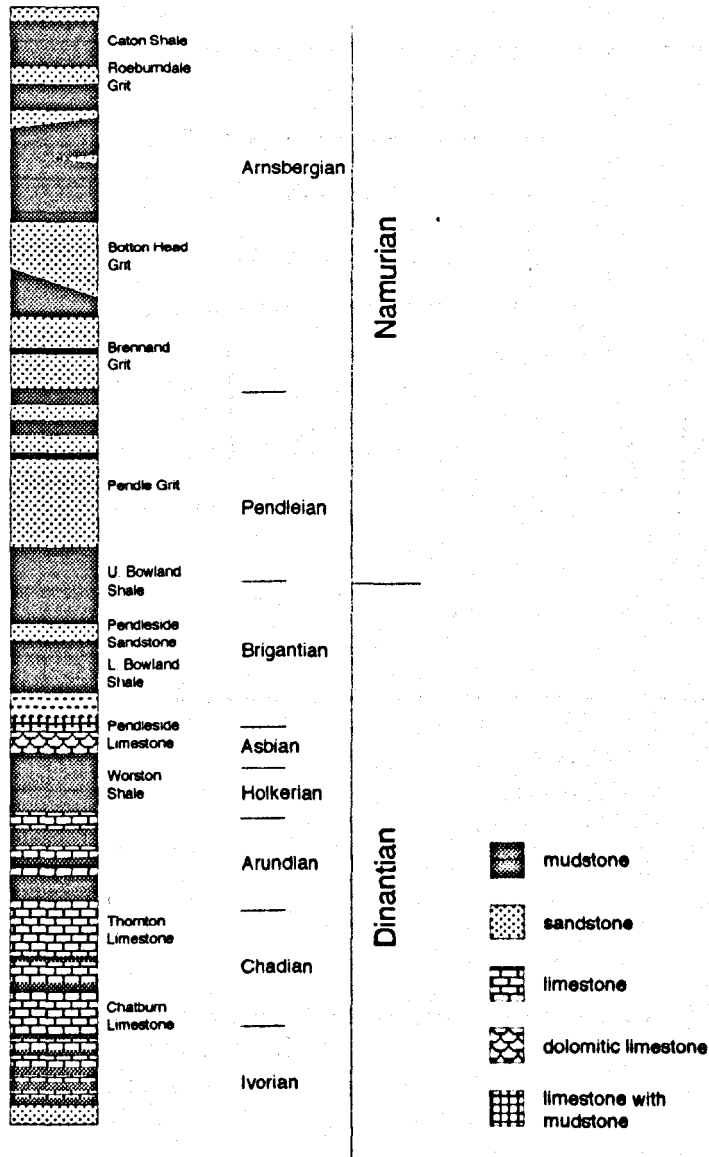
During the initial stages of subsidence, sedimentation was slow but continuous and bituminous limestones were deposited. The underlying basement became active in Chadian times causing extension of the basin which led to a subsequent transition of carbonate ramp to slope sedimentation (Gawthorpe 1986, 1987a). By the Holverian, a marine transgression culminated in the formation of clastic shale sequences. Carbonate supply had returned to the basin during Asbian times, but in the late Asbian/early Brigantian the margin of the northern basin began to break up due to a second phase of basement extension. This gave rise to shale sedimentation in the area. Figure 4.2 shows a generalised sedimentary sequence for the lower Carboniferous in the area of the Craven Basin.

## 4.3 Burial history of the shales

Apatite fission track analysis (AFTA) was performed on four sandstone samples through the auspices of British Gas and produced as Geotrack Report #381. All the AFTA data presented in this discussion is taken from that report. Two samples were from the Pendle Grit (Pendleian) and two from the Pendleside Sandstone (Brigantian). Although they were taken from stratigraphically lower units than the Caton Shales (Figure 4.2), they will record the maximum burial of the Namurian sediments on the flanks of the Bowland Basin.

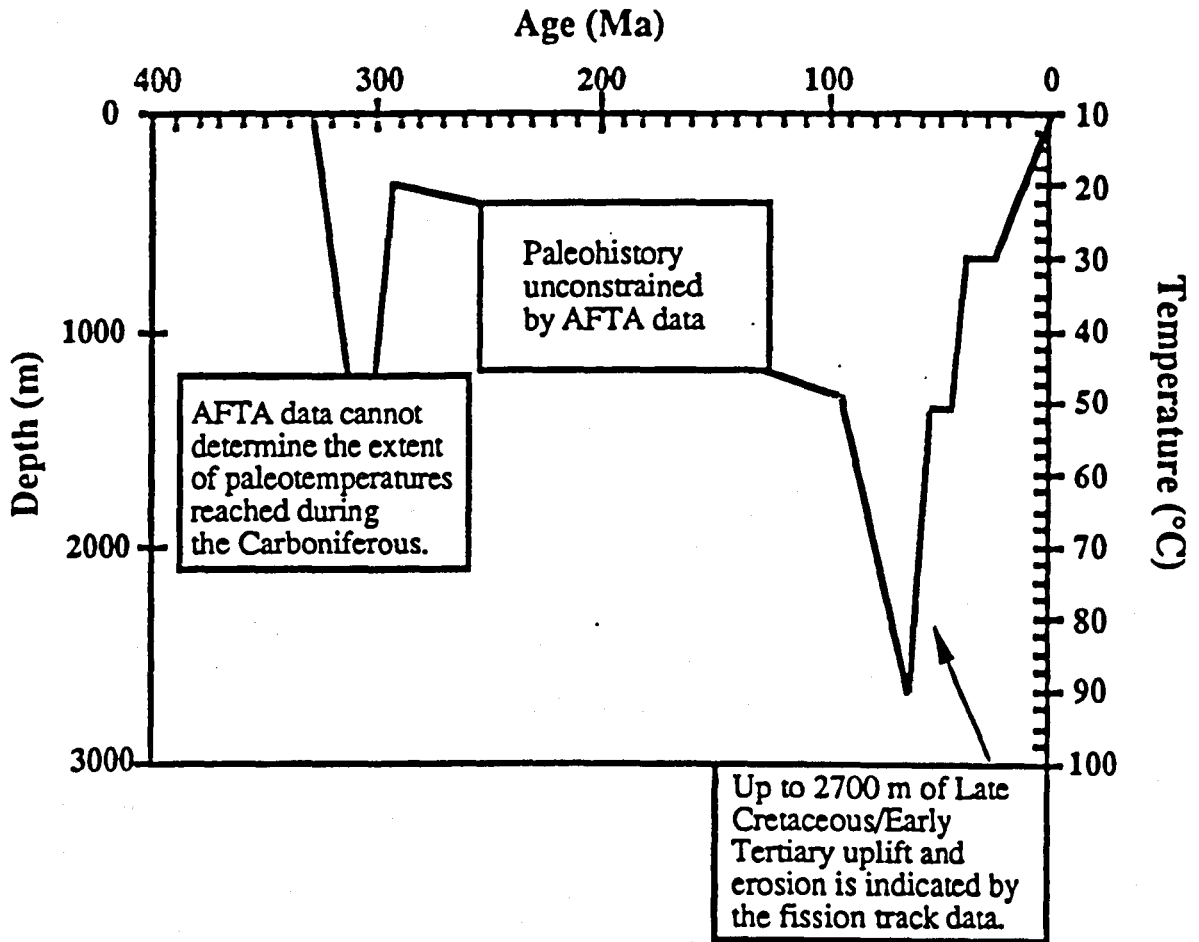
The AFTA data show a maximum palaeotemperature of  $\sim 90^{\circ}\text{C}$  during the late Cretaceous/Early Tertiary at about 65Ma. This data is in agreement with the findings of Lewis *et al.* (1992) who studied a much larger set of samples from

Figure 4.2



Generalised sedimentary sequence of the Lower Carboniferous sediments in the Craven Basin.

Figure 4.3



Schematic illustration of a thermal history interpretation of AFTA data from outcrop samples in the Bowland Basin.  
(After Lewis and Moore, 1992)

Northern England. Therefore assuming a typical geothermal gradient of 30°C per km, there must have been something in the order of 3km section removed by erosion. Although Hercynian uplift seems to be the dominant event in annealing apatite grains, heating during the Carboniferous cannot be neglected without taking  $R_0$  values into account. Predicted values of the vitrinite reflectance for the Pendlian/Brigantian samples are in the region of 0.57. They were found to be in the range 0.5 to 0.6, indicating that temperatures did not exceed 90°C during the Carboniferous. The thermal history interpretation of AFTA data has been reproduced from the Geotrack report and is shown in Figure 4.3.

## 4.4 Caton Shales

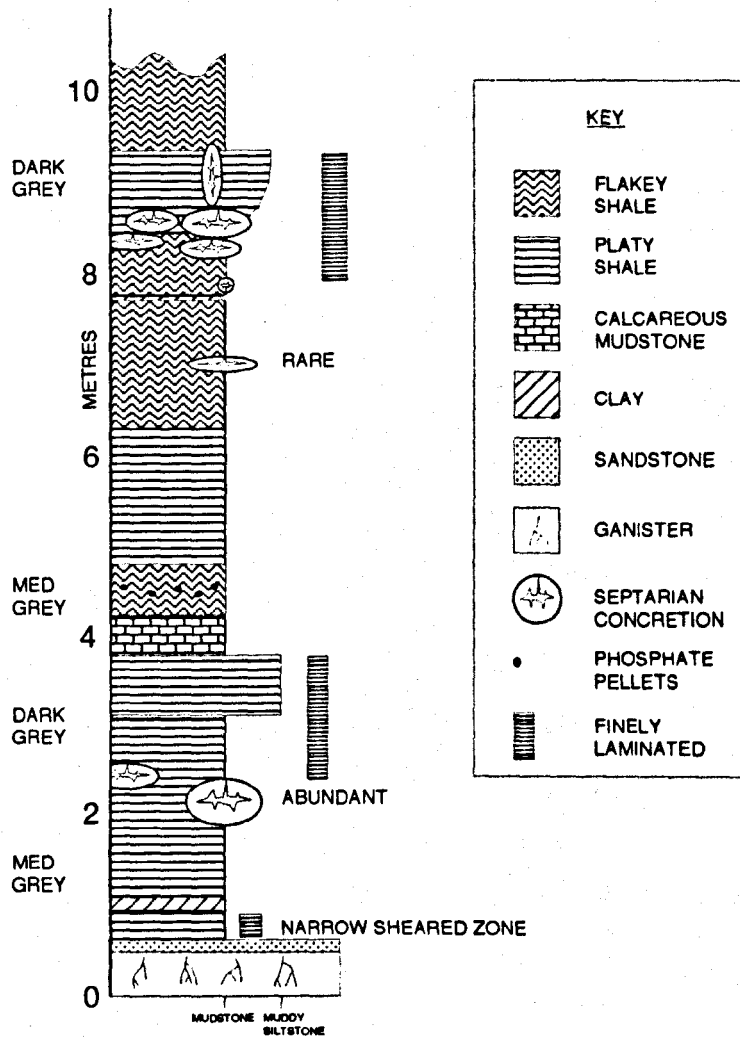
The Caton Shales ( $E_{2b}$ ) have been studied by a variety of authors, e.g. Bisat (1934), Hudson (1944), Slinger (1936) and Moseley (1952, 1956). The *Cravenocereatoides nitidus* Zone ( $E_{2b}$ ) was divided into 4 subzones by Hudson (1944) and later (1945) modified into 3 subzones (*Ct. bisati*, *Ct. nitidus*, *Ct. stellarum*) and was again modified by Moseley (1952).

The Caton Shales have been separated into two divisions, the Upper (*Ct. bisati* and *Ct. nitidus*) and the Lower (*Ct. holmesi* and ?*Ct. stellarum*). In this study, a section from the Lower Caton Shales (GR. 3648 4638) was investigated. The Lower Caton Shales lie conformably on the Roeburndale Grit (Moseley 1952, 1956) and contain bands of septarian concretions. About 10m of the sequence was studied in detail (Figure 4.4).

A ganister marks the base of the section which passes up through a mud rich sequence of fossiliferous shales. A dark muddy limestone occurs about 4 metres above the ganister and is thought to correlate with the limestone described by Holmes and Bisat (1925) and Moseley (1956) occurring approximately 11 feet above the Roeburndale Grit at Keasden Beck (GR. 3727 4645) and Kettles Beck (GR. 3729 4641).

Septarian concretions dominate two main zones within the sequence. Large (~70 cm) ovoid concretions occur at 1.5m and about 8m above the ganister. The concretions range in size and shape from: spheroidal (10cm diameter) through oblate spheres (long axis 50cm short axis 35cm) to discoidal (diameter 15cm, long axis 50cm). These concretions were ubiquitous along a 50cm wide band

Figure 4.4

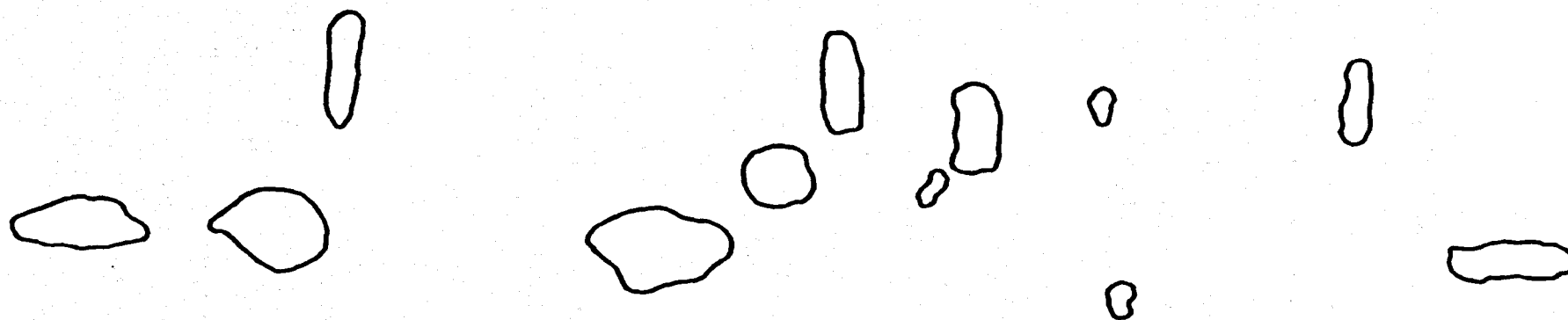


Sedimentary log of the Caton Shales at Lowgill.

Figure 4.5

NE

SW



Distribution of the concretions exposed laterally over approximately 6m of outcrop.  
The vertical concretions are more dominant in the upper horizon.

along the whole exposure. The distribution of the concretions is shown in Figure 4.5, and Enclosure 1.

## 4.5 Geochemistry of the sequence

The environmental conditions at the time of sediment deposition and the nature of organic matter input during deposition was established by a geochemical study of the sequence of the Caton Shales. Twenty 'fresh' samples of shale were collected at approximately equal intervals throughout the exposed section in addition to in situ measurements of the radioactivity of the sediments by gamma ray spectrometry (Table 4.1).

### 4.5.1 Radioactive characterisation of the Caton Shales

The total natural gamma-ray count was measured at twenty one sites along the stream section to determine the uranium content (ppm), thorium content (ppm) and  $^{40}\text{K}$  content (%K). The measurements were made according to the criteria of Myers and Wignall (1987) i.e. relatively fresh flat surfaces permanently saturated with water using the Exploranium detector. The precision of the measurements is thought to be better than 2% (Maynard, 1991) with a count time of 120 seconds.

The radioactivity measurements are plotted against height above the ganister (Figure 4.6). Several distinctive horizons can be picked out from this data.

#### 4.5.1.1 Ganister

The base of the sequence shows the lowest amount of radioactivity at 7.7ur (1ur or unit of radioelement concentration is equivalent to 1ppm U, 2.1ppm Th or 0.38% K). It exhibits approximately half the total radioactivity of the shale making up the rest of the sequence. The low concentrations of clay minerals and K-feldspars in the ganister account for low  $^{40}\text{K}$  concentrations and the oxic environment in which the sandstone was deposited would inhibit the fixation of uranium, as it is highly mobile in such conditions.

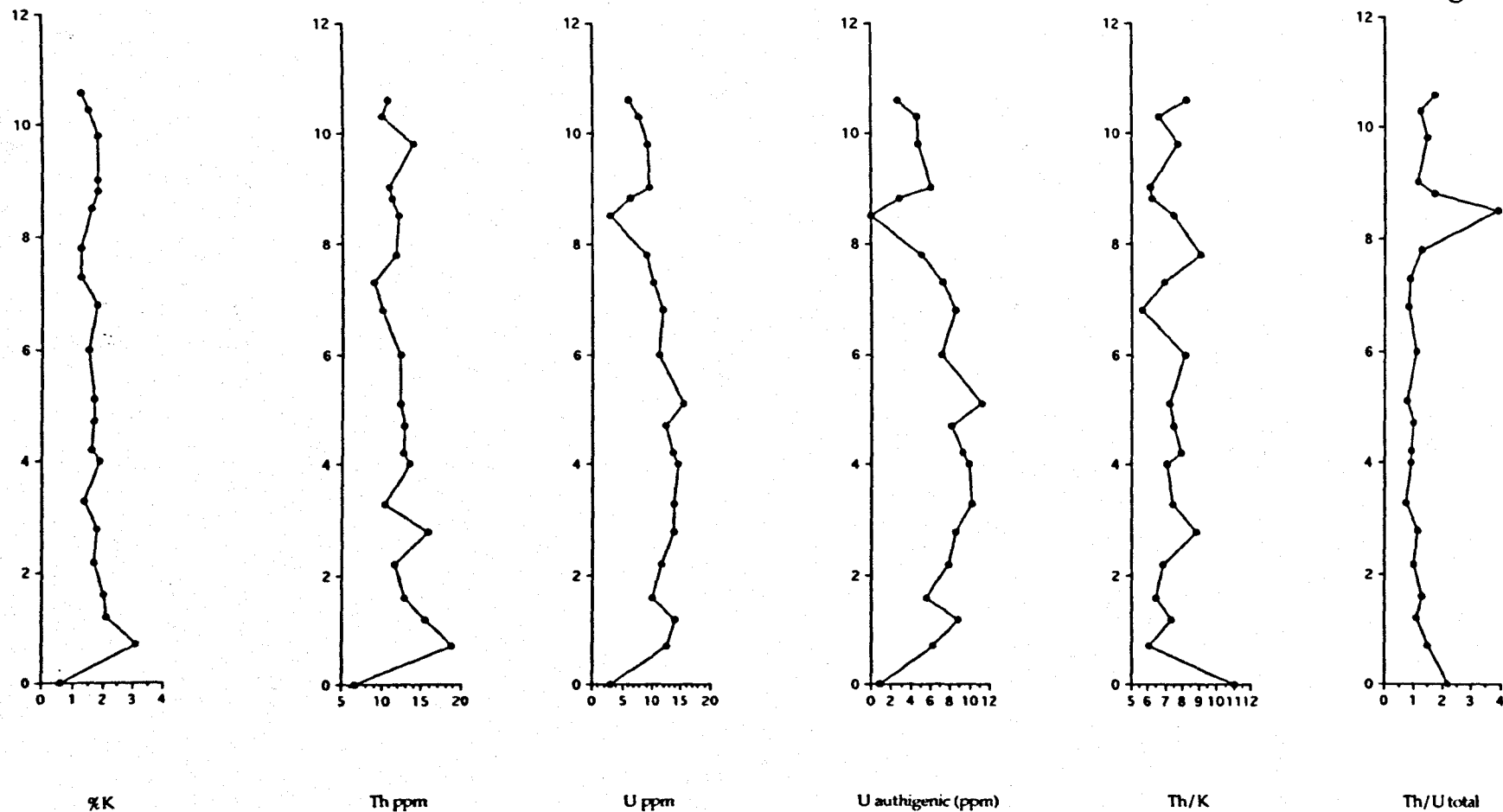


Table 4.1

Sample	Depth (m)	%K	U ppm	Th ppm	Th/U	K/Th	U auth
LG1	10.6	1.3	6.2	10.7	1.7	8.2	2.6
LG2	10.3	1.5	8.0	10.0	1.3	6.7	4.7
LG3	9.8	1.8	9.4	14.0	1.5	7.8	4.7
LG4	9.0	1.8	9.6	11.0	1.1	6.1	5.9
LG6	8.8	1.8	6.5	11.2	1.7	6.2	2.8
LG7	8.5	1.6	3.1	12.1	3.9	7.6	0.0
LG8	7.8	1.3	9.0	11.8	1.3	9.1	5.1
LG9	7.3	1.3	10.2	9.0	0.9	6.9	7.2
LG10	6.8	1.8	11.9	10.1	0.8	5.6	8.5
LG11	6.0	1.5	11.2	12.3	1.1	8.2	7.1
LG12	5.1	1.7	15.3	12.4	0.8	7.3	11.2
LG13	4.7	1.7	12.4	12.8	1.0	7.5	8.1
LG14	4.2	1.6	13.5	12.7	0.9	7.9	9.3
LG15	4.0	1.9	14.4	13.5	0.9	7.1	9.9
LG16	3.3	1.4	13.7	10.4	0.8	7.4	10.2
LG17	2.8	1.8	13.8	15.9	1.2	8.8	8.5
LG18	2.2	1.7	11.7	11.7	1.0	6.9	7.8
LG19	1.6	2.0	9.9	12.9	1.3	6.5	5.6
LG20	1.2	2.1	13.9	15.5	1.1	7.4	8.7
LG21	0.7	3.1	12.6	18.8	1.5	6.1	6.3
LG22	0.0	0.6	3.0	6.6	2.2	11.0	0.8

Radiogeochemical data measured at 21 sites along the Lowgill stream section of the Caton Shales. The depth is a measure of the distance above the ganister, which marks the base of the sequence.

Figure 4.6



Log of potassium, thorium and uranium for the Caton Shale sequence exposed at Lowgill. The vertical axis is the distance (measured in metres) above the top of the ganister.

#### 4.5.1.2 Shale

The shale sequence shows a marked difference in radioactivity. Table 4.2 shows a summary of the mud rock radio geochemistry. The potassium values vary by a factor of 2.5 throughout the shale sequence (1.3 to 3.10%, median 1.7%). There is a positive correlation between Th and K (Figure 4.7), indicating that indeed the clay fraction contains most of the K and Th. The more dense accessory minerals, the K-feldspars and micas, which carry K and Th will be deposited before the clay fraction. The ratio of Th/K remains relatively constant throughout the sequence, decreasing in the horizons with concretions present. This indicates increased potassium input at times of concretion growth possibly due to a change from a montmorillinite clay to a more illitic clay (illite has similar U and Th contents to montmorillinite but much higher concentrations of potassium (Table 4.3)). An alternative for the increased potassium concentrations within the concretionary horizons can be explained by diagenetic potassium migration.

The uranium curve for the sequence represents a mixture of authigenic and detrital sources. Authigenic uranium tends to be fixed in more anoxic, reducing conditions where organic matter fixes uranium into the sediment by the reduction of the uranyl ion. The authigenic uranium content was estimated using the method of Myers and Wignall (1987). However, uranium can be remobilised in oxidising environments and removed from the system. Therefore care must be taken when interpreting uranium concentrations within shales.

The cross plot of organic carbon with uranium (Figure 4.8) gives a weak positive correlation, indicating that organic matter partly controlled the precipitation of authigenic uranium. It is interesting to note that the concentration of authigenic uranium increases in the horizon with the phosphate pellets. This is probably due to preferential absorption of uranium by the phosphate. The authigenic uranium content decreases at the two dominant concretionary horizons (at 2m and 8.3m above the ganister). The Th/U indicates that the stratigraphically lower decrease in uranium is not significant. However, the upper concretionary horizon shows a marked depletion in uranium. This is probably associated with a later oxidising fluid remobilising the uranium as discussed later in this chapter.

**Table 4.2**

Clay	%K	U ppm	Th ppm
Illite	6.7	1.5	10 - 25
Glauconite	4.5	10	?
Montmorillinite	1.6	2-5	10 - 24
Chlorite	0.1	?	3-5
Kaolinite	0.3	1.5 - 9	6 - 42

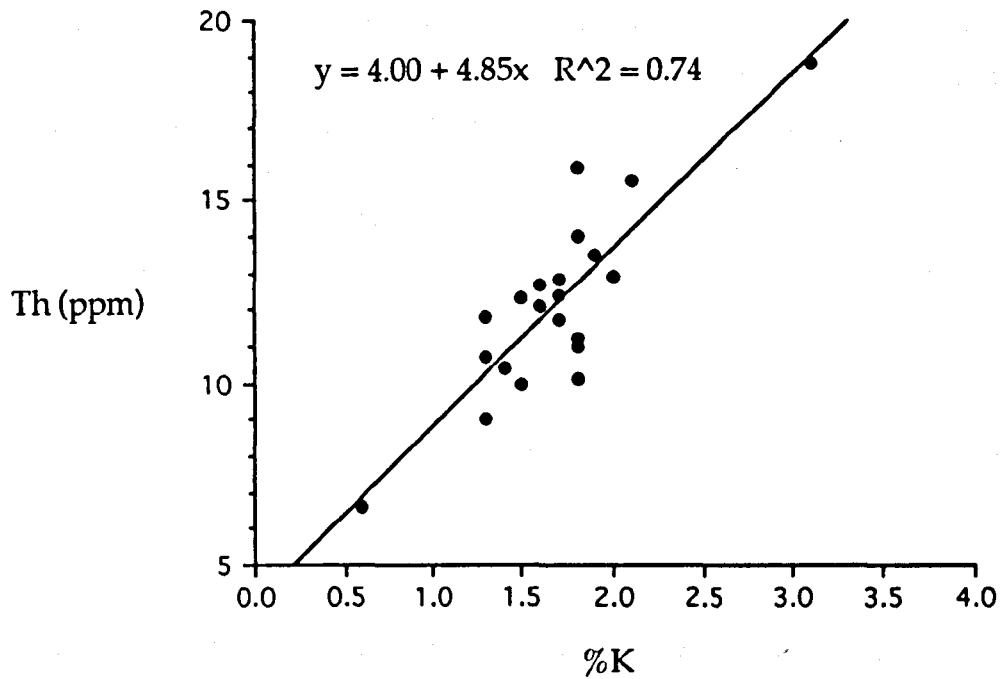
Distribution of U, Th and K within a selection of clay minerals (after Myers and Wignall, 1987).

**Table 4.3**

	range	mean	median	$\sigma_{n-1}$
U ppm	3.1 - 15.3	10.81	11.45	3.16
Th ppm	9 - 18.8	12.44	12.20	2.30
%K	1.3 - 3.1	1.73	1.70	0.39
U <sub>auth</sub> ppm	0.0 - 9.9	5.75	6.13	2.96

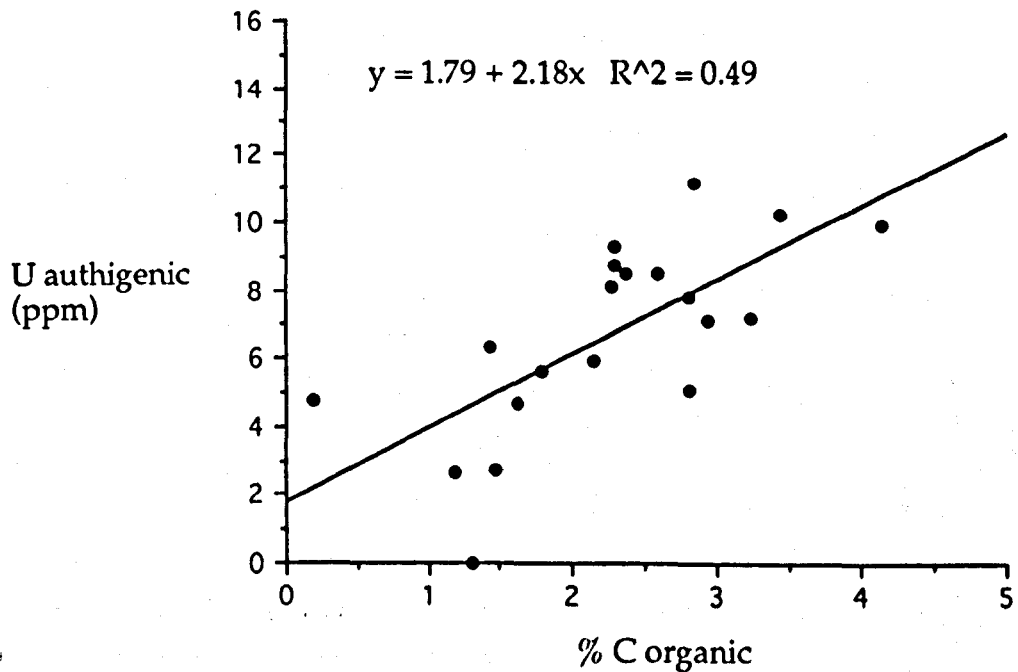
Distribution of U, Th and K within the Caton Shales (excluding the ganister).

Figure 4.7



Relationship between thorium and potassium in the Caton Shales as measured by gamma ray spectrometry.

Figure 4.8



Relationship between authigenic uranium and organic carbon in the Caton Shales.

### 4.5.2 Carbon, Iron, Sulphur relationships

Berner and Raiswell (1983) noted a positive linear relationship between organic carbon and reduced sulphur in modern sediments deposited in oxygenated marine bottom waters. They used the C/S ratio to distinguish marine from non marine rocks (Berner and Raiswell, 1984) because marine rocks have lower C/S values (~2.8) than fresh water sediments (C/S >10). Table 4.4 and Figure 4.9 show the C/S ratio for the Caton Shales. The carbon sulphur cross plot shows a nearly uniform pyrite sulphur content of  $0.2 \pm 0.1\%$ .

It would seem that, based upon the C/S ratios, some of the shale samples have fresh water signals i.e. high C/S. This is clearly not the case as the palaeontology of the sequence shows assemblages typical of marine conditions (P. Wignall, pers comm.).

There is no obvious relationship between the degree of pyritisation and organic carbon content (Figure 4.10). The DOP values are all very low <0.35 indicating oxygenated bottom water conditions at the time of deposition (Raiswell *et al.*, 1988).

Simple mass balance calculations show that the total sulphur content (mean 2.20%) in the shales is much greater than the reduced pyritic sulphur (mean 0.21%), in Table 4.4. There is negligible organically bound sulphur (see later) and a maximum of 0.3% elemental sulphur. Therefore the remaining sulphur must be in the form of sulphate (mean 1.82% by difference). This suggests some form of oxidative process converting diagenetically formed pyrite into oxidised and partially oxidised sulphur species which have not been lost from the system.

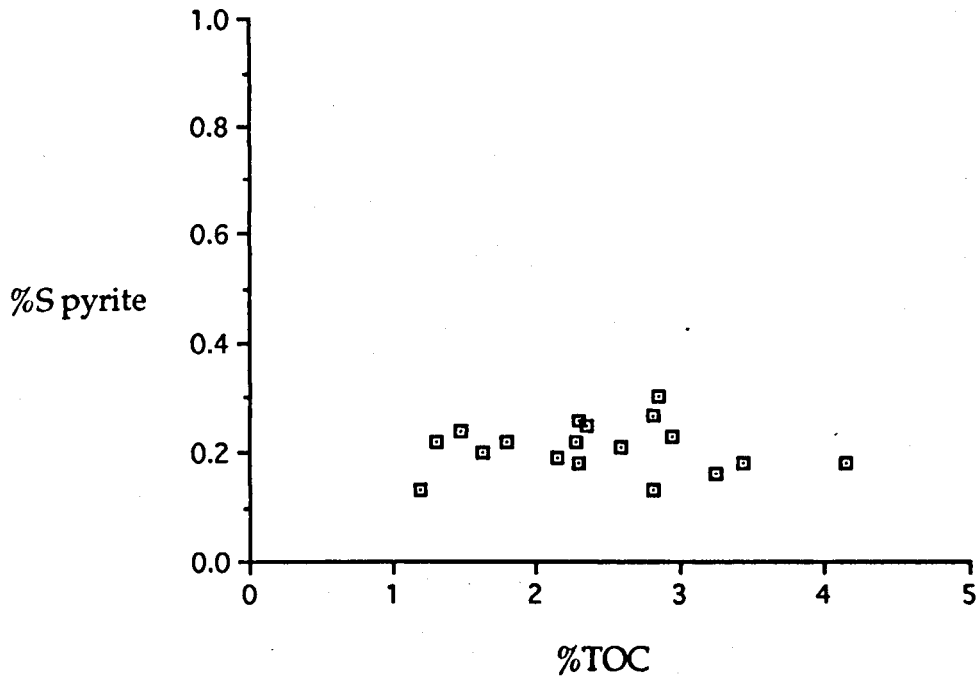
Pyrite weathering was modelled on computer to establish its effects on the C/S ratio. Assuming organic carbon content remains constant, sulphur was removed systematically from the pyrite pool. The results are shown in Figure 4.11. Shales with low organic carbon contents (<0.5%) and high pyrite sulphur (>3.0%) show little change in their C/S ratios up to approximately 90% sulphur loss. However, shales with high organic carbon and low reduced sulphur show marked changes in C/S at low levels of pyrite weathering. Therefore, in reality it is likely that organic carbon will not be constant throughout weathering processes. The relative rates of loss of the two components (pyrite sulphur and organic carbon) must therefore be considered.

Table 4.4

Sample	% TOC	%Stotal	%Spyrite	%Fe acid soluble	%Fepyrrite	%FeR	DOP
LG1	1.19	1.18	0.13	2.11	0.11	2.22	0.05
LG2	1.63	1.71	0.20	0.91	0.17	1.09	0.16
LG3	1.79	2.23	0.22	0.63	0.19	0.82	0.23
LG4	2.15	1.73	0.19	0.33	0.16	0.50	0.33
LG6	1.47	2.24	0.24	1.85	0.21	2.06	0.10
LG7	1.30	1.20	0.22	3.13	0.19	3.32	0.06
LG8	2.82	1.46	0.13	2.96	0.11	3.07	0.04
LG9	3.25	2.49	0.16	1.37	0.14	1.51	0.09
LG10	2.36	1.79	0.25	2.33	0.22	2.55	0.09
LG11	2.94	2.04	0.23	1.37	0.20	1.57	0.13
LG12	2.85	1.30	0.30	2.25	0.26	2.51	0.10
LG13	2.27	1.70	0.22	1.30	0.19	1.49	0.13
LG14	2.29	3.02	0.18	1.52	0.16	1.67	0.09
LG15	4.14	2.88	0.18	2.16	0.16	2.32	0.07
LG16	3.44	4.99	0.18	1.65	0.16	1.81	0.09
LG17	2.59	2.47	0.21	0.76	0.18	0.94	0.20
LG18	2.81	3.30	0.27	0.72	0.24	0.96	0.25
LG19	1.79			0.62			
LG20	2.29		0.26	0.66	0.23	0.89	0.26
LG21	1.43			0.49			

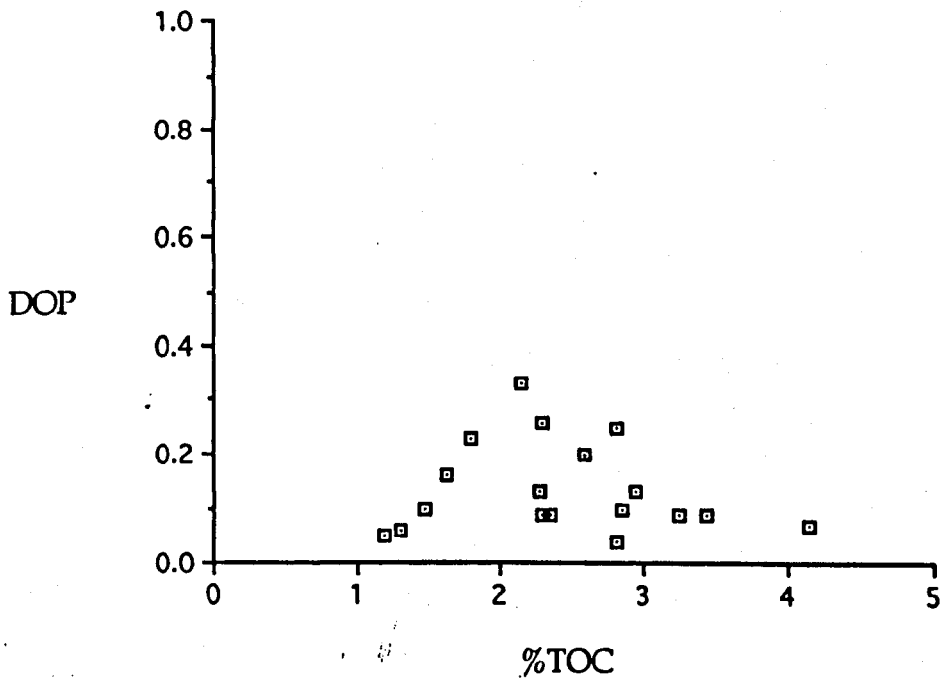
Summary of the inorganic geochemical data for the Caton Shales.

Figure 4.9



C/S relationship for the Caton Shales.  
There is little variation in either the TOC or the content of reduced sulphur.

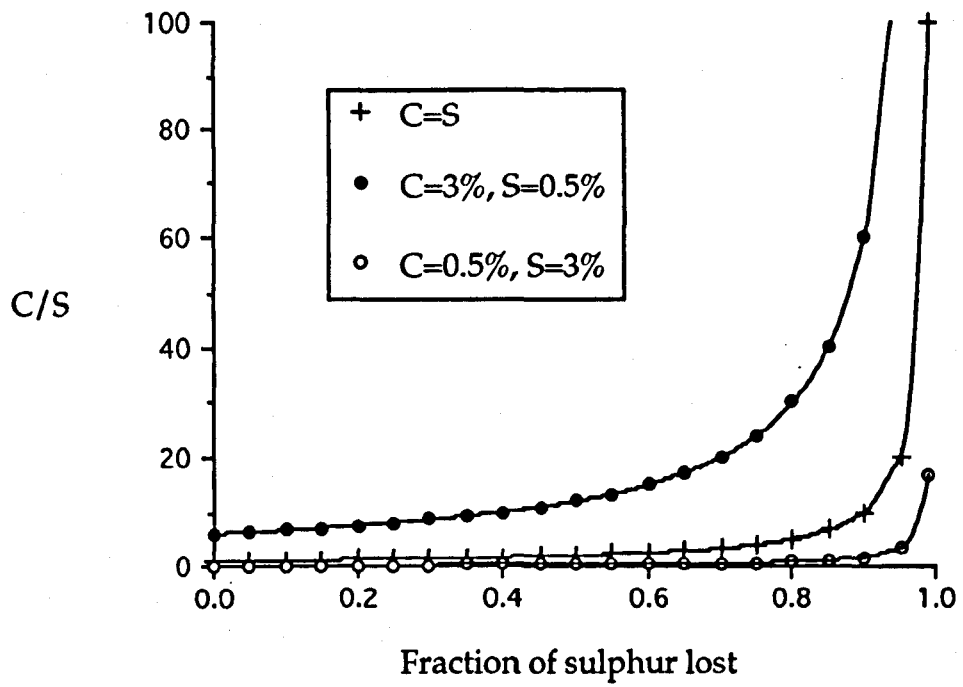
Figure 4.10



The relationship between degree of pyritisation (DOP) and organic carbon.  
All the DOP values are low (<0.35) indicating oxygenated bottom water conditions at the time of deposition.



Figure 4.11



Model values for C/S ratios.  
See text for discussion.

The samples collected in the field were carefully selected to obtain what was thought to be fresh material i.e. the outer 30cm of rock was removed prior to collection. The C/S data reveals that the samples have undergone significant weathering and obviously the DOP data will also be affected. The weathering of the Caton Shales together with other shales will be discussed in detail in Chapter 6.

A second suite of shale samples was collected from just one location. Additional care was taken to avoid weathering by first removing approximately 1.0m of shale from the surface then, using a core drill, samples were taken up to a depth of 20cm into the newly exposed surface (Tables 4.5 and 4.6). The samples were taken from the concretion bearing horizon approximately 8m above the ganister.

The total sulphur values for the drilled samples were greater than the pyrite sulphur in all cases, but the measured elemental sulphur content gave very good mass balance with a two component system i.e. the total sulphur equals elemental sulphur plus pyrite sulphur. Elemental sulphur accounts for no more than 10% of the total sulphur in most cases. However the sample 5.5BO had much higher elemental sulphur contents (0.8% S<sup>0</sup> vs. a total sulphur of 3.06%). There is a shortfall of 0.3% S which is presumed to be sulphate sulphur, indicating some weathering of pyrite. This sample has the lowest C/S ratio (0.62).

The carbon sulphur ratios are all very similar as would be expected from samples collected within the same sedimentary horizon (mean 0.69,  $\sigma_{n-1}$  0.07). These values are much lower than the expected C/S ratio of 1.6 (assuming normal marine conditions) as predicted from Raiswell and Berner (1987). The data suggest that there has been minor pyrite sulphur oxidation, but there has also been significant loss of organic carbon from the shale samples during maturation, depressing the C/S ratio significantly.

The minor weathering of the pyrite suggests that the DOP values for the drilled samples should be more reliable than those samples collected without extensive removal of surface layers of rock. The DOP values (mean 0.71,  $\sigma_{n-1}$  0.06) indicate restricted bottom water conditions. The sedimentological evidence to confirm this prediction is limited. There is evidence of lamination with little trace of bioturbation, which may indicate less oxygenated bottom waters; however the field observations are far from conclusive.

Table 4.5

Sample	% Total S	% Reduced S	% Pyrite	% Fe acid sol	% Reactive iron	DOP	$\delta^{34}\text{S}$ pyrite
3DR	1.63	1.53	2.85	1.40	4.25	0.67	-20.4
41DR	2.01	1.85	3.47	1.47	4.94	0.70	-17.6
42DR	2.00	1.90	3.55	1.76	5.31	0.67	-17.3
5BD	2.08	2.05	3.83	1.17	4.99	0.77	-17.5
5.5BO	3.06	2.00	3.75	1.11	4.86	0.77	-17.5
5.5BD	2.12	1.67	3.12	0.98	4.10	0.76	-16.9
5.5D	2.00	1.81	3.39	1.12	4.51	0.75	-18.0
5O	1.96	1.72	3.22	1.23	4.45	0.72	-18.7
3O	1.78	1.55	2.90	1.89	4.79	0.60	-20.2
3M	1.99	1.56	2.93	1.38	4.31	0.68	-20.2
3D	2.15	1.93	3.61	1.42	5.03	0.72	-18.7

Summary of geochemical data from the Caton Shales. Samples taken at least 1m into the outcrop.

Table 4.6

Sample	TOC	% EOM	S1	S2	S3	PI	HI	OI	T max
41DR	1.20	0.14	0.69	1.01	0.61	0.41	84.2	50.8	439
42DR	1.26	0.13	0.82	1.18	0.67	0.41	93.7	53.2	438
5BD	1.30	0.14	0.68	1.36	0.66	0.33	104.6	50.8	441
5.5BO	1.24	0.14	0.99	1.35	0.66	0.42	108.9	53.2	437
5.5BD	1.23	0.14	0.38	1.11	0.67	0.26	90.2	54.5	436
5.5D	1.20	0.11	0.51	1.47	0.58	0.26	122.5	48.3	441
5O	1.20	0.07	0.66	1.34	0.70	0.33	111.7	58.3	443
3O	1.26	0.07	0.32	0.97	0.69	0.25	77.0	54.8	438
3M	1.24	0.13	0.69	1.37	0.73	0.34	110.5	58.9	440
3D	1.28	0.15	0.67	1.26	0.70	0.35	98.4	54.7	439

Rock Eval data for shale samples from the Caton Shales. Samples taken at least 1m into the outcrop.  
(EOM=Extractable Organic Matter, PI=Production Index, HI=Hydrogen Index, OI=Oxygen Index)

### 4.5.3 Organic matter within the Caton Shales

The kerogen and bitumen from the Caton Shales were analysed for chemical and stable isotope (carbon) composition.

#### 4.5.3.1 Kerogen

Visual determination of the main kerogen components was performed on a single sample from the concretionary horizon 8.3m above the ganister (Table 4.7). The dominant component was vitrinitic material including non-fluorescent amorphous kerogen (three quarters of total kerogen). This is the main component of a terrestrially derived kerogen dominated by higher plants.

Hydrogen (HI) and oxygen indices (OI) plotted on a van Krevelen type diagram (Figure 4.12) also indicate that the kerogen is of Type III composition. Maturity profiles plotted on a HI- $T_{\max}$  cross plot suggest that the Caton Shales have a vitrinite reflectance in the order of 0.8 (Figure 4.13). Table 4.8 shows the results of optical measurements on a kerogen isolate confirming a vitrinite reflectance of 0.84 together with other optical maturity parameters.

#### 4.5.3.2 Bitumen

The elemental composition of the average content of bitumen is given in Table 4.9, together with the elemental composition of chemically separated fractions (asphaltenes, aliphatic, aromatic and polar fractions). The relative proportions of the fractions of the bitumen are given in Table 4.10. The deviation from the mass balance is an indication of the cumulative errors associated with the various separation and analytical steps. Nitrogen in particular does not balance, probably because of the difficulty in measuring low concentrations in such an organic rich matrix by GC.

The asphaltene fraction is particularly rich in hetero-atoms, especially S and O, whereas the aliphatic fraction, as expected, contains low amounts of N, S and O relative to the bitumen. Gas chromatography and gas chromatography-mass spectrometry have been used to determine molecular characteristics of the soluble organic matter (Figures 4.14 and 4.15). A summary of these results is given in Table 4.11.

**Table 4.7**

Kerogen Data		
%Sapropel	% Vitrinite	% Inertinite
10	75*	15

Relative proportions of the maceral groups isolated from kerogen from the Caton Shales.

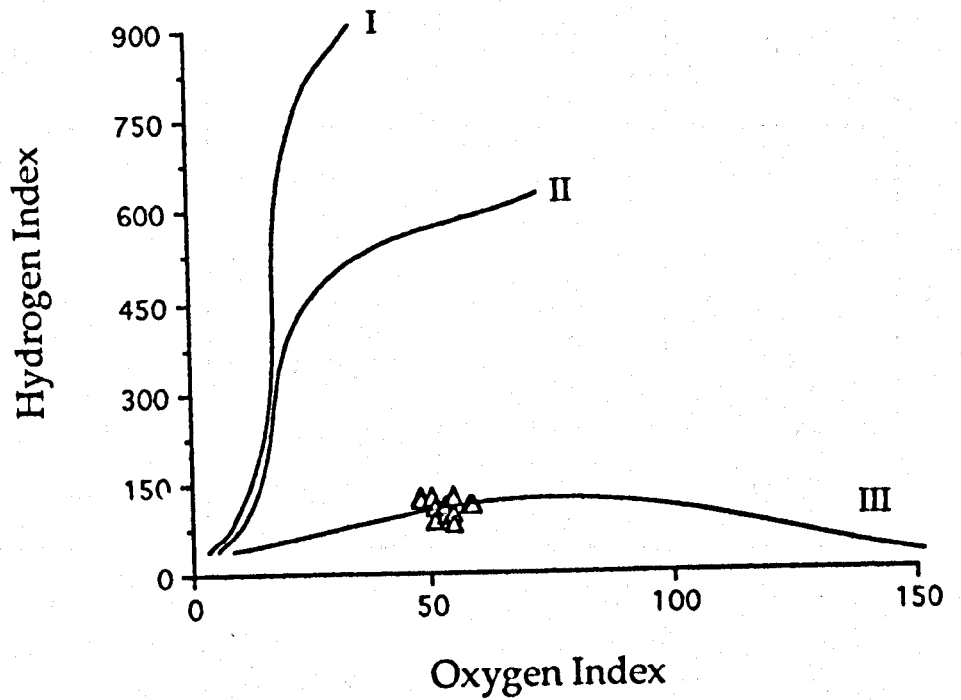
\*Mainly degraded (including "Non-Fluorescent Amorphous" kerogen)

**Table 4.8**

Vitrinite Reflectance	Spore colouration	Spore fluorescence
0.84 (n=16)	6.0 (n=9)	4-5 (n=9)

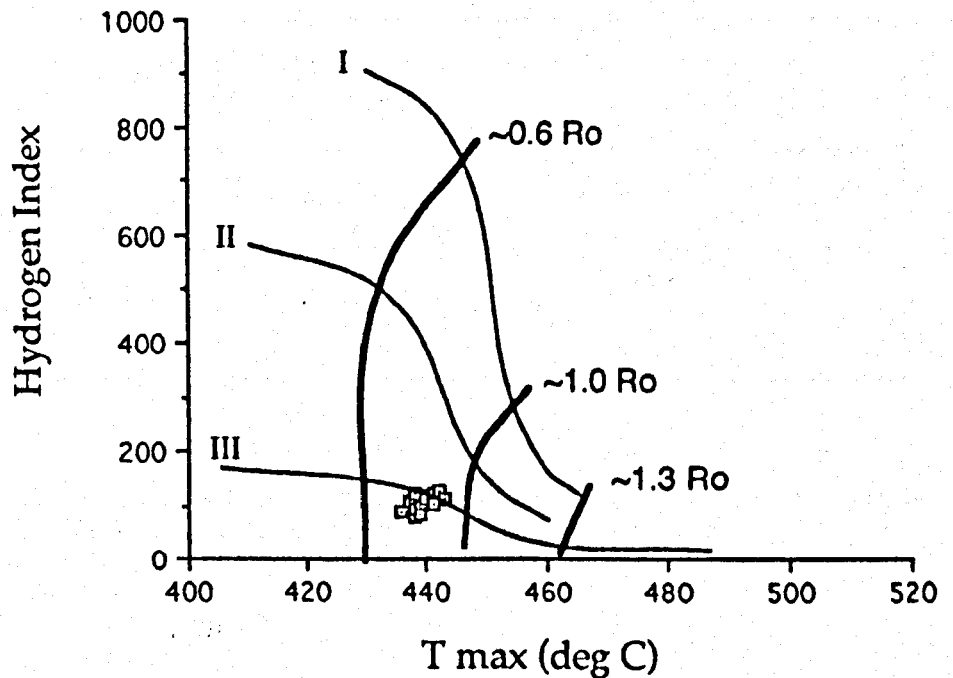
Thermal maturity parameters as measured optically on organic matter from within the Caton Shales.

Figure 4.12



A van Krevelen 'type' plot of Rock Eval parameters (Oxygen Index and Hydrogen Index) to indicate the kerogen type of the Caton Shales. The data cluster around the Type III line.

Figure 4.13



A van Krevelen 'type' plot (based on Rock Eval data) contoured with iso-maturity lines, indicating a vitrinite reflectance of approximately 0.8.

**Table 4.9**

	%C	%H	%N	%S & %O*
Bitumen	80.37	10.21	1.34	8.08
Asphaltene	68.51	6.60	2.75	22.14
Aliphatic	83.69	12.82	2.14	1.35
Aromatic	83.18	8.51	5.95	2.36
Polar	80.40	5.29	0.74	13.57

Average chemical compositions of the bitumen and fractions of the bitumen extracted from the Caton Shales.

\*Calculated by difference.

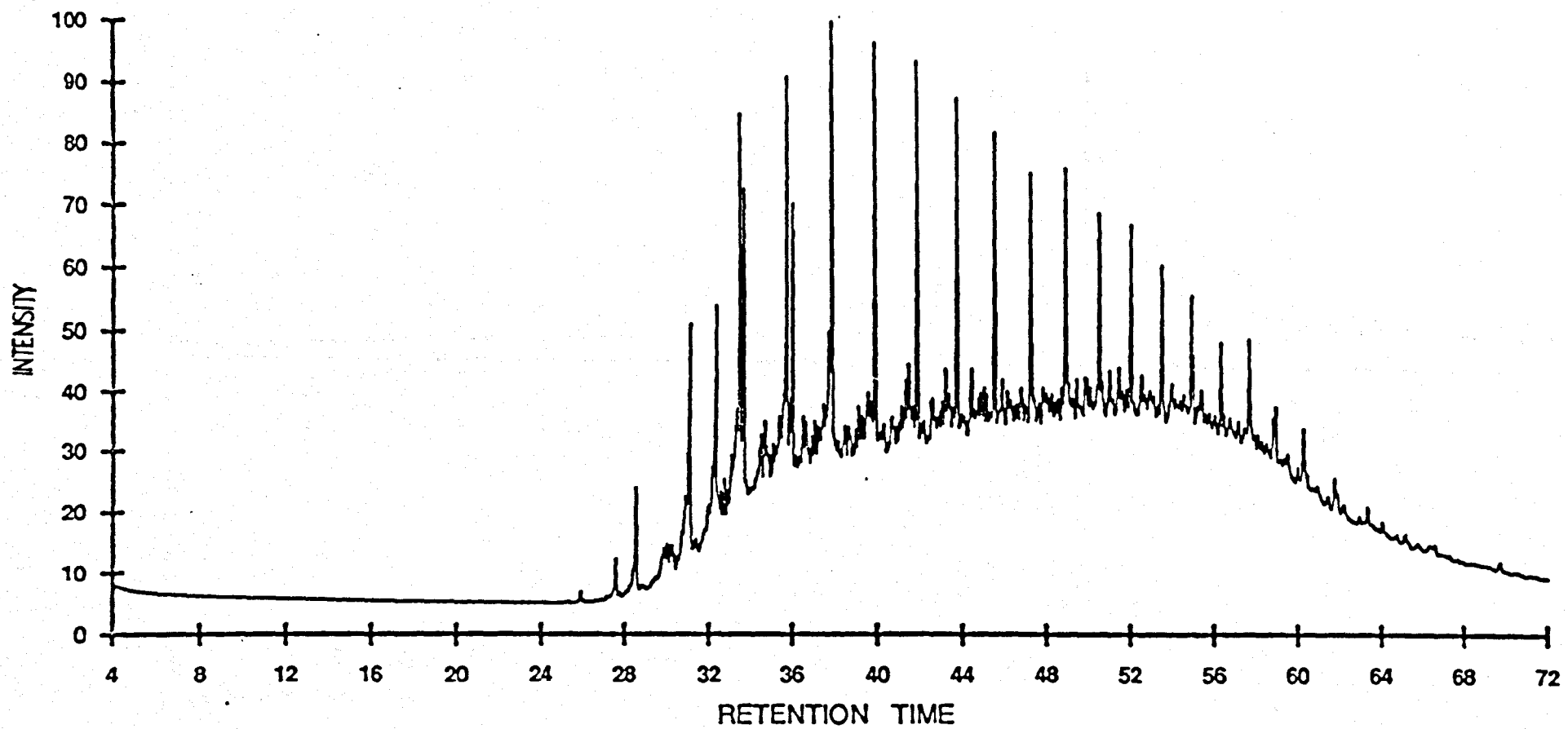
**Table 4.10**

	% Asphaltene	% Aliphatic	% Aromatic	% Polar
oil	46.8	31.3	12.9	9.0
bitumen	39.3	19.3	15.0	26.4

Average composition of the soluble organic matter from the Caton Shales and from within the septarian concretions as "oil".

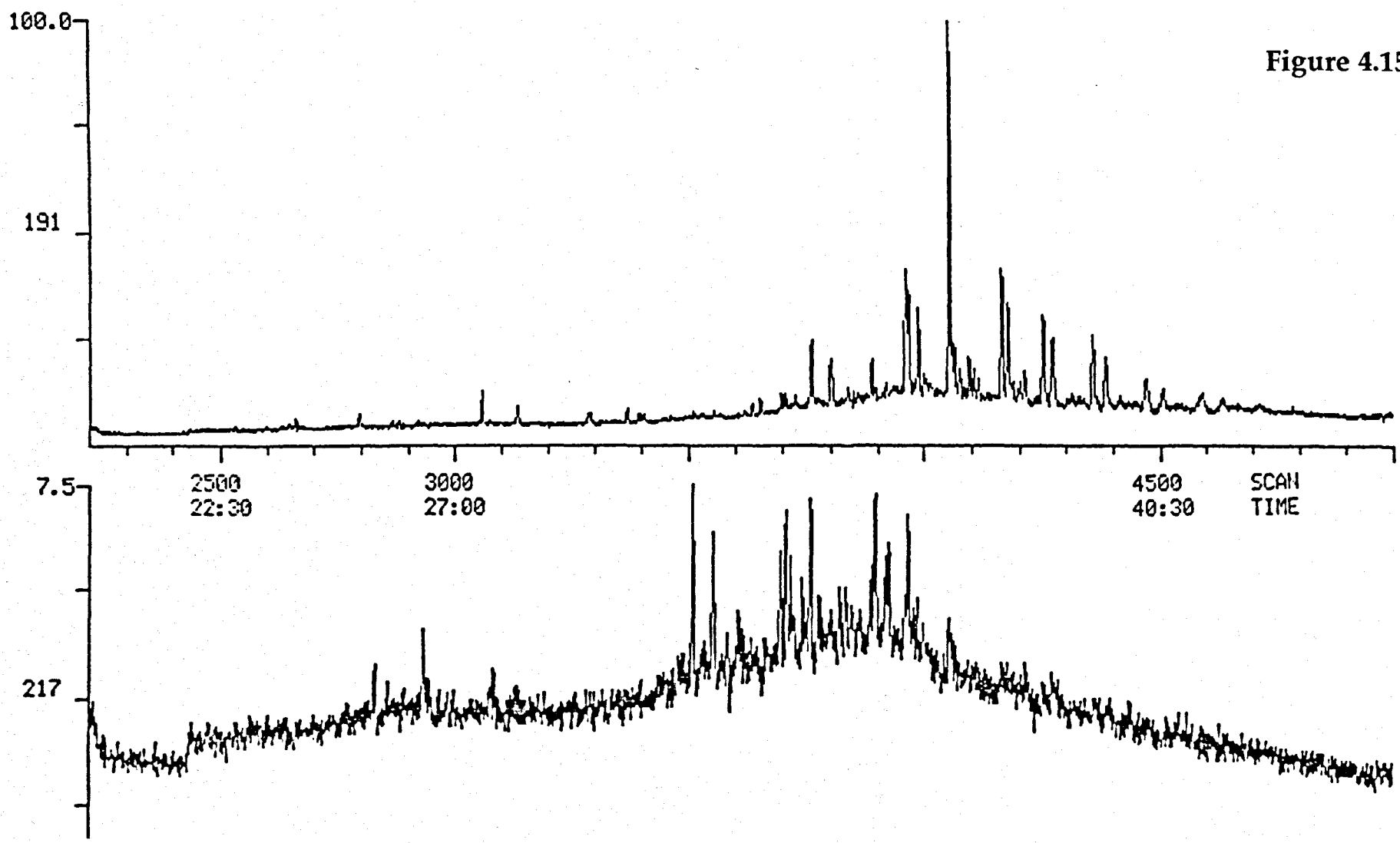


Figure 4.14



GC trace for extracted shale.

Figure 4.15



GC-MS trace for extracted shale (m/e 191 and m/e 217).

**Table 4.11**

Molecular parameter	Shale	Oil
CPI	1.00	1.17
Pr/Ph	0.94	0.87
Pr/nC-17	1.02	6.43
Ph/nC-18	0.70	3.74
Sterane (20S/20S+20R)	0.49	0.54

Summary of molecular parameters measured using GC and GC-MS techniques on the aliphatic fractions, separated from the soluble organic matter.

Although the kerogen is Type III, the CPI (carbon preference index) is 1.00. A CPI greater than 1 would be expected, given that the principal organic component has been derived from higher land plants. However maturation effects are known to decrease the proportion of odd relative to even alkanes, so that a CPI of 1 may result from maturation effects here (vitrinite reflectance of 0.84).

The pristane/phytane ratio is close to unity, providing little information about the redox conditions during early diagenesis. The isoprenoids pristane and phytane (normalised to nC-17 and nC-18 respectively) indicate conflicting biodegradation interpretations. The Ph/nC-18 ratio is less than 1 showing a preferential degradation of nC-18 characteristic of maturation processes, but the Pr/nC-17 is slightly greater than 1 (1.02) suggesting some loss of n-alkanes by moderate biodegradation.

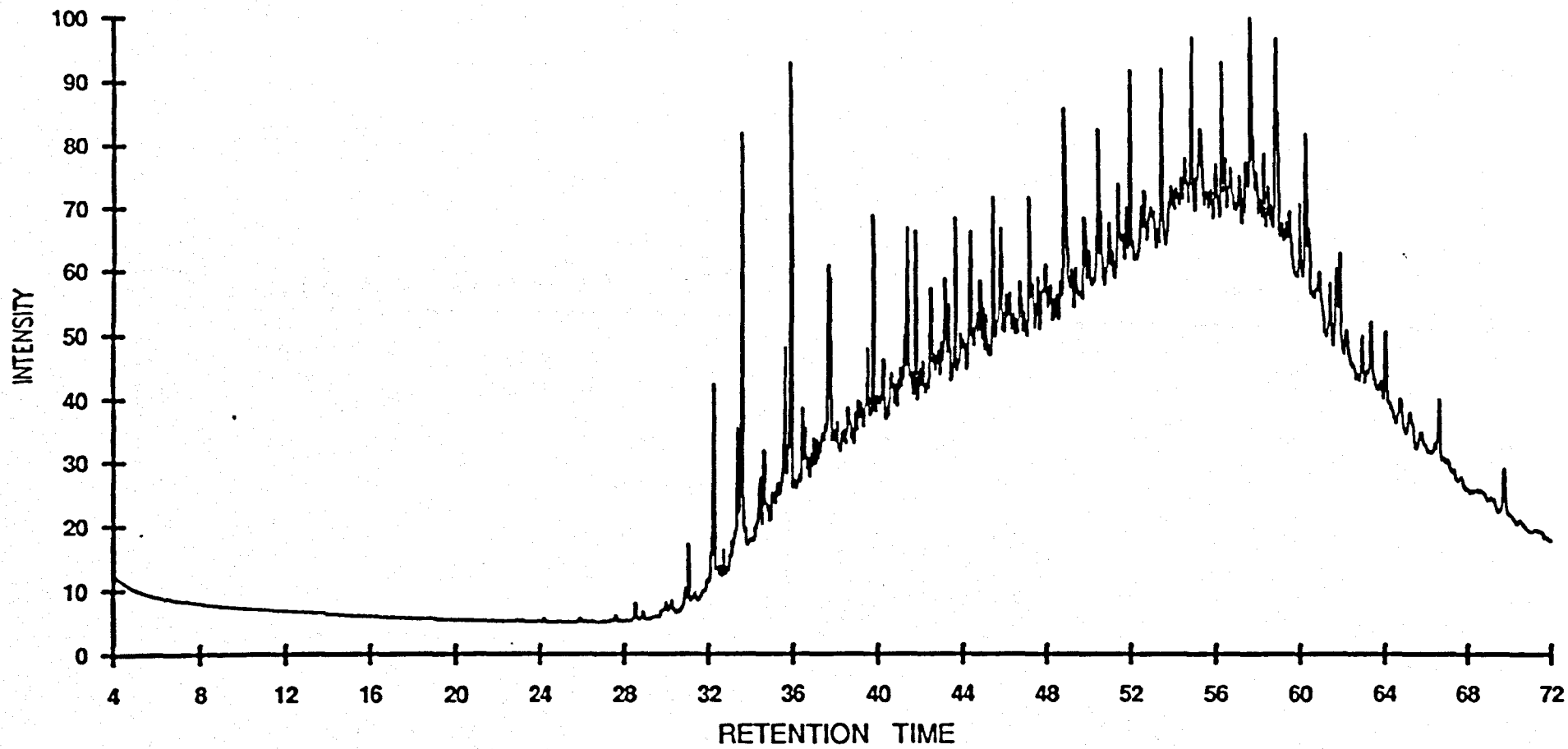
Samples from the oil contained within some of the septarian concretions were also analysed by GC and GC-MS to obtain selected biomarker ratios (Figures 4.16 and 4.17, Table 4.11). The odd over even n-alkanes and the GC traces suggest that the oil is less mature than the shale in which the concretion occurs. The oil also appears to be biodegraded to a greater extent relative to the host shale given the sizes of the unresolved humps in the GC trace. However the m/e 177 scan did not show any indication of demethylated hopanes, which were expected given the large UCM (unresolved complex mixture), indicating the possibility of a different source of organic matter.

The steranes (m/e 217; see 2.9.4 and Figures 4.15 and 4.17) in the oil sample show a 20S/(20S+20R) ratio of 0.54 where as the shale shows a less mature ratio of 0.49. There also appears to be more C28 steranes in the concretion oil. The triterpane (m/e 191 Figures 4.15 and 4.17) appear similar. From the data the precise origin of the 'oil' contained within the concretions cannot be established. However, the results point to it being locally derived, with minor alteration by intense microbial activity.

#### 4.5.3.3 Organic carbon isotopes

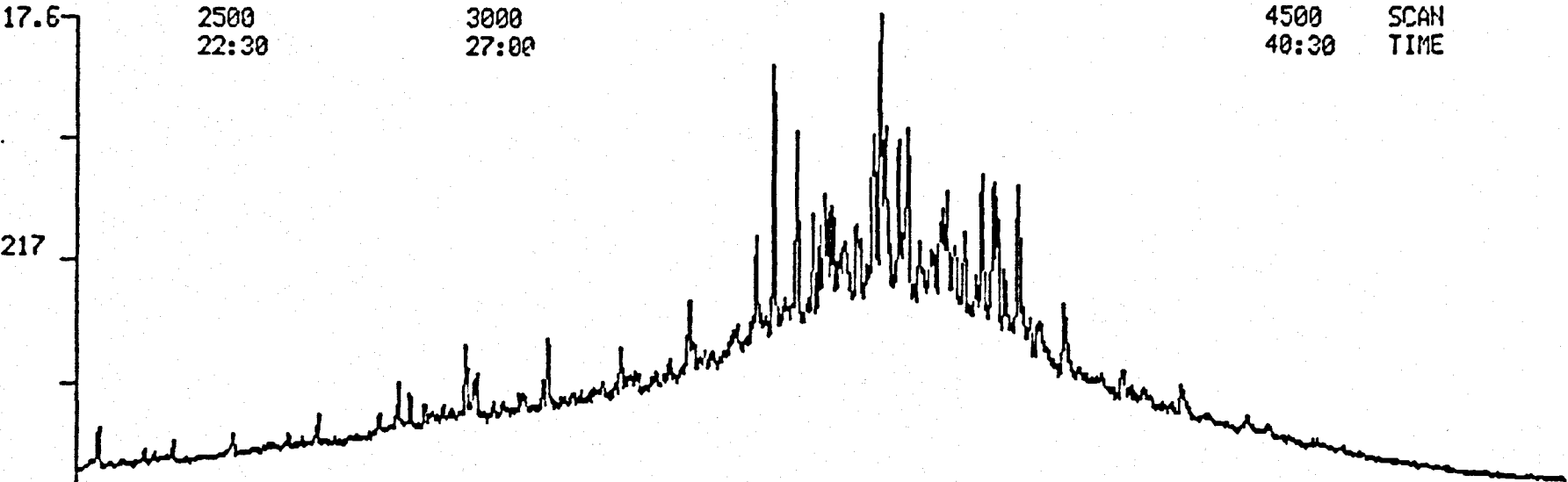
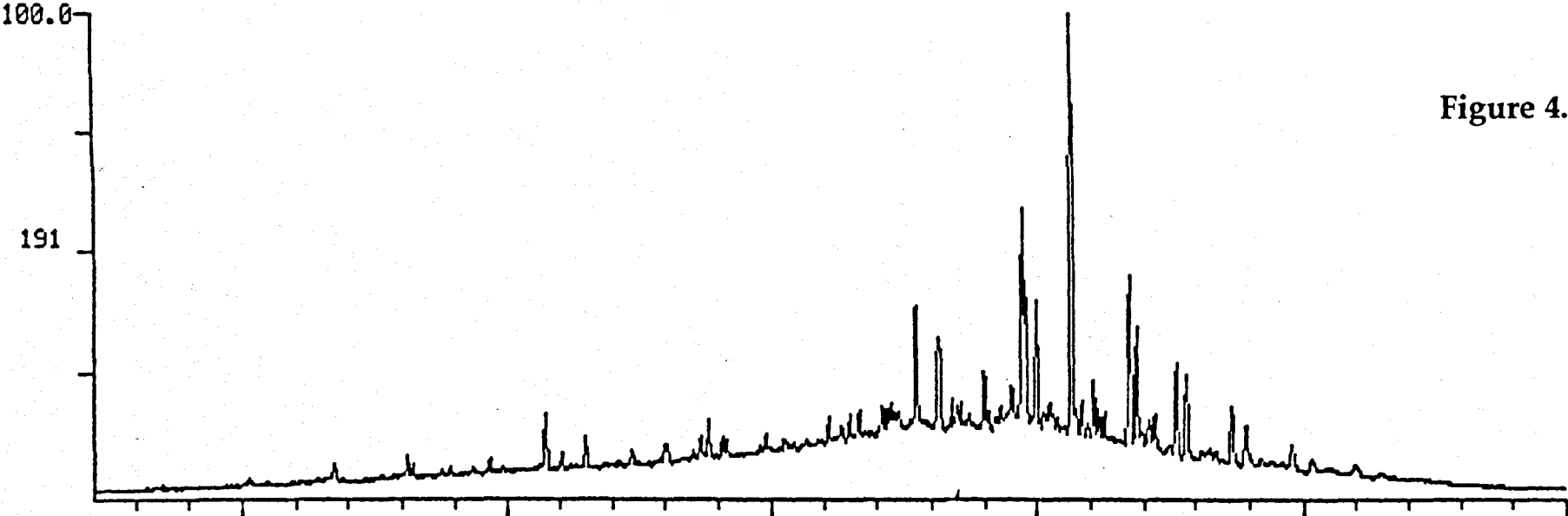
The  $\delta^{13}\text{C}$  for a selection of bitumens extracted from the Caton Shales are shown in Table 4.12. The mean bitumen value is  $-27.53 \pm 0.47\text{‰}$  and the mean for the concretion oil is  $27.71 \pm 0.06\text{‰}$ . Terrestrial organic matter typically has a

Figure 4.16



GC trace for concretion "oil".

Figure 4.17



GC-MS trace for concretion "oil" (m/e 191 and m/e 217).

Table 4.12

Sample	$\delta^{13}\text{C}$ organic carbon
LG1	-27.97
LG2	-27.82
LG3	-27.55
LG4	-27.81
LG6	-27.72
LG8	-27.36
LG10	-27.14
LG12	-27.07
LG18	-28.28
LG20	-27.48
LG21	-26.64
Concretion Oil	-27.75
	-27.67

$\delta^{13}\text{C}$  values for the organic carbon in the bitumens (LG) and the concretion oil.

$\delta^{13}\text{C}$  of  $-27\text{‰}$  providing further evidence of a higher land plant derived organic component to the Caton Shales. The 'oil' within the concretions appears to have the same type of precursor material.

#### 4.6 Origins of carbonate concretions

Concretions (localised masses of carbonate cementation) are found in both marine and non-marine argillaceous and arenaceous sediments from the Cambrian (e.g. Raiswell, 1970) throughout the geological record.

The timing of concretionary growth was a major focus of early researchers e.g. Tarr (1921), Tomkiewf (1927) and Weeks (1957). Together with more recent studies e.g. Raiswell (1971), Oertel and Curtis (1972), Raiswell (1976), Astin and Scotchman (1988) and Al-Biatty, (1990) it was recognised that the distortion of host sediment laminae around the concretion indicated that the formation of the concretions must be early during diagenesis. Estimates of the sediment porosity can be obtained using the assumptions of Lippmann (1955) and Raiswell (1971) who suggested that the pore spaces within the host sediment are passively filled by carbonate cement. Thus the volume of carbonate will reflect the porosity of the sediment. However, textural studies must also be taken into account when porosity estimates are used to establish the time of concretion formation. Feistner (1989) has demonstrated the existence of displacive/replacive textures within concretions thus rendering porosity estimates as only approximate.

Fossil preservation within concretion matrices also indicate an early formation. Early diagenetic cementation will prevent distortion of fossils from compaction by the overlying sediments. Other features preserved in concretions e.g. faecal pellets (Gautier and Claypool, 1984) have also been used as evidence of early formation of concretions.

Oertel and Curtis (1972) noted that in some concretions, clay minerals are oriented radially in a progressive "centre-to-outside" distribution. They interpreted this to be evidence of a long period of growth of the concretions, as compaction alters the position of the clay minerals with time.

Organic matter decomposition and carbonate precipitation have most recently been reviewed by Canfield and Raiswell (1991). The nature of organic matter



dissimilatory reactions is dependant on the nature of the oxidant (either dissolved oxygen, sulphate, or oxidised detrital matter) and the organic matter (reducing agent). A succession of reactions can be recognised during early diagenesis which alters the carbonate saturation state of pore waters through organic carbon oxidation. Hence the precipitation of carbonate (calcite, dolomite, siderite or rhodocrosite) either as individual minerals or as mixtures will reflect the alkalinity generated from the microbial decay of organic matter. Both the anion and stable isotopic composition of the concretionary cements record the pore water chemistry at the time of formation (Hudson, 1978; Coleman and Raiswell, 1981; Marshall, 1982; Boles *et al.*, 1985; Curtis *et al.*, 1986; Astin and Scotchman, 1988; Scotchman, 1988; Al-Biatty, 1990).

#### 4.6.1 Timing and growth of the concretions

##### 4.6.1.1 Porosity

Raiswell (1971) estimated the porosity of the uncompacted sediment to establish the depth at which concretions were formed. Assuming that concretionary cement passively fills pore space, the amount of cement within the concretion is a measure of the porosity of the sediment at the time of precipitation. Useful porosity is defined as:

$$\text{useful porosity, } \phi = \frac{\text{volume of interconnected water}}{\text{volume of total sediment}}$$

Given that an average composition of the concretionary matrix comprises of 83% CaCO<sub>3</sub>, the porosity can be calculated. The composition of the carbonate free residue is shown in Table 4.13.

On a mass balance approximation, the density of the residue is approximately equal to that of calcite (2.71 gcm<sup>-3</sup>). Thus the porosity can be approximated to the weight percent of calcite cement expressed as a fraction i.e. 0.83. This value indicates concretion formation at very shallow depths, near to the sediment water interface.

**Table 4.13**

Mineral	% abundance	density / gcm <sup>-3</sup>	density of component/gcm <sup>-3</sup>
Illite	40	2.75	1.1
Quartz	15	2.65	0.4
Kaolinite	25	2.55	0.6
Pyrite	2	4.90	0.1
Chlorite & Muscovite	10	2.70	0.3
Others	8	? assumed 2.7	0.2
total			2.7

Mineral abundance in the carbonate free residue of concretion matrix material.

**Table 4. 14**

v / cm yr <sup>1</sup>	x / cm
0.0001	3.1x10 <sup>6</sup>
0.001	3.1x10 <sup>5</sup>
0.01	3.1x10 <sup>4</sup>
0.1	3.1x10 <sup>3</sup>
1	3.1x10 <sup>2</sup>

Values for the migration distances and flow velocities expected to be seen in a typical muddy sediment assuming diffusion and flow are of equal importance with  $D=10^{-5}\text{cm}^2\text{sec}^{-1}$  ( $D=314\text{cm}^2\text{yr}^{-1}$ ).

#### 4.6.1.2 Depth

As argillaceous sediments become buried, they become more compact. It has been shown that a simple empirical relationship exists between porosity and burial, irrespective of the specific physical properties of the sediment. One such relationship is given by Baldwin and Butler (1985) which estimates the burial depth using:

$$\text{burial depth (in km)} = 6.02 (1 - \phi)^{6.35}$$

where  $\phi$  is the porosity.

Thus for the Caton Shale samples with a porosity of  $\sim 0.83$ , the depth of formation can be estimated to be less than 1m. The estimate for burial depth cannot be used with any degree of certainty, but it does indicate a shallow depth of concretion formation.

#### 4.6.1.3 Duration

The transport of calcium and carbonate to a site of concretionary growth can be either dominated by molecular diffusion or by flow. The Peclet number can be used to establish the relative importance of the two transport mechanisms. Where,

$$\text{Peclet Number } (P_N) = D/xv,$$

$D$  = molecular diffusion coefficient,

$x$  = average distance of migration,

$v$  = interstitial water flow velocity.

The typical values for water flow within mud rocks during compaction are in the range  $0.0001$  to  $1\text{cmyr}^{-1}$  (Berner, 1980). Thus for a molecular diffusion coefficient of  $10^{-5}\text{cm}^2\text{sec}^{-1}$  (value for sodium ions in a fine grained clay with 80% porosity (Manheim, 1970)), the distances can be calculated over which diffusion is the major process i.e.  $D \gg xv$ . Berner (1980) lists the molecular diffusion coefficients of other ions in sediments of comparable porosity. These values are in the range  $10^{-6}\text{cm}^2\text{sec}^{-1}$  to  $10^{-5}\text{cm}^2\text{sec}^{-1}$ .

It can be seen from Table 4.14 that for sediments with a molecular diffusion coefficient of  $10^{-5}\text{cm}^2\text{sec}^{-1}$ , diffusion is the dominant process up to distances in the order of hundreds of centimetres i.e.  $D \gg xv$ .

A theoretical model for diffusion controlled concretion formation, limited by transport has been proposed by Berner (1968). This provides an estimate for the time taken for concretion growth:

$$t = \frac{R^2}{2vD(C_\infty - C_R)}$$

t time

R concretion radius

v molar volume of the concretionary cement

D diffusion coefficient

$(C_\infty - C_R)$  = degree of super saturation

Thus for a concretion with  $R=5\text{cm}$ ;  $v=35\text{ cm}^3\text{mol}^{-1}$  (for calcite);  $D=10^{-5}\text{cm}^2\text{sec}^{-1}$  and  $(C_\infty - C_R)=10^{-7}\text{M}$  (values for D and  $C_\infty - C_R$  taken from Berner (1968)), the time for concretion formation is:

$$t = \frac{5^2}{2 \times \left(\frac{35}{0.83}\right) \times 10^{-5} \times 10^{-7}} \times (60 \times 60 \times 24 \times 7 \times 52)$$

~9,500 years

This value must be used with caution. Raiswell (1973) points out some errors in using this approach and other workers e.g. Thyne and Boles (1989) have noted the difficulty in estimating realistic values for  $(C_\infty - C_R)$ .

It is thought that concretion growth could be controlled by surface reactions (Raiswell, 1988), because dissolved species e.g. phosphate and organic matter may inhibit  $\text{CaCO}_3$  precipitation. The value obtained by the calculation is therefore only an estimate of the minimum length of time needed for concretion growth with the given assumptions. However, with an estimated sedimentation rate of say  $0.2\text{cm yr}^{-1}$ , the depth of formation for a typical concretion at the above rate would be about 20m.

#### 4.6.1.4 Temperature

Oxygen isotope ratios can be used as geothermometers. For low temperature systems, i.e. those within the diagenetic regime, there is an approximate relationship between temperature (T) and the fractionation factor ( $\alpha$ ) such that:

$$\ln \alpha \propto \frac{1}{T^2}.$$

By fitting experimental data to this relationship, Clayton *et al.* (1966) derived an empirical relationship between calcite and water (the reservoirs of oxygen) expressed as:

$$10^3 \ln \alpha = \left[ 2.78(10^6 T^{-2}) \right] - 2.89.$$

Since,

$$10^3 \ln \alpha \approx \delta_A - \delta_B = \Delta_{A-B},$$

the empirical relationship can be readily used to estimate the temperature of formation of calcite, given the isotopic composition of the cement and the formation water.

Carboniferous sea water had a  $\delta^{18}\text{O}$  of about +1‰. Thus, the temperature at which this cement ( $\delta^{18}\text{O} = +25‰$ , Table 4.16) may have formed is estimated to be +45°C.

#### 4.6.1.5 Shape

Given the variation in the size, shapes and orientation of the concretions, it seems improbable that they all formed by the same mechanism. For carbonate to precipitate, there must be localised supersaturation with respect to the carbonate mineral(s). This supersaturation can be derived by shell debris acting as nucleation sites (Raiswell, 1976) or by concentrations of organic matter acting as localised sites for sulphate reduction and hence calcite supersaturation (Raiswell, 1987). Alkalinity may also be generated by other organic matter oxidation reactions such as anaerobic methane oxidation, Raiswell (1987). The vertical concretions may have formed from the total decomposition of drift wood during sulphate reduction. Wignall (pers. comm.) rules out the concretions as burrow sites, given their morphology. The more spherical concretions may have formed by nucleating around shell debris, producing a more isotropic carbonate concentration.

#### **4.6.1.6 Sedimentology**

Uncrushed shells are common within some of the concretions, indicating cementation has protected the host sediment before appreciable compaction had occurred during lithification. Sediment laminae of the enclosing shale are distorted conformably around all the concretions. This again indicates that the concretions had formed prior to significant sediment compaction.

### **4.7 Septa formation**

The formation of septarian cracks within concretions is not clearly understood. Traditionally it was thought that dehydration of a 'proto-concretion' consisting of a hard cemented shell containing a soft interior resulted in shrinkage cracks (e.g. Lippman, 1955; Raiswell, 1971; Pettijon, 1975). Such dehydration has been ascribed to chemical desiccation by clay minerals (Raiswell, 1971).

An alternative mechanism has been proposed by Astin (1986) whereby septarian cracks form as tensile fractures during rapid burial and compaction of the host mud rocks. This is based on the observation that septa have a preferred vertical orientation in vertical sections compared with a more irregular polygonal pattern in sections parallel to bedding. Astin (1986) suggests that fracturing will be possible by overpressuring during the burial of shales.

#### **4.7.1 Septarian concretions from the Caton Shales**

Detailed chemical and isotopic analysis of the cements infilling the septa from the concretions in the upper horizon provides information about the timing of fracturing and the origins of the pore fluids.

Septarian cracks cross cut all the concretions studied. They have several common characteristics some of which were noted by Astin (1986):

1. Septarian cracks are widest in concretion centres, narrowing towards concretion margins.

2. Some concretions show two generations of cracks. The later cracks cross cut the earlier ones.
3. In general, second generation septa continue up to the concretion margins where as the first generation of cracks terminate more frequently before the concretion margins.
4. Early cracks cut through sediment laminae preserved in the concretion matrix indicating crack formation after significant cementation. Later cracks run parallel with preserved sediment bedding.
5. Sections parallel to bedding of large concretions show a polygonal pattern of early cracks with no preferred orientation. Vertical sections show dominant vertical cracks. Second generation cracks show a preferred NE-SW orientation in sections parallel to bedding whilst vertical sections show septa propagating outwards, parallel to bedding (Figure 4.18).

## 4.8 Geochemistry of the concretion cements

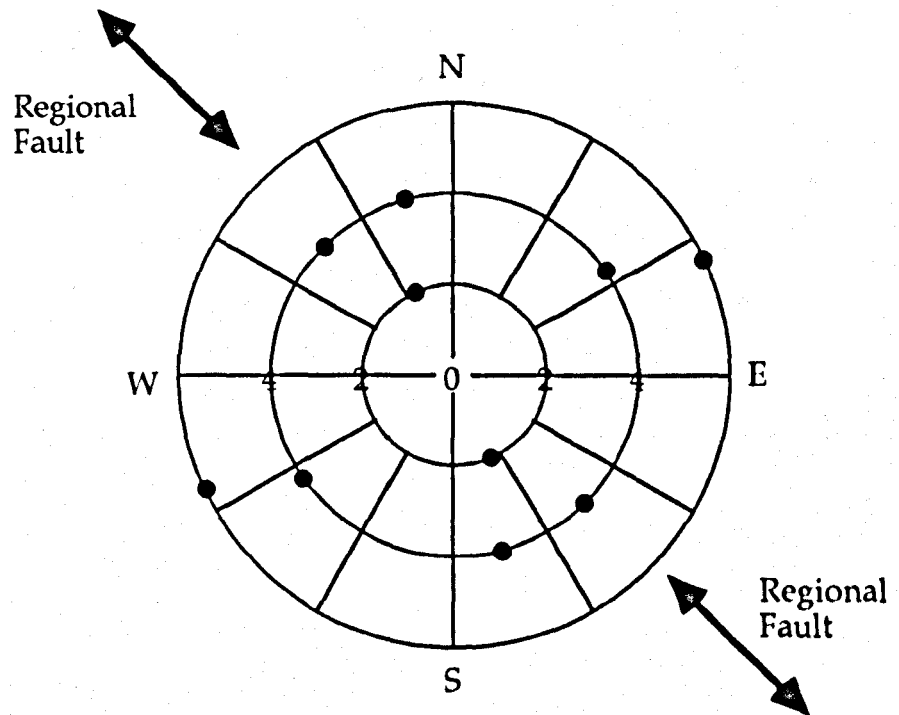
Scotchman (1991) and references therein show that the cation chemistry and the stable isotope ratios of oxygen and carbon provide information enabling the timing of septa formation and cementation to be established.

### 4.8.1 Stable isotopes

The trend in isotope evolution in septarian cements are shown in Figure 4.19. They are similar to the findings of Hudson (1978), Coleman and Raiswell (1981), Astin and Scotchman (1988) and Scotchman (1991b). The evolution is from a heavy (-1.5‰ PDB) to a light (-14.5‰ PDB) oxygen composition and a light (-29‰ PDB) to a heavy (-7‰ PDB) carbon composition. The generations of septa show different isotopic compositions indicating formation under different diagenetic regimes. The  $\delta^{13}\text{C}$  and  $\delta^{18}\text{O}$  are shown in Table 4.15.

Enclosures 2 and 3 show the distribution of the samples taken for carbonate isotope analyses.

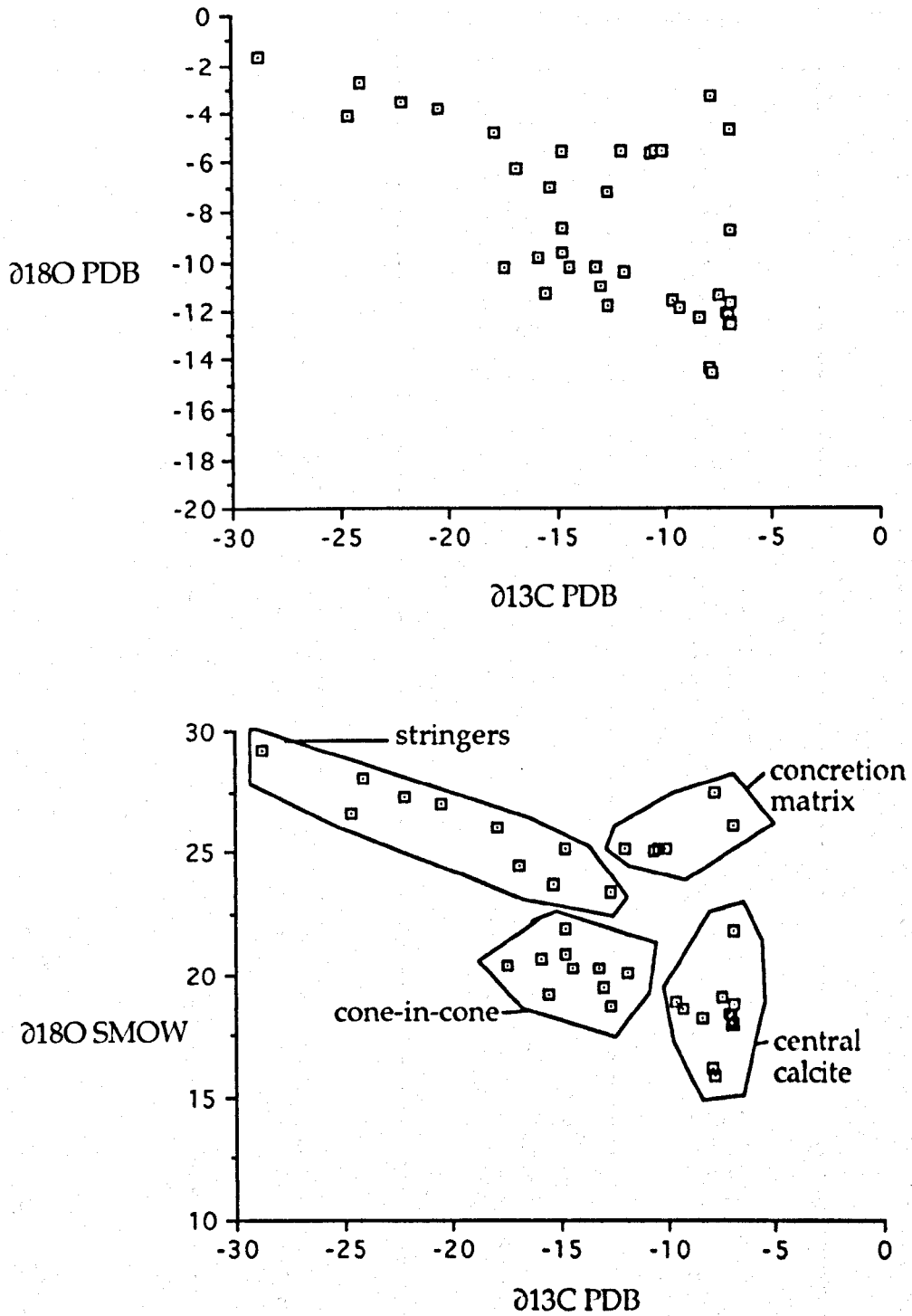
Figure 4.18



Principle crack orientations in the septarian concretions.  
(direction is measured horizontal to bedding)



Figure 4.19



Trends in isotope evolution in the septarian cements from the Caton Shale concretions. The  $\delta^{18}\text{O}$  is presented as PDB and as SMOW.

Table 4.15

Sample	Generation	$\delta^{13}\text{C}$ PDB	$\delta^{18}\text{O}$ PDB	$\delta^{18}\text{O}$ SMOW
1-A	2.00	-24.11	-2.73	28.05
2-A	2.00	-24.61	-4.12	26.61
6-A	3.00	-15.58	-11.34	19.18
8-A	4.00	-7.88	-14.56	15.85
10-A	3.00	-17.43	-10.25	20.30
9-B	4.00	-7.05	-12.59	17.88
4-A	1.00	-11.99	-5.60	25.09
12-A	2.00	-20.53	-3.78	26.97
2-B	2.00	-17.89	-4.75	25.97
8-B	3.00	-8.35	-12.29	18.19
9-B	4.00	-6.99	-12.52	17.95
12-B	3.00	-11.87	-10.49	20.05
1-C	1.00	-10.05	-5.55	25.14
4-C	2.50	-14.47	-10.29	20.25
6-C	3.00	-13.21	-10.27	20.27
8-C	4.00	-9.32	-11.92	18.58
10-E	1.50	-28.74	-1.62	29.19
2-F	2.00	-6.96	-12.56	17.92
4-F	4.00	-7.08	-12.21	18.27
6-F	4.00	-6.97	-8.76	21.84
2-D	3.00	-7.11	-12.12	18.37
5-D	4.00	-7.86	-3.34	27.42
6-D	2.00	-14.79	-5.56	25.13
4-E	4.00	-7.50	-11.39	19.12
5-E	4.00	-15.87	-9.90	20.65
9-E	3.00	-12.70	-11.79	18.70
9-A	4.00	-7.97	-14.29	16.13
11-A	3.00	-14.79	-8.66	21.93
2-C	1.00	-10.66	-5.66	25.03
3-C	2.50	-22.21	-3.52	27.23
7-C	4.00	-9.59	-11.60	18.91
9-C	3.00	-14.74	-9.69	20.87
11-C	1.00	-10.36	-5.56	25.13
5-F	4.00	-6.91	-11.73	18.77
10-C	2.00	-15.37	-7.02	23.62
1-D	4.00	-16.87	-6.25	24.42
7-E	5.00	-12.60	-7.26	23.38
10-B	5.00	-12.93	-11.03	19.49
1-F	5.00	-6.91	-4.66	26.05

Stable oxygen and carbon isotope data from carbonate samples from the septarian concretions of the Caton Shales.

Generation: 1=matrix, 2=stringer, 3=cone-in-cone, 4=central calcite, 5=dolomite.

#### 4.8.1.1 Concretion matrix

The carbon isotope composition of diagenetic cements reflect the source of the carbon. Curtis (1977) shows depth related diagenetic processes associated with different characteristic  $\delta^{13}\text{C}$  values. The sulphate reduction zone shows a composition near to that of the organic matter source. In the case of the Caton Shales, the organic matter shows  $\delta^{13}\text{C}$  values typical of those shown by marine organic matter, in the order of  $-27\text{‰}$  PDB. Fermentation produces very heavy  $\text{CO}_2$  whereas decarboxylation produces  $\text{CO}_2$  with a similar isotopic composition to that of sulphate reduction.

The concretion matrix is comprised of carbon with a  $\delta^{13}\text{C}$  in the range  $-10.5$  to  $-12.0\text{‰}$  PDB. These values are at least  $+15\text{‰}$  heavier than those expected if the concretions were from carbonate derived wholly from sulphate reduction. It is therefore suggested that the concretion cement is made up of a mixture of carbon sources:

	$\delta^{13}\text{C}$
sulphate reduction carbon	$-28\text{‰}$
methanogenic carbon	$+15\text{‰}$ (variable)
marine carbonate	$0\text{‰}$

The proportions of methanogenic derived carbon and marine carbonate are uncertain, but as Scotchman (1991b) points out, the lack of  $\delta^{13}\text{C}$  values close to zero or positive values would indicate an insignificant proportion of methanogenic carbon relative to marine derived carbonate. However, there is some shell carbonate present within the concretion matrices which may be evidence for some methanogenic  $\text{CO}_2$  contribution as there was obviously not complete dissolution of primary carbonate (Raiswell and Coleman, 1981).

Geological evidence suggests that the concretions formed early during diagenesis. However, the oxygen isotope ratios used simplistically as a geothermometer indicate precipitation at a temperature in the order of  $+45^\circ\text{C}$ . This would clearly indicate a depth out of the range of early diagenetic processes, assuming a typical geothermal gradient of  $30^\circ\text{C}$  per 1km depth. Since the oxygen isotope composition of the carbonate is dependant on the isotopic compositions of the fluid from which it precipitated as well as the temperature at which it precipitated, precipitation probably occurred from a porewater more  $^{18}\text{O}$  depleted than the Carboniferous seawater value assumed above.

Such depletion can result either by:

1. Mixing with meteoric waters which have  $\delta^{18}\text{O}$  values in the range -3 to -11‰ PDB (Dansgaard, 1964).
2. Formation of diagenetic minerals may fractionate oxygen by 3‰ over a depth interval of 600m (Lawrence *et al.*, 1976).
3. Ultrafiltration by clay minerals e.g. Benzel and Graf (1984).

SEM studies show no evidence for the formation of smectite in large quantities and clay mineral ultrafiltration has only been demonstrated in the laboratory therefore the source of  $^{18}\text{O}$  depleted water is thought to be meteoric water mixing with marine water.

#### 4.8.1.2 Early septarian cements

The carbon isotopic composition of the early septarian cements is dominated by carbon derived from sulphate reduction. Values range from -29‰ to -10‰. The concentration of  $\text{HCO}_3^{2-}$  is in the order of 2mmol in marine waters. Therefore the heavy marine signal is rarely preserved in early diagenetic cements as the concentration of dissolved bicarbonate is insufficient to initiate precipitation and diagenetic  $\text{HCO}_3^-$  sources are required.

The oxygen isotopes show palaeotemperatures ranging from:

$$\begin{aligned} \delta^{18}\text{O} &= -8\text{‰}_{\text{PDB}}, \text{ temperature} = 58^\circ\text{C} \text{ to} \\ \delta^{18}\text{O} &= -1\text{‰}_{\text{PDB}}, \text{ temperature} = 21^\circ\text{C}. \end{aligned}$$

The apparently elevated temperatures are associated with heavier carbon isotope values and are thus thought to be penecontemporaneous with the formation of the concretion matrix. The lower temperatures ( $\sim 21^\circ\text{C}$ ) are comparable with warm sea temperatures and correspond to the lightest  $\delta^{13}\text{C}$  values produced from sulphate reduction.

Table 4.16

Sample I-D	Generation	$\delta^{13}\text{C}$ PDB	$\delta^{18}\text{O}$ PDB	$\delta^{18}\text{O}$ SMOW	mol% Mn	mol% Fe	mol% Ca	mol% Mg	Mn/Fe	Mg/Fe
1/C	1	-10.05	-5.55	25.14	0.12	1.44	93.29	5.14	0.08	3.57
10/E	2	-28.74	-1.62	29.19	0.14	5.04	87.21	7.61	0.03	1.51
2/A	2	-24.61	-4.12	26.61	0.14	3.11	88.73	8.02	0.05	2.58
12/A	2	-20.53	-3.78	26.97	0.23	3.61	95.50	0.65	0.06	0.18
3/C	2	-22.21	-3.52	27.23	0.46	12.53	82.96	4.05	0.04	0.32
6/C	3	-13.21	-10.27	20.27	0.00	1.04	95.96	3.00	0.00	2.88
9/C	3	-14.74	-9.69	20.87	0.06	1.67	94.49	3.77	0.04	2.26
6/A	3	-15.58	-11.34	19.18	0.19	5.00	87.29	7.53	0.04	1.51
1/D	3	-16.87	-6.25	24.42	0.16	3.01	96.25	0.58	0.05	0.19
2/B	3	-17.89	-4.75	25.97	0.16	2.50	97.02	0.32	0.06	0.13
6/D	3	-14.79	-5.56	25.13	0.34	7.17	88.73	3.76	0.05	0.52
9/A	4	-7.97	-14.29	16.13	0.23	3.86	95.24	0.66	0.06	0.17
9/B	4	-7.05	-12.59	17.88	0.26	4.13	93.08	2.52	0.06	0.61
2/D	4	-7.11	-12.12	18.37	0.26	4.64	88.44	6.66	0.06	1.44
4/E	4	-7.50	-11.39	19.12	0.00	7.00	93.14	6.17	0.00	0.88
5/F	4	-6.91	-11.73	18.77	0.36	7.55	89.51	2.59	0.05	0.34
2/F	4	-6.96	-12.56	17.92	0.22	3.46	95.94	0.38	0.06	0.11
8/B	4	-8.35	-12.29	18.19	0.21	3.51	95.84	0.43	0.06	0.12
9/E	5	-12.70	-11.79	18.70	0.99	10.45	66.31	22.25	0.09	2.13

Summary of stable isotope and geochemical composition of cements from the septarian concretions of the Caton Shales. Cement generation: 1=matrix, 2=stringer, 3=cone-in-cone, 4=central calcite, 5=dolomite.

### 4.8.1.3 Late Septarian cements

The  $\delta^{13}\text{C}$  of the later cements shows a continuing trend to heavier values. The lightest values overlap the heaviest values of the first generation of septarian cements ranging from  $-18\text{‰}$  to  $-7\text{‰}$  PDB. The carbon isotope ratios infer mixing from carbon sources with a greater proportion of carbon derived from methanogenesis.

The oxygen isotopic composition shows a continuing trend to lighter values from  $-8$  to  $-15\text{‰}$  PDB. The apparent palaeotemperatures range from:

$$\begin{aligned}\delta^{18}\text{O} &= -8\text{‰}_{\text{PDB}}, \text{ temperature} = 58^{\circ}\text{C} \text{ to} \\ \delta^{18}\text{O} &= -15\text{‰}_{\text{PDB}}, \text{ temperature} = 110^{\circ}\text{C}.\end{aligned}$$

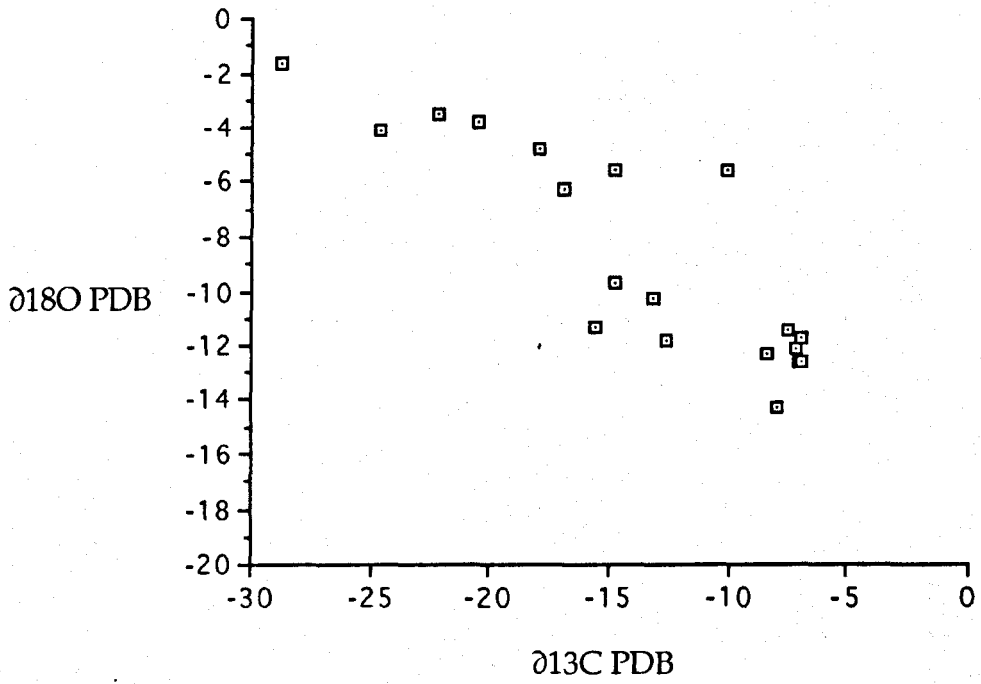
Such depletion in  $^{18}\text{O}$  cannot be explained by simple mixing of fluids alone as the minimum  $\delta^{18}\text{O}$  is outside the range for meteoric waters and cannot be directly accounted for by organic matter oxidation, as suggested by Raiswell and Coleman (1981) and Sass *et al.* (1991).

Fluid inclusions were observed in wafers cut from the youngest generation of cement. The inclusions were predominantly aqueous, however approximately 10% of all the inclusions were hydrocarbons. Poor data was obtained from the samples observed. Homogenisation temperatures were often impossible to determine as the cements had probably suffered from stress and the inclusions leaked. An estimated homogenisation temperature of  $+60^{\circ}\text{C}$  was measured (D. Banks, pers. comm.). This value is much lower than that predicted from oxygen isotope thermometry.

### 4.8.2 Cation chemistry

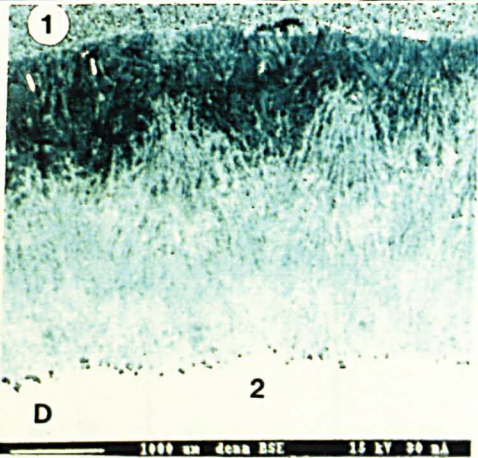
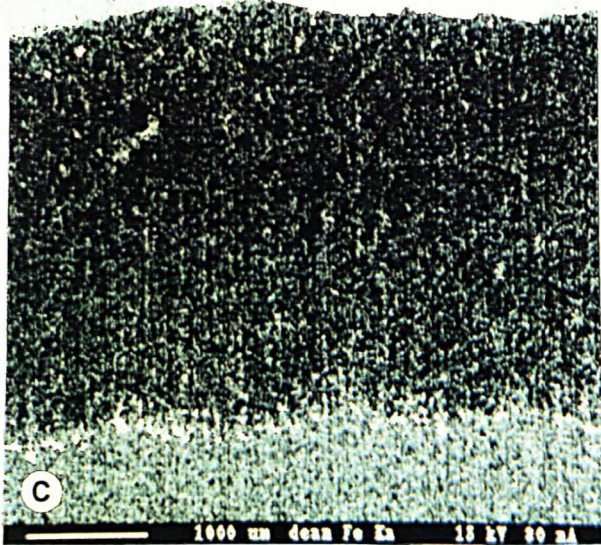
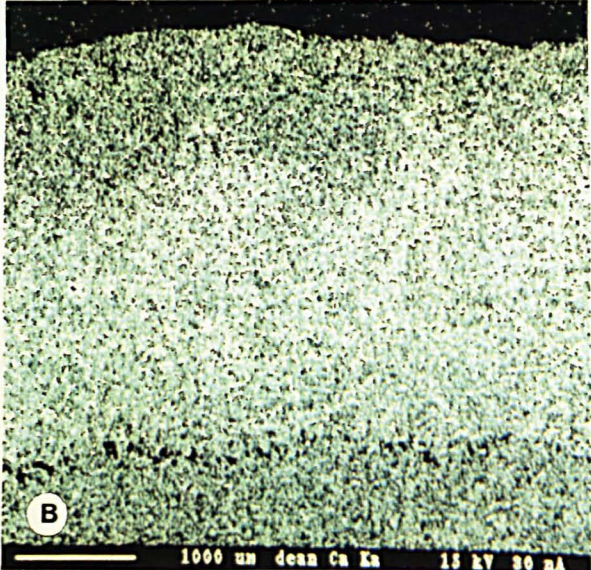
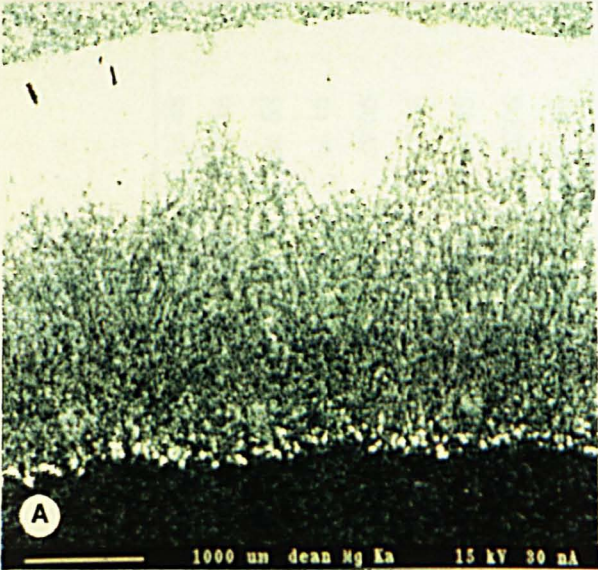
Atomic absorption was used to determine the concentrations of Fe, Mn, Mg and Ca in twenty of the samples used for isotopic analysis (Table 4.16), together with electron microprobe analysis for a much greater number of samples. The  $\delta^{18}\text{O}$ ,  $\delta^{13}\text{C}$  cross plot for these samples is shown in Figure 4.20 confirming a representative sub-sample of the total samples analysed for  $\delta^{18}\text{O}$  and  $\delta^{13}\text{C}$ . The probe  $\text{K}\alpha$  X-ray maps summarise the Fe, Mg and Ca chemistry of the second generation carbonate cements (Plate 4.1). Detailed probe analyses for Mn, Fe Mg and Ca are presented in Table 4.17.

Figure 4.20



The relationship between  $\delta^{18}\text{O}$  and  $\delta^{13}\text{C}$  of the carbonates from a sub-set of 20 concretion and septa samples.





The major cation chemistry of the carbonate cement of a typical septarian crack is revealed by  $K_{\alpha}$  X-ray maps of: **A**=magnesium; **B**=calcium; **C**=iron. The lighter regions mark areas of higher concentration. **D** is a back-scattered electron micrograph of the area analysed showing the change in chemistry from the concretion matrix (1) to the central calcite (2).



Table 4.17

Traverse 1				Traverse 2			
%Mg	%Ca	%Mn	%Fe	%Mg	%Ca	%Mn	%Fe
0.00	0.00	0.00	0.00	0.00	0.00	0.00	0.00
9.89	89.74	0.21	0.15	2.65	96.38	0.15	0.82
7.53	92.17	0.13	0.18	6.70	93.00	0.05	0.26
8.42	91.38	0.08	0.13	6.89	93.11	0.00	0.00
7.38	92.01	0.22	0.39	6.79	93.06	0.10	0.05
8.65	91.02	0.13	0.20	10.26	89.70	0.00	0.04
8.76	91.15	0.00	0.09	6.49	93.46	0.05	0.00
8.82	90.99	0.13	0.06	6.81	93.09	0.10	0.00
10.34	89.48	0.12	0.06	7.92	92.00	0.00	0.08
9.04	90.81	0.06	0.08	8.30	91.64	0.00	0.06
11.30	88.56	0.07	0.07	8.27	91.55	0.15	0.02
9.17	90.76	0.08	0.00	9.21	90.77	0.00	0.03
8.29	91.60	0.06	0.04	8.76	91.19	0.05	0.00
8.74	91.05	0.08	0.13	12.47	87.40	0.13	0.00
10.03	89.87	0.08	0.02	10.99	88.84	0.15	0.02
9.95	89.96	0.06	0.03	9.37	90.55	0.00	0.08
9.71	89.82	0.18	0.29	8.66	91.28	0.06	0.00
9.27	90.61	0.02	0.09	8.24	91.70	0.00	0.05
9.95	89.98	0.07	0.00	11.22	88.78	0.00	0.00
9.68	90.16	0.12	0.04	9.70	90.21	0.03	0.06
9.36	90.52	0.02	0.11	9.08	90.90	0.02	0.00
10.90	89.02	0.06	0.02	10.52	89.48	0.00	0.00
9.76	90.21	0.02	0.00	9.34	90.65	0.00	0.00
9.41	90.47	0.13	0.00	9.46	90.54	0.00	0.00
8.21	91.79	0.00	0.00	9.48	90.52	0.00	0.00
10.10	89.78	0.08	0.05	8.77	91.14	0.00	0.09
8.30	91.66	0.02	0.03	8.51	91.49	0.00	0.00
10.32	89.51	0.13	0.04	8.04	91.96	0.00	0.00

Table 4.17 continued

Traverse 1 continued			
%Mg	%Ca	%Mn	%Fe
8.04	91.81	0.14	0.00
9.14	90.70	0.08	0.07
9.62	90.12	0.21	0.05
8.41	91.52	0.07	0.00
8.40	91.52	0.05	0.03
8.99	90.85	0.12	0.04
7.28	92.64	0.02	0.05
8.42	91.51	0.06	0.00
7.98	91.95	0.05	0.03
7.23	92.58	0.15	0.03
9.07	90.80	0.13	0.00
8.59	91.31	0.08	0.03
7.36	92.46	0.13	0.04
8.04	91.75	0.09	0.12
7.40	92.45	0.13	0.01
7.27	92.65	0.02	0.05
7.17	92.73	0.03	0.07

Traverse 2 continued			
%Mg	%Ca	%Mn	%Fe
9.03	90.92	0.06	0.00
7.64	92.31	0.05	0.00
7.92	92.08	0.00	0.00
9.55	90.38	0.06	0.00
9.54	90.46	0.00	0.00
7.15	92.72	0.00	0.13
8.06	91.88	0.00	0.06
7.96	92.04	0.00	0.00
9.77	90.13	0.05	0.05
9.68	90.19	0.13	0.00
8.66	91.10	0.02	0.21
8.22	91.65	0.10	0.03
8.15	91.85	0.00	0.00
7.04	92.88	0.00	0.08
10.30	89.70	0.00	0.00
7.56	92.33	0.08	0.03
8.02	91.90	0.08	0.00
6.28	93.57	0.01	0.13
10.94	89.06	0.00	0.00
7.27	92.61	0.00	0.12

Normalised X-ray microprobe analyses for Ca, Mg, Fe and Mn from two traverses across septarian veins. The sample measurements were taken every 10 $\mu$ m, starting near to the concretion matrix and ending in approximately the centre of the vein.

The changes in cation chemistry can be seen using the relationships of  $\delta^{13}\text{C}$  with respect to the molar ratios of Mg/Fe and Mn/Fe. Curtis *et al.* (1986) and Scotchman (1991b) used the Mn/Fe ratio as a measure of pore water variation, given the complex variation and partitioning of Ca, Mg, Fe and Mn within carbonate cements. Sample 5/D has not been incorporated into the data set as it contains anomalous  $\delta^{18}\text{O}$  values.

#### 4.8.2.1 Calcium

There is no obvious trend in the content of calcium within any of the samples. The difference between the composition of pure calcite can be ascribed to the incorporation of Mg and Fe into the lattice of the calcite.

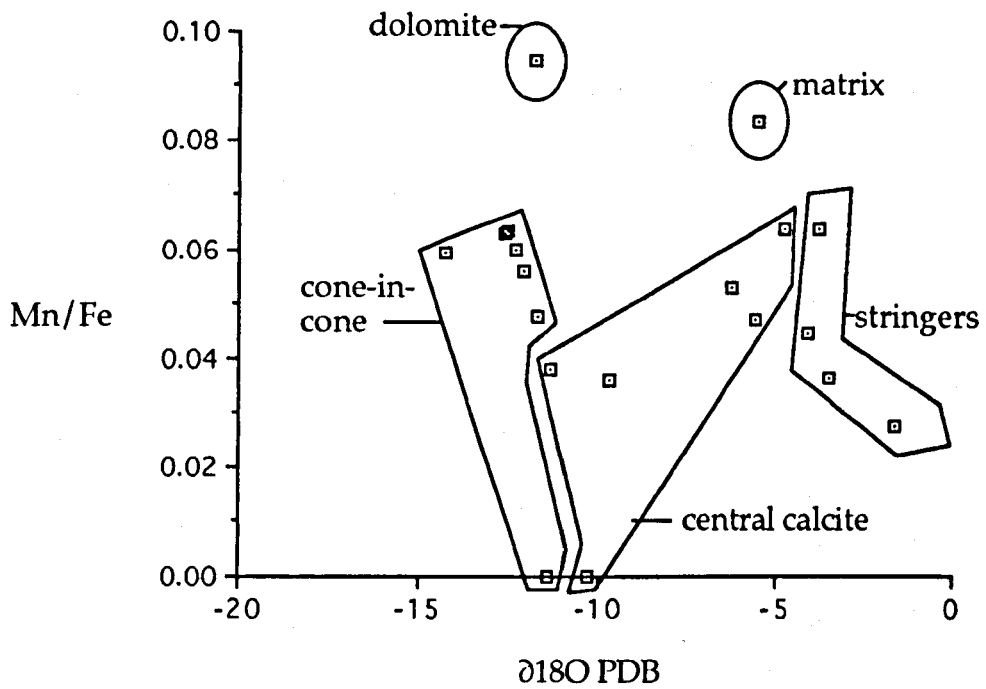
#### 4.8.2.2 Manganese

The manganese concentration in all the samples analysed was  $< 1.0\text{mol}\%$ . The highest concentration was found in the dolomitic sample where the concentration was found to be  $0.9\text{mol}\%$ . Figures 4.21 and 4.22 show the variation of the Mn/Fe ratio with  $\delta^{18}\text{O}$  and  $\delta^{13}\text{C}$ . The matrix and the dolomite cements show the highest Mn/Fe ratios. Within each of the other generations of cements, there is a progressive change from a Mn/Fe of  $\sim 0.6$  to one indicating little or no Mn present. The Mn/Fe ratio increases with increasing  $\delta^{13}\text{C}$  in the early septarian cements and it has a negative relationship with  $\delta^{18}\text{O}$ . However, in the second generation the Mn/Fe increases with the increasing  $\delta^{18}\text{O}$  and decreases with increasing  $\delta^{13}\text{C}$ . The final central calcite shows a varying Mn/Fe with a relatively constant  $\delta^{13}\text{C}$  and  $\delta^{18}\text{O}$ .

#### 4.8.2.3 Iron

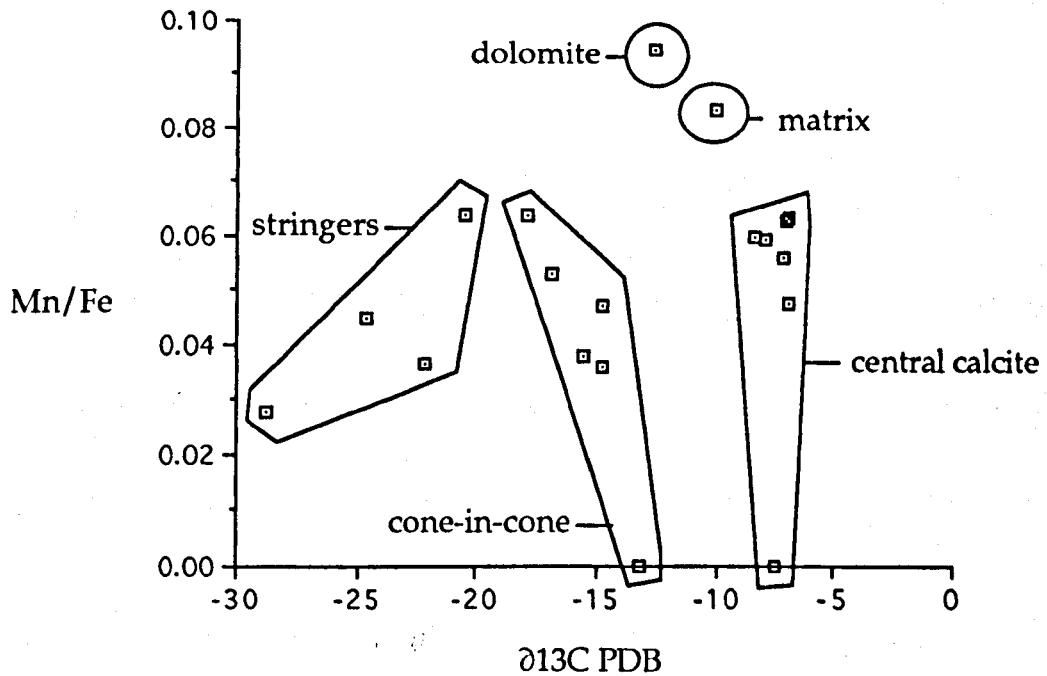
The concentrations in all the samples show similar iron values. The clear calcite has a range  $3.5$  to  $7\text{mol}\%$ , the bundled calcite  $1$  to  $7\text{mol}\%$  and the first generation of calcite  $3$  to  $5\text{mol}\%$  (with the exception of sample 3/C which has a high Fe content).

Figure 4.21



Evolution of the carbonate chemistry 1: Mn/Fe with  $\delta^{18}\text{O}$ .

Figure 4.22



Evolution of the carbonate chemistry 2: Mn/Fe with  $\delta^{13}\text{C}$ .

#### 4.8.2.4 Magnesium

There is a wide spread of magnesium concentrations in all of the generations of cements. The Mg/Fe ratios plotted against  $\delta^{18}\text{O}$  and  $\delta^{13}\text{C}$  (Figure 4.23 and 4.24) show a complex picture of cement evolution within each generation. The K $\alpha$  X-ray maps (Plate 4.1) clearly shows the change from a Mg rich early second generation cement to a Mg poor late clear calcite cement.

### 4.9 Authigenesis and evolution of the concretions

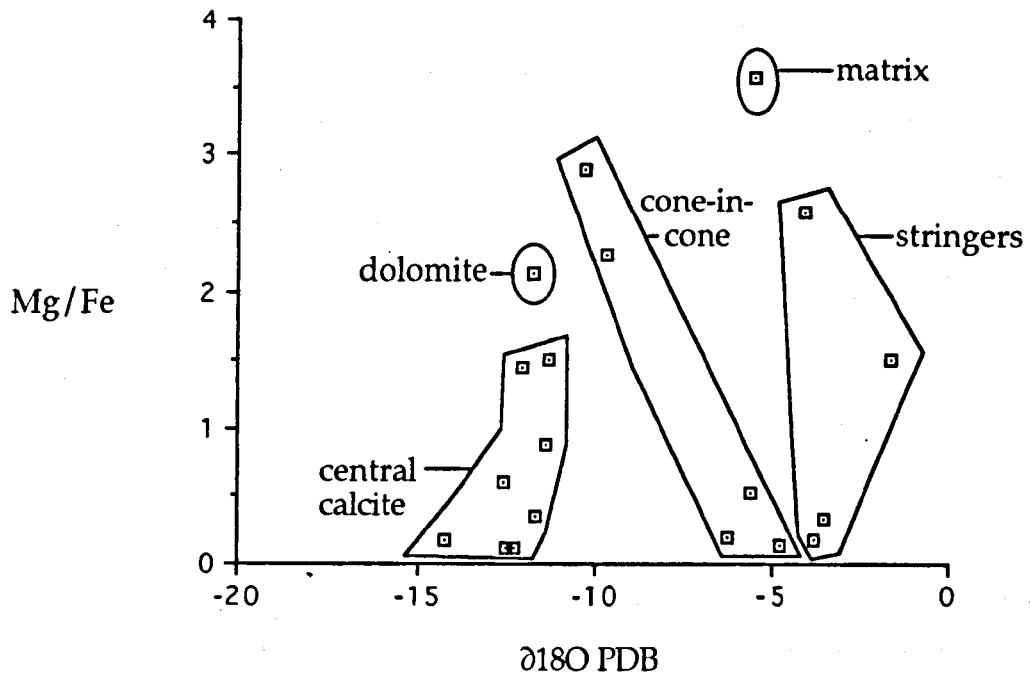
#### 4.9.1 Stage 1 - concretion formation

The formation of the concretions occurred early during diagenesis, close to the sediment water interface based on the porosity estimates, the geological relationships of compacted bedding, and the preservation of uncrushed fossils within the concretion matrix. The carbon and oxygen stable isotope ratios indicate the concretionary cement formed from a mixture of carbonate. This was probably derived from both dissolved shell fragments and bicarbonate produced during sulphate reduction, with a possible meteoric water influence accounting for the depletion of  $\delta^{18}\text{O}$  values.

#### 4.9.2 Stage 2 - initial septarian crack formation

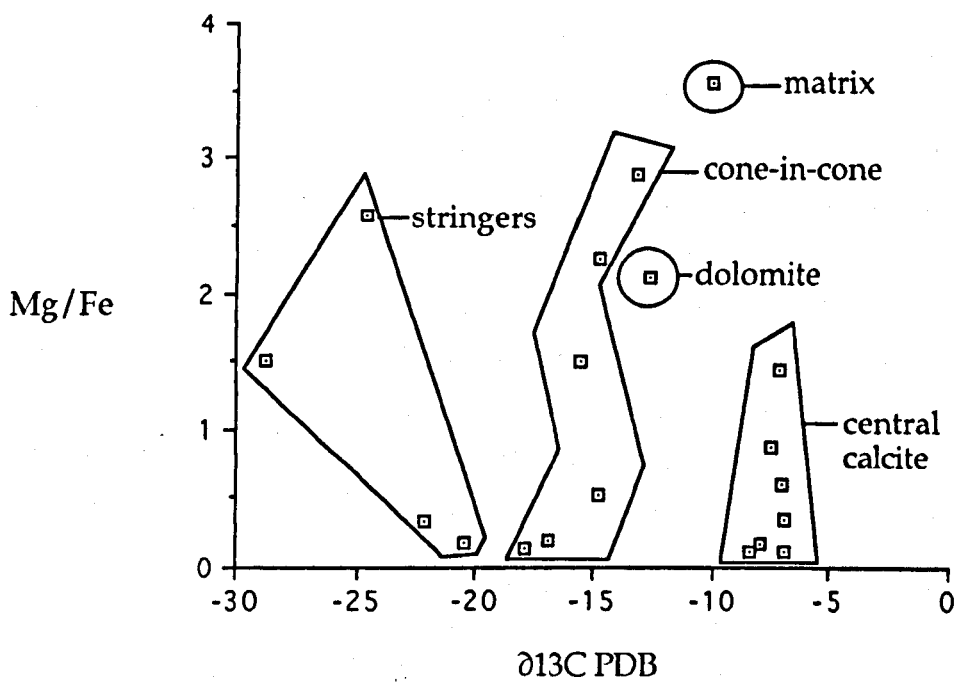
Septarian cracks occur as two obvious generations. The early septa cut through sediment laminae showing a polygonal pattern of cracks in horizontal section and vertical cracks in vertical section. These cracks are thought to result from a stress field in which the principal stress is vertical and the horizontal stresses were lower and roughly equal (Astin, 1986). Such a condition could result by shale overpressuring. However, Astin (1986) points out that Eocene concretions from the London Clay formation have septarian cracks but have only been buried to a maximum depth of 50m. It would seem that local factors such as size and shape play a major role in crack formation. Therefore the initial formation of sub-critical cracks which led to major fracturing was possible in the Caton Shales within the upper 10's of metres of the sediment.

Figure 4.23



Evolution of the carbonate chemistry 3: Mg/Fe with  $\delta^{18}\text{O}$ .

Figure 4.24



Evolution of the carbonate chemistry 4: Mg/Fe with  $\delta^{13}\text{C}$ .

### 4.9.3 Stage 3 - cementation of the septarian cracks

The  $\delta^{13}\text{C}$  values of the carbonate cement indicate that the source of the cement was dominated by carbon derived from sulphate reduction, together with a lesser contribution from aragonitic shell carbonate. The Mn/Fe and Mg/Fe ratios also suggest mixing of a higher Fe, Mg composition associated with carbon derived from sulphate reduction and a meteoric fluid with a higher Mn and  $^{18}\text{O}$  composition.

### 4.9.4 Stage 4 - late septarian crack formation

A second generation of septarian cracks cross cuts the first. Unlike the early cracks, the second generation cracks form within sediment laminations and have a preferential orientation in a NE-SW direction with an associated conjugate set in a NW-SE direction. A different mechanism must be invoked for the second set of septa. The regional geology shows major faulting across the area with a NW-SE orientation, indicating that the second stage concretion fracturing was associated with the faulting. A tectonic mode of formation would produce greater stress in a horizontal orientation fitting in with the observed fracture pattern.

### 4.9.5 Stage 5 - cementation of the late septa

Three distinct generations of cement fill the septa formed from the second fracturing event. The earliest bundles of calcite show  $\delta^{18}\text{O}$  palaeotemperatures in the range of  $70^\circ\text{C}$ , suggesting precipitation at much greater temperatures and or depletion in  $^{18}\text{O}$ . Heavier  $\delta^{13}\text{C}$  values indicate a carbon input from methanogenic processes. The progressive change from a magnesium rich to a low magnesium, low iron cement is clearly illustrated in the Plate 4.1, showing the  $\text{K}\alpha$  X-ray maps across a second generation septa. The formation of dolomite is associated with this event as revealed by textural relationships and confirmed by the overlap of the isotopic signature within the fibrous calcite field.

The last generation of clear calcite is separated by a sharp boundary. In some cases this is marked by small euhedral crystals of barite. Due to the very small size, sulphur isotopic analysis proved impossible to perform on these samples.

Perhaps the sulphur was produced by the decomposition of organo-sulphur compounds or may have been formed by TSR. The clear calcite is generally rich in iron as shown by the  $K\alpha$  X-ray maps, but not revealed by AA. This generation of cement is contemporaneous with hydrocarbon migration as shown by hydrocarbon inclusions and bituminous oil residues in the central cavities of the concretions. The  $\delta^{13}\text{C}$  of the cement is much heavier than would be expected if the source of the carbon was originally organically bound, indicating a basinal brine influence which is not unexpected given the temperature of formation ( $\sim 60^\circ\text{C}$  from fluid inclusion data) and the presence of hydrocarbons which are not derived locally.

## 4.10 Conclusions

Weathering of shales is a very important process in the oxidation and subsequent loss of pyrite from sediments. The weathering of shales is discussed in more detail in Chapter 6.

The Caton Shales were deposited under normal marine conditions with a dominant terrestrial component to the organic matter. Concretions within the shales were formed early during diagenesis. Sediment overpressure caused initial fracturing of these concretions, followed by calcite cementation. The source of the carbon being derived from sulphate reduction. A later fracturing associated with regional tectonic events led to the emplacement of a migrated oil into the centres of the late stage septa.



# Chapter 5

## Geochemistry of the Jet Rock

### 5.0 Introduction

This chapter is an investigation of the diagenesis of the Jet Rock (Upper Lias, Lower Toarcian, Figure 5.1) and in particular the relationships between various forms of inorganic and organic sulphur.

A variety of palaeoenvironmental indicators have been compared (Pr/Ph, C/S and DOP) to establish their validity in what is generally considered to be a marine shale sequence representing strongly dysaerobic or euxinic conditions at the time of deposition. The type and nature of the organic matter has been studied with particular attention given to organosulphur compounds.

The Jet Rock is a potentially good system to study for organic sulphur investigations. Most of the reactive iron minerals within the Jet Rock were thought to have formed early syngenetic pyrite and the pore waters were dominated by dissolved sulphide (Raiswell *et al.*, 1993a). The sediments are at an early stage of thermal maturity (vitrinite reflectance 0.6) being buried to a maximum of 2.5km (Pye, 1985). Thus, hydrocarbon generation has started within the Jet Rock. Most of the hydrocarbons generated in the sediments have remained in situ, evidenced by the small amounts of compaction waters which were expelled during maturation.

Stable sulphur isotopes have been used to time the relative formation of pyrite and organosulphur compounds (OSC) whilst concretion matrix studies enable the mobility of some elements to be assessed during diagenesis.

### 5.1 Geological Setting

The Jurassic in Northeast England is marked by a marine transgression, which continued a late Triassic invasion of marine waters onto the epicontinental shelf. Sedimentation was controlled by eustatic sea level changes and the

Figure 5.1

<b>Mesozoic</b>	Cretaceous		
	<b>Jurassic</b>	Malm	Tithonian Kimmeridgian Oxfordian
		Dogger	Callovian Bathonian Bajocian Aalenian
		Lias	Toarcian Pliensbachian Sinemurian Hettangian
Triassic			

<b>LOWER TOARCIAN</b>	<b>Whitbian</b>	bifrons	braunianus	<b>Lias Group</b>	<b>Whitby Mudstone Formation</b>	Alum Shale Member
			fibulatum			
			commune			
		falciferum	falciferum			Jet Rock Member
			exaratum			
		tenuicostatum	semicelatum			Grey Shale Member
	tenuicostatum					
	cecelandicum					
	paltum					

Stratigraphy of the Jet Rock on the Yorkshire Coast.

elevation and collapse of rift related crustal upwarps of the North Sea Graben (Anderton *et al.*, 1985).

A reactivation of ancient faults enabled an accumulation of thick basinal marine shales to form. The extensive development of restricted basinal marine environments allowed the accumulation of bituminous shales. Jenkyns (1988) called the lower *falciferum* zone an 'anoxic event' as the deposition of Toarcian black shales has occurred in several distinct basins across Europe, Farrimond *et al.* (1989).

## 5.2 The Jet Rock

Much work has been focussed on the Jet Rock. Howarth (1962) has described the sequence of the Jet Rock, providing detailed stratigraphical descriptions of exposures on the Yorkshire coast. Hallam (1967) has studied the sedimentology as has Morris (1979, 1980), together with the palaeoecology. Wignall and Hallam (1991) also give details about the fauna in a palaeoenvironmental context.

The mineralogical composition and major and minor element compositions of the Jet Rock have been studied by Gad *et al.* (1969). Further geochemical studies of the series have been made by Raiswell and Berner (1985), Raiswell and Al-Biatty (1989) and Al-Biatty (1990). The main focus of this later work was on the carbon-iron-sulphur geochemistry of the Jet Rock. A positive correlation between carbon and sulphur was found to exist together with constant DOP (independent of carbon). Pyrite formation in the Jet Rock is thought to be limited by iron and dominantly syngenetic.

Farrimond *et al.* (1989) have made an organic geochemical investigation of Toarcian black shales, including the Jet Rock. Myers and Wignall (1987) have made a combined study of palaeoecology and gamma ray spectrometry of the Jet Rock showing maximum authigenic uranium 4.5m above the base of the Jet Rock, representing the most intense period of anoxia.

Raiswell (1976, 1987) and Coleman and Raiswell (1981) have studied the isotopic compositions of carbonate concretions. Carbonate carbon is derived principally from organic matter during sulphate reduction. Isotopically light pyrite from open system sulphate reduction is found as framboids throughout

the sediment and large crystals of isotopically heavy pyrite are found in greater abundance at concretion margins. The oxygen isotopes suggest that the cements formed at a temperature close to that of sea water.

Recent work by Raiswell *et al.* (1993a) following the results of Tan (1985) and Al-Biatty (1990) have looked at the organosulphur compounds in the Jet Rock in relation to the other forms of sulphur. The formation of organic sulphur compounds are thought to post date syngenetic pyrite, forming after most reactive iron minerals have been pyritised. Late stage isotopically heavy pyrite forms contemporaneously with the incorporation of sulphur into organic compounds.

The deposition of the Jet Rock has been discussed by Wignall and Maynard (1993) in terms of sequence stratigraphy. They conclude that the Jet Rock is an early transgressive marine shale sequence. All the authors agree that the Jet Rock was deposited under marine waters which were probably anoxic. The position of the  $H_2S/O_2$  interface has not yet been established, therefore euxinicity cannot be excluded.

### 5.3 Samples

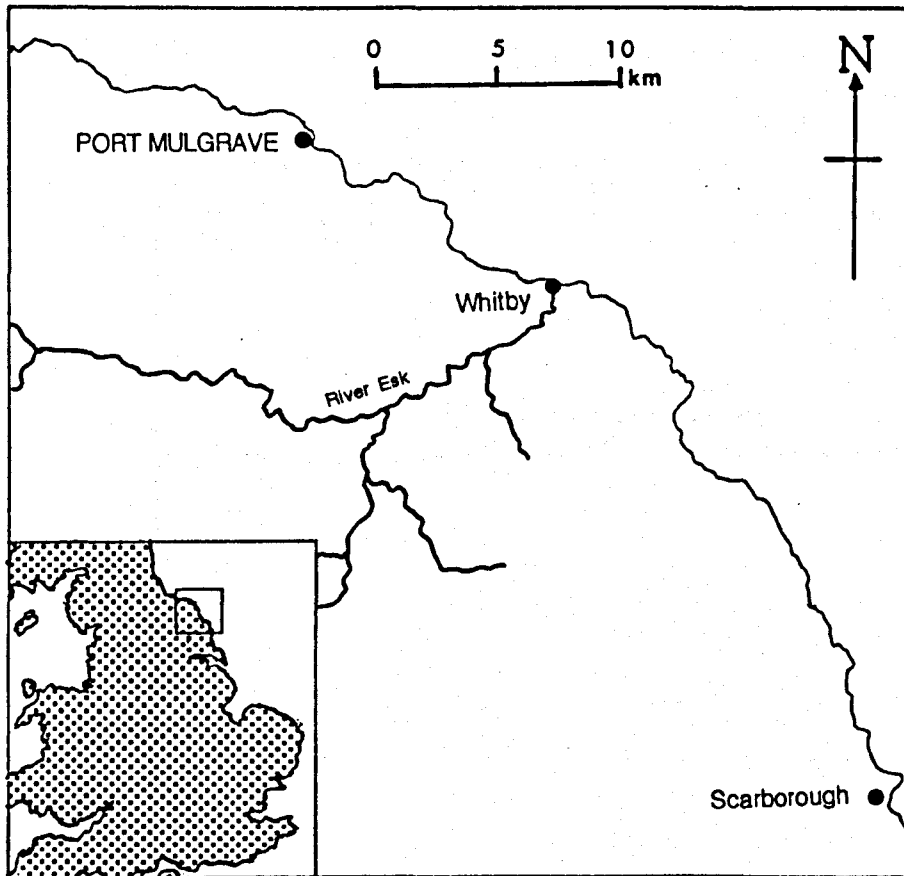
Samples were collected from a well exposed wave cut platform at Port Mulgrave, approximately 11km NW of Whitby (Figure 5.2). The exposed section comprises of 9m of gently dipping, finely laminated dark grey shales. The sequence is dominated by concretions described by Howarth (1962) and shown on the log (Figure 5.3). Table 5.1 shows the Jet Rock sample locations.

Samples were collected at regular intervals throughout the exposed sequence, the lowest being at the top of the Grey Shales exposed only at low tide. Care was taken to ensure fresh samples, therefore large (<1kg) blocks of shale were cut from the exposure after surface weathering was removed. A further 2cm layer of rock was removed from each sample prior to crushing by Tema.

### 5.4 Gamma Ray Spectrometry

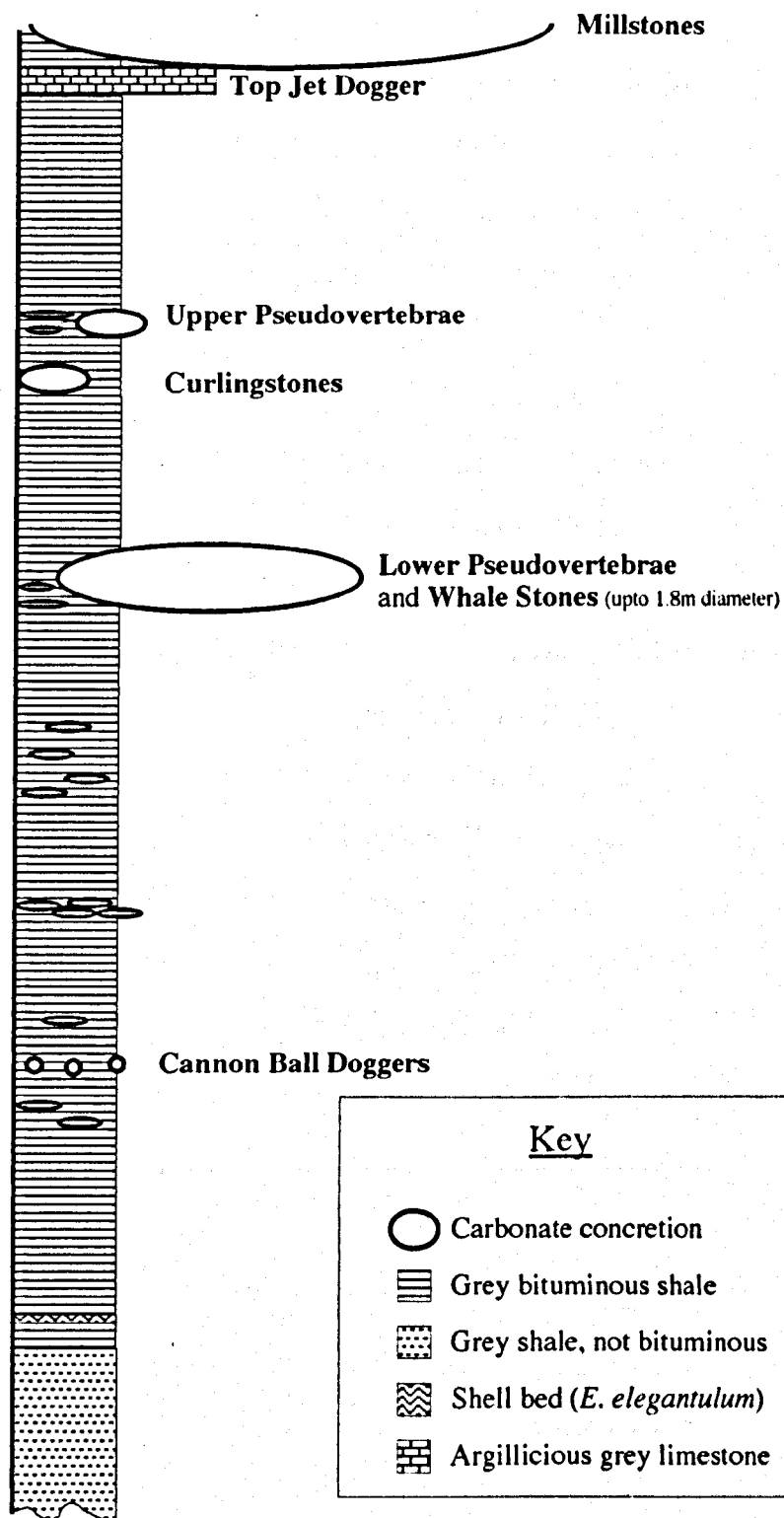
The total natural gamma-ray count was measured at thirteen sites along the beach section to determine the uranium content (ppm), thorium content (ppm)

Figure 5.2



Map showing the location of Port Mulgrave on the east coast of Yorkshire.

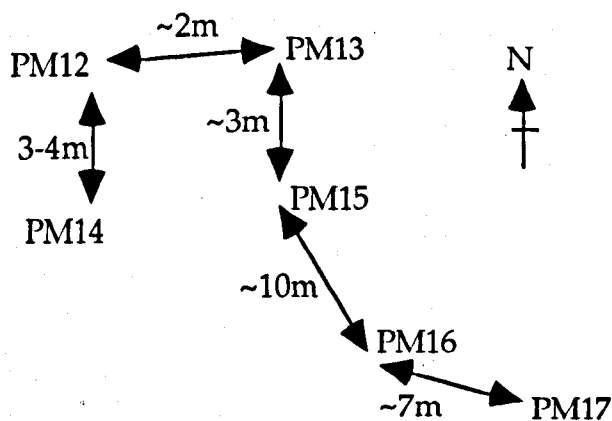
Figure 5.3



Sedimentary log of the Jet Rock sequence at Port Mulgrave.

Table 5.1

Sample	Location relative to concretion horizons
PM1	Top Jet Dogger (top part)
PM2	30cm below PM1
PM3	30cm below PM2
PM4	Upper Pseudovertebrae
PM5	Curlingstones
PM6	45cm below PM5
PM7	30cm below PM6 (base of bed 36)
PM8	Whalestones (top)
PM9	Whalestones (base)
PM10	45cm below PM9 (just above layer of flat pyritic nodules)
PM11	60cm below PM10
PM12	Cannon Ball Doggers
PM13	Cannon Ball Doggers
PM14	Cannon Ball Doggers
PM15	Cannon Ball Doggers
PM16	Cannon Ball Doggers
PM17	30cm below CBDs



Spatial distribution of the Cannon Ball Dogger samples.

Jet Rock sample locations.

and  $^{40}\text{K}$  content (%K) (Table 5.2). The measurements were made according to the criteria of Myers and Wignall (1987), i.e. by placing the Exploranium detector on relatively fresh flat surfaces permanently saturated with water. The precision of the measurements is thought to be better than 2% (Maynard, 1991) with a count time of 120 seconds.

The values obtained in this study compare favourably with those previously published for the Jet Rock (Myers and Wignall, 1987). The total radioactivity (ROI) remains essentially constant throughout the sequence. The Top Jet Dogger is however clearly picked out, being depleted in radioactive minerals relative to the rest of the argillaceous sediment.

There is a weak correlation between the organic carbon content and the authigenic uranium concentration (Figure 5.4), indicating that anoxia contributed to the accumulation and fixation of uranium into the sediment. Authigenic uranium is ubiquitous throughout the succession. The lowest level of  $U_{\text{auth}}$  is found at the base of the sequence but in general, the lower part of the sequence has a higher authigenic uranium content. The maximum  $U_{\text{auth}}$  also corresponds to the maximum TOC content.

The Th/K ratio has been used as a grain size indicator (van Buchem *et al.*, 1992). The Jet Rock shows little change in grain size and composition except for the limestone at the top of the section. The Th/K ratio remains essentially constant ( $7.51 \pm 1.06$ ) apart from the limestone horizon.

## 5.5 Carbon, Iron and Sulphur Relationships

The relationships between carbon, iron and sulphur have been discussed in Chapter 2. The aim of this section is to examine the C/S relationships throughout the sequence and to use DOP to act as a palaeoenvironmental indicator. These parameters will then be compared with organic palaeoenvironmental indicators. The relative importance of iron as a sink for reduced sulphur will also be discussed in relation to the formation of organo-sulphur compounds.

The C, S and Fe geochemistry of the Jet Rock has been studied extensively by Raiswell with co-workers (Raiswell and Berner, 1985; Raiswell *et al.*, 1988; Raiswell *et al.*, 1993a). The C/S, FeR/C and DOP/C relationships have been



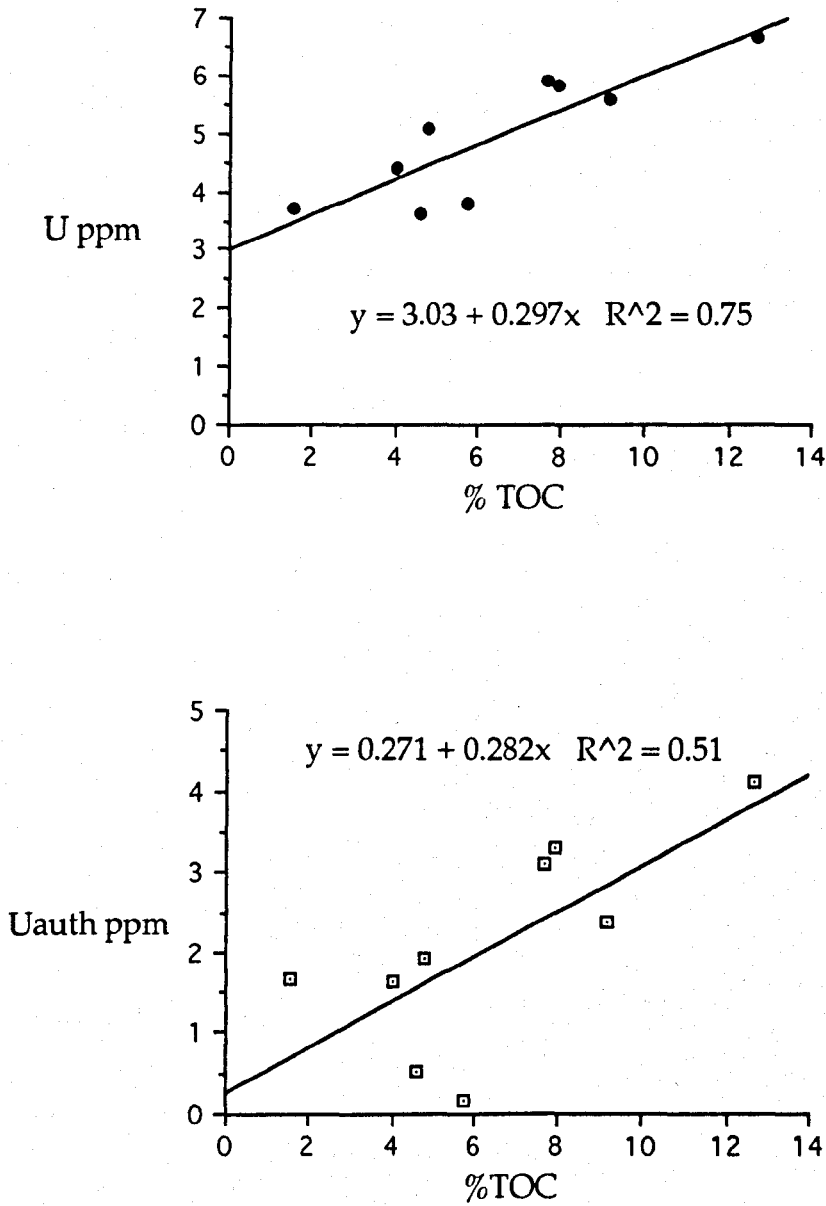
Table 5.2

Sample	%K	U ppm	Th ppm	U/Th
	1.50	5.80	10.30	0.56
PM1	0.80	3.70	6.10	0.61
PM3	1.30	4.40	8.30	0.53
	1.20	6.50	10.00	0.65
	1.50	4.80	8.60	0.56
	1.10	3.30	8.10	0.41
PM5	1.30	5.10	9.50	0.54
PM7	1.00	3.60	9.20	0.39
PM8	1.10	6.70	7.70	0.87
PM9	1.00	5.60	9.60	0.58
PM10	1.10	5.80	7.50	0.77
PM12	1.20	5.90	8.40	0.70
PM17	1.30	3.80	10.90	0.35

Gamma ray log of the Jet Rock.

Readings were taken from the Top Jet Dogger (above PM1) to the Grey Shales (PM17).

Figure 5.4



Relationship between uranium (total and authigenic uranium) and organic carbon.

interpreted as showing a carbon-reduced sulphur distribution parallel to that of a normal marine shale but with a syngenetic offset. The positive correlation between reactive iron and organic carbon suggests that the C/S pattern results from the coupling of iron and organic carbon i.e. the pyrite formation is iron limited. The DOP remains constant with increasing TOC indicating a marked syngenetic pyrite component with little pyrite forming after the iron bearing minerals have reached the sediment water interface. These results are shown in Figure 5.5 and Table 5.3.

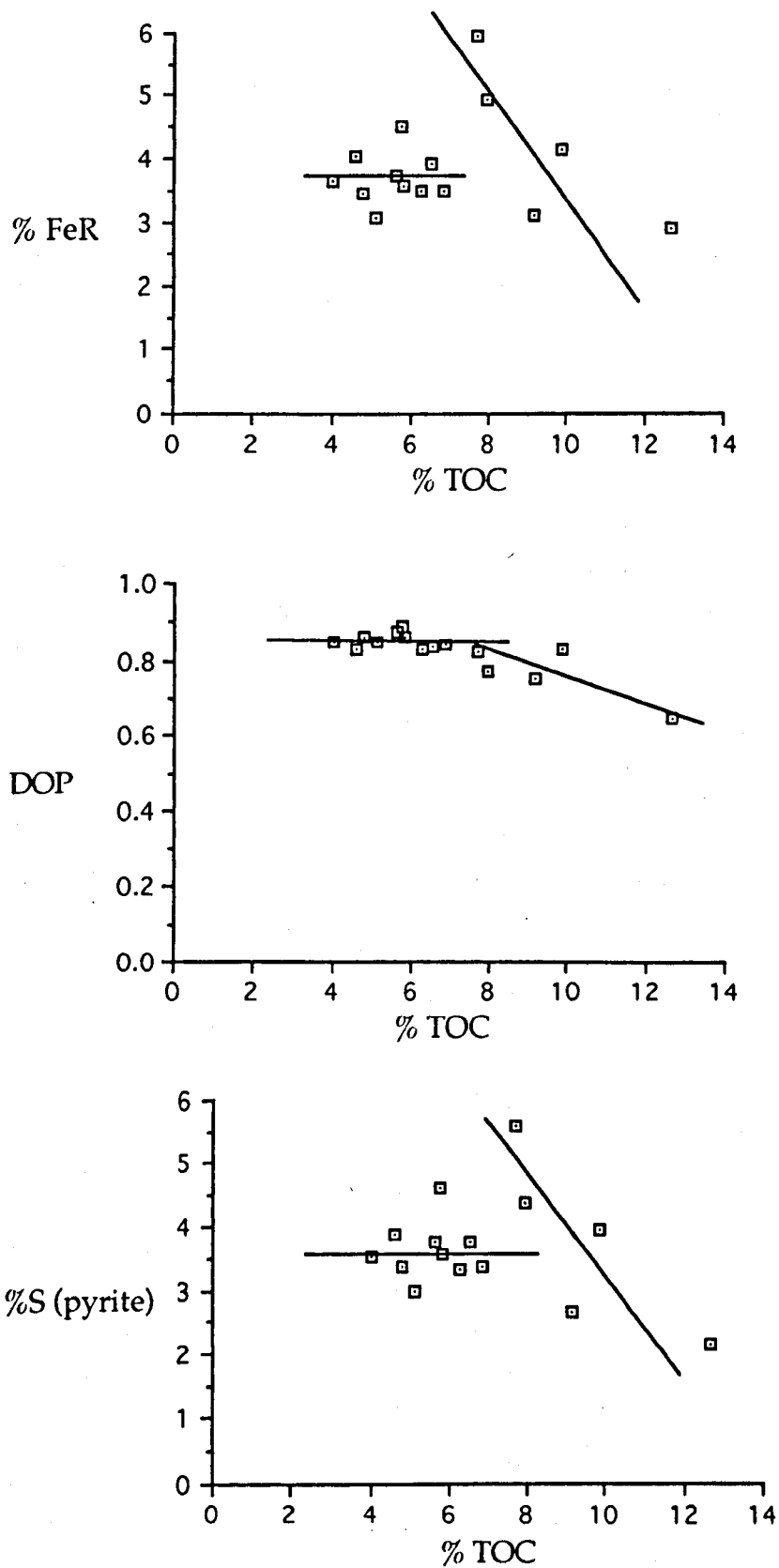
However it can be seen that there are conflicting trends in samples with  $\text{TOC} > 8\%$ . This observation is also picked out in the data obtained by Al-Biatty (1990). Little attention has been paid to these trends. Raiswell *et al.* (1993a) published another data set showing the same decreasing S/C, FeR/C and DOP/C relationships with samples having TOC greater than 8%.

There is an apparent lithological control on the distribution of organic carbon. Samples with  $\text{TOC} > 8\%$  are exclusively found around the Whalestone concretions (Bed 35) comprising of approximately 1m of sediment. The gamma ray logs show an increased authigenic uranium content at this stratigraphic level (this study and Myers and Wignall, 1987), suggesting that there was a change in the diagenetic conditions affecting this horizon.

Organic matter preservation is usually associated with very low levels of oxygen, as is the presence of authigenic uranium. Indeed, Myers and Wignall (1987) state that the maximum authigenic uranium value represents "the most intense period of anoxia" of the Jet Rock. However, it is in these samples which show the lowest DOP values (mean 0.76, this study), decreasing with increasing organic carbon content and a very wide range in pyrite content (3.9 to 7.2%, Raiswell *et al.*, 1993a; 2.1 to 5.6%, this study). Clearly there must be some factor controlling the pyrite formation unique to these particular samples in the middle of the sequence studied.

Raiswell and Berner (1985) considered the idealised relationships between organic carbon and pyrite sulphur in euxinic sediments. They used DOP to establish the controlling (limiting) factor of pyrite formation i.e. exhaustion of either the carbon or iron reservoir. Figure 2.5 shows the two scenarios discussed. Syngenetic pyrite formed in the water column will be independent of the organic carbon content of the sediment, hence the positive value for S at zero organic carbon. In general, organic carbon and iron minerals are thought

Figure 5.5



The relationship between reactive iron (FeR), degree of pyritisation (DOP) and pyrite sulphur with total organic carbon (TOC).

Table 5.3

Sample	%FeR	%TOC	% S	DOP
PM1	2.37	1.56	1.18	0.43
PM2	4.36		4.15	0.83
PM3	3.64	4.03	3.54	0.85
PM4	3.07	5.11	2.99	0.85
PM5	3.44	4.81	3.39	0.86
PM6	3.57	5.84	3.55	0.87
PM7	4.05	4.60	3.88	0.83
PM8	2.92	12.65	2.17	0.65
PM9	3.08	9.14	2.65	0.75
PM10	4.95	7.95	4.38	0.77
PM11	5.95	7.68	5.61	0.82
PM12	4.16	9.83	3.97	0.83
PM13	3.74	5.61	3.75	0.87
PM14	3.48	6.85	3.36	0.84
PM15	3.93	6.54	3.77	0.83
PM16	3.49	6.27	3.34	0.83
PM17	4.52	5.74	4.62	0.89

Summary of the reactive iron (FeR), organic carbon (TOC), pyrite sulphur (S) and degree of pyritisation (DOP) for the Jet Rock

to have a positive correlation (Berner 1984), due to the presence of colloidal organic material adsorbed onto clay minerals. Thus, where argillaceous sediments are deposited, there is commonly a correlation between iron and carbon. Carbon limited and iron limited sediments show the same general increase in pyrite content with increasing organic matter, but DOP increases with TOC in carbon limited situations, whereas DOP is uniform with increasing organic carbon where iron is the limiting factor.

The data for the Jet Rock suggests that the bulk of the sediment was iron limited (DOP generally greater than 0.85). Most of the pyrite being formed in the water column syngenetically. However, around the Whalestones the limiting factors change. Similar results have been reported by Fisher and Hudson (1987) from samples taken from the Lower Oxford Clay. Both DOP and FeR decrease with organic carbon greater than about 8%. There is a conflict in interpretation of this data. Fisher and Hudson (1987) argue that pyrite formation is limited by sulphate availability. Raiswell and Berner (1985) suggest that sulphate is not a limiting factor for pyrite formation in marine sediments with normal salinity therefore iron is the controlling factor in pyrite formation within the Lower Oxford Clay. However, the sulphur isotopic composition of the pyrite from the Lower Oxford Clay is relatively heavy, suggesting that there has been some closed system sulphate reduction and incorporation of heavy H<sub>2</sub>S into pyrite.

Williams (1978) notes a positive correlation of organic-C and sulphide-S in ancient sediments in the Cambrian Alum Shale. In samples with a carbon concentration greater than 10 moles /kg (~12 wt %), there is a distinct negative correlation with sulphide-S. Most samples analysed plot within this field (61 out of 68 samples). No explanation is given for this trend in data by Williams. Authigenic carbonate concentrations are in general positively correlated with organic carbon concentrations. Where this is the case, dilution of clastic iron-rich clays by iron poor carbonates can lead to a negative correlation between iron and organic carbon (Raiswell and Berner 1985). Therefore one possible explanation of the samples containing high organic carbon in the data presented by Williams (1978) is that of a carbonate dilution effect.

It is obvious that there is a significant negative correlation between reduced sulphur (as pyrite) and organic carbon in ancient anoxic marine sediments in three examples where the TOC is greater than 8wt%. The Jet Rock samples have been studied in detail to provide a reinterpretation of the existing data

and by analogy to provide a model for the organic carbon rich parts of the Lower Oxford Clay and the Cambrian Alum Shale.

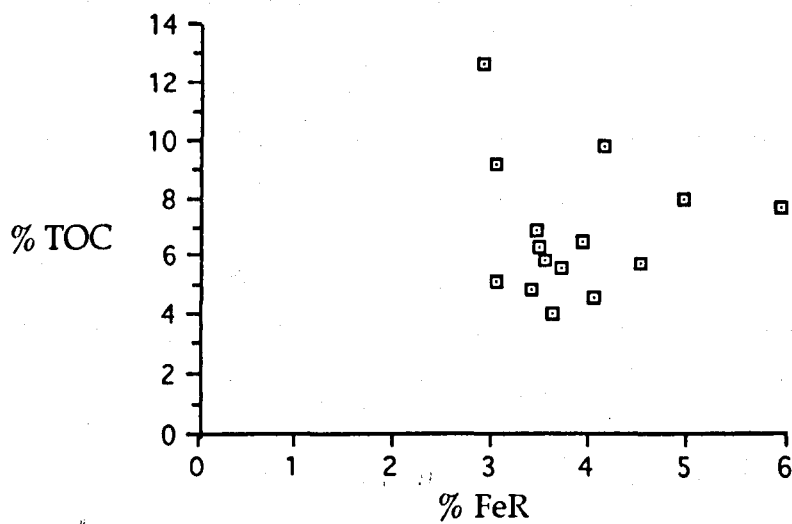
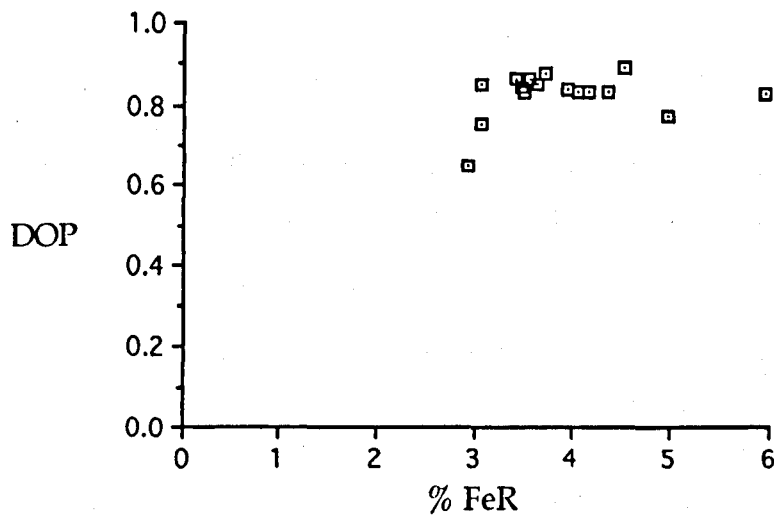
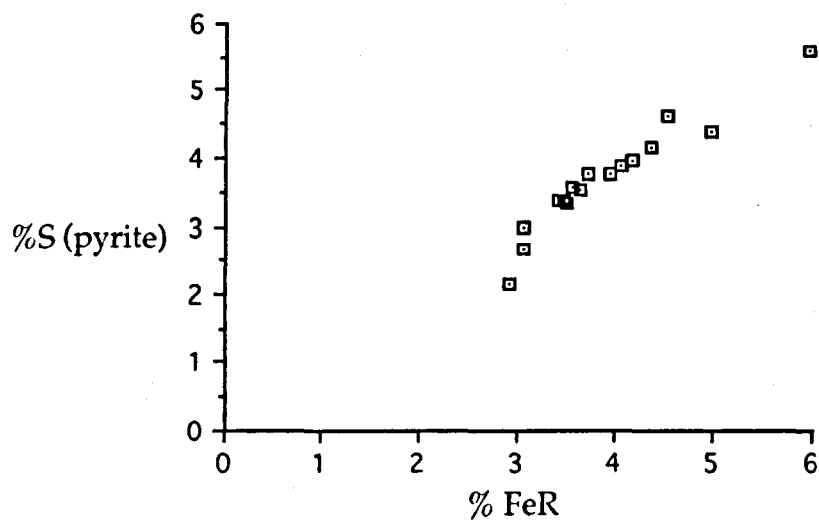
The cross plot of reactive iron (FeR) and pyrite sulphur shows excellent correlation (correlation coefficient 0.9) over the entire range of values (Figure 5.6). The concentration of reactive iron decreases markedly with increasing organic carbon and because of the relationship between reactive iron and pyrite sulphur there is a corresponding decrease of pyrite as organic carbon increases. At very high organic carbon levels (>10%), the amount of pyrite within the sample is at the same concentration as samples with the lowest organic carbon contents. The correlation between FeR and pyrite concentration also helps to explain the trends in DOP. At low FeR the difference between HCl soluble Fe and Fe as pyrite will be significant therefore the DOP values are expected to be low. With increasing FeR concentrations (and hence pyrite Fe), the difference between [Fe-HCl soluble + Fe-pyrite] and Fe-pyrite will decrease, thereby increasing the DOP.

If the argument presented above is the mechanism for generating the negative correlations between C and FeR and between C and S then, why does either FeR or S (whichever is the limiting factor) decrease? It is unlikely that iron is the limiting factor in the Jet Rock. As Raiswell and Berner (1985) point out, DOP would be high and constant relative to organic carbon. Therefore given the abundance of organic carbon in the section the limiting factor for pyrite formation must be sulphide.

The concentration of sulphide in the diagenetic regime is determined by organic carbon, a sink for the sulphide (generally iron minerals), diffusion and a source of sulphate (see Chapter 2). The unknown factors in the Jet Rock are the sulphate supply and the diffusion out of the system of hydrogen sulphide. If conditions were euxinic as the geochemical data suggests, syngenetic pyrite would form by the reaction of iron bearing minerals with sulphidic bottom waters. The pyrite so formed would be independent of organic carbon concentrations. If the sulphate resupply to the anaerobic sulphate reducing bacteria was cut off a closed system of sulphate reduction would be established. Euxinic conditions would prevent bioturbation by benthic fauna.

The hydrogen sulphide produced by such closed system sulphate reduction would become isotopically heavier. Any subsequent diagenetically formed pyrite would be enriched in  $^{34}\text{S}$ . If the heavy  $\text{H}_2\text{S}$  were to diffuse into the water

Figure 5.6



The relationship between pyrite sulphur, degree of pyritisation (DOP) and total organic carbon (TOC) with reactive iron (FeR).



column, isotopically heavy syngenetic pyrite may also form. A plot of data from this study including the data of Raiswell *et al.* (1993) shows the relationship between  $\delta^{34}\text{S}_{\text{pyrite}}$  and organic carbon (Figure 5.7). There appear to be two sets of samples. Below 8% C the samples cover a wide spread of  $\delta^{34}\text{S}$  from -30‰ to -22‰. The samples containing over 8% carbon show a positive correlation with  $^{34}\text{S}$  i.e. they become isotopically heavier from -24‰ to -20‰.

## 5.6 Organic matter

### 5.6.1 Kerogen

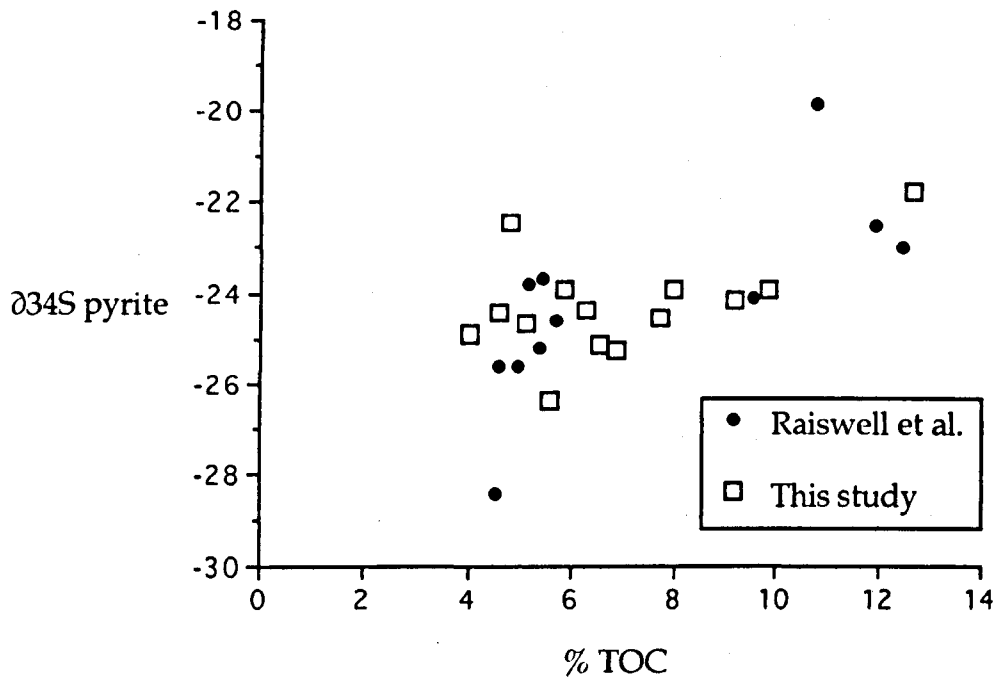
Two kerogen samples isolated by demineralisation (HF, 100%) were examined optically to determine the principle kerogen constituents (Figure 5.8). The results indicate that the Top Jet Dogger (PM1) is a mixture of fluorescent amorphous material derived from marine phytoplankton and palynomorphs from a terrestrial source. The shales stratigraphically lower in the sequence, represented by PM2 indicate a much greater marine component. The limestone (PM1) shows coarser, less well sorted organic material than PM2 which has fine, well sorted organic matter.

The Rock Eval results (Table 5.4) also indicate a kerogen of Type II origin. Van Krevelen type plots of hydrogen index against oxygen index and hydrogen index against  $T_{\text{max}}$  both suggest the organic matter within the Jet Rock is of Type II composition (Figures 5.9 and 5.10). Figure 5.10 indicates a thermal maturity less than 1.0%. This was confirmed by vitrinite reflectance measurements (0.55 to 0.65) and the spore colouration index reported by Raiswell *et al.* (1993a) of 3.5 to 4.5. It is thought that the Jet Rock has been buried to a depth less than 2.5km (Pye, 1985) suggesting that the maximum temperatures reached were in the region of 60-80°C.

### 5.6.2 Bitumen

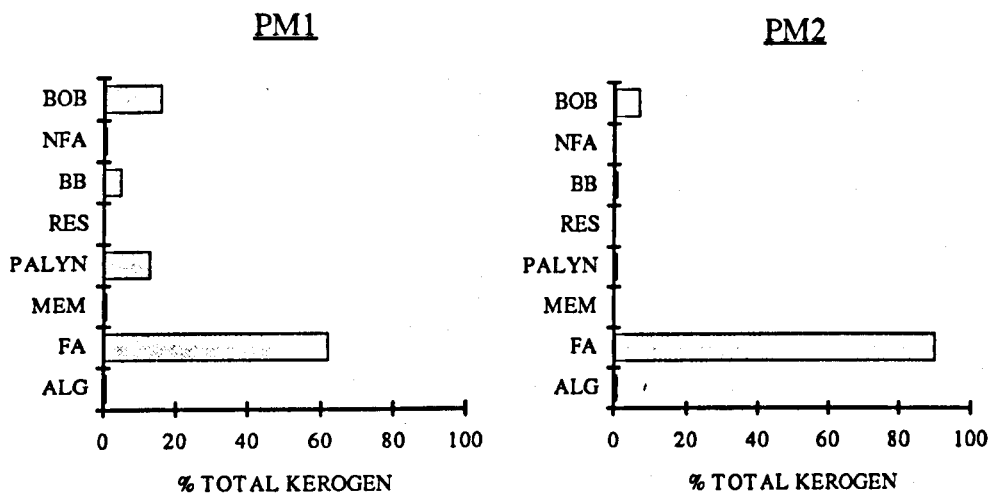
The bitumen from the Jet Rock was soxhlet extracted in an azeotropic mixture of DCM and methanol. The percentage of soluble organic matter in the Jet Rock ranges from 0.5% to 2.4% (Table 5.5). The amount of bitumen in a sample expressed as a proportion of the total organic carbon content is defined as the Transformation Ratio. This ratio remains roughly constant throughout the sequence indicating constant factors affecting all the organic material and also suggesting that the organic matter throughout the sequence was of

Figure 5.7



The relationship between total organic carbon and  $\delta^{34}\text{S}$  pyrite. The data presented by Raiswell *et al.* (1993a) is shown together with data from this study.

Figure 5.8



Constituents of the kerogen isolated from samples PM1 and PM2.

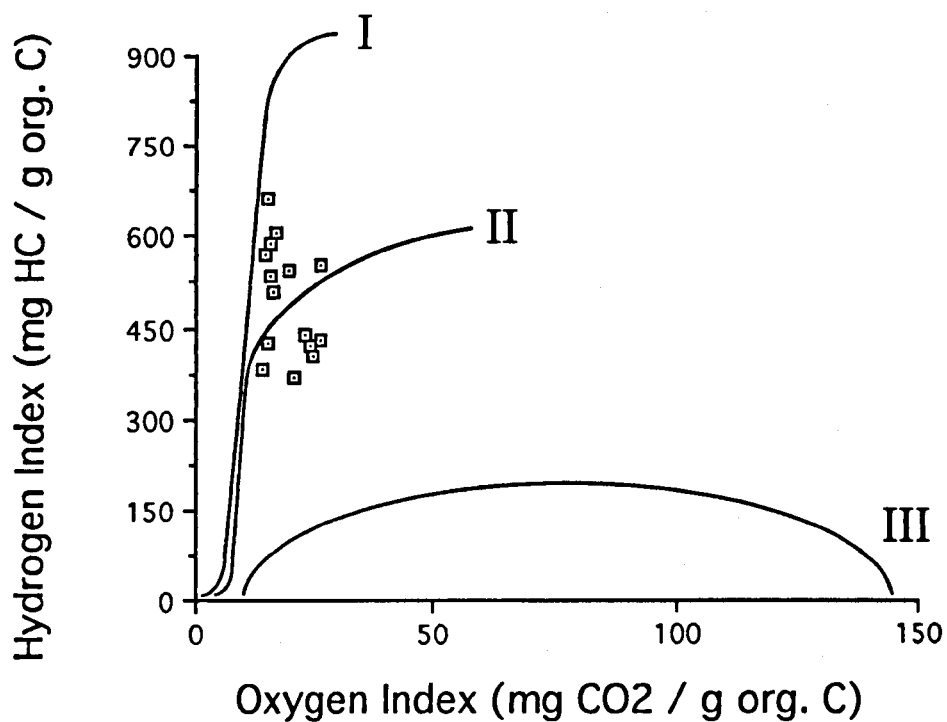
<u>Abbreviation</u>	<u>Kerogen Type</u>
BOB	Black Opaque Blocky
NFA	Non-Fluorescent Amorphous
BB	Brown Blocky
RES	Resinous
PALYN	Palynomorphs
MEM	Membranes
FA	Fluorescent Amorphous
ALG	Algae

Table 5.4

Sample	%TOC	S1	S2	S3	PI	HI	OI	T <sub>max</sub>
PM1	1.56	1.96	6.74	1.09	0.23	432.05	69.87	438
PM3	4.03	2.07	16.28	0.99	0.11	403.97	24.57	438
PM4	5.11	4.72	18.89	1.06	0.20	369.67	20.74	439
PM5	4.81	5.09	20.27	1.15	0.20	421.41	23.91	437
PM6	5.84	4.83	25.05	1.55	0.16	428.94	26.54	437
PM7	4.60	4.22	20.16	1.06	0.17	438.26	23.04	436
PM8	12.65	6.96	48.14	1.79	0.13	380.55	14.15	440
PM9	9.14	4.57	38.92	1.36	0.11	425.82	14.88	437
PM10	7.95	4.80	52.82	1.21	0.08	664.40	15.22	440
PM11	7.68	3.77	45.10	1.19	0.08	587.24	15.49	439
PM12	9.83	4.70	55.91	1.43	0.08	568.77	14.55	439
PM13	5.61	2.74	30.91	1.49	0.08	550.98	26.56	439
PM14	6.85	3.19	35.00	1.10	0.08	510.95	16.06	439
PM15	6.54	3.25	34.97	1.04	0.09	534.71	15.90	443
PM16	6.27	3.51	38.00	1.07	0.08	606.06	17.07	441
PM17	5.74	3.04	31.23	1.12	0.09	544.08	19.51	438

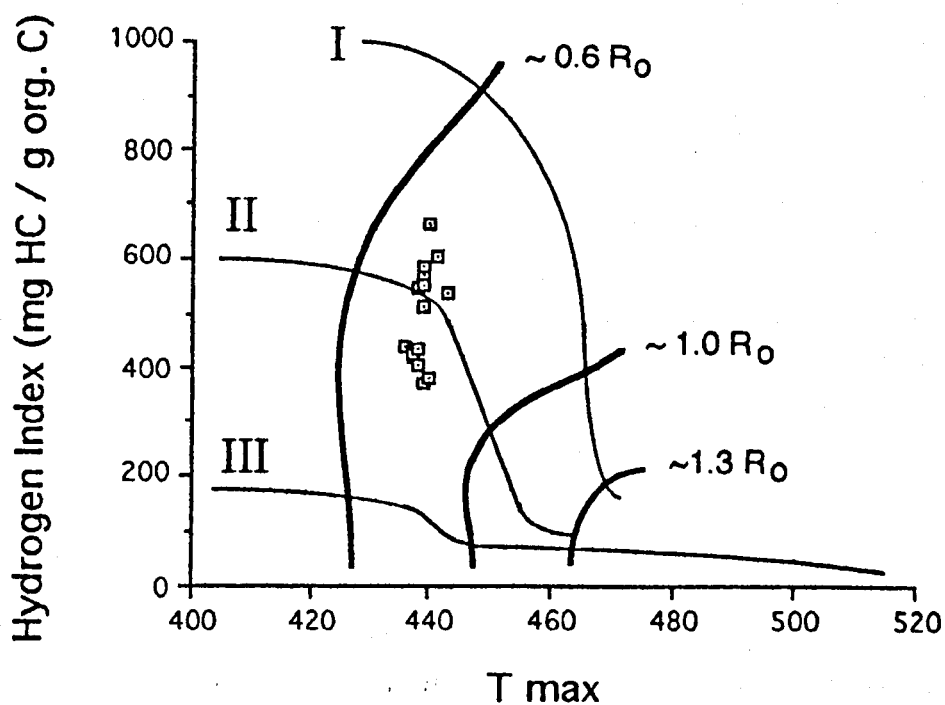
Rock Eval data for the Jet Rock.

Figure 5.9



Van Krevelen type plot for the Jet Rock indicating Type II kerogen.

Figure 5.10



Van Krevelen type plot for the Jet Rock indicating Type II kerogen with  $R_0 \sim 0.7$ .

Table 5.5

Sample	% TOC	% EOM	Transformation Ratio
PM1	1.56	0.56	0.36
PM2		1.27	
PM3	4.03	1.29	0.32
PM4	5.11	1.42	0.28
PM5	4.81	1.52	0.32
PM6	5.84	1.84	0.31
PM7	4.60	1.94	0.42
PM8	12.65	2.37	0.19
PM9	9.14	2.34	0.26
PM10	7.95		
PM11	7.68	2.16	0.28
PM12	9.83	2.14	0.22
PM13	5.61	1.52	0.27
PM14	6.85	1.70	0.25
PM15	6.54	1.96	0.30
PM16	6.27	2.00	0.32
PM17	5.74	1.83	0.32

Extractable organic matter (EOM), total organic carbon (TOC) and the transformation ratio for the Jet Rock samples.

approximately the same composition relative to its hydrocarbon generating potential (Figure 5.11).

The bitumen extracted from each sample was chemically separated firstly into asphaltene and maltene fractions. Subsequent separation of the maltene fractions into aliphatic, aromatic and polar fractions were performed. The relative proportions of each of the fractions are given in Table 5.6. The bitumen is of a relatively constant composition. The ratio of maltene to asphaltene is roughly 3:1 (Table 5.5), the maltene is dominated by aliphatic and aromatic compounds with the polar compounds typically being less than 10% of the maltene fraction.

The chemical composition (C,H,N,O and S) of the bitumen and the fractions are given in Table 5.7a,b,c,d,e. The marked variations in the constituent elements cannot be ascribed wholly to sample variation. The analytical and experimental error is thought to have been significant in the analysis of the fractions. Although the separation of the fractions is thought to be good giving 100% yields  $\pm$  1%, the samples collected from the Cannon Ball Dogger Horizon (PM12 to PM16) show significant variation, therefore the data must be treated with some caution. Relative trends are however easily identified.

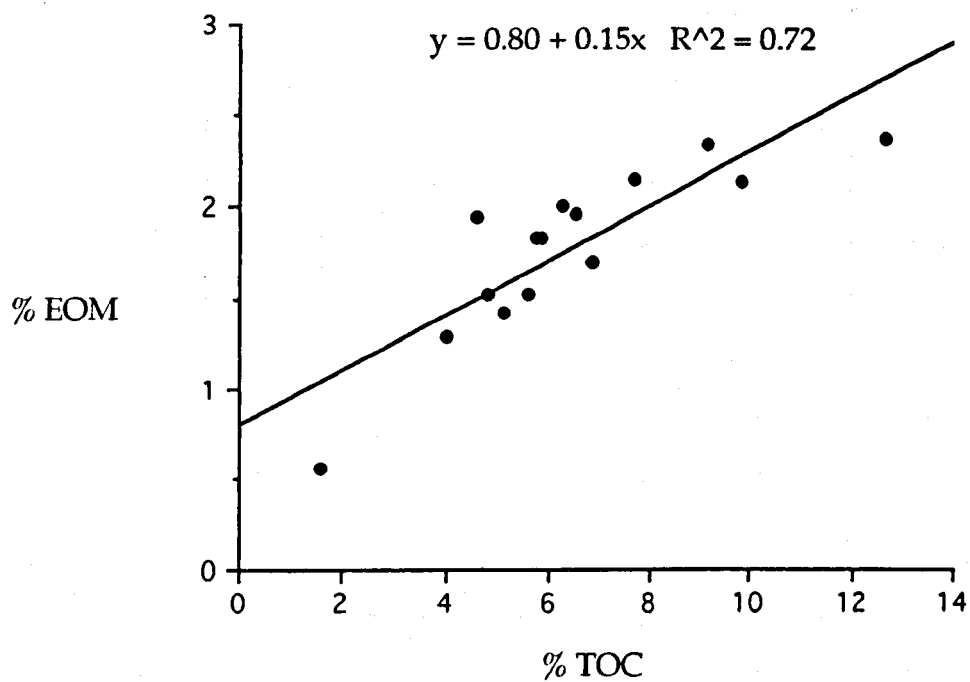
The samples which are relatively rich in hetero atoms (N,S and O) are those with a more polar nature (asphaltene, aromatic and polar). The aliphatic fraction is devoid of sulphur and contains mainly nitrogen as the dominant heteroatom. The ternary diagram (Figure 5.12) shows the distribution of nitrogen, oxygen and sulphur in the samples. The data for the total bitumens plots in similar fields to that of Raiswell *et al.*, 1993a.

### 5.6.3 Biological markers

The fractions separated by liquid chromatography have been investigated at a molecular level by GC, GC-MS, GC-FID/FPD and GC-AED to establish the nature of the organic material and to speciate the compounds in which sulphur is present.

The ratio of odd carbon number n-alkanes to even number n-alkanes was measured from GC of the aliphatic fraction and is shown on Table 5.8 expressed as the CPI (Carbon Preference Index). Examples of these traces are

Figure 5.11



The relationship between extractable organic matter (EOM) and total organic carbon (TOC) for the Jet Rock.



Table 5.6

Sample	% maltene	% asphaltene	%aliphatic of bitumen	%aromatic of bitumen	%polar of bitumen	%aliphatic of maltene	%aromatic of maltene	%polar of maltene
PM1	61.60	38.30	33.14	23.16	5.30	53.80	37.60	8.60
PM2	83.60	16.40	42.64	34.53	6.35	51.00	41.30	7.60
PM3	83.30	16.70	28.91	44.90	9.58	34.70	53.90	11.50
PM4	73.60	26.30	23.40	39.82	10.38	31.80	54.10	14.10
PM5	77.10	22.90	29.30	36.16	11.57	38.00	46.90	15.00
PM6	85.20	14.80	39.11	36.47	9.63	45.90	42.80	11.30
PM7	65.90	34.20	23.13	34.40	8.30	35.10	52.20	12.60
PM8	83.70	16.40	30.55	43.61	9.54	36.50	52.10	11.40
PM9	67.40	32.50	23.12	33.70	10.58	34.30	50.00	15.70
PM10	83.40	16.50	35.86	37.28	10.26	43.00	44.70	12.30
PM11	81.80	18.20	34.93	37.14	9.73	42.70	45.40	11.90
PM12	79.40	20.50	33.82	37.00	8.65	42.60	46.60	10.90
PM13	72.40	27.50	46.55	17.30	8.54	64.30	23.90	11.80
PM14	77.10	22.90	34.16	34.70	8.25	44.30	45.00	10.70
PM15	85.40	14.50	44.66	31.94	8.71	52.30	37.40	10.20
PM16	76.10	23.80	44.52	22.91	8.68	58.50	30.11	11.40
PM17	69.40	30.50	36.50	23.94	8.95	52.60	34.50	12.90

Relative proportions of the organic fractions from the extracted bitumen.

**Table 5.7a**

Sample	%C	%H	%N	%S	%O
PM1	88.29	8.80	0.14	2.10	0.67
PM2	88.63	9.47	0.03	0.82	1.05
PM3	88.07	9.45	0.48	1.22	0.78
PM4	88.03	9.43	0.20	1.01	1.33
PM5	84.07	13.96	0.21	0.75	1.01
PM6	88.91	9.53	0.26	0.88	0.42
PM7	87.86	9.06	0.47	1.13	1.48
PM8	87.76	8.97	0.35	1.40	1.52
PM9	87.58	8.83	0.46	1.46	1.67
PM10	88.88	9.05	0.35	1.14	0.58
PM11	88.10	9.19	0.27	0.97	1.47
PM12	89.07	9.22	0.25		
PM13	87.64	8.90	0.63	1.55	1.28
PM14	88.55	8.85	0.54	0.98	1.08
PM15	88.04	8.91	0.53	1.00	1.52
PM16	88.02	9.20	0.20	0.96	1.62
PM17	87.23	9.00	0.46	0.97	2.34

Elemental composition of bitumen extracted from the Jet Rock.

Table 5.7b

Sample	%C	%H	%N	%S	%O*
PM1	88.99	4.70	2.34	3.59	3.59
PM2	88.73	4.67	1.86	3.93	3.93
PM3	88.72	3.61	1.92	2.03	2.03
PM4	88.95	4.98			
PM5	87.69	5.35	2.00	10.09	10.09
PM6	88.16	3.15	2.22	7.90	7.90
PM7	88.27	2.41	2.12	4.23	4.23
PM8	88.06	2.50	1.82	3.90	3.90
PM9	88.23	2.36	1.72	5.26	5.26
PM10	88.29	3.85	1.37	4.99	4.99
PM11	88.00	2.69	1.83	5.57	5.57
PM12	87.69	5.35	1.75	10.34	10.34
PM13	87.89	5.60	1.69	7.97	7.97
PM14	88.08	4.07	1.40	9.31	9.31
PM15	88.11	2.63	2.06	8.74	8.74
PM16	87.68	4.57	1.41	12.41	12.41
PM17			1.51		

Elemental composition of the asphaltene fraction of the bitumen extracted from the Jet Rock.

\* calculated by difference.

Table 5.7c

Sample	%C	%H	%N	%S	%O*
PM1	85.15	13.36	0.05	0.00	1.44
PM2	78.39	13.18	0.00	0.00	8.43
PM3	86.61	14.32	0.05	0.00	0.00
PM4	89.59	13.86	0.00	0.00	0.00
PM5	85.83	12.16	2.11	0.00	0.00
PM6	77.08	12.54	0.50	0.00	9.88
PM7	80.61	13.21	0.92	0.00	5.26
PM8					
PM9	94.43	12.55	0.00	0.00	0.00
PM10	83.50	13.59	0.13	0.00	2.78
PM11	76.81	11.41	0.74	0.00	11.04
PM12	80.94	12.69	0.00	0.00	6.37
PM13	86.75	11.98	0.00	0.00	1.27
PM14	83.21	6.71	0.22	0.00	9.86
PM15	86.39	9.72	0.50	0.00	3.39
PM16	85.23	13.68	0.23	0.00	1.09
PM17	81.01	10.32	0.10	0.00	8.57

- Elemental composition of the aliphatic fraction of the bitumen extracted from the Jet Rock.

\* calculated by difference.

Table 5.7d

Sample	%C	%H	%N	%S	%O*
PM1	88.43	10.39	0.45	1.38	0.00
PM2	89.25	10.76	1.55	0.77	0.00
PM3	89.30	10.99	0.39	0.78	0.00
PM4	86.53	9.78	1.51	1.26	0.92
PM5	86.00	9.93	1.46	0.98	1.63
PM6	88.70	11.15	0.50	0.88	0.00
PM7	85.19	10.54	0.15	0.90	3.19
PM8					
PM9	84.94	9.70	0.25	1.32	3.97
PM10	85.43	12.93	0.05	1.07	0.59
PM11	76.81	11.41	0.74	1.74	9.37
PM12	86.32	4.16	0.82	1.78	6.73
PM13	85.06	9.48	0.06	1.04	4.63
PM14	82.01	8.83	0.24	1.89	7.30
PM15	83.06	7.89	0.70	0.97	7.83
PM16	84.28	8.36	0.63	1.23	5.05
PM17	85.90	9.64	0.83	1.13	2.50

Elemental composition of the aromatic fraction of the bitumen extracted from the Jet Rock.

\* calculated by difference.

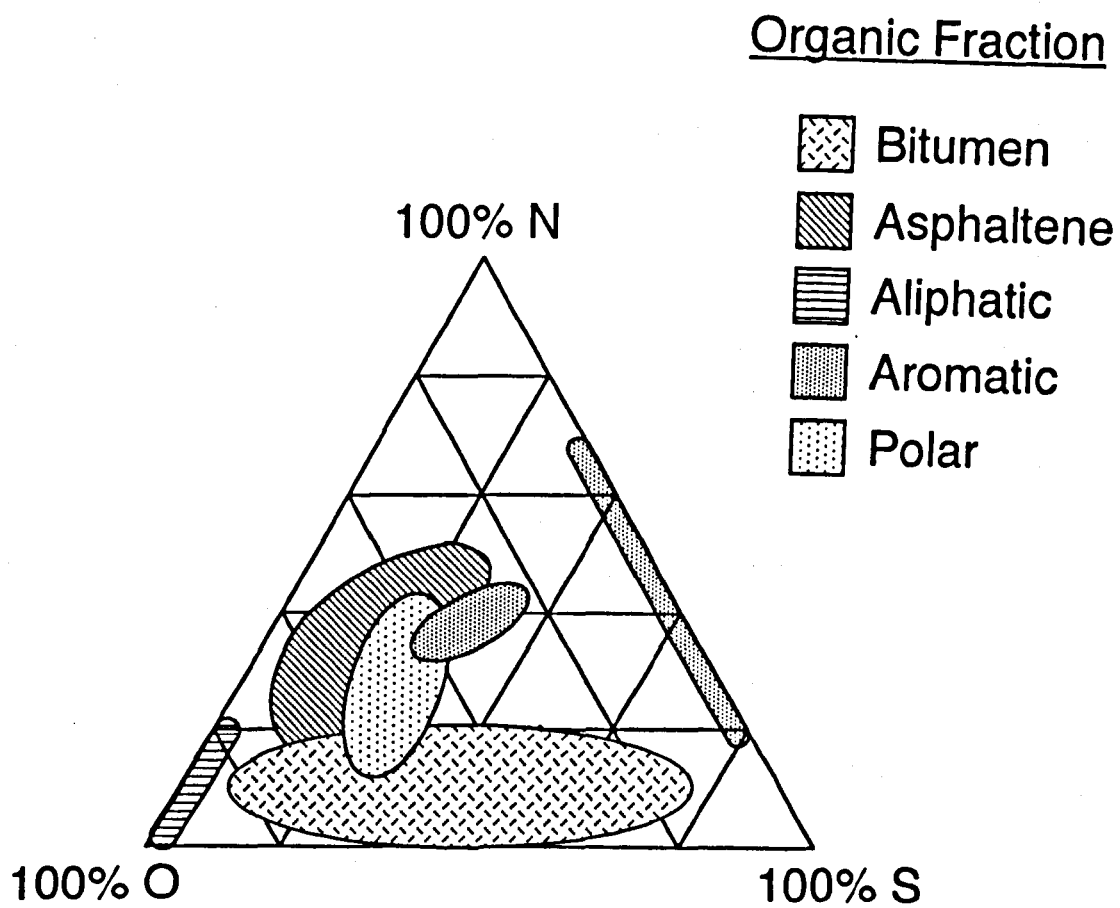
Table 5.7e

sample	%C	%H	%N	%S	%O *
PM1		9.17	4.12	2.42	4.70
PM2	81.65	10.02	1.33	1.98	5.02
PM3	82.39	9.23	2.25	1.91	4.22
PM4	89.59	13.86	0.00	2.03	5.48
PM5	82.23	8.68	1.23	2.69	5.17
PM6	81.94	9.70	5.16	2.58	0.62
PM7	83.08	9.73	1.50	1.87	3.80
PM8	78.75	9.18	1.95	1.46	8.66
PM9	81.05	8.45	1.31	2.13	7.06
PM10	75.46	8.23	1.81	2.15	12.35
PM11	78.21	8.56	1.20	1.48	10.55
PM12	77.16	8.32	1.65	1.89	10.98
PM13	77.04	4.23	1.07	1.56	16.10
PM14	78.50	9.89	1.50	1.68	8.43
PM15	79.45	9.60	1.89	2.50	6.56
PM16	77.48	9.16	1.54	2.46	9.36
PM17	80.49	8.98	1.00	1.80	7.73

Elemental composition of the polar fraction of the bitumen extracted from the Jet Rock.

\* calculated by difference.

Figure 5.12



Hetero-atom plot of the organic fractions of the Jet Rock.

**Table 5.8**

Sample	Pr/nC17	Ph/nC18	Pr/Ph	Ts/Tm	hopane	sterane	CPI
PM1	2.34	0.99	1.38	0.48	0.62	0.45	1.01
PM6	1.60	1.38	1.54	0.50	0.63	0.41	0.94
PM7	1.47	1.36	1.24	0.51	0.62	0.50	1.05
PM8	0.97	1.02	1.33	0.78	0.61	0.46	1.09
PM9	1.20	1.05	1.33	0.68	0.61	0.46	0.97
PM10	1.18	1.15	1.36	0.56	0.61	0.45	1.00
PM11	1.24	1.13	1.28	0.66	0.60	0.47	1.06
PM12	1.14	1.20	1.26	0.57	0.58	0.46	1.01
PM14	1.37	1.18	1.36	0.68	0.57	0.42	1.02
PM15	1.14	1.15	1.24	0.51	0.61	0.49	1.50
PM16	1.22	1.30	1.28	0.59	0.59	0.46	1.06
PM17	1.85	1.12	1.44	0.62	0.62	0.43	1.03

Summary of biomarker ratios measured on samples from the Jet Rock.



shown in Figure 5.13. The CPI for the Jet Rock has a value typical for mature oils. However, the maturity for the sequence is  $R_o \sim 0.6\%$  therefore the low CPI must be due to the dominance of plankton derived material in the kerogen.

The pristane/phytane ratio (Pr/Ph) is greater than 1 in all the samples measured. Traditional interpretations of such a result would be to imply oxidising conditions. The isoprenoids pristane and phytane normalised to nC-17 and nC-18 respectively indicate moderate biodegradation (Figure 5.14), but again the data do not plot in the field usually representing reducing palaeoenvironmental conditions.

The hopanes trisnorhopane ( $T_m$ ) and trisneonorhopane ( $T_s$ ) used as a ratio of abundance ( $T_s/T_m$ ) indicate that the Jet Rock is at the early to peak maturity stage of evolution, with values ranging from 0.48 to 0.78. The hopane 22S/22R biomarker ratio suggests a slightly higher maturity ( $R_o$  equivalent  $\sim 0.7\%$ ) and the sterane 20S/20R ratio indicates an even higher maturity.

The biomarker ratios obtained by GC peak area and peak height measurements are relatively easy to obtain from the aliphatic extract of shales but there seems to be poor correlation between several parameters. Therefore no single biomarker ratio should be considered as a reliable estimate. Only when several are compared in conjunction with each other should firm conclusions be drawn. The palaeoenvironmental indicators pristane and phytane clearly do not support the sedimentological and inorganic geochemical interpretations of the conditions at the time of burial.

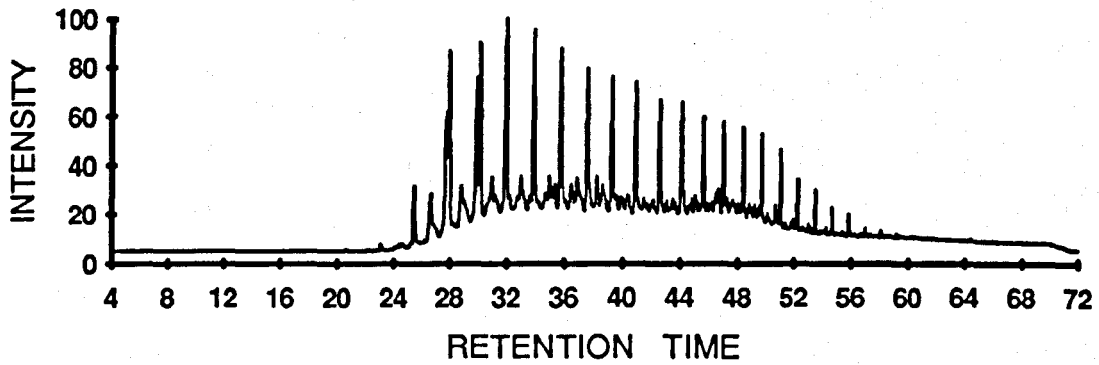
## 5.7 Organo-sulphur compounds

The identification of organo-sulphur compounds was tentatively made using a Finnigan TSQ 70 Triplequadrupole Mass Spectrometer. Positive identification of the species was not made despite attempts using GC-FID/FPD in conjunction with GC-MS. Dibenzothiophene was positively identified later in the same samples (A. Gize, pers. comm.).

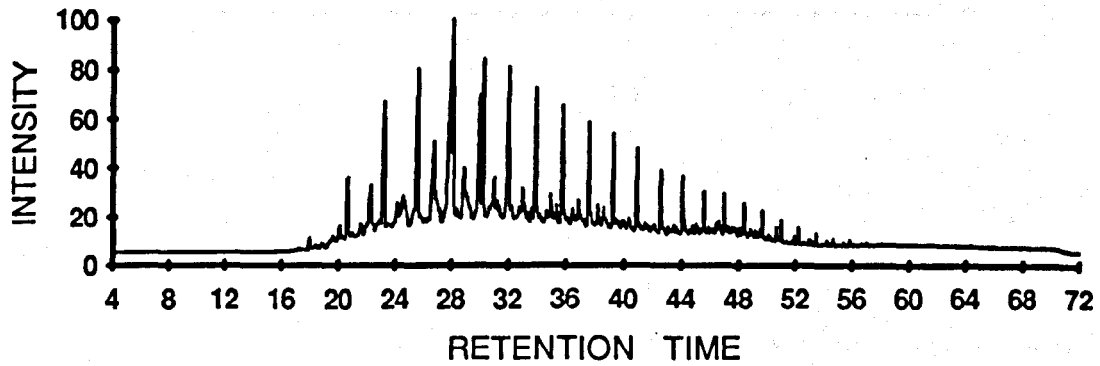
A more sulphur specific technique was employed (GC-AED) which confirmed the identification of dibenzothiophene together with alkylated dibenzothiophenes (Figure 5.15) in all the bitumens analysed (P. Louie, pers. comm.). The aromatic fractions were found to contain  $C_1$  to  $C_3$

Figure 5.13

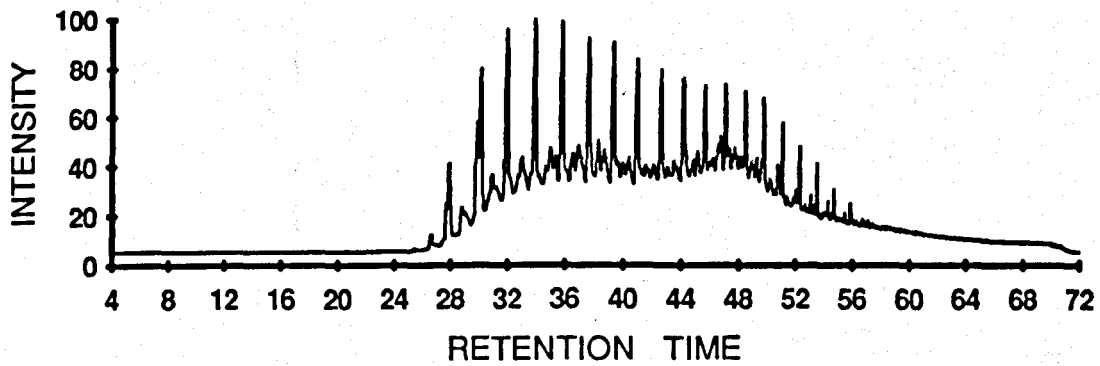
PM 1



PM 8

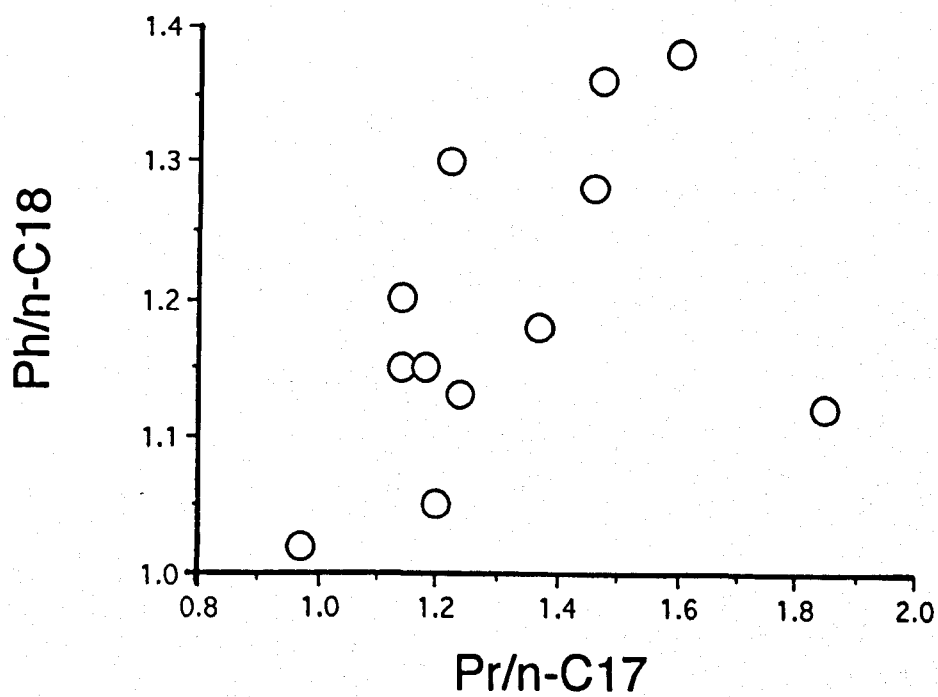
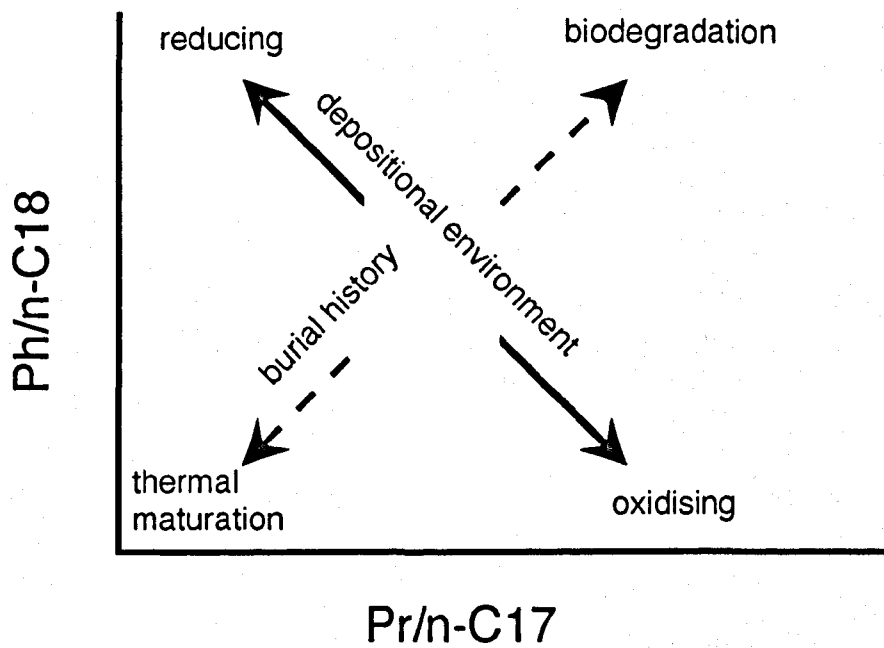


PM 17



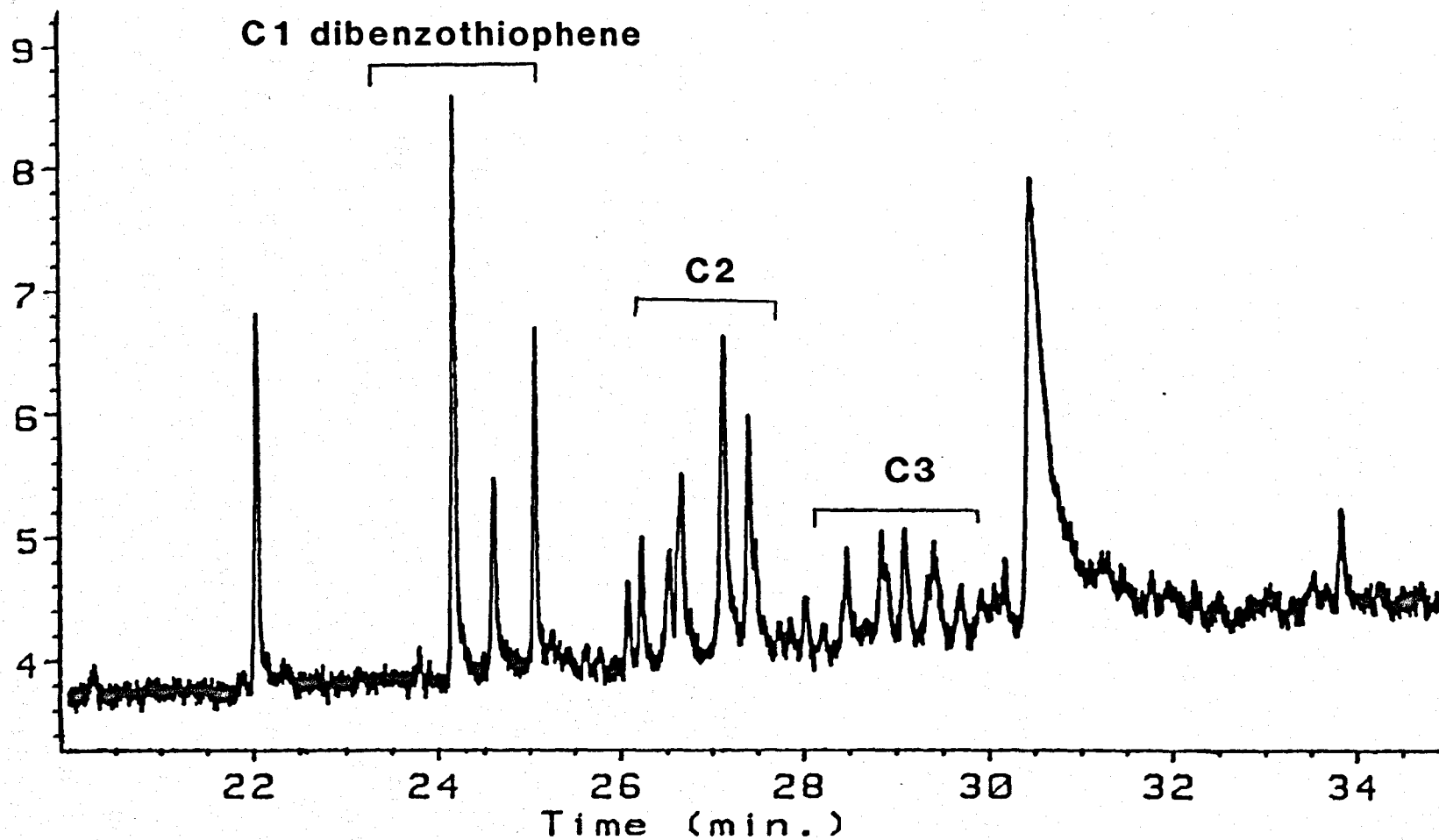
GC traces for aliphatic material extracted from the Jet Rock.

Figure 5.14



The pristane/heptadecane against phytane/octadecane cross plot used as a palaeoenvironmental indicator for the Jet Rock.

Figure 5.15



GC-AED trace showing the presence of dibenzothiophene and alkylated dibenzothiophenes in the bitumen from the Jet Rock.

dibenzothiophenes as the dominant sulphur bearing compounds. Most studies of the formation of organo-sulphur compounds use either modern sediments or sediments which are at a low thermal maturity. The Jet Rock samples have vitrinite reflectance in the order of 0.6%, clearly the early less stable OSC will not be present in samples of such relatively high maturity.

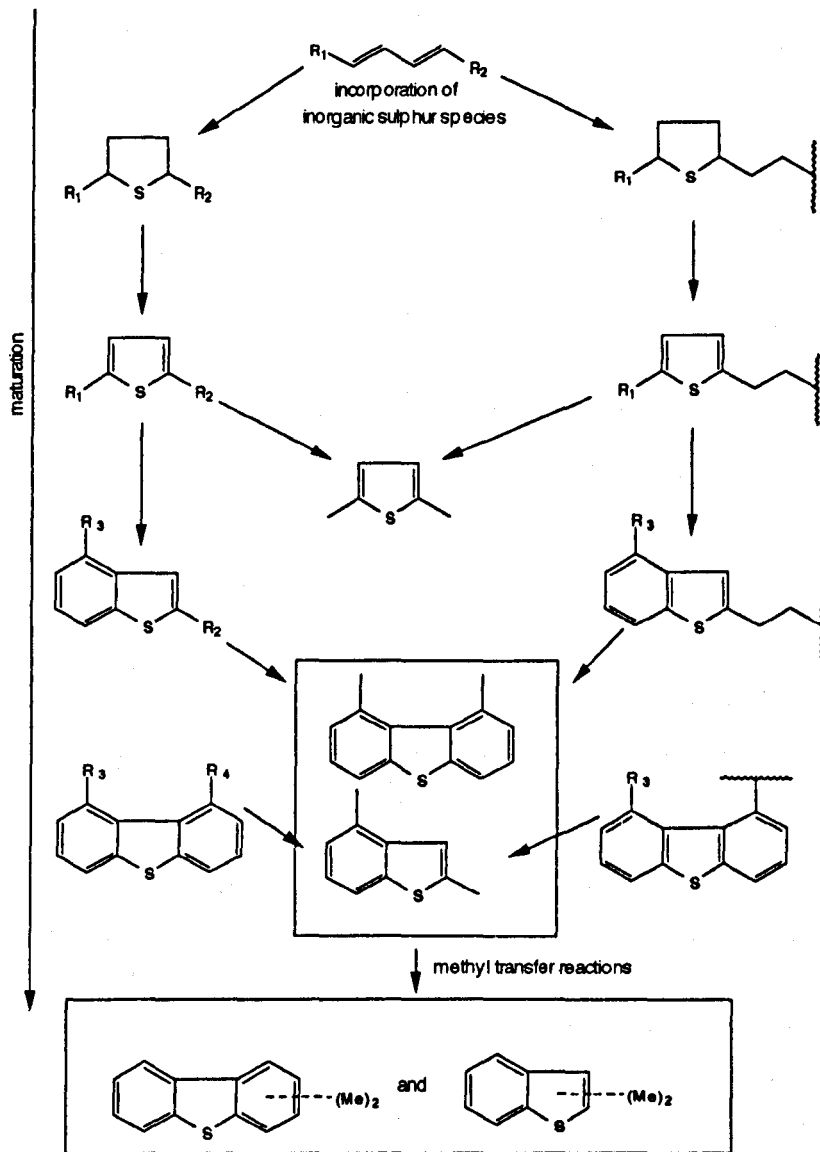
Dibenzothiophenes do not represent geochemical fossils in the strictest sense. The aromatic thiophenic structure is thought to form during the diagenesis of organic matter as rearrangement and degradational reactions proceed. Sinninghe Damsté and de Leeuw (1989) have reviewed the formation of organo-sulphur compounds including the generation of alkylated dibenzothiophenes. Figure 5.16 shows how a sulphur bearing alkane can be transformed through a sequence of reactions from thiolanes/thioanes to thiophenes to benzo[b]thiophenes to finally form dibenzothiophenes. Subsequent methyl transfer reactions are thought to explain the isomerisation observed (Radke, 1987).

The mechanism proposed for the formation of dibenzothiophene (alkylated or otherwise) assumes sulphur is incorporated into reactive organic material either by addition across double bonds or by nucleophilic addition or addition/elimination reactions. The isotopic composition of sulphur either fully reduced as  $\text{HS}^-$  or partially oxidised as a polysulphide, which is incorporated into organic matter, will be preserved during diagenesis.

Primary assimilated sulphur cannot be discounted from such a study without consideration of the relative proportions of diagenetically formed OSC and naturally occurring OSC in materials such as proteins. The main organic component of the Jet Rock is material derived from phytoplankton. The average protein content of phytoplankton is approximately 50%. Given that 1% of this is made up of sulphur then 0.005% of the primary organic matter is expected to be sulphur. Amino acids are readily degraded during diagenesis (M. Collins, pers. comm.; Mossman *et al.*, 1991) therefore it is expected that any surviving primary assimilated sulphur in the sediment will be negligible relative to any incorporated during diagenesis.

Organically bound sulphur in kerogens within marine sediments is thought to be derived either by assimilation or by the incorporation of sulphur initially derived from sulphate reduction. Recent studies have confirmed that sulphur can become incorporated into kerogen and bitumen during early diagenesis

Figure 5.16



Incorporation of sulphur into organic compounds.  
After Sinninghe Damsté and de Leeuw (1989).

(e.g. Sinninghe Damsté and de Leeuw, 1989), although the controls exerted by sediment composition are not yet known.

## 5.8 Sulphur Isotopes

Measurements of the sulphur isotopic composition of pyrite, elemental sulphur, kerogen, bitumen, asphaltene and maltene were determined by the methods described in Chapter 2. The sulphur isotope data are shown in Table 5.9.

Inspection of the bitumen, asphaltene and maltene values does not show isotopic mass balance i.e. the mass-weighted sum of the asphaltene and the maltene fractions should equal the isotopic composition of the bitumen. The deviation is not constant however, the maltenes seem to be lighter in general than the bitumens. The asphaltenes show a wide variation to the bulk bitumen value but are significantly heavier than the kerogen values in most cases. This suggests either error in the determination of the  $\delta^{34}\text{S}$  ratios or some process(es) which fractionates particular functionalities of sulphur. This anomaly and the presence of sulphate sulphur and elemental sulphur will be discussed in Chapter 6.

The bulk bitumen and kerogen fractions are used to constrain the incorporation of sulphur into organic matter relative to pyrite. This approach has been adopted by Raiswell *et al.* (1993a). Jurassic sea water has a sulphur isotopic composition of +17‰ (Claypool *et al.*, 1980). Therefore any assimilated sulphur would be expected to have a value in the region of +17‰. The microbial reduction of sea water sulphate is the primary mechanism whereby isotopically light  $\text{H}_2\text{S}$  is generated. The hydrogen sulphide evolved during sulphate reduction is fixed by detrital iron minerals to eventually form pyrite and by organic matter to produce organically bound sulphur bearing compounds.

Two texturally and isotopically distinct generations of pyrite can be found within the Jet Rock. The first to be formed is framboidal pyrite having an isotopically light  $\delta^{34}\text{S}$  signature (-30.1 to -21.7‰). This type of pyrite is characteristic of early diagenetic pyrite formed in a system with an open sulphate supply. The typical size of the framboids is between 10 and 15  $\mu\text{m}$ . The second generation of pyrite is in the form of euhedral cubes. This form of pyrite is concentrated in

Table 5.9

Sample	Pyrite	Elemental	Kerogen	Bitumen	Asphaltene	Maltene
PM1	-28.1		-12.3		-1.6	
PM2	-27.6		-13.9	-14.0		
PM3	-24.9		-11.9	-14.9	-7.3	
PM4	-24.7			-4.0	1.0	
PM5	-22.4		-7.7	-3.9	-3.5	
PM6	-23.9		-12.7	-4.9	-4.1	-0.3
PM7	-24.4		-13.6	-0.3	-3.8	-2.4
PM8	-21.7	-16.8	-0.8	2.5	-5.8	0.2
PM9	-24.2		-0.3	-0.1	-0.6	0.4
PM10	-23.9	-10.4	-8.7	3.6		1.2
PM11	-24.6	-6.1	-10.3	-3.6	-1.4	
PM12	-23.9	-8.3	-5.9	1.2	-9.2	0.7
PM13	-25.2		-4.5	-0.7		0.7
PM15	-24.4		-7.5	-0.4		
PM17	-30.1		-10.0	-0.2		

$\delta^{34}\text{S}$  for organic and inorganic forms of sulphur (excluding sulphate sulphur), found within the Jet Rock.



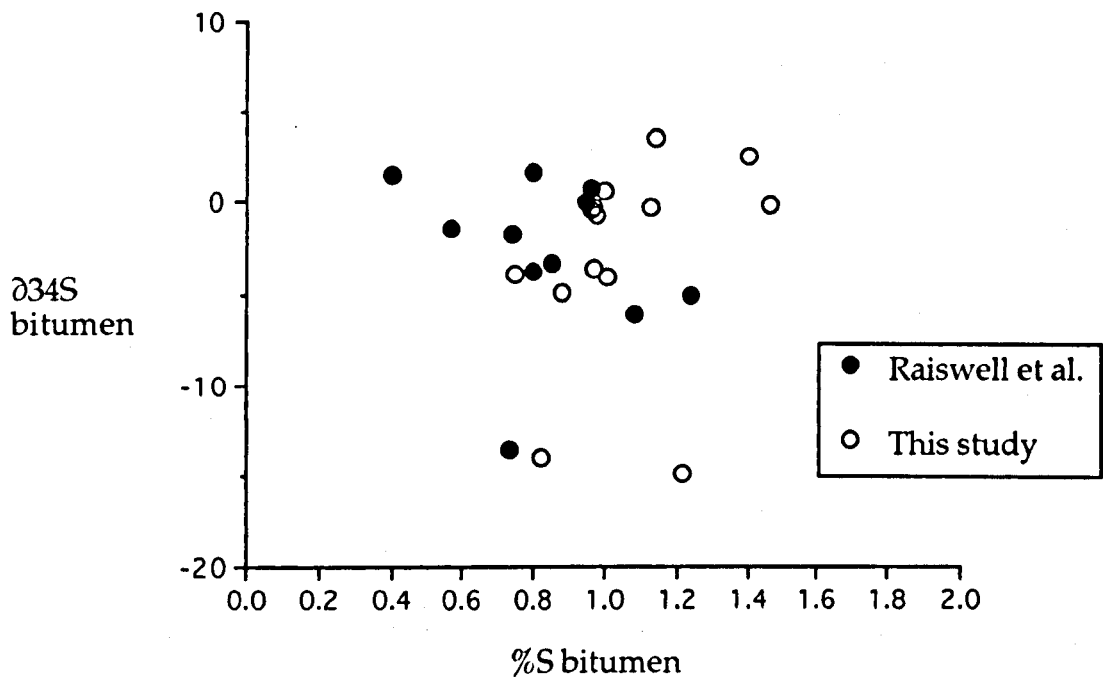
patches within the sediment and also forms a rim on some of the concretions. This late stage pyrite ranges in isotopic composition from  $-12.8\text{‰}$  to  $-9.8\text{‰}$ . However Raiswell *et al.* (1993a) report concretionary pyrite with a value of  $-3\text{‰}$ .

The  $\Delta^{34}\text{S}_{\text{sea water-pyrite}}$  is in the order of  $42\text{‰}$  for the Jet Rock. The organic sulphur  $\delta^{34}\text{S}$  values are all isotopically heavier than the first generation of pyrite. However, the  $\delta^{34}\text{S}$  organic sulphur compositions are all lighter than the  $+17\text{‰}$  of Jurassic sea water, indicating a diagenetic origin for the sulphur.

The cross plot between sulphur concentration versus  $\delta^{34}\text{S}$  values for the bitumens is shown in Figure 5.17 incorporating the data of Raiswell *et al.* (1993a). The data can be divided into two groups; light bitumen  $\text{S} < -10\text{‰}$  and heavy bitumen  $\text{S} > -10\text{‰}$ . The light samples are from the top of the sequence near to the Top Jet Dogger. The second group of samples are distributed with  $\delta^{34}\text{S}$  of  $0\text{‰} \pm 5\text{‰}$ . The data sets of Raiswell *et al.* (1993a) and this study show opposing trends of variation of isotopic composition with increasing S content when examined individually. When the data is taken as a whole, there appears to be no relationship of  $\delta^{34}\text{S}$  to the amount of sulphur contained in the bitumen. The data obtained in this study does suggest that there is a progressive increase in  $^{34}\text{S}$  with increasing sulphur content. This is indicative of sulphur incorporation into the bitumen over time, with the pool of sulphur becoming progressively heavier as incorporation progresses. The anomalous light values may be due to a change in organic matter type or reactivity enabling lighter sulphur to be incorporated. The relationship between oxygen index and the  $\delta^{34}\text{S}$  of the bitumen is shown in Figure 5.18. There appears to be a systematic increase in  $\Delta^{34}\text{S}$  with increasing oxygen index suggesting that the more polar the sample, the earlier the  $\text{H}_2\text{S}$  incorporation. However the available data is inconclusive to confirm such a mechanism. This observation supports the mechanism for the formation of organic sulphur compounds proposed by Raiswell *et al.* (1993a). A trend of high sulphur and low oxygen to low sulphur and high oxygen contents within the bitumen were ascribed to the possible formation of OSC via the elimination of oxygen by dehydration reactions. Subsequent sulphur incorporation can then take place via addition of sulphur across the double bond.

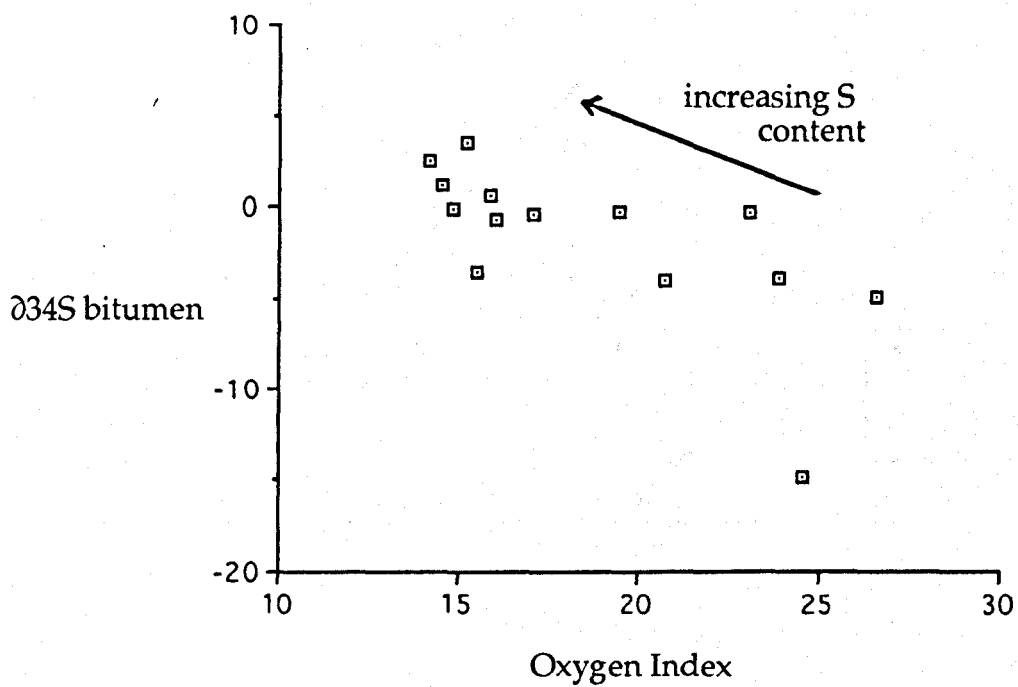
The isotopic compositions of the bitumen and pyritic sulphur are covariant although the bitumen S is isotopically heavier by approximately  $15\text{‰}$  (Figure 5.19). The  $\delta^{34}\text{S}$  of framboidal pyrite becomes progressively enriched in  $^{34}\text{S}$ ,

Figure 5.17



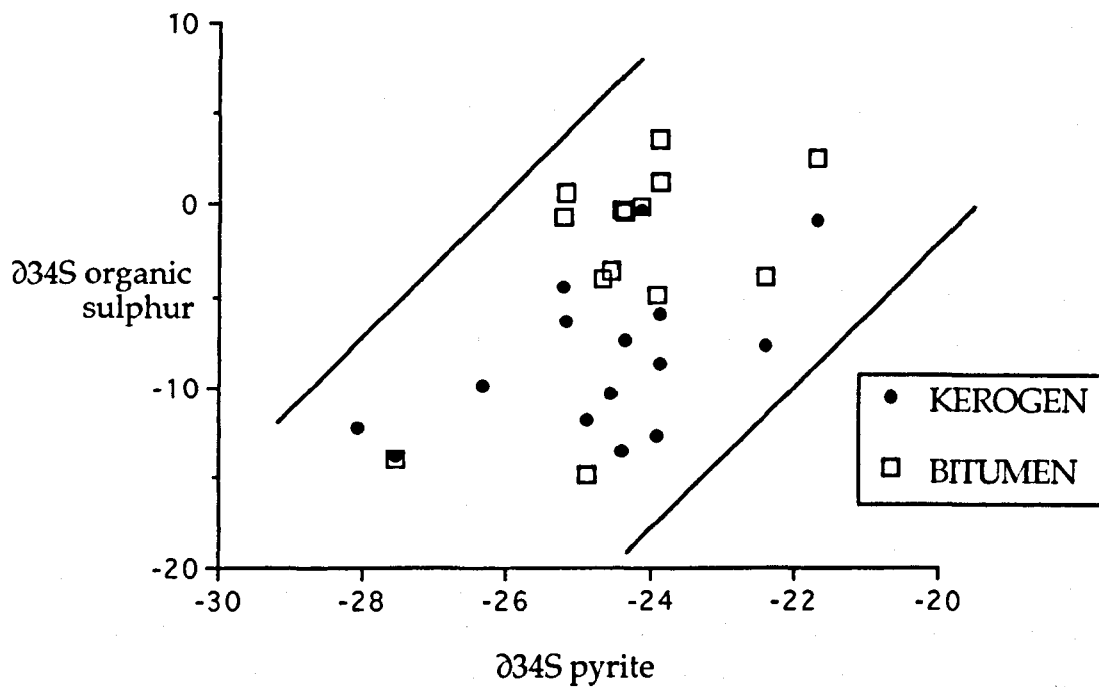
Relationship between  $\delta^{34}\text{S}$  and sulphur concentration from bitumens extracted from the Jet Rock. The graph shows data from this study and data from Raiswell *et al.* (1993a).

Figure 5.18



Relationship between the oxygen index and the  $\delta^{34}\text{S}$  of the bitumens extracted from the Jet Rock.

Figure 5.19



Relationship between the pyrite and organic sulphur isotopic composition within the Jet Rock.

suggesting that sulphate supply became partially closed. The organic sulphur in both kerogen and bitumen show a similar trend but with an isotopic offset between OSC and pyrite. Raiswell *et al.* (1993a) suggested two possible mechanisms for generating such results.

1. The sulphur incorporated into the bitumen and pyrite may have evolved from the same source but the organic matter incorporates more  $^{34}\text{S}$  relative to the pyrite.
2. Late, isotopically heavy pyrite formed from an evolving pool of  $\text{H}_2\text{S}$  (becoming depleted in  $^{32}\text{S}$ ) contemporaneously with organo-sulphur compounds. The late pyrite which was formed modified the bulk pyrite values to show an evolving trend towards heavier isotopic compositions.

The reactions forming pyrite and organo-sulphur compounds are not thought to be associated with different isotopic fractionations as such reactions involving reduced sulphur usually have similar small isotopic fractionations (Raiswell *et al.*, 1993a from the conclusions of Mossman *et al.*, 1991). Therefore the second suggestion of Raiswell (1993a) seems to be the most appropriate for the data.

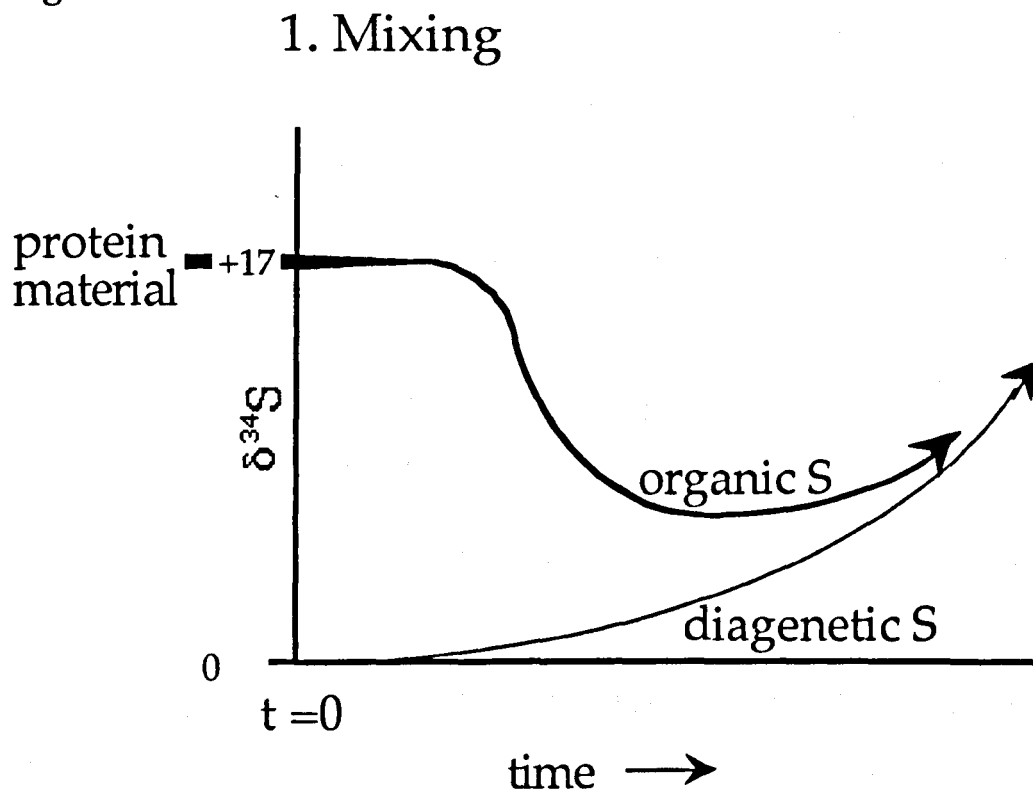
## 5.9 A Model for the Formation of Organic Sulphur Compounds

Traditionally, it is believed that iron competes successfully with organic matter as a sink for reduced sulphur during early diagenesis e.g. Berner (1985). Thus the amount of hydrogen sulphide formed must exceed the amount of iron available in the sediment before OSC can form.

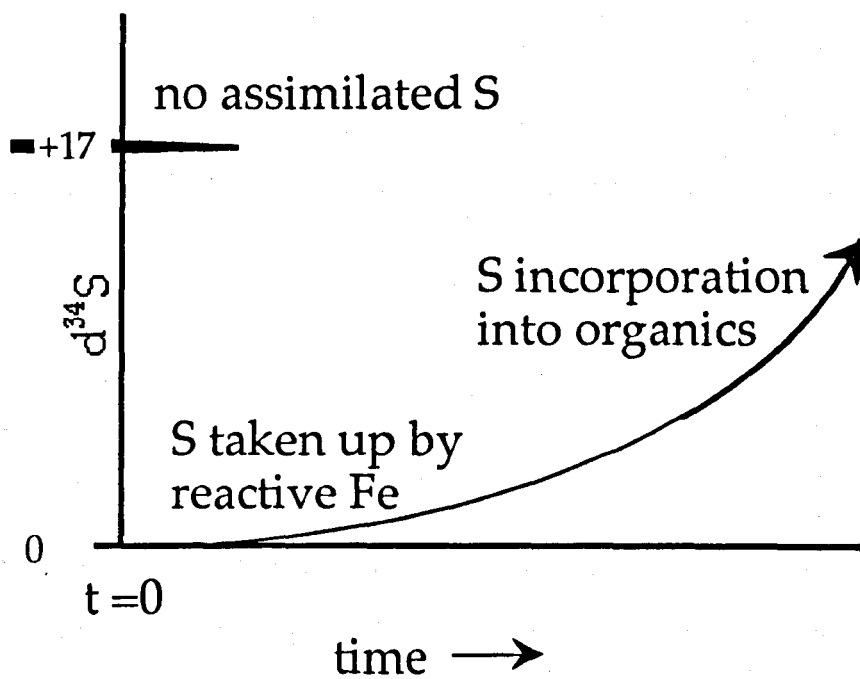
A model is proposed for the formation of OSC based on the relative timing of sulphur incorporation into pyrite and organic matter as determined by stable sulphur isotopes. A summary of this model is shown in Figure 5.20.

The evolution of the overall isotopic composition of organically bound sulphur can be regarded either as one of mixing assimilated sulphur (+17‰) with diagenetic  $\text{H}_2\text{S}$  (initially very light but becoming progressively heavier as the system becomes closed), or as incorporation of sulphur into organic matter

Figure 5.20



## 2. Post pyrite incorporation



Summary of the sulphur incorporation model based on sulphur isotope information.

after an early phase of pyrite formation (but contemporaneously with a late stage isotopically heavy pyrite). The second of these two models seems the most likely.

The high DOP values measured in the Jet Rock suggest that there was a significant amount of pyrite formed from the readily available iron and the light isotopic composition indicates that this formation was early during diagenesis. The table of rate constants and half-lives for iron bearing minerals (Table 5.10) shows that such reactive iron minerals would be haematite, goethite, lepidocrocite and ferrihydrite. Therefore, in future studies, if iron mineralogies were carefully determined, it may be possible to relate the formation of sulphur bearing compounds to specific iron minerals and hence to a half-life. In the case of the organic matter within the Jet Rock, the incorporation of sulphur into bitumen probably occurred after the formation of the main phase of isotopically light open system pyrite, but was contemporaneous with the formation of a small amount of isotopically heavy pyrite, from H<sub>2</sub>S in a closed system.

## 5.10 The geochemistry of the Cannon Ball Doggers and their host sediment

The stratigraphically lowest set of concretions (Cannon Ball Doggers) of the Jet Rock were studied to determine the time of concretion formation and the diagenetic processes affecting the bulk geochemistry of the host shale.

The Cannon Ball Dogger horizon makes up the lowest set of concretions within the *falciferum* zone of the Toarcian. They are spherical or sub-spherical ranging in size from a few centimetres to a maximum diameter of 30cm. A thick pyritic rim of up to 7mm surrounds the carbonate concretion.

### 5.10.1 Origin of the Cannon Ball Doggers

The Cannon Ball Doggers have been studied extensively by Raiswell (1976,1987) and Coleman and Raiswell (1981). The concretions formed early during diagenesis. This conclusion is based upon several observations:

- i. compaction of host sediment laminae around the concretions

Table 5.10

Iron Mineral	k (year <sup>-1</sup> )	Half-life
Ferrihydrate	10,000	3 hours
Lepidocrodite	1,000	9 hours
Goethite	100	12 days
Hematite	10	115 to 1100 days
	1	
"Reactive" silicates	10 <sup>-1</sup>	230 years
	10 <sup>-2</sup>	
Magnetite (covered)	10 <sup>-3</sup>	533 years
	10 <sup>-4</sup>	
Sheet silicates	10 <sup>-5</sup>	84,000 years
Ilmonite, Garnets	10 <sup>-6</sup>	
	Augite, Amphibole	

Iron bearing minerals and their associated half-lives with respect to their sulphidation.

After Raiswell *et al.* (1993b).



- ii. uncrushed fossils within the concretion matrix
- iii. porosity estimates of 77-87% (Raiswell, 1976) 81-90% (this study)
- iv. geochemical evidence

The geochemical evidence can be sub-divided into bulk geochemistry and stable isotope geochemistry. The stable isotopes of carbon, oxygen and sulphur have been used to determine the mode of formation of the concretions and the bulk geochemistry to establish diagenetically controlled mineral changes, and major element mobility.

### 5.10.2 Organic Carbon

The  $\delta^{13}\text{C}$  of organic carbon found within the concretions has a range -32.1 to -33.9‰ (Coleman and Raiswell, 1981). The kerogen has an isotopic value of -28‰ and the asphaltene -31.0‰. As Coleman and Raiswell note, the  $\delta^{13}\text{C}$  values for organic matter are controlled by the isotopic composition of the source material. The kerogen composition for the Jet Rock is dominated by fluorescent amorphous material (Figure 5.8) which is thought to be derived from the preferential preservation of the resistant tissues of phytoplankton (Raynaud *et al.*, 1989). The light  $\delta^{13}\text{C}$  values can therefore be explained by a mixture of marine plankton (typically in the order of -30‰) and a terrestrial component (~10% of the kerogen, which has been found to have a range of -16 to -23‰, the lipid fraction of land plants have  $\delta^{13}\text{C}$  values in the range -30 to -35‰).

Coleman and Raiswell (1981) propose two ways of generating such light values:

- i. abundant terrestrial input
- ii. preferential degradation of isotopically heavy organic matter

The second is thought to be correct, given the composition of the kerogen.

The isotopic composition of the organic matter found within the concretion is lighter than that of the organic matter in the surrounding sediment, suggesting some diagenetic modification has occurred to the organic matter within the concretions. This conflicts with the findings of Coleman and Raiswell (1981) who report  $\delta^{13}\text{C}$  values for the shale to be -33.2‰. However, the value determined in this study fits with the suggestion by Coleman and Raiswell (1981) that the Cannon Ball Doggers contain light organic carbon which is

thought to result from preferential degradation of isotopically heavy parent organic matter.

### 5.10.3 Carbonate Carbon and Oxygen

Coleman and Raiswell (1981) report  $\delta^{13}\text{C}$  values for inorganic carbon within the concretion cement in the range -12.9 to -14.4‰. The carbonate carbon in the host sediment has  $\delta^{13}\text{C}$  of -6.8‰. The  $\delta^{18}\text{O}$  composition of the concretion cement is similar to that shown by the host shale -8.9 to -9.9‰ and -9.8‰ respectively.

The carbonate carbon is thought to be derived from a mixture of carbon from sulphate reduction, fermentation and marine carbonate derived carbon. The sediment has a heavier value suggesting an increased component of fermentation or increased marine carbonate.

The carbonate oxygen values of the concretion cement and the host shale are very similar. Palaeotemperature calculations based on the  $\delta^{18}\text{O}$  yield temperatures in the region of +60°C. This clearly conflicts with the idea of a very shallow depth of formation. Coleman and Raiswell (1981) suggest that local diagenetic factors are responsible for the seemingly anomalous  $\delta^{18}\text{O}$  values as concretions higher in the sequence show oxygen palaeotemperatures of about +25°C. Meteoric waters passing through the Cannon Ball Dogger horizon was suggested as a possible means of producing light  $\delta^{18}\text{O}$  values. The geochemistry of the concretions and the host shale were investigated in more detail to establish the chemical changes which have occurred since concretion formation.

### 5.10.4 Sulphur Isotopes and Bulk Geochemistry

Evans (1989) has used the non-carbonate fraction from concretion centres/host shale pairs to quantify the overall changes in shale chemistry during burial. The same method has been used in this study to assess the mobility of selected elements during the diagenesis of the Jet Rock.

Twelve Cannon Ball Doggers were chosen at random along the line of strike together with a fresh sample of host shale adjacent to each concretion. Of this

set of specimens, the four most spherical concretions and their corresponding shale samples were chosen for analysis. The middle 2cm of each concretion was cut (parallel to bedding) to produce five sub-samples. All the rock samples were ground to a +90 mesh size (the shales were crushed in a terra with a tungsten carbide barrel and the concretion samples were crushed by hand in a steel mortar).

The carbonate component of each sample was dissolved out using HCl (10% v/v). The resulting residues were analysed for major elements, uranium and thorium (using XRF techniques) and carbon and sulphur by GC. Table 5.11 shows the results obtained during carbonate removal. It can be clearly seen that the bulk of the concretions are made up of carbonate. The percentage weight loss of the concretions being a measure of the sediment porosity at the time of formation (Raiswell, 1971).

The chemical analysis of the HCl residues are shown in Table 5.12. Two types of concretion have been sampled. Concretions #1 and #3 show high carbon and sulphur contents relative to the host shale. Microscopic study of these concretions reveal whorls of ammonites, fragments of bivalves and small whole ammonites (probably *Eleganticeras elegantulum*) in much greater numbers than in concretions #2 and #11. Fish scales are also common in all the concretions at higher concentrations than in the host sediment. Such biogenic material may have acted as a nucleus for initial concretionary growth (Canfield and Raiswell, 1991b).

The enrichment of sulphur in concretions #1 and #3 is due to an increased amount of pyrite (Table 5.13). The  $\delta^{34}\text{S}$  of pyrite from concretions #1 and #11 were measured together with the pyrite sulphur from the host shales (Table 5.13). The pyrite within the concretion is heavier than that of the surrounding sediment, indicating a partially closed system of sulphate. The concretion with the higher organic carbon content (#1) shows slightly heavier  $\delta^{34}\text{S}$  values. This together with the increased pyrite content suggests greater microbial sulphate reduction induced by a more abundant source of organic matter. The  $\delta^{34}\text{S}$  of the pyrite rim is heavier than the pyrite inside the concretion (-9.4‰) and is cubic in morphology unlike the finely dispersed framboids within the concretions. Such heavy sulphur is indicative of late stage closed system sulphate reduction

Table 5.11

Sample	Percentage change in mass
1.0	11.04
1.1	90.71
1.2	90.26
1.3	90.19
1.4	89.40
1.5	89.60
2.0	11.03
2.1	90.71
2.2	90.26
2.3	90.20
2.4	89.4
2.5	90.74
3.0	11.79
3.1	81.34
3.2	84.19
3.3	81.79
3.4	80.99
3.5	81.95
11.0	10.04
11.1	90.90
11.2	86.63
11.3	89.61
11.4	86.83
11.5	89.54

Change in mass after carbonate removal from samples of the Cannon Ball Doggers and host sediment.

Suffix: 0 host sediment

5

3 1 2 distribution of samples from within the concretion

4

Table 5.12

Sample	%C	%S	%Si	%Al	%Fe	%Mg	%Ca	%Na	%K	%Ti
1.0	4.97	4.44	48.13	20.02	7.78	1.36	0.08	1.40	2.91	0.91
1.1	6.54	5.17	44.38	17.05	7.74	1.03	1.76	0.39	2.32	0.05
1.2	6.99	6.56	42.03	16.76	9.12	1.03	1.65	0.35	2.34	0.78
1.3	6.45	6.54	43.19	17.08	9.93	1.04	1.24	0.52	2.49	0.81
1.4	6.64	5.56	40.93	16.11	8.40	0.97	2.40	0.36	2.27	0.77
1.5	6.74	5.13	43.16	17.05	8.02	1.01	1.96	0.47	2.36	0.81
2.0	4.40	4.31	46.26	18.61	12.66	1.16	0.05	0.70	2.49	0.85
2.1	2.26	3.31	59.24	13.03	6.82	0.79	1.12	1.52	1.90	0.99
2.2	2.41	4.62	59.65	13.79	7.29	0.84	0.86	0.83	2.00	0.98
2.3	2.35	4.60	60.72	13.62	7.36	0.86	0.98	0.83	2.01	0.98
2.4	2.28	6.08	59.45	14.78	9.47	0.91	1.15	0.81	2.15	1.03
2.5	2.62	5.37	63.09	13.86	8.48	0.86	0.56	1.03	2.07	0.98
3.0	4.95	4.28	53.62	22.29	8.41	1.43	0.07	0.33	3.18	0.98
3.1	5.85	11.98	43.50	15.88	18.17	0.88	1.88	0.53	2.29	0.83
3.2	5.25	11.33	38.93	14.89	16.77	0.90	1.04	0.91	2.23	0.72
3.3	6.79	6.47	47.13	17.76	10.10	1.13	1.81	1.02	2.69	0.87
3.4	6.53	13.84	40.43	15.49	21.11	1.06	3.37	0.27	2.28	0.75
3.5	4.59	5.77	47.79	18.22	10.12	1.16	3.12	0.38	2.70	0.89
11.0	4.48	4.14	48.87	19.83	7.56	1.32	0.25	0.53	2.73	0.90
11.1	2.44	3.21	54.93	13.60	7.08	0.84	1.71	0.92	2.00	0.94
11.2	2.48	5.72	55.85	13.98	8.53	0.83	1.20	1.22	2.06	0.92
11.3	2.52	4.86	56.52	13.96	7.62	0.83	1.28	0.85	2.01	0.99
11.4	2.57	4.72	54.84	13.86	7.86	0.92	1.44	1.66	2.21	1.01
11.5	2.63	4.72	55.89	13.76	7.26	0.84	1.40	0.91	1.99	0.96

Summary of the chemical analyses of the carbonate free residues from the Cannon Ball Doggers and the host sediment.

Suffix: 0 host sediment

5

3 1 2 distribution of samples from within the concretion

4

Table 5.13

Sample	% pyrite (carbonate free basis)	$\delta^{34}\text{S}$
1.0	8.30	-22.10
1.2	12.27	-16.62
1.3	12.23	-19.28
1.4	10.40	-16.69
pyritic rim of concretion 1	~95	-9.84
11.0	7.56	-25.17
11.2	8.53	-18.07
11.3	7.62	-20.06
11.5	7.86	-20.41
pyritic rim of concretion 11	~95	-9.42

Isotopic composition of pyrite from two Cannon Ball Dogger concretions.

### 5.10.5 Clay Mineral Reactions

The approximate mineralogy of the shales under investigation was found by Morris (1980), a modified version is shown in Table 5.14. The minerals are predominantly clay minerals and quartz (making up about 80% of the rock). Such a composition resembles a weathered shale. The process of diagenesis involves the hydrolysis of minerals at elevated temperatures and so is a subterranean process directly analogous to chemical weathering and halmyrolysis (weathering on the ocean bottom). It is probable that the initial sediment deposited during the Jurassic contained clays which were produced during terrestrial weathering processes.

One of the first reactions to occur as detrital material enters the marine sedimentary basin is cation exchange. The activities of most species found in natural waters are greater in marine environments, thus increasing the potential for such reactions to occur. The results of this process would be preserved within the concretions, enabling exchange reactions taking place after early diagenesis to be measured. No data was obtained on the mineralogy of the material inside the concretion.

The type of clay mineral produced depends greatly on the environment of initial formation. Once formed, the clays are thought to be kinetically stable for long periods of time, even though their geochemical environment may change. The paragenesis of kaolinite is usually regarded as a hydrolysis reaction of a feldspar. Equation 5.1 shows an idealised reaction for the formation of kaolinite, which has not been duplicated in laboratory studies, but it does indicate that there may be an increase in pH (OH<sup>-</sup> formed), dissolution of silicon and liberation of potassium in the form of K<sup>+</sup> ions.



Illite is the most abundant clay mineral found in the sediment. This indicates that the environment in which the illite formed was rich in K<sup>+</sup> ions. The source of these ions being the marine environment where the fluids are rich in alkali metals, or from hydrolysis reactions such as that shown in Equation 5.3. The apparent lack of montmorillinite (or other smectites) may be due to their conversion to illite with time. Such a reaction is shown in Equation 5.2.

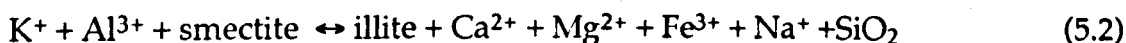


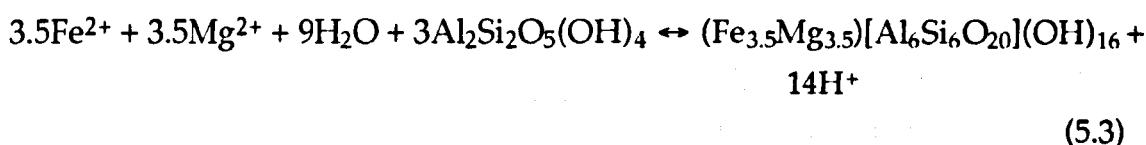
**Table 5.14**

	Mineral	Abundance (%)
Clay Minerals	Illite	35
	Kaolinite	20
	Chlorite	5
Others	Quartz	20
	Pyrite	8
	Oligoclase	5
	Muscovite	5
	Calcite	2
	Organics	5

Mineralogy of the Jet Rock.



It has been shown (Burst, 1959) that there are progressive changes in clay mineral expansion rates with depth. That is, the ability of cation exchange decreases with depth as sites become substituted with ions like K<sup>+</sup>. In practice this means that clays with a high ion exchange capacity (like montmorillinite) become converted to mixed layer clays (montmorillinite-illite) until at deep burial, the clay becomes illitic. Some of the dissolved metal ions from Equation 5.2 may react with the kaolinite produced in Equation 5.1 to form chlorite, as shown in Equation 5.3.



Such clay mineral reactions account for the difference in chemistry between the concretions and the host sediment. There have obviously been significant changes in the silicate mineralogy from the time of deposition until the present. If the concretions represent the composition of the sediment at the time of deposition, the following conclusions can be made:

Authigenic illite and chlorite increase the Mg, K and Al contents of the sediment. Calcium concentrations are higher in the concretions due to an increase in the amount of biogenic material such as apatite. Sodium has been lost from the sediment due to the attack of sodium plagioclase forming kaolinite which has been preserved in the concretion.

Concentrations of uranium determined by XRF were on the detection limits (<5ppm). Their values have not been tabulated given the accuracy of ~40% (A. Gray, pers. comm.). Gamma ray spectrometry indicates that the concentrations of uranium in the host shale are in the order of 5.8ppm of which approximately 2ppm is authigenic (this study and Myers and Wignall, 1987). No value for the uranium content within the concretion was determined.

The thorium value found for the host sediment ( $12.25 \pm 1.92\text{ppm}$ ) is typical of that for a marine shale and consistent with findings of other workers. Myers and Wignall (1987) reported Th levels in the order of 13ppm measured by gamma ray spectrometry; Raiswell (pers comm.) has analysed five samples from the Jet Rock by neutron activation giving a mean of  $11.6 \pm 1.4\text{ppm}$ . Every concretion sample was found to have a concentration of thorium of 3ppm.

Without any normalisation or standardisation it is clear to see that there has been a large efflux of Th from the concretions.. Thorium only occurs as the  $\text{Th}^{4+}$  ion in geological environments, but it will form soluble complexes with water enabling thorium to be transported in aqueous solutions. The hydrated cations are thought to be 8 or 9 coordinated and are strong acids (because of the high charge on the ions). In strongly acidic conditions  $\text{pH} < 3$  the dimeric ion  $[\text{Th}_2(\text{OH})_2]^{6+}$  predominates. With increasing alkalinity, polymerisation increases and the solubility of the resulting amorphous oxy-hydroxide decreases. Most thorium salts are soluble in acidic solutions. Thorium is also selectively adsorbed onto clay minerals in less acidic conditions. However, such a marked change in the composition of the thorium contents within concretion/sediments pairs have (to the authors knowledge) never been reported before. In fact Evans (1989) normalises elements to thorium, assuming that thorium is immobile.

The high abundances of both illite and kaolinite indicate that there were not distinct phases of authigenic clay mineral growth, but a continual series of clay mineral reactions. As the more acidic reactions of diagenesis took place (kerogen maturation) the pH of the environment would drop. An acid dominated environment with low activities of cations would lead to the formation of kaolinite (liberating silicon and alkali metals and fractionating uranium and thorium). This process would inevitably lead to an increase in pH (by liberating the more soluble alkali and alkaline-earth metals in favour of aluminium and silicon) which may induce the formation of smectites. Illite is more likely to form in such an environment as the activity of potassium will be enhanced, and the illite/smectite transition will be thermodynamically favourable.

## 5.11 Conclusions

The Jet Rock was iron limited (DOP generally greater than 0.85) with significant amounts of pyrite added syngenetically. The light isotopic composition of the framboidal pyrite suggests the sulphur was derived from open system sulphate reduction. However there are exceptions to this. Samples with  $\text{TOC} > 8\%$  contain isotopically heavy pyrite ( $-24$  to  $-20\%$ ) which was formed from  $\text{H}_2\text{S}$  produced during closed system sulphate reduction.

The organic matter within the Jet Rock is early mature ( $R_0 = 0.55$  to  $0.65$ ) Type II kerogen, dominated by material derived from the resistant tissues of phytoplankton.

Organo-sulphur compounds are present within the solvent soluble organic matter. These have been identified principally as dibenzothiophenes.

The concentration of sulphur in the bitumens is found to be inversely proportional to the oxygen index, suggesting elimination of oxygen during sulphur incorporation into the organic compounds.

The organically bound sulphur is isotopically heavier than the framboidal generation of pyrite within the Jet Rock, but isotopically similar to the massive pyrite (ascribed to be a later generation of pyrite).

A model is presented to describe the isotopic evolution of sulphur in the Jet Rock. A first generation of framboidal pyrite formed during open system sulphate reduction. Massive pyrite and OSC then formed contemporaneously during closed system sulphate reduction, forming isotopically heavy compounds.

The Cannon Ball Dogger concretions formed early during diagenesis. The pyritic rim of the concretions formed later than pyrite contained within the concretions. The differences in the chemical composition of the concretion matrix and host sediment is due to a continuous series of clay mineral reactions.

The anomalous light oxygen isotope data for the Cannon Ball Doggers may be explained by invasive meteoric waters in to the shale sequence. However the chemistry of the concretion/shale pairs would suggest that the concretions have remained closed to diagenetic transformations after the pyrite rim of the concretions was formed. Therefore the principle source of isotopically light oxygen is thought to be from sulphate, trapped organic matter and from the encapsulating silicates undergoing limited transformations.

# Chapter 6

## Weathering of Shales

### 6.0 Introduction

Weathering has been defined as the sum of the processes that change the inorganic and organic constituents of rocks in contact with the atmosphere, hydrosphere and biosphere (Valeton, 1988). This chapter presents a study of the weathering of sulphur species in marine mud rocks. Most studies of oxidation reactions have concentrated upon specific minerals in laboratory studies or as soil formation reactions. Shale samples over a geographical and chronological age range have been chosen for a study of in situ weathering.

### 6.1 Sulphate in Shales

The sources of sulphur in ancient marine sedimentary rocks are in pyrite elemental sulphur, organic sulphur and sulphate sulphur. The formation of pyrite and organic sulphur compounds are discussed in Chapter 2.

Sulphate sulphur and elemental sulphur are thought to be the result of oxidation of reduced sulphur species, generally regarded as pyrite sulphur, Littke *et al.*(1991). Laboratory studies of pyrite oxidation by Steger (1977a,b), Steger and Desjardins (1977) and Steger (1979) have determined the products of sulphide oxidation. Reviews of the kinetics of the oxidation of pyrite are presented by de Haan (1991). In most cases, the iron systematics have been used to trace the oxidation process and little attention has been paid to the sulphur bearing species during the reactions.

In mud rocks, there are several possible sources of sulphur which are prone to oxidation, forming sulphate:

- i pyrite S
- ii elemental S
- iii organic S
- iv polysulphides

This chapter aims to investigate the nature of the oxidation reactions of reduced sulphur bearing species and the source of oxygen making up the sulphate i.e. water or atmospheric oxygen.

The *Thiobacteriaceae* bacteria are thought to be the dominant family of bacteria involved in the oxidation of reduced sulphur species into sulphate (Goldhaber and Kaplan, 1974). The *Thiobacillus* (commonly known as thiobacilli) are the most commonly studied genus of the sulphur oxidising bacteria.

The mechanism of biological oxidation of inorganic sulphur compounds is poorly understood. The mechanism of oxidation has not been established, although attempts to distinguish between biological and abiological sulphide oxidation have been attempted using stable isotopes e.g. review by Toran and Harris (1989).

One of the major problems in interpreting the mechanism of sulphide oxidation is the reaction of unstable partially oxidised intermediates with initial starting material and other intermediates. Roy and Trudinger (1970) suggested that the first step in sulphide oxidation was abiological oxidation to elemental sulphur. Figure 6.1 shows the pathways in the oxidation of reduced sulphur compounds by thiobacilli (Goldhaber and Kaplan, 1974). Physiological oxidation of the elemental sulphur would result in the formation of thiosulphate, polythionates, sulphite and sulphate.

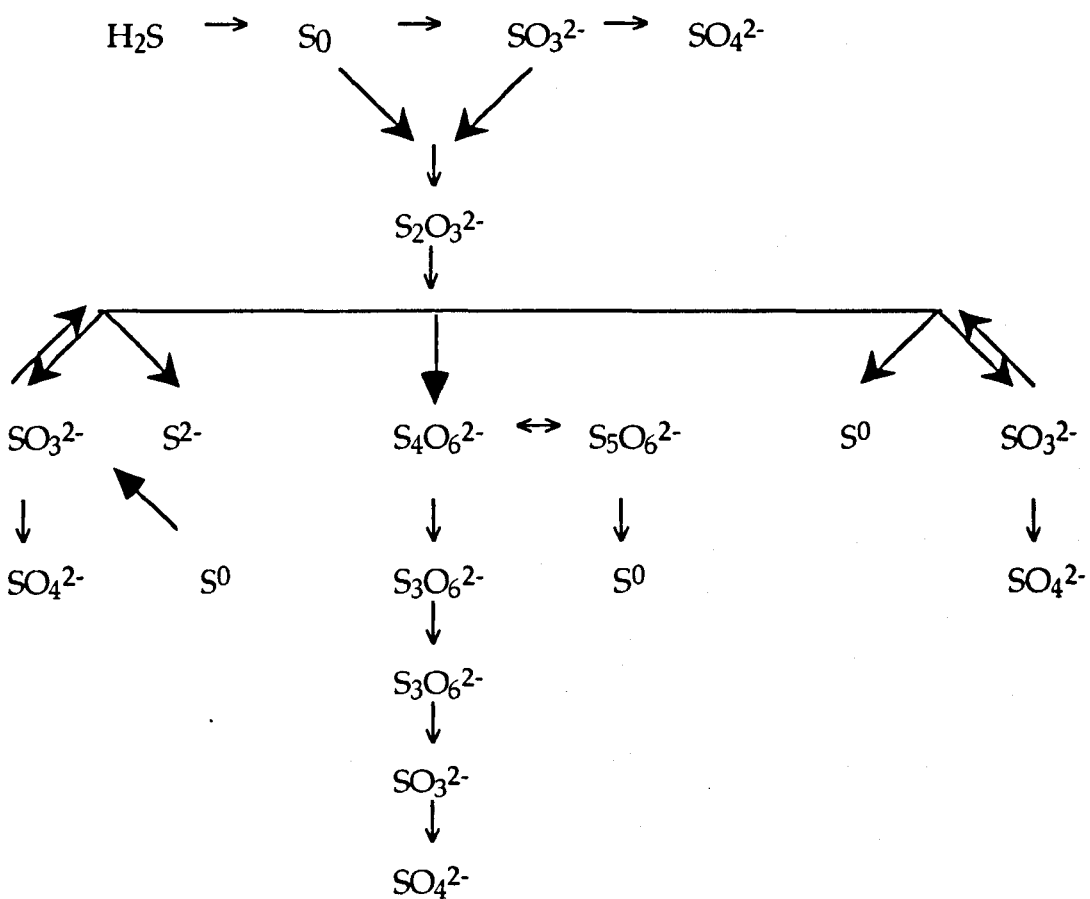
The mechanism of the oxidation of sulphide minerals is dependent on the intermediate reaction steps and on the process i.e. biological or abiological. As Toran and Harris (1989) noted, the exact mechanism of the process for a particular reaction is difficult to establish because of the complex nature and reactivity of the intermediate reaction products and the competition between the biological and abiological reaction steps.

## 6.2 Oxidation of reduced sulphur

### 6.2.1 Inorganic Sulphur

The oxidation of pyrite has been extensively studied and reviewed by Lawson (1982) and de Haan (1991). These oxidation reactions are generally catalysed by

Figure 6.1

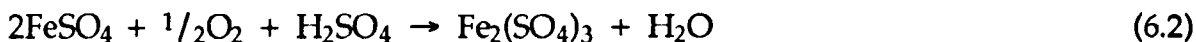


Pathways in the oxidation of reduced sulphur compounds by thiobacilli.  
After Goldhaber and Kaplan (1974).

*Thiobacillus* bacteria in the presence of molecular oxygen and water, the sulphur becomes oxidised to sulphate (Equation 6.1).



The iron may also become oxidised with additional oxygen in the newly formed acidic aqueous conditions (Equation 6.2).



Iron (III) is a powerful oxidising agent. Under acidic conditions Fe(III) is thought to be important in the oxidation of pyrite and at higher pH oxygen is regarded as the dominant oxidising agent. However, Luther *et al.* (1985) suggest that Fe(III) may be significant at pH close to 7. The kinetic constraints suggest that the reaction with molecular oxygen is significantly faster.

Elemental sulphur can be oxidised to sulphuric acid in an environment where free oxygen and water are available (Equation 6.3). This reaction is catalysed by *Thiobacillus ferrooxidans* (Margalith *et al.*, 1966).



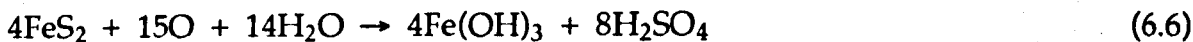
Elemental sulphur also forms when ferric sulphate reacts with pyrite. This reaction is represented by Equation 6.4.



The generation of acidic conditions during the oxidation of pyrite is well known. Iron (III) is very insoluble e.g.  $K_{\text{sp}} \text{Fe}(\text{OH})_3 = 2.0 \times 10^{-39} \text{ (mol dm}^{-3}\text{)}$  c.f.  $K_{\text{sp}} \text{Fe}(\text{OH})_2 = 7.9 \times 10^{-16} \text{ mol dm}^{-3}$ . Therefore, in reactions involving the oxidation of pyrite where both sulphur and iron are oxidised, significant acidity will be generated (Equations 6.5 and 6.6).



or

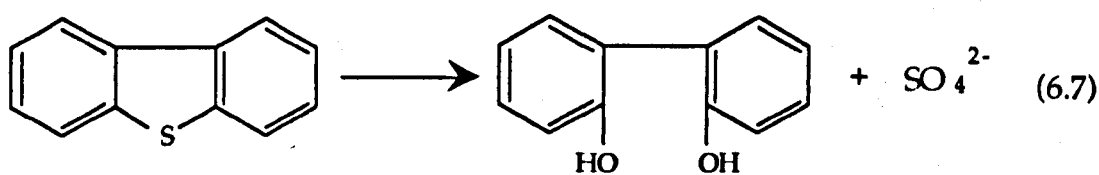


The precipitation of iron(III) oxides or hydroxides is thought to inhibit the further oxidation of pyrite. Coatings of such precipitates are thought to greatly reduce the kinetics of the oxidation reactions, Morse (1991). This has important implications for the preservation of pyrite within oxic environments and will be discussed later in this Chapter.

Zaback and Pratt (1992) noted the isotopic similarity of sulphate and elemental sulphur to sulphur in bitumens found within the Miocene Monterey Formation. They suggest that the elemental sulphur and sulphate were the product of the oxidation (chemical or biological) of pyrite and organic sulphur.

## 6.2.2 Organic Sulphur

Biodesulphurization has been recognised by the petroleum industry as a possible means of selectively removing sulphur bearing compounds from petroleum prior to refining (Fredorack, 1990 and references therein). Micro-organisms oxidise OSC to form 'water soluble sulphur compounds'. There are a wide variety of OSC found within the Jet Rock e.g. thiophenes, dibenzothiophene and alkylated dibenzothiophene which may undergo such biodesulphurization reactions. The bacterium *Sulfolobus acidocaldarius* has been found to metabolise dibenzothiophene to yield 2,2'-dihydroxybiphenol and sulphate (Equation 6.7). This reaction was found to take place under aerobic conditions (Fredorack, 1990).



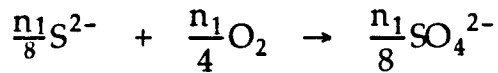
## 6.3 Oxidation Mechanisms

Oxidation (loss of electrons) of pyrite can be achieved by many different mechanisms. Toran and Harris (1989) have proposed a classification scheme for sulphide oxidation based upon the electron transfer reactions which take place during the incorporation of oxygen from  $\text{H}_2\text{O}$  or  $\text{O}_2$  into the oxidation product. Although the exact mechanism for oxidation is not described, the general



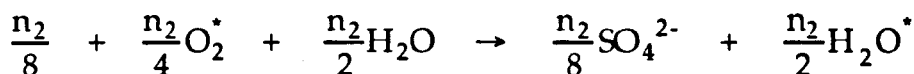
reaction in unknown proportions is considered. Three basic mechanisms have been suggested to incorporate oxygen into sulphate.

1. Atmospheric oxygen alone acts as the terminal electron acceptor via either a biological or abiological route to give the following stoichiometric equation:



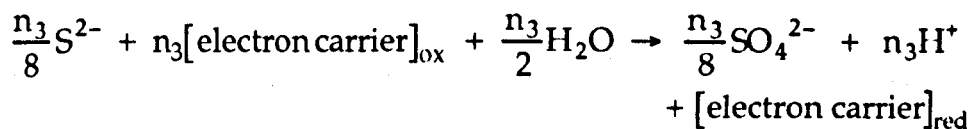
where  $n_1$  is the number of electrons transferred directly by the electron acceptor.

2. Electron transfer may take place by molecular oxygen accepting sulphide electrons but incorporation of oxygen is achieved via  $H_2O$  oxygen donation according to the reaction:

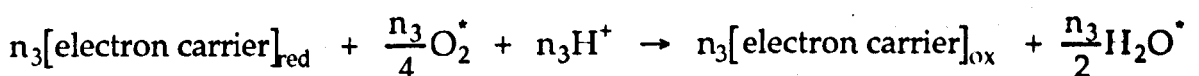


This oxygen from  $O_2$  is incorporated into water. This reaction is abiological. The number of electrons transferred by the electron acceptor in the reaction is given by  $n_2$ .

3. Electron carriers may be involved in the oxidation of pyrite. The number of electrons involved in such a reaction ( $n_3$ ) is shown in the following reaction:



The electron carrier (e.g.  $Fe^{3+}$ ) is re-oxidised by atmospheric oxygen according to the reaction:

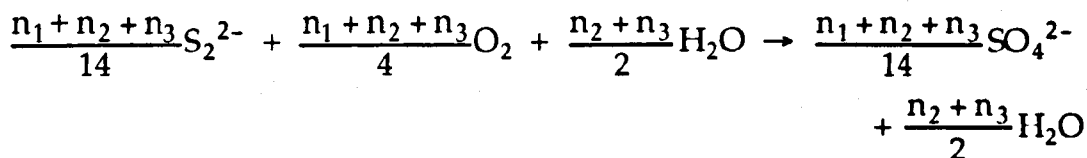


Pyrite contains partially reduced sulphur, with sulphur in the -1 oxidation state. Therefore, the oxidation of pyrite involves the loss of 7 electrons for each atom

of sulphur in pyrite, giving a total of 14 electrons to change from the -1 to the +6 oxidation state in sulphate.

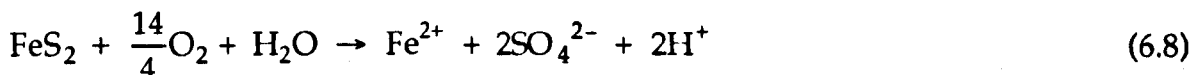
Reconsidering the second mechanism, in order to balance the reaction, 1 oxygen atom from O<sub>2</sub> must be incorporated into sulphate during the oxidation of FeS<sub>2</sub>. Therefore 7 out of the 8 electrons are H<sub>2</sub>O derived i.e. 87.5% is H<sub>2</sub>O derived oxygen.

The overall mechanism for these reactions can be expressed as:



However, the number of electrons transferred in each reaction remains uncertain.

Goldhaber (1983) proposed direct incorporation of O<sub>2</sub> derived oxygen into sulphate as the mechanism for pyrite oxidation by abiological reaction according to the reaction shown in Equation 6.8,



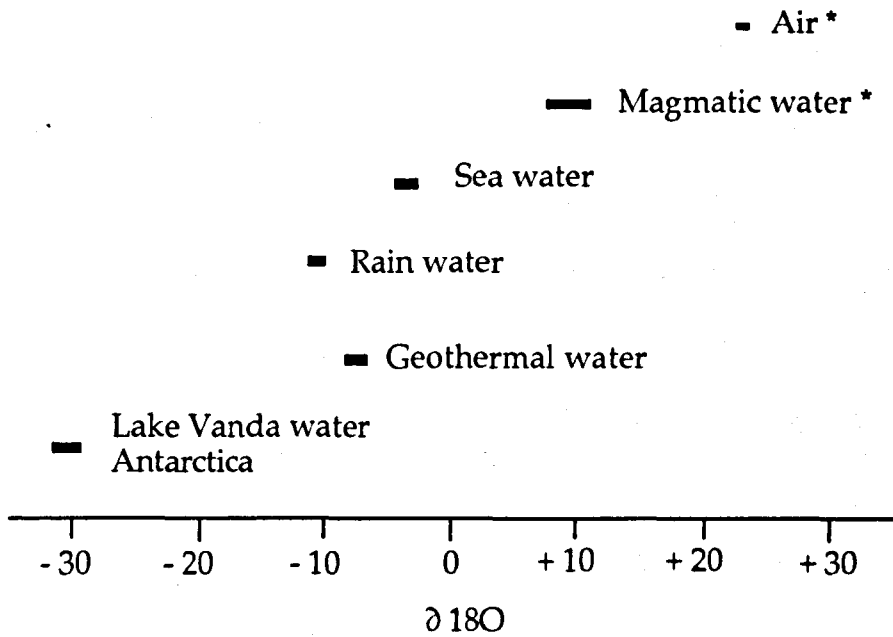
giving sulphate containing 87.5% O<sub>2</sub> derived oxygen.

## 6.4 Oxygen isotope systematics

Oxygen exists as two dominant stable isotopes <sup>18</sup>O and <sup>16</sup>O (Table 2.5). The δ<sup>18</sup>O for water is varied depending on the nature of the water. Fresh water samples tend to have negative δ<sup>18</sup>O values with respect to SMOW, whilst atmospheric oxygen has a high positive value (+23.5‰). Magmatic water has been shown to have positive values in the range +5 to +10‰ (Taylor, 1974). The distribution of δ<sup>18</sup>O compositions are illustrated in Figure 6.2.

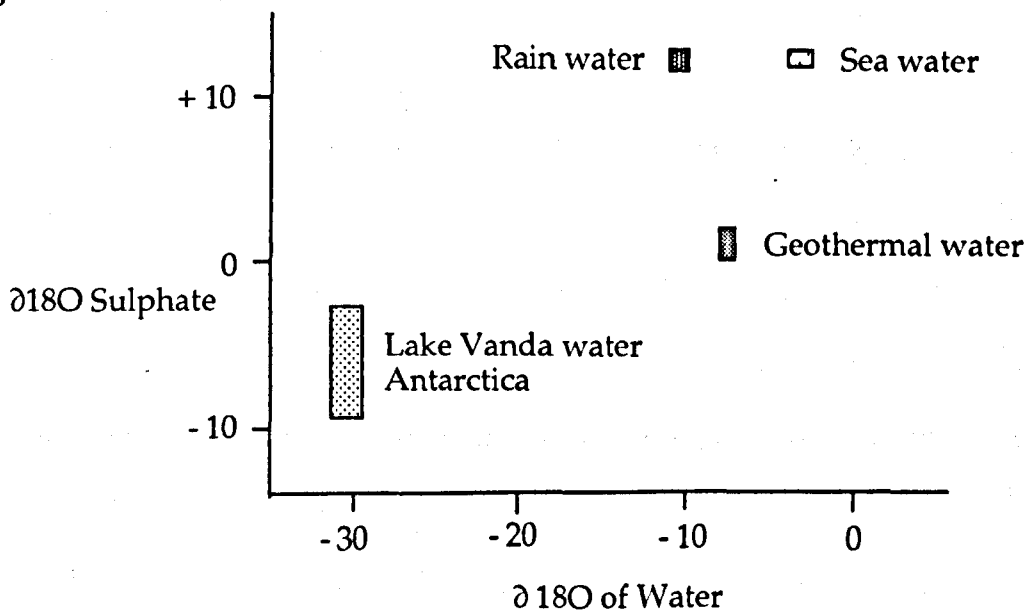
Rafter and Mizutani (1967) discuss the relationships between sulphate oxygen and associated water oxygen. There is a positive correlation between δ<sup>18</sup>O values in sulphate and water for Antarctic lake water, geothermal water and

Figure 6.2



Oxygen isotopic compositions of waters and air. Values from Rafter and Mizutani (1967) and Krauskopf\* (1985).

Figure 6.3



Distribution of oxygen isotopic composition of sulphates and the associated waters. After Rafter and Mizutani, 1967.

sea water but not for rain water. (Figure 6.3). The rain water sulphate is susceptible to marked change depending on local environmental conditions.

The oxygen incorporated into sulphate is derived from a reaction either with atmospheric oxygen (which may be dissolved) or water. The isotopic signature of the oxygen in the source is reflected in the  $\delta^{18}\text{O}$  of the sulphate oxygen. Thus the nature of the oxygen source may be distinguished, given that the  $\delta^{18}\text{O}$  of ground water is negative (  $-8\text{‰}$  for Northeast England, S. Bottrell, pers. comm.) and the  $\delta^{18}\text{O}$  of atmospheric oxygen is  $+23.5\text{‰}$  (Koopnick and Craig, 1972).

Given the complexities of the mechanisms for sulphide oxidation via biological or abiological oxidation, they shall not be considered in detail in this study. However, the  $\delta^{18}\text{O}$  values of the oxygen can be used to establish the source of the oxygen when taking the fractionations into consideration.

The  $\delta^{18}\text{O}$  for sulphate oxygen can be expressed as a mixture of atmospheric oxygen and water derived oxygen as shown by:

$$\delta^{18}\text{O}_{\text{SO}_4} = (\delta^{18}\text{O}_{\text{O}_2} + \epsilon_{\text{O}_2}) \cdot f_a + (\delta^{18}\text{O}_{\text{H}_2\text{O}} + \epsilon_{\text{H}_2\text{O}})(1-f_a)$$

where  $f$  is the proportion of oxygen from the reservoir and  $\epsilon$  is the fractionation. Experimental studies show a range of  $\epsilon$  values. These are summarised by Toran and Harris (1989) and are shown in Table 6.1.

Oxygen isotope exchange is controlled by pH, as the  $[\text{H}_2\text{SO}_3]$  intermediate species is unstable disassociating into:



The exchange reactions between atmospheric oxygen and water bound oxygen are very slow, therefore the oxygen isotope signal is dominated by water bound oxygen and the reservoir oxygen (water) can be represented as:



Sulphite is oxidised to sulphate by a variety of reactions. Three such reactions are shown in more detail in Table 6.2. Each reaction incorporates a different

**Table 6.1**

Experiment	$\epsilon_{O_2}$	$\epsilon_{H_2O}$
Abiological, high $P_{O_2}$ submersed	-8.7	0
Abiological, aerobic submersed	-4.3	
T. ferroxidans, aerobic submersed	-11.4	
Abiological, anaerobic with $Fe^{3+}$ submersed		4.1
Acid mine drainage (assumed 100% $H_2O$ incorporation)		2.6
Calculated	(-4.3) assumed	-6
Calculated	(-8.7) assumed	0

Isotope fractionation measurements for oxygen incorporation into sulphate.  
After Toran and Harris (1989).

**Table 6.2**

Reaction	% atmospheric oxygen
$SO_3^{2-} + H_2O + 2Fe^{3+} \rightarrow SO_4^{2-} + 2H^+ + 2Fe^{2+}$	0
$SO_3^{2-} + \frac{1}{2}O_2 \rightarrow SO_4^{2-}$	25
$SO_3^{2-} + O_2 \rightarrow SO_5^{2-} \rightarrow SO_4^{2-} + \frac{1}{2}O_2$	40

The proportion of atmospheric oxygen incorporation into sulphate via the oxidation of sulphite.

proportion of atmospheric oxygen. Once sulphate has formed, there is no further exchange of oxygen in the diagenetic environment if pH does not fall below 1 and temperature remains less than 100°C. Thus the identity of the last incorporated oxygen should be preserved.

## 6.5 In situ weathering of shales

Samples from the Jurassic (Jet Rock) and the Carboniferous (Caton Shales and Bowland Shales) were studied to determine the effects of in situ weathering on iron mineralogy, organic carbon and sulphur species.

### 6.5.1 Iron

Two samples were taken from this section of Jurassic Jet Rock at Port Mulgrave (see Chapter 5 for location and geological setting). Sample WPM12 was taken from the top few centimetres of the outcrop, whereas the sample PM12 was taken from the same site but from much deeper in the outcrop, as described in Chapter 2.

Sequential extractions of crushed samples were performed to determine iron concentrations using a modified version of the scheme described by Raiswell *et al.* (1994). About 100mg of rock sample was mixed with ammonium oxalate (50ml, 0.2M, pH=2) for two hours. The residue filtered and extracted using sodium dithionite for an hour (50ml, 0.3M) buffered to pH 4.8 with acetic acid and sodium citrate.

The residue was finally extracted using the hot HCl extraction technique described in Chapter 3. Iron concentrations were measured by atomic absorption as described in Chapter 3.

Canfield (1989a) found that  $\text{Fe}(\text{OH})_3$  and lepidocrocite ( $\gamma\text{FeOOH}$ ) were completely extracted with the oxalate solution. Dithionite was found to dissolve all major iron oxide phases whilst having only a limited effect on iron bearing silicates. Hot hydrochloric acid was found to attract all the iron oxides and hydroxides together with silicates. The results for the extractions of the two samples are shown in Table 6.3.

**Table 6.3**

	Wt % Fe extracted	
	PM12	WPM12
Oxalate	0.24	0.29
Dithionite	0.07	0.11
HCl	0.28	0.60

Results of the extractions of samples PM12 and WPM12.

**Table 6.4**

	Wt % Fe extracted	
	PM12	WPM12
Oxalate	0.24	0.29
Ox + dith	0.31	0.40
Ox + dith +HCl	0.59	1.00
Single Step HCl	0.71	1.07
%Fe as Pyrite	3.45	3.13
%FeR	4.16	4.20

Extraction data for samples PM12 and WPM12 showing cumulative iron extracted together with pyritic iron and reactive iron (FeR).

There seem to be two distinct pools of iron bearing minerals found in the Jet Rock samples. Those extracted by the oxalate i.e. the reactive oxides and oxyhydroxides and the much less reactive iron silicates, extracted by the hot HCl but not with the dithionite.

The sample taken at the surface of the exposure shows similar concentrations of iron extracted by oxalate and dithionite solutions, with slightly greater amounts being extracted from the weathered sample. There is a significant difference between the amount of iron extracted by HCl. Almost twice as much iron was extracted from the weathered sample.

Both samples were crushed to a size not greater than 250 mesh. Clearly, the weathered sample reacts more with HCl than does the 'fresh' sample. A typical mineralogy of the Jet Rock is given in Table 5.12, the iron bearing minerals being principally chlorite (~5%) and pyrite (~7%). Berner (1970) showed that fine grained pyrite was insoluble in hot hydrochloric acid, therefore any iron extracted from the Jet Rock must be either from trace amounts in illites, from chlorite or from the oxidation products of pyrite. Raiswell *et al.* (1994) found that chlorite was attacked to a small extent with boiling HCl (~2.2% iron extracted). Table 6.4 shows the extraction data as cumulative iron extracted together with a single step hot HCl extraction and pyrite iron concentrations.

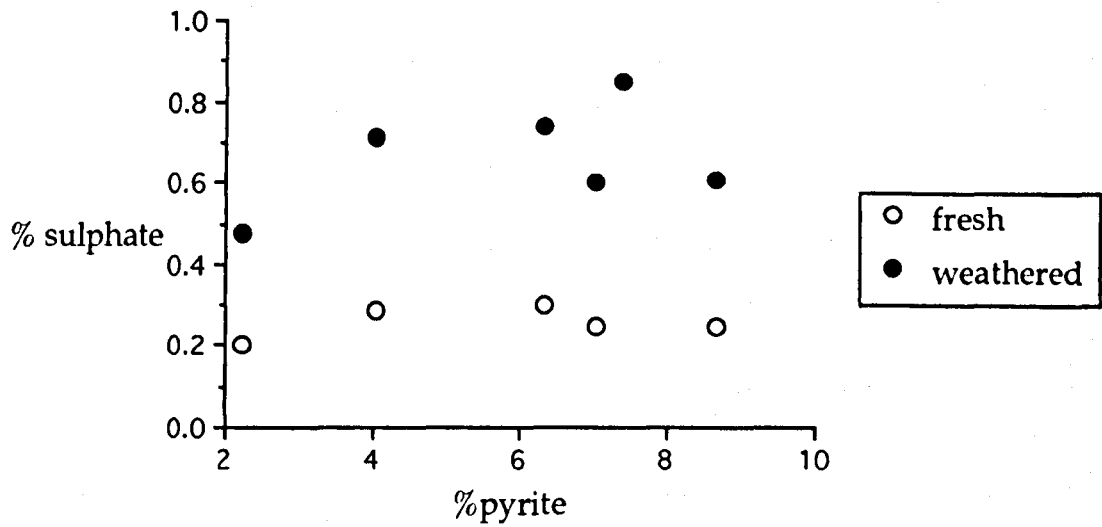
Given that the precision for each step in the sequential extraction is in the order of 3% (Raiswell *et al.* 1994, Canfield 1989a), the single step HCl extraction and the three step combined iron extraction are within error. There is very little difference between the FeR for the two samples. However, there is less pyrite in WPM12. The difference between the iron extracted by hot HCl in the two samples can be accounted for on a mass balance basis by pyritic iron.

In terms of mineralogy however, it seems hard to rationalise the data. Pyrite is unreactive to hot HCl. Simple oxidation products of pyrite are iron oxides, oxyhydroxides or sulphates, all of which would be expected to react with oxalate and dithionite. One possibility is that pyrite was oxidised into a reactive oxyhydroxide which subsequently reacted with carbonate to form siderite.

Extraction experiments performed on siderite showed that about 10 wt % Fe was extracted by dithionite and almost 40 wt % Fe by hot HCl (Raiswell *et al.* 1994). To envisage a situation where pyrite is oxidised (and acidity generated) then the oxidised iron reacting to precipitate a carbonate seems very unlikely.

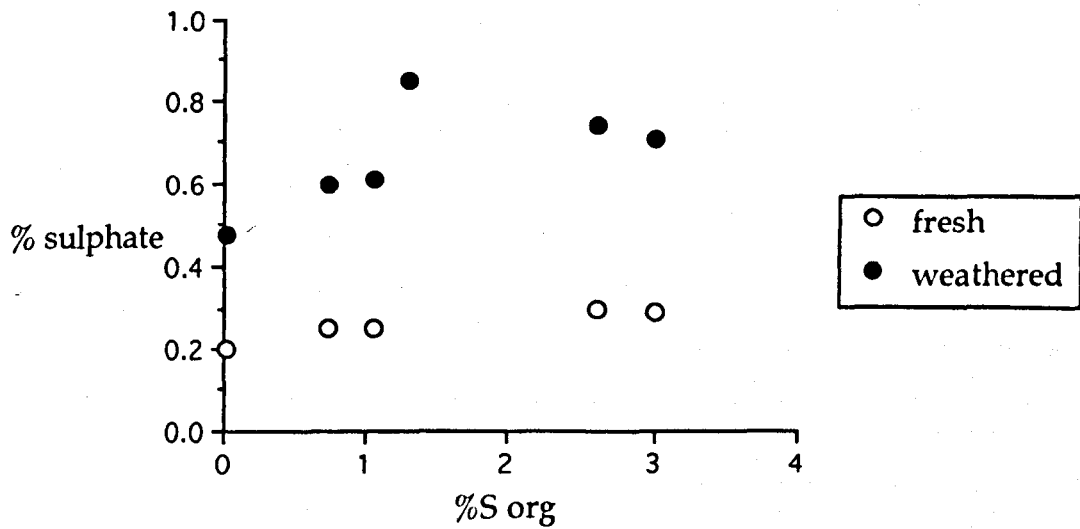


Figure 6.4



The relationship between pyrite concentration and acid soluble sulphate concentration in the Jet Rock.

Figure 6.5



The relationship between organic sulphur and sulphate sulphur in the Jet Rock.

Pye and Miller (1990) performed a very simple leaching experiment using a pyritic shale sample and water or dilute sulphuric acid. They found that there was rapid loss of exchangeable cations, but with time the rate of Fe and Mg loss increased. This suggests that the extrahedral layers (containing Fe and Mg) within the lattices of chlorites, illitic clays and micas were slow to react, but did indeed react.

The weathered Jet Rock is constantly being removed by the action of the sea. Therefore, any significant physical weathering will result in the removal of the material. The surface weathering environment is dominated by sea water although the outcrop is situated in the intertidal zone exposing the rocks to the air for several hours each day. This environment may lead to the alteration of chlorite into swelling chlorite and mixed layer species. Although retaining iron within the lattice the chemistry and therefore the reactivity of such material is significantly different to 'pure' shale. Such a situation can explain the discrepancy between the dithionite and HCl extractions.

The constant washing of the shale would dissolve the soluble phase and remove it out of the system. One of the suggested products of pyrite oxidation is iron sulphate (both ferric and ferrous) which could easily account for the loss of iron. There would be some residual sulphur (as elemental sulphur) left if ferrous sulphate was produced by the reaction shown in Equation 6.9.



### 6.5.2 Organic Matter

Samples from the Caton Shales (see Chapter 4 for location details) were taken with a view to investigate the surface weathering effects of organic matter as measured by Rock Eval analysis. This is a rapid and routinely implemented technique used to determine the chemical composition of kerogens and hence their hydrocarbon generating potential.

Samples were taken from four depths at one area on the outcrop of the Caton Shales in the Lowgill stream section. The first few centimetres of rock were classed as 'outer', subsequent samples were taken by excavation of the outcrop by chisel and finally using a rock core drill. The depths are shown in Table 6.5.

**Table 6.5**

Sample descriptor	Depth into rock face
Outer (O)	0 - 10 cm
Middle (M)	30 - 50 cm
Deep (D)	70 - 80 cm
Drill (DR)	100 - 110 cm

Depth of samples taken from the Caton Shales.

**Table 6.6**

Sample Number	Sample Reference	S1	S2	T <sub>max</sub>	TOC
1	3DR	-	-	-	-
2	41DR	0.310	1.010	424.000	1.28
3	42DR	0.320	0.890	424.000	2.00
4	5BD	-	-	-	-
5	5.5BO	0.050	0.810	428.000	1.86
6	5.5BM	0.040	0.800	425.000	2.04
7	5.5BD	0.040	0.800	425.000	1.72
8	5.5O	0.060	0.730	430.000	1.42
9	5.5M	0.050	0.870	424.000	-
10	5.5D	0.040	0.760	426.000	1.73
11	5O	0.040	0.640	433.000	1.42
12	5M	0.040	1.280	430.000	-
13	3O	0.130	1.050	425.000	1.59
14	3M	0.070	0.750	427.000	1.65
15	3D	0.070	0.870	430.000	1.68

Summary of the Rock Eval data for weathered Carboniferous shale samples.

Taking note of the limitations of Rock Eval information in that it can be affected by hydrocarbon contamination mineral matrix effects, the results are compared internally within the data set. The drill was cooled during cutting by stream water, thus the risk of hydrocarbon contamination by this extraction process is minimal. Table 6.6 shows the S1, S2 and  $T_{\max}$  pyrolysis data for 14 samples, together with TOC values.

Bitumen was extracted from some of these samples. The amount extracted expressed as a percentage of the whole rock is shown in Table 6.7.

The samples drilled were not Soxhlet extracted due to lack of material collected. The data available suggests that there is no appreciable difference in the amount of bitumen extracted from any of the samples near to the surface (<100cm). The variance in the reproducibility of the extraction of sample 5.5O is  $\pm 0.01$  which provides an envelope for almost all of the data.

There appears to be a marked difference between the drilled samples and the samples collected from within 1m of the outcrop surface. The volatilisation of pre-existing hydrocarbons in the samples during the Rock Eval process produces the S1 peak. The data suggests that up to 85% of these products (the bitumen) may be lost during the surface weathering of shales. More data must be collected and a detailed chemical comparison of extracted bitumens from shale samples collected by deep drilling and surface samples should be undertaken.

Jørgensen (1982) found that sulphate reduction and oxic respiration oxidise equal amounts of organic carbon in recent near shore marine sediments. During burial and subsequent diagenetic reactions, further loss of organic matter is observed. Raiswell and Berner (1987) showed that for normal marine sediments, the ratio of organic carbon to pyrite sulphur (C/S) could be used to estimate the level of thermal maturity for sediments as old as Devonian. This relationship is used to provide an estimate for organic sulphur loss, as pyrite sulphur is not lost in significant amounts by microbial methanogenesis, thermal maturation and low grade metamorphism, unlike organic carbon.

Assuming an initial C/S ratio of 2.8 (Goldhaber and Kaplan, 1974), the data presented by Raiswell and Berner (1987) can be used to provide an estimate of the percentage carbon loss, see Table 6.8. Linear regression produces the following expression:

**Table 6.7**

Sample	Mass of Rock	Mass of Bitumen	%
5.5 O	51.56006	0.07844	0.15
5.5 O	46.99545	0.06581	0.14
5.5 O	49.96278	0.07824	0.16
5.5 O	44.23035	0.06349	0.14
5.5 M	51.32352	0.06871	0.13
5.5 D	44.23035	0.06349	0.14
5.5 b O	46.17474	0.06520	0.14
5.5 b D	44.53259	0.06445	0.14
3 M	58.98409	0.07500	0.13
3 D	52.54810	0.07703	0.15

Bitumen extracted from the Caton Shales.

**Table 6.8**

C/S	R <sub>0</sub>	Estimated %C loss
2.8	0	0
2.1	0.5	25
1.6	0.7	42
1.4	1.0	50
1.3	1.0	55
0.7	2.0	75

Estimated loss of organic carbon with increasing thermal maturity.

$$\%C_{\text{loss}} = 7.96 + 36.90R_0$$

$$r^2 = 0.94$$

This enables approximate carbon loss to be readily calculated for normal marine shales with thermal maturities up to  $R_0 = 2.0$ . The limitations noted by Raiswell and Berner (1987) must be taken into account for use with this method (see Chapter 3).

Although not a weathering reaction, it must be remembered that the shales in this study are at least 190 million years old. With  $R_0$  in the range 0.4 to 0.85 (Table 6.7), there has been significant loss of organic matter. The shales in this study probably contained at least 30% more organic carbon than they do at present (Tables 6.8 and 6.9). During thermal maturation, the loss of organic carbon is accompanied by the loss of organic sulphur, both residual assimilated sulphur and sulphur added during incorporation reactions earlier in diagenesis. The sulphur-carbon bond strengths in organic compounds are weaker than the comparable bond for carbon-carbon (Table 6.10). The thermal stability of sulphur bearing organic compounds will, therefore be lower than those compounds without sulphur.

Primary protein material is thought to contain approximately 1% sulphur, zooplankton being comprised of 60% protein. Given the thermal maturation processes, the effects of biodegradation and reoxidation, the organosulphur compounds found in ancient shales are likely to be some of the most stable and resistant molecules out of the range of possible compounds which may have made up the sediment at some stage in its history.

### 6.5.3 Sulphur

#### 6.5.3.1 Sulphate in Jurassic Shales

Six pairs of samples from the Jet Rock were taken to investigate the effects of weathering on sulphur compounds within organic rich shales. Each pair was taken as a block cut from the beach section using a stihl saw. The block was then divided into two parts to produce a weathered and 'unweathered' or fresh sample. The concentrations of sulphur bearing compounds are summarised in Table 6.11. The concentration of elemental sulphur in the samples was very low - less than 0.01 wt%.

**Table 6.9**

Sample	R <sub>0</sub>
Jet rock	0.6
Bowland Shales	0.7
Caton Shales	0.85
[Chatburn Limestone	0.4]

The thermal maturity (as measured by vitrinite reflectance) of shale samples analysed in this study.

**Table 6.10**

Bond	$\Delta H$ kJ mol <sup>-1</sup>
C-C	348
C-H	412
S-S	264
S-H	338
C-S	272
C=C	612
C=S	477

Average bond energies for selected bonds.  
(After Stark and Wallace, 1986)

**Table 6.11**

Sample	% Pyrite	% Organic S	% SO <sub>4</sub> Fresh	% SO <sub>4</sub> Weathered
PM 1	2.21	0.01	0.20	0.48
PM 5	6.35	2.61	0.30	0.74
PM 8	4.06	3.60	0.29	0.71
PM12	7.42	1.29	-	0.85
PM 15	7.05	0.74	0.25	0.60
PM 17	8.65	1.05	0.25	0.61
PM 10	8.21	1.45	-	-
PM 11	10.52	1.68	-	-

Summary of the proportions of sulphur bearing compounds in the Jet Rock.



In order to obtain sufficient CuS to enable isotopic analysis multiple soxhlet extractions were performed and the resulting residues were combined. The fresh samples contain less acid soluble sulphate than is found within the weathered samples. There is very little variation with sulphate concentration within the fresh samples ( $0.26 \pm 0.04$  %) but a slightly greater increase is shown within the weathered samples ( $0.67 \pm 0.12$  %). Approximately 0.4 % more sulphate is found in the weathered samples.

The concentration of acid soluble sulphate appears to be independent of pyrite sulphur (Figure 6.4) but there is good independent correlation between the organic sulphur content and sulphate concentration in the fresh samples ( $r^2 = 0.89$ ). The correlation between the weathered sample and the organic sulphur concentrations of the fresh sample ( $r^2 = 0.39$ ) is not as good. These relationships are shown in Figure 6.5.

There is a positive correlation between the concentration of sulphate within the weathered and fresh samples. Figure 6.6 illustrates this data with  $r^2 = 0.99$ . Such a good correlation indicates the evolution from the fresh to the weathered sample by progressive addition by some mechanism.

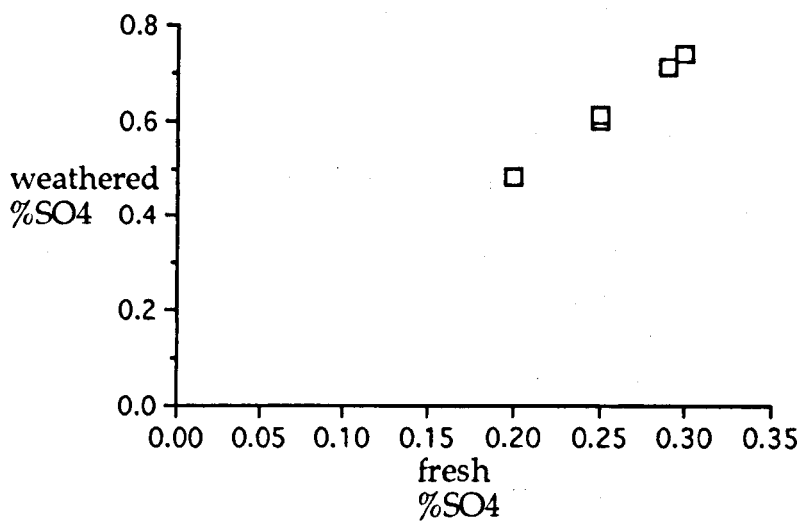
### 6.5.3.2 Isotopic composition of sulphate in the Jet Rock

A combined sulphur and oxygen isotopic study has been made of the sulphate found in the fresh and weathered samples collected from the Jet Rock. The main purpose of such an investigation was to try to determine the source of sulphur, within the sulphate.

The possibility of the sulphate being derived from sea water, either Jurassic or present day must first be considered. Present day sea water sulphate has a sulphur isotope composition of  $+21\text{‰}$  (Rees *et al.*, 1987) and Jurassic sea water sulphate is thought to have a  $\delta^{34}\text{S}$  of  $+17\text{‰}$  (Claypool *et al.*, 1980). Clearly the sulphate in this study is not the result of dissolved sea water sulphate precipitating directly into the rock and becoming incorporated, as the  $\delta^{34}\text{S}$  of the acid soluble sulphate is negative for all samples (Table 6.12).

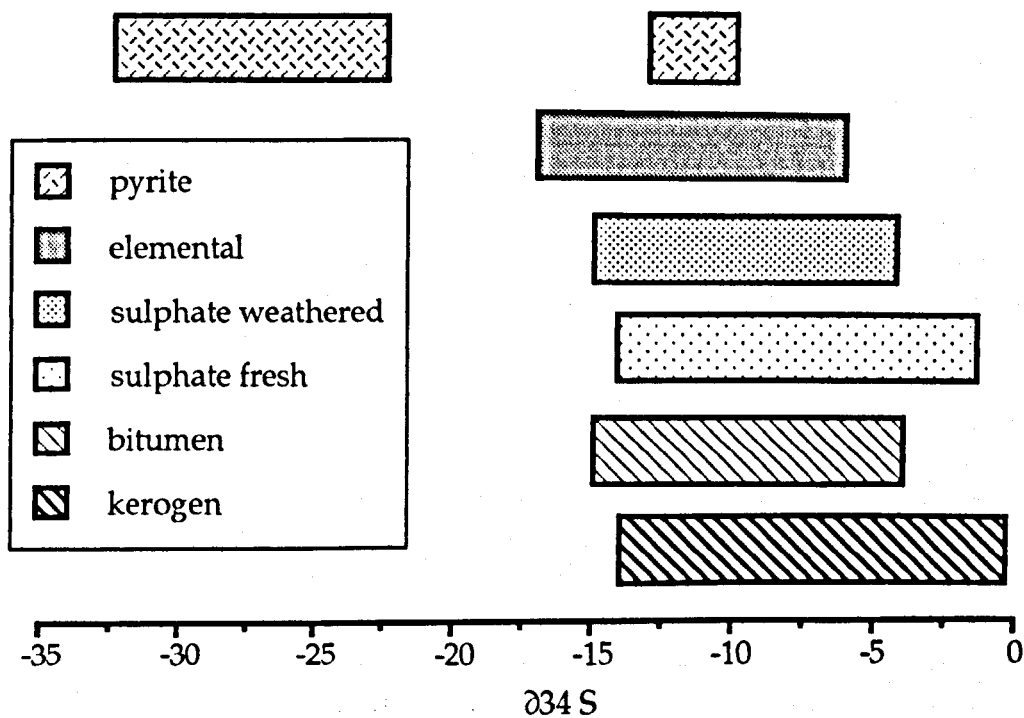
The sulphur isotopic composition of the different forms of sulphur (sulphate, pyrite, elemental kerogen and bitumen) is discussed in order to propose the origin of the sulphate and elemental sulphur in the Jet Rock.

Figure 6.6



The relationship between sulphate concentration in the weathered and fresh samples from the Jet Rock.

Figure 6.7



Summary of the distribution of the isotopic composition sulphur species found within the Jet Rock.

Table 6.12

Sample	Fresh Sulphate		Pyrite $\delta^{34}\text{S}$	Elemental $\delta^{34}\text{S}$	Kerogen $\delta^{34}\text{S}$	Bitumen $\delta^{34}\text{S}$	Weathered Sulphate	
	$\delta^{34}\text{S}$	$\delta^{18}\text{O}$					$\delta^{34}\text{S}$	$\delta^{18}\text{O}$
PM 1	-13.94	5.60	-28.20		-12.29	-	-14.90	-0.10
PM 5	-6.12	4.20	-22.40		-7.74	-3.90	-7.20	0.80
PM 8	-2.29	2.10	-21.70	-16.81	-0.82	2.53	-8.00	2.00
PM 12	-3.68	2.60	-24.90	-8.27	-5.89	1.15	-6.80	1.80
PM 15	-1.16	2.60	-25.17		-6.43	0.62	-5.60	-0.10
PM 17	-2.10	2.80	-32.03		-10.00	-0.18	-4.10	2.20
PM 10	-4.80	2.40	-23.89	-10.36	-	-3.61	-	-
PM 11	-6.10	2.50	-24.57	-86.08	-5.89	1.15	-	-

$\delta^{34}\text{S}$  for sulphur bearing compounds in the Jet Rock. All values are in ‰.

The distribution of the isotopic compositions of sulphur bearing compounds is shown in Figure 6.7. There are two distinct generations of pyrite found in the Jet Rock. They can be distinguished texturally and by  $\delta^{34}\text{S}$  composition into an early isotopically light, framboidal phase and a later, isotopically heavy, massive euhedral phase. This is discussed in Chapter 5. Both generations of pyrite are displayed in Figure 6.7 as separate fields.

The first generation of pyrite is by far the lightest and most distinct sulphur bearing phase based upon the isotopic evidence. There is considerable overlap between the other phases. It seems unlikely that either the elemental sulphur or the sulphate sulphur was derived from the oxidation of the first generation of pyrite, given the large difference in their  $\delta^{34}\text{S}$ .

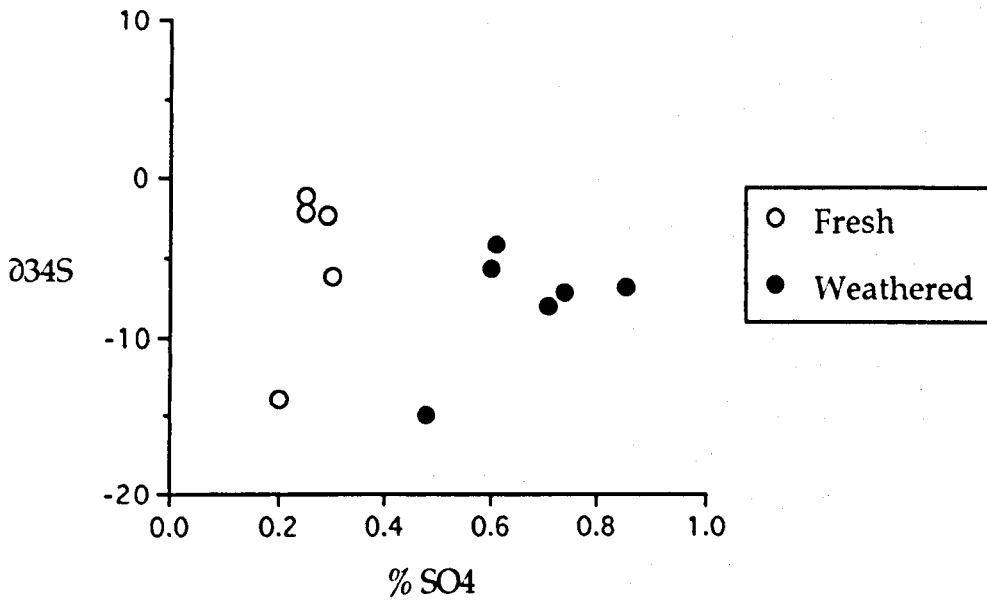
In all cases, the weathered samples contain at least 0.4% sulphate, and the fresh samples less than 0.4% sulphate, irrespective of sulphur isotopic composition (Figure 6.8). The weathered samples contain sulphate enriched with  $^{32}\text{S}$  being approximately  $3.0 \pm 1.9\text{‰}$  lighter than the corresponding fresh samples (Figure 6.9).

A single source of sulphate sulphur in the Jet Rock cannot be unambiguously identified using sulphur isotopes alone. The data suggests that sulphate sulphur is a mixture of organic sulphur and pyrite sulphur. The organic sulphur appears to be dominant in most cases. Sample PM1 has the lightest sulphate sulphur ( $-13.94\text{‰}$ ) indicating a significant pyrite sulphur contribution. The weathered samples show lighter sulphate sulphur values than the fresh samples, suggesting more pyrite oxidation.

The sulphate oxygen isotopic compositions of the weathered and fresh samples are shown in Table 6.11. The fresh samples analysed have a mean  $\delta^{18}\text{O}$  value of  $3.1 \pm 1.2\text{‰}$  and the mean  $\delta^{18}\text{O}$  value for the weathered samples was  $1.1 \pm 1.0\text{‰}$ . There is an apparent difference in the oxygen isotopic composition of the sulphate from fresh and weathered samples. Figure 6.10 shows the relationship between sulphate content and  $\delta^{18}\text{O}$ . As the concentration of sulphate increases, the sulphate oxygen becomes progressively lighter. In general, fresh samples have  $\delta^{18}\text{O}$  greater than  $+2\text{‰}$  and the weathered samples show lighter values i.e. less than  $+2\text{‰}$ , suggesting a greater influence of water derived oxygen.

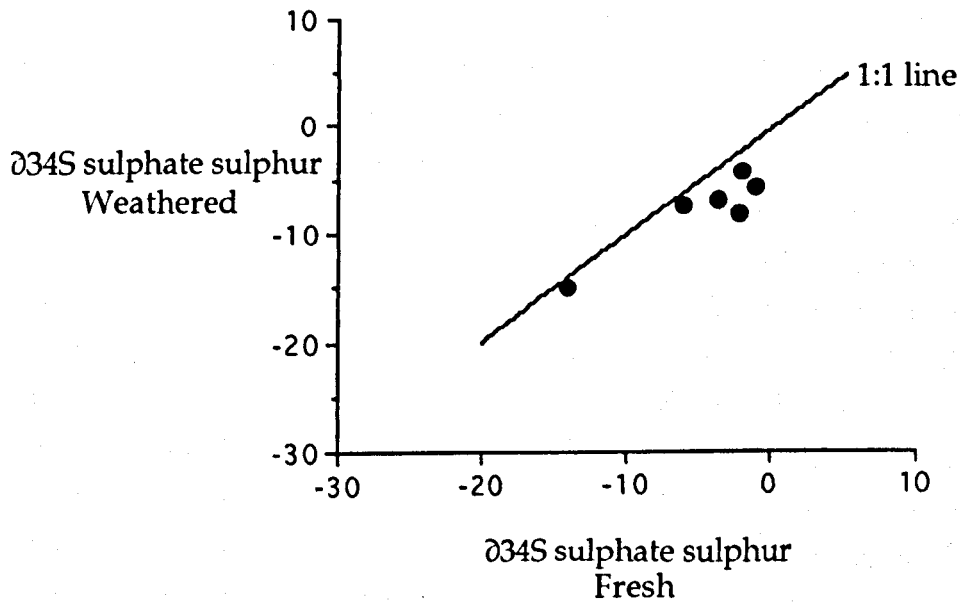
Unlike the sulphur isotope data, the oxygen values in the weathered and fresh samples do not show a positive linear correlation, but a negative one (Figure

Figure 6.8



Relationship between sulphate concentration and  $\delta^{34}\text{S}$  of the sulphate extracted from fresh and weathered samples of the Jet Rock.

Figure 6.9



$\delta^{34}\text{S}$  of sulphate extracted from weathered and fresh samples from the Jet Rock.

6.11). The lightest  $\delta^{18}\text{O}$  in the fresh samples correspond to the heaviest sulphates in the weathered samples. Considering this and the relationship shown in Figure 6.12 an evolution of  $\delta^{18}\text{O}$  compositions can be established. Initially sulphate with heavy oxygen is formed at low concentrations. As oxidation continues and sulphate concentrations build up, the relative importance of water derived oxygen becomes apparent. One possible explanation of this observation could be that biological oxidation takes place on or near to the rock surface utilising more water derived oxygen.

A plot of  $\delta^{34}\text{S}$  against  $\delta^{18}\text{O}$  for the sulphate summarises the data (Figure 6.12). The trend can be explained by either:

1. different enrichment factors for oxygen isotopes in the oxidation of pyrite versus organic sulphur, or
2. a correlation between oxidant source (atmospheric oxygen and water oxygen) and sulphur source.

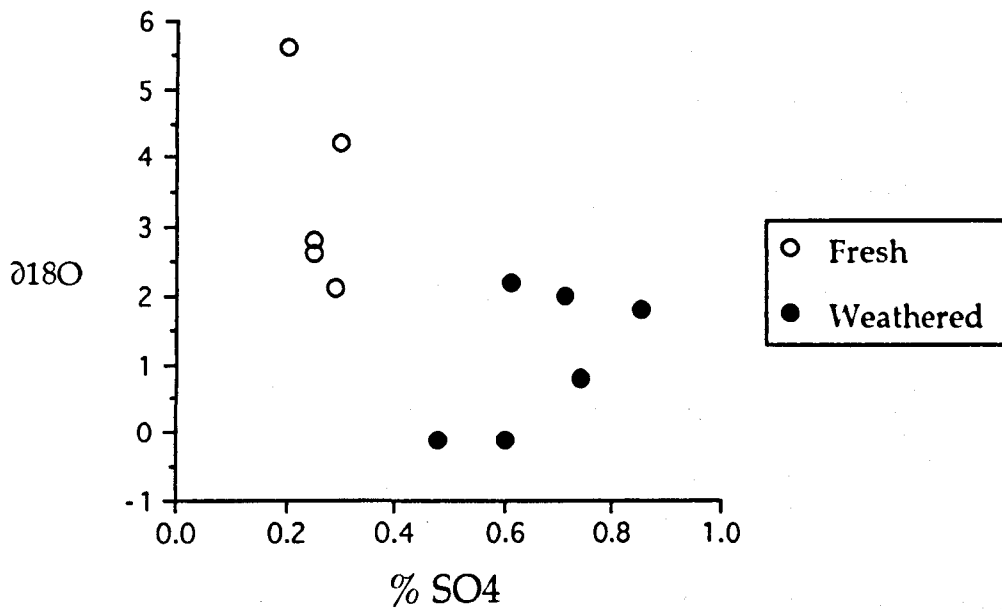
The weathered samples show slightly lighter  $\delta^{34}\text{S}$  suggesting more pyrite derived sulphur and much lighter  $\delta^{18}\text{O}$  from water.

### 6.5.3.3 Sulphate in Carboniferous Shales

Shale samples from weathered Carboniferous shales were collected to compare the sulphate sulphur and oxygen isotopic compositions with those of the Jurassic. Four sample locations were visited (Table 6.9).

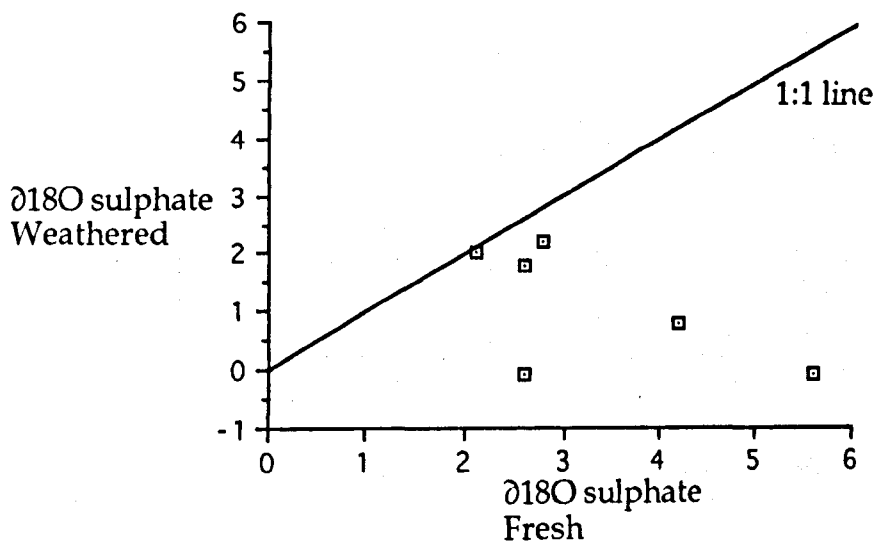
The Bowland Shales are a Dinantian/Namurian mudrock sequence found within the Bowland Basin of Northern England. The structure and sedimentology of the area has been extensively studied by Gawthorpe and co-workers e.g. Gawthorpe (1986), (1987a,b), Gawthorpe and Clemmey, (1985) and Gawthorpe *et al.* (1989). The two sample localities visited for the Bowland Shales (Dinkley and Crag Wood) represent contrasting sites of palaeodeposition. Dinkley was thought to lie in a position distal to the main turbidite fan. Crag Wood represents a condensed sequence lying on an intrabasinal topographic high (Clemmey, pers. comm.). The Chatburn Limestone group comprises of Ivorian and Early Chadian sediments. Gawthorpe (1986), interpreted the progression of limestones to shales as the

Figure 6.10



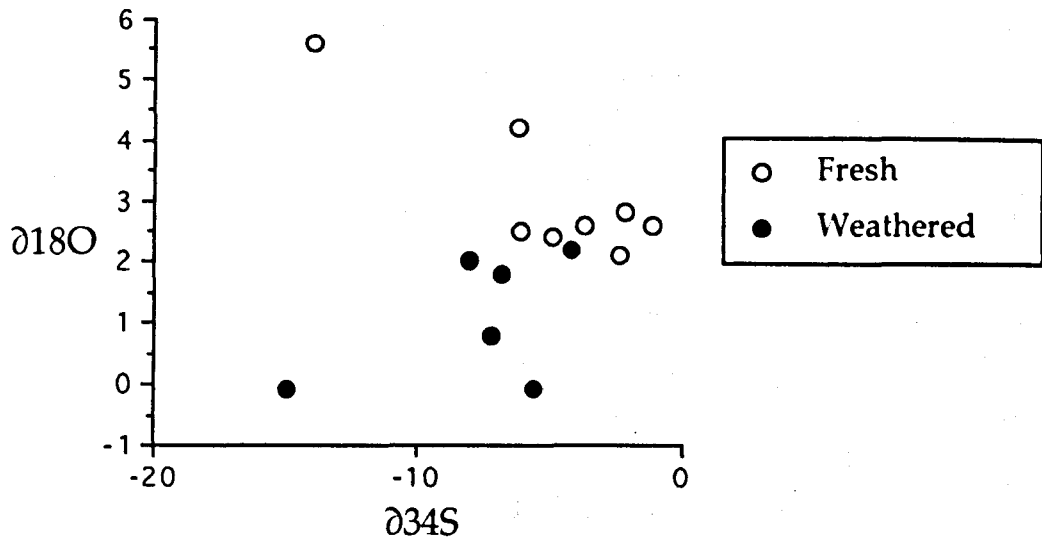
Relationship between sulphate concentration and  $\delta^{18}\text{O}$  of the sulphate extracted from fresh and weathered samples of the Jet Rock.

Figure 6.11



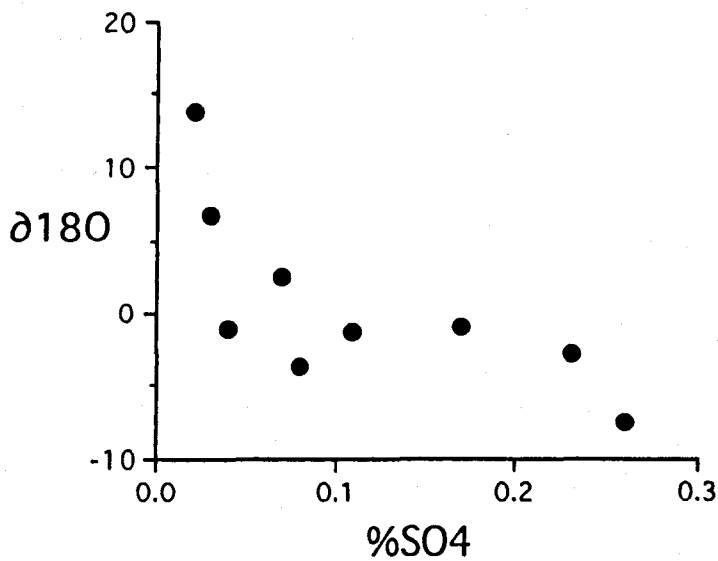
$\delta^{18}\text{O}$  of sulphate extracted from weathered and fresh samples from the Jet Rock.

Figure 6.12



Variation of  $\delta^{18}\text{O}$  and  $\delta^{34}\text{S}$  in sulphate extracted from fresh and weathered samples of the Jet Rock.

Figure 6.13



Variation of  $\delta^{18}\text{O}$  and sulphate concentration for Carboniferous shales.



evolution of a carbonate ramp-to-slope environment. The samples from the Caton Shales were collected from the Lowgill section as described in Chapter 4. All the Carboniferous samples were crushed and soluble sulphate was extracted with 0.01M HCl. These samples were not originally selected for a study of weathering and therefore were collected in the usual way i.e. the weathered crust of rock removed prior to sample collection. The results of the analyses are shown in Table 6.13.

The mean sulphate concentration in the Bowland Shales was found to be  $0.10 \pm 0.10\%$ , the Caton Shales had a mean sulphate concentration of  $0.10 \pm 0.07\%$  and the sample from the Chatburn Limestone group contained  $0.23\%$  soluble sulphate. These values are lower than those for the Jet Rock samples (mean fresh =  $0.26\%$  and mean weathered =  $0.67\%$ ). There was very little organic sulphur within the bitumen fraction of any of the Carboniferous samples. Often the values were less than the detection limits. The concentrations of pyrite are in general considerably lower in the Carboniferous samples than in the Jurassic with means of  $3.02 \pm 1.74\%$  ( $n=9$ ) and  $6.81 \pm 2.63\%$  ( $n=8$ ).

The  $\delta^{34}\text{S}$  of pyrite from the Carboniferous is characteristic of each group of sediments: Bowland Shales, mean  $\delta^{34}\text{S} = -32.45\text{‰}$ ; Chatburn Limestone Group,  $\delta^{34}\text{S} = -6.40\text{‰}$  and the Caton Shales, mean  $\delta^{34}\text{S} = -17.70\text{‰}$ . These fall within the mean value for the Jet Rock (mean  $\delta^{34}\text{S} = -25.69$ ).

#### 6.5.3.4 Isotopic Composition of sulphate from Carboniferous Shales

The  $\delta^{18}\text{O}$  and  $\delta^{34}\text{S}$  values for acid soluble sulphate from nine Carboniferous shale samples are shown in Table 6.13. One sample (SDK8) shows a very light sulphur isotopic composition ( $\delta^{34}\text{S} = -30.00\text{‰}$ ). With the exception of this sample, the mean  $\delta^{34}\text{S}$  of the sulphate is  $-1.70 \pm 4.3\text{‰}$  and the mean  $\delta^{18}\text{O}$  is  $1.70 \pm 5.90\text{‰}$ .

There is a similar trend to that seen in Figure 6.10 with the Carboniferous samples. Although the range of  $\delta^{18}\text{O}$  and sulphate concentrations are different, there is a marked increase in  $^{16}\text{O}$  as the sulphate concentration increases i.e. samples with the most soluble sulphate have the lowest  $\delta^{18}\text{O}$  values (Figure 6.13). Data from the Carboniferous and the Jurassic samples are shown together on Figure 6.14.

Table 6.13

Sample	% Sulphate	% Pyrite	$\delta^{34}\text{S}$ Pyrite	$\delta^{18}\text{O}$ Sulphate	$\delta^{34}\text{S}$ Sulphate
SDK1	0.11	6.82	-28.63	-1.3	3.70
SDK4	0.03	1.18	-41.40	6.8	-4.2
SDK8	0.26	1.76	-35.83	-7.4	-30.0
SCL2	0.23	1.03	-6.40	-2.7	-1.7
SCW1	0.02	3.71	-27.93	13.8	-2.3
SCW6	0.07	3.26	-28.48	2.5	-8.7
LG30	0.04	2.90	-17.81	-1.1	-5.2
LG3M	0.08	2.93	-17.41	-3.6	1.1
LG5M	0.17	3.56	-17.87	-0.9	3.4

$\delta^{18}\text{O}$  and  $\delta^{34}\text{S}$  values from sulphate extracted from Carboniferous shales.

Table 6.14

Sample	$\text{S}^0$	$\text{SO}_4\text{-S}$	Pyrite	Kerogen	Bitumen
LG30	-7.66	-5.20	-17.81	xx	xx
LG3M	-6.00	1.10	-17.41	xx	xx
LG5M	-4.73	-3.40	-17.87	xx	xx
WPM8	-16.81	-8.00	-21.70*	-8.28*	2.53*
WPM12	-8.27	-6.80	-24.90*	-5.89*	1.15*
PM10	-10.63	-4.80	-23.89		-3.61
PM11	-6.08	-6.10	-24.57	-5.89	1.15
mean	-8.60	-4.74	-21.16		
$\sigma_{n-1}$	4.09	2.97	3.40		

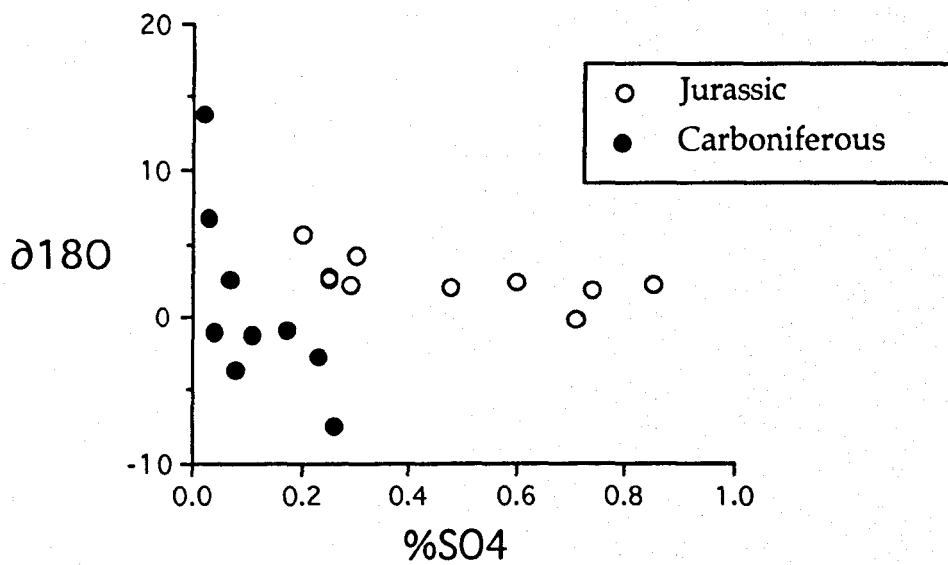
$\delta^{34}\text{S}$  values for sulphur species found in shales.

All values are expressed in ‰.

\* denotes the values for 'fresh' samples, therefore only represent an approximation for the weathered samples.

xx denotes concentration of sulphur too small to perform isotopic analysis.

Figure 6.14



Variation of  $\delta^{18}\text{O}$  and soluble sulphate extracted from fresh and weathered shale samples.

The  $\delta^{18}\text{O}$  and  $\delta^{34}\text{S}$  cross plot of the Carboniferous samples shows no obvious pattern (Figure 6.15). Taking each sample locality individually, the Dinkley samples suggest a progressive decrease in  $\delta^{34}\text{S}$  as  $\delta^{18}\text{O}$  increases. The Lowgill samples cluster at the high  $\delta^{34}\text{S}$  low  $\delta^{18}\text{O}$  end of the range and the samples from Crag Wood and the Chatburn Limestone Group lie almost within this range.

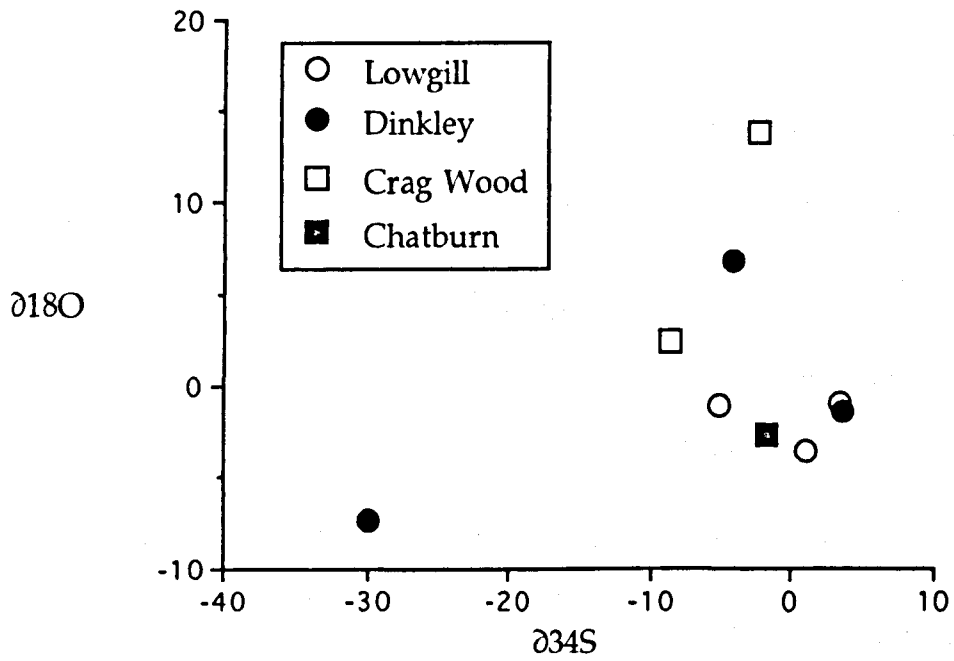
### 6.5.3.5 The evolution of sulphate isotopic composition

The sulphate isotopic data show clear trends. The 'fresh' (unweathered) samples have relatively heavy sulphur and oxygen isotopic compositions at the lower sulphate concentrations. This trends towards lighter isotopic compositions of both sulphur and oxygen with increasing sulphate concentration (Figures 6.8, 6.10, 6.13 and 6.14). The weathered Jurassic shale samples form an extension of this trend. These samples show the highest sulphate concentration and lightest oxygen and sulphur isotopic compositions (with the exception of SDK8 which has very light S and O isotopic compositions). This trend can be interpreted as mixing of two sulphate sources:

1. A primary sulphate, present in the rock at low concentration (<0.1 wt%) prior to any weathering and characterised by relatively heavy isotopic compositions of sulphur and oxygen.
2. An additional component generated by near-surface weathering reactions characterised by lighter isotopic compositions of both sulphur and oxygen. It is an increase in the proportions of this component that produces the shift in sulphate isotopic compositions observed between the weathered and unweathered Jurassic shale sample pairs (Table 6.12).

Original sea water sulphate is ruled out as a significant component of the sulphate on the basis of sulphur isotope composition. Carboniferous and Jurassic sea water sulphate was significantly  $^{34}\text{S}$  enriched relative to all of the sulphate values reported in this study (+25‰ and +17‰, Claypool *et al.*, 1980). Early diagenetic pore waters probably contained sulphate which was further enriched in  $^{34}\text{S}$  by the effects of bacterial sulphate reduction (Goldhaber and Kaplan, 1974). The observed spread in the sulphate-oxygen isotopic values seem unlikely to be a result of a shift in the proportion of atmospheric derived oxygen and water derived oxygen. The weathered samples of the Jurassic

Figure 6.15



The relationship between  $\delta^{34}\text{S}$  and  $\delta^{18}\text{O}$  isotopic compositions of the sulphate extracted from Carboniferous shales. Samples of the Bowland Shales were taken from Dinkley and Crag Wood, from the Chatburn Limestone Group near Chatburn and from the Caton Shales at Lowgill.

shales are always  $^{18}\text{O}$  depleted relative to their unweathered counterparts (Table 6.12). This would necessitate that more atmospheric oxygen was incorporated in the deeper part of the weathering profile which seems extremely unlikely.

### Primary sulphate

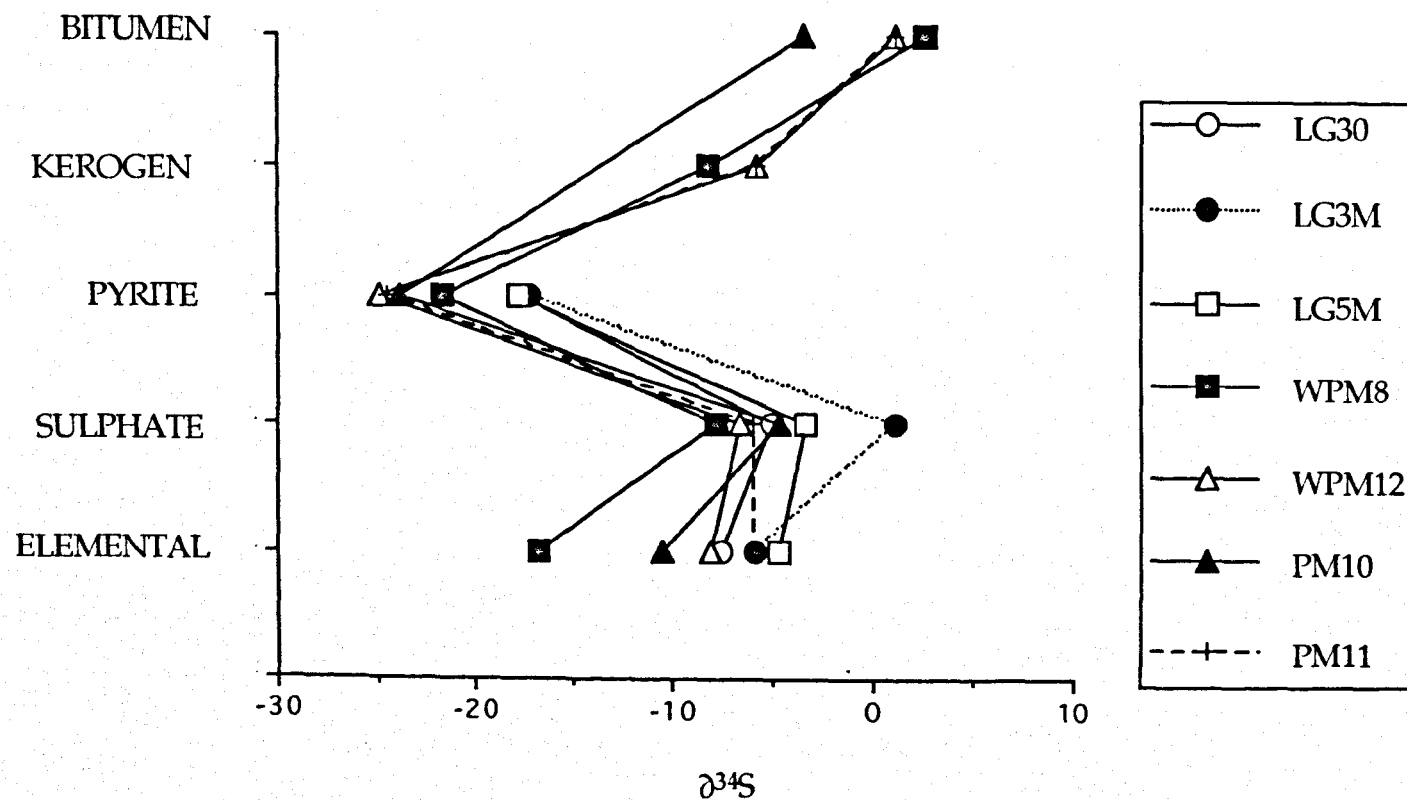
The range in sulphate-sulphur isotopic compositions in the unweathered shales is generally similar to the organic sulphur (kerogen and bitumen). The groundmass pyrite is substantially depleted in  $^{34}\text{S}$  relative to the sulphate-sulphur (Figure 6.16). There is a broad relationship between sulphate and organic sulphur isotopic compositions (Figure 6.17). This suggests that the degradation of OBS was the source of the primary sulphate. The heaviest oxygen compositions are associated with this sulphate component.

Using the heaviest oxygen isotopic composition (13.8‰) and assuming a marine derived pore water (0‰) an isotopic equilibrium temperature calculated from the relationship determined by Lloyd (1968) would be 136°C. This temperature is slightly higher than those calculated for thermal maximum achieved during the maturation of these shales (90-100°C from AFTA, 110°C from carbonate thermometry). The discrepancy probably results because even this sample contains some component of later sulphate with lighter oxygen. However, the heavy sulphate-oxygen isotope compositions of primary sulphate do imply that it was produced before or during maturation of the shales in order that isotopic equilibration with the pore fluid could occur. Lloyd (1968) also reports the kinetics of some of the isotope exchange reactions in the sulphate-water system. At 80°C and pH=7, the half life for the exchange reaction is in the order of 100 years. In more acidic conditions (pH=4) the half life is in the order of 10 years. Thus the exchange reactions could reach equilibrium given the geological time scale of events.

### Late "weathering" sulphate

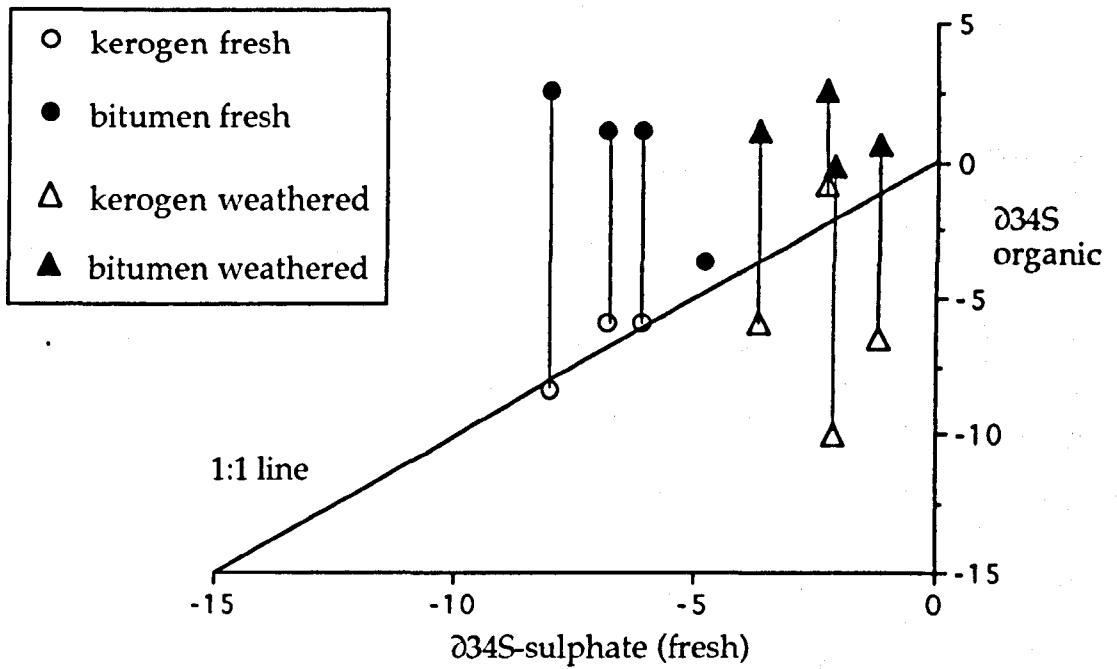
A second generation of sulphate can be identified in the shales. It is characterised by lighter sulphate-sulphur isotopic compositions, probably the result of oxidation of pyrite as well as organic sulphur during weathering. The lighter oxygen isotopic compositions are consistent with a value for the weathering sulphate of around -2‰, which would represent approximately  $3/4$  meteoric water derived oxygen (at approximately -8‰ in N. England; S.

Figure 6.16



Distribution of  $\delta^{34}\text{S}$  values for sulphur species (bitumen, kerogen, pyrite, sulphate and elemental sulphur) found in shales.

Figure 6.17



The relationship between sulphate and organic sulphur isotopic concentrations from both fresh (unweathered) and weathered shale samples from the Jurassic.



Bottrell, pers. comm.) and  $1/4$  atmospheric oxygen (at 23.5‰ with an enrichment factor of -8.7‰ on incorporation; Torran and Harris, 1989 and references therein). Such a ratio is common for sulphates produced by weathering reactions (e.g. Taylor *et al.*, 1984).

### 6.5.3.6 Elemental Sulphur in Shales

The concentration of elemental sulphur was determined for a selection of samples under investigation. Due to the low concentrations of elemental sulphur it was often impractical to determine the sulphur concentrations or to establish the  $\delta^{34}\text{S}$  of the elemental sulphur. Up to 6 aliquots of activated copper wool added to individual samples undergoing soxhlet extraction had to be combined in order to produce enough copper sulphide precipitate (after chromous chloride reprecipitation, see 3.8.3) to determine the  $\delta^{34}\text{S}$  of samples. Thus, a large mass of rock powder was needed (in the order of 300g per sample).

The  $\delta^{34}\text{S}$  for elemental sulphur is shown in Table 6.14. Elemental sulphur has  $\delta^{34}\text{S}$  values between sulphate sulphur and pyrite sulphur for each sample, or in the case of PM11, the  $\delta^{34}\text{S}$  of sulphate sulphur and elemental sulphur are the same. Organic sulphur (kerogen or bitumen) appears to be the isotopically heaviest sulphur bearing phase. The data suggests that the elemental sulphur derives from the oxidation of pyritic sulphur. There is a difference in the isotopic composition in the elemental sulphur and pyrite sulphur of  $\sim 10\text{‰}$ .

It is interesting to compare the data in this study with that of Zaback and Pratt (1991). They studied the isotopic composition of different forms of sulphur in the Miocene Monterey Formation. A similarity between the isotopic composition of sulphate and elemental sulphur was found. The sulphate had more negative  $\delta^{34}\text{S}$  values than the elemental sulphur. The isotopic composition of the sulphate appears to be dependent on the lithofacies (values in the phosphatic lithofacies  $> 15\text{‰}$ , in a siliceous lithofacies  $< -25\text{‰}$  with organic sulphur in the range +5 to +20‰ in both cases). The presence of sulphate and elemental sulphur was put down to biological or abiological processes oxidising pyrite and organic sulphur.

## 6.6 Conclusions

Shale samples are prone to weathering. Visual inspection of the surface of shale prior to collection will not necessarily ensure a fresh sample. Weathering effects samples to depths greater than 1m in well consolidated shale outcrops. Geochemical data obtained from surface samples should be treated with caution.

Weathered shales contain more soluble iron than fresh samples. This has obvious implications for the DOP parameter. Reactive iron values will be falsely high, thus lowering the measured DOP of the sample.

Organic matter is lost from shales during diagenesis by a variety of processes. Weathering also reduces the organic matter content of shales. Rock Eval results show significant loss of S1 yields. Hydrocarbon exploration data is susceptible to error if the analysis is performed on weathered source rocks.

Soluble sulphate and elemental sulphur may be present in apparently fresh shales. They are probably derived from the oxidation of organo-sulphur compounds and pyrite respectively.

The use of  $\delta^{18}\text{O}$  measurements on soluble sulphate enables the source of the oxygen to be established. For the shales studied, the oxygen is comprised of a mixture of atmospheric oxygen and water derived oxygen. The apparent atmospheric oxygen component within the sulphate from the unweathered samples can be ascribed to the oxygen isotopes reaching equilibrium with marine derived pore-waters at elevated temperatures.

## Chapter 7

# General Conclusions and Suggestions for Further Work

This chapter presents a summary of the main findings in this study. Suggestions for future research and the continuation of work initiated by the studies presented in this thesis are also made.

### 7.1 Analytical methods for determining sulphur compounds in shales

A systematic approach to the determination of sulphur compounds in shales has been established. Experimental methodologies have been developed and modified where necessary, to enable both the concentrations and isotopic composition of sulphur compounds in shales to be determined. The analytical methodology to produce stable sulphur isotope data is not consistent in the literature. Further experiments should be undertaken to establish the analytical errors and precision of the individual techniques, leading to the publication of suggested standard methods.

### 7.2 Geochemistry of the Caton Shales

The Caton Shales contain a mixture of authigenic (range 3.1 to 15.3ppm) and detrital (range 0 to 9.99ppm) uranium. The precipitation of authigenic uranium was partly controlled by organic carbon. Preferential absorption of uranium by phosphate produced authigenic uranium enrichment within a horizon containing phosphate pellets.

Palaeoenvironmental conditions at the time of deposition of the Caton Shales were determined using a variety of parameters. A palaeontological study shows marine fauna are present indicating oxic marine conditions. The DOP is low (<0.35) again suggesting oxic conditions. The C/S ratio (mean 0.69) is lower

than expected because there has been significant loss of organic carbon and a small loss of pyrite sulphur.

The organic matter in the Caton Shales is Type III kerogen ( $R_0=0.84$ ). The pristane/phytane ratio and other organic geochemical parameters have been influenced by biodegradation and are of limited use in determining palaeoredox conditions.

### 7.3 Formation of Septarian Concretions

The septarian concretions found at the Lowgill stream section of the Caton Shales have had a complex history. A combined isotopic and geochemical study has enabled the diagenetic evolution to be established. The carbonate cements evolved from a heavy ( $-1.5\text{‰}$  PDB) to a light ( $-14.5\text{‰}$  PDB) oxygen composition and a light ( $-29\text{‰}$  PDB) to a heavy ( $-7\text{‰}$  PDB) carbon composition.

Initial formation of the concretion matrix took place early during diagenesis, close to the sediment water interface. Overpressuring of the sediment resulted in the formation of cracks which were filled by cements derived from a mixture of meteoric water and sulphate reduction. Regional tectonic activity initiated a later generation of cracks which were filled by three distinct generations of carbonate cements. The last cementation phase was accompanied by hydrocarbon migration.

The use of  $K\alpha$  X-ray maps of large areas of diagenetic cement provide a rapid method of obtaining geochemical data. The subsequent use of the electron microprobe over selected areas enables quantitative measurements to be taken to calibrate the X-ray maps. Electron microscopy has been shown to be a powerful tool in the elucidation of diagenetic events.

A detailed organic geochemical study of hydrocarbons within concretions provides useful information about the hydrocarbon migration within an area. By comparing biomarkers characteristic to a shale sequence, migration and biodegradation of organic compounds within source rocks can be established.

## 7.4 Geochemistry of the Jet Rock

There is a positive correlation between reactive iron and organic carbon and DOP is independent of organic carbon indicating significant syngenetic pyrite formation. High TOC concentrations (>8%) are found around the Whalestone concretions where different diagenetic conditions prevailed. Samples with TOC<8% contain framboidal pyrite with  $\delta^{34}\text{S}$  in the range -30 to -22‰. At higher TOC the pyrite is produced with a closed sulphate supply ( $\delta^{34}\text{S}$  -24‰ to -20‰).

The Jet Rock contains Type II kerogen ( $R_0=0.55$  to 0.65). Organo-sulphur compounds are present within the solvent soluble organic matter. These have been identified principally as dibenzothiophenes.

Authigenic uranium is ubiquitous throughout the succession. The Top Jet Dogger is depleted in radioactive minerals relative to the rest of the sediment. Organic carbon correlates positively with authigenic uranium.

The organic matter within the Jet Rock is early mature ( $R_0 = 0.55$  to 0.65) Type II kerogen, dominated by material derived from the resistant tissues of phytoplankton.

The organically bound sulphur ( $\delta^{34}\text{S}$  -14.0‰ to 3.6‰) is isotopically heavier than the framboidal generation of pyrite within the Jet Rock, but isotopically similar to the massive pyrite ( $\delta^{34}\text{S}$  -12.8‰) ascribed to be a later generation of pyrite.

A model is presented to describe the isotopic evolution of sulphur in the Jet Rock. A first generation of framboidal pyrite formed during open system sulphate reduction. Massive pyrite and OSC then formed contemporaneously during closed system sulphate reduction, creating isotopically heavy compounds.

The Cannon Ball Dogger concretions formed early during diagenesis. The pyritic rim of the concretions precipitated later than pyrite contained within the concretions. The differences in the chemical composition of the concretion matrix and host sediment is due to a continuous series of clay mineral reactions.

The anomalous light oxygen isotope data for the Cannon Ball Doggers may be explained by invasive meteoric waters entering the shale sequence. However the chemistry of the concretion/shale pairs would suggest that the concretions have remained closed to diagenetic transformations after the pyrite rim of the concretions was formed. Therefore the principle source of isotopically light oxygen is thought to be from sulphate, trapped organic matter and from the encapsulating silicates undergoing limited transformations.

## 7.5 Weathering of Shales

Shale samples are prone to weathering. Visual inspection of the surface of shale prior to collection will not necessarily ensure a fresh sample. Weathering affects samples to depths greater than 1m in well consolidated shale outcrops. Geochemical data obtained from surface samples should be treated with caution.

Weathered shales contain more soluble iron than fresh samples. This has obvious implications for the DOP parameter. Reactive iron values will be falsely high, thus lowering the measured DOP of the sample.

Organic matter is lost from shales during diagenesis by a variety of processes. Weathering also reduces the organic matter content of shales. Rock Eval results show significant loss of S1 yields. Hydrocarbon exploration data is susceptible to error if the analysis is performed on weathered source rocks.

Soluble sulphate and elemental sulphur may be present in apparently fresh shales. They are probably derived from the oxidation of organo-sulphur compounds and pyrite respectively.

The use of  $\delta^{18}\text{O}$  measurements on soluble sulphate enables the source of the oxygen to be established. For the shales studied, the oxygen is comprised of a mixture of atmospheric oxygen and water derived oxygen. Oxygen values which are isotopically similar to atmospheric oxygen can be produced during equilibration reactions of pore waters at elevated temperatures.

## 7.6 Concluding Remarks

This thesis has provided a further insight into the formation, evolution and weathering of sulphur bearing compounds within shales. A range of samples from the Carboniferous and Jurassic have been analysed by a combination of isotopic, organic and inorganic techniques.

Organic and inorganic parameters have been used to identify the palaeoenvironmental conditions at the time of deposition of the shales. The nature of the organic material within the sediment has also been established. Detailed molecular studies have enabled the identification of organo-sulphur compounds to be made. Isotopic analysis of the sulphur-bearing species has provided an insight into the relative timing of the formation of sulphur compounds. A greater understanding of the effects of weathering has been gained from a combined sulphur and oxygen isotopic analysis of sulphate extracted from shales.

# Appendix

## Statistical methods used

### A.1 Linear Correlation Analysis

The strength of a linear relationship between two variables can be measured by linear correlation analysis. There is a perfect correlation between bivariate data when all the data fall exactly along a straight line. The correlation is said to be positive if  $y$  tends to increase and negative when  $y$  tends to decrease.

### A.2 Least Squares Estimate

The method of least squares enables the line of best fit through bivariate data to be determined. Given that  $\hat{y} = mx + c$  is the equation of a straight line,  $\hat{y}$  is a predicted value of  $y$  corresponding to a particular value of  $x$ . The least squares criterion requires the constants  $m$  and  $c$  to be such that  $\sum (y - \hat{y})^2$  is a minimum. The constants  $m$  and  $c$  can be calculated using

$$m = \frac{\sum (x - \bar{x})(y - \bar{y})}{\sum (x - \bar{x})^2} \quad \text{and} \quad c = \frac{1}{n} (\sum y - m \sum x).$$

### A.3 Coefficient of Linear Regression

The coefficient of linear regression  $r$ , is a measure of the strength of the linear relationship between two variables. A value of  $-1$  indicates a perfect negative correlation and a value of  $+1$  shows a perfect positive correlation. The value of  $r$  is calculated using

$$r = \frac{\sum (x - \bar{x})(y - \bar{y})}{(n - 1)s_x s_y}$$

where  $s_x$  and  $s_y$  are the standard deviations of  $x$  and  $y$ .



The standard deviation ( $s_x$ ) being the positive square root of the variance,

$$s_x = \sqrt{\frac{\sum (x - \bar{x})^2}{n-1}}$$

## A.4 Coefficient of Determination

The coefficient of determination  $r^2$  is an additional measure of the 'goodness of fit' of the linear regression line. The value  $r^2$  is the proportion of the total variation (variance) in  $y$  values explained by variation (variance) in  $x$  values, whereas  $r$  is the proportion of standard deviation of  $y$  values explained by variation (standard deviation) of  $x$  values. The range of  $r^2$  is between 0 and +1. If  $r^2$  is close to 1 then there is a strong relationship between the two data sets. Values close to zero indicate a weak relationship.

## A.5 Significance of Linear Correlation Coefficient

The significance of the value of the linear correlation coefficient ( $r$ ) can be established using a simple hypothesis test. The null hypothesis being "the two variables are linearly unrelated" ( $\rho=0$ ), where  $\rho$  is the linear correlation coefficient for the population. If there is thought to be only a positive or only a negative correlation, the alternative hypothesis should be a one-tail test, otherwise the alternative hypothesis should be a two-tail test. The number of degrees of freedom for the  $r$  statistic is given by  $(n-2)$ . The rejection of the null hypothesis means that there is a linear relationship between the two variables at the given level of significance. Critical values of  $r$  can be found from standard statistical tables e.g. Calcutt and Boddy (1983) and are shown in Table A1.

## A.6 Confidence Limits

It is possible to set limits about an experimentally derived mean ( $\bar{x}$ ) where the population mean ( $\mu$ ) is expected to lie within a given degree of probability. If  $s_x$  is calculated from a small data set, there may be considerable uncertainty

associated with this value as it is a poor estimate of  $\sigma$ , the population standard deviation. Using the parameter  $t$  where,

$$t = \frac{x - \mu}{s},$$

the potential variability can be accounted for. The confidence limits for the mean ( $\bar{x}$ ) of  $n$  measurements is given by

$$\text{confidence limits for } \mu = \frac{\bar{x} \pm ts}{\sqrt{n}}.$$

Using the values in Table A.2, where  $(n-1)$  is the number of degrees of freedom, the confidence limits can be calculated.

Table A.1

	0.1	0.05	0.02	0.01	0.001
v=1	0.9877	0.9969	0.9995	0.9999	1.0000
2	0.9000	0.9500	0.9800	0.9900	0.9990
3	0.8054	0.8783	0.9343	0.9587	0.9912
4	0.7293	0.8114	0.8822	0.9172	0.9741
5	0.6694	0.7545	0.9329	0.8745	0.9507
6	0.6215	0.7067	0.7887	0.8343	0.9249
7	0.5822	0.6664	0.7498	0.7977	0.8982
8	0.5494	0.6319	0.7155	0.7646	0.8721
9	0.5214	0.6021	0.6851	0.7348	0.8471
10	0.4973	0.5760	0.6581	0.7079	0.8233
11	0.4762	0.5529	0.6339	0.6835	0.8010
12	0.4575	0.5324	0.6120	0.6614	0.7800
13	0.4409	0.5139	0.5923	0.6411	0.7603
14	0.4259	0.4973	0.5742	0.6226	0.7420
15	0.4124	0.4821	0.5577	0.6055	0.7246
16	0.4000	0.4683	0.5425	0.5897	0.7084
17	0.3887	0.4555	0.5285	0.5751	0.6932
18	0.3783	0.4438	0.5155	0.5614	0.6787
19	0.3687	0.4329	0.5034	0.5487	0.6652
20	0.3598	0.4227	0.4921	0.5368	0.6524
25	0.3233	0.3809	0.4451	0.4869	0.5974
30	0.2960	0.3494	0.4093	0.4487	0.5541
35	0.2746	0.3246	0.3810	0.4182	0.5189
40	0.2573	0.3044	0.3578	0.3932	0.4896
45	0.2428	0.2875	0.3384	0.3721	0.4648
50	0.2306	0.2732	0.3218	0.3541	0.4433
60	0.2108	0.2500	0.2948	0.3248	0.4078
70	0.1954	0.2319	0.2737	0.3017	0.3799
80	0.1829	0.2172	0.2565	0.2830	0.3568
90	0.1726	0.2050	0.2422	0.2673	0.3375
100	0.1638	0.1946	0.2301	0.2540	0.3211

Values of the linear correlation coefficient for different levels of significance. The number of degrees of freedom  $v$ , is given by  $(n-2)$  where  $n$  is the number of pairs of data. The probabilities (at the head of the columns) refer to the two-tail test of significance and give the probability that  $|r|$  will be greater than tabulated values. For a single-tail test the probabilities should be halved. After Calcutt and Boddy (1983).

Table A.2

Degrees of Freedom	Factor for Confidence Interval				
	80%	90%	95%	99%	99.9%
1	3.08	6.31	12.7	63.7	637
2	1.89	2.92	4.30	9.92	31.6
3	1.64	2.35	3.18	5.84	12.9
4	1.53	2.13	2.78	4.60	8.60
5	1.48	2.02	2.57	4.03	6.86
6	1.44	1.94	2.45	3.71	5.96
7	1.42	1.90	2.36	3.50	5.40
8	1.40	1.86	2.31	3.36	5.04
9	1.38	1.83	2.26	3.25	4.78
10	1.37	1.81	2.23	3.17	4.59
11	1.36	1.80	2.20	3.11	4.44
12	1.36	1.78	2.18	3.06	4.32
13	1.35	1.77	2.16	3.01	4.22
14	1.34	1.76	2.14	2.98	4.14
$\infty$	1.29	1.64	1.96	2.58	3.29

Values of t for various levels of probability.

## References

- Al-Biatty, H.J., 1990. Aspects of carbon-sulphur-iron geochemistry and diagenesis. Ph.D. Thesis, Univ. Leeds, 428 pp. (Unpubl.).
- Abbott, G.D., Lewis, C.A. and Maxwell, J.R., 1985. The kinetics of specific organic reactions in the zone of catagenesis. *Phil. Trans. R. Soc. Lond.*, 315: 107-122.
- Alperin, M.J., Reeburgh, W.S. and Whiticar, M.J., 1988. Carbon and hydrogen isotope fractionations resulting from anaerobic methane oxidation. *Global Biogeochem. Cycles*, 2: 279-288.
- Adams, J.A.S. and Weaver, C.E., 1958. Thorium to uranium ratios as indicators of sedimentary processes; example of the concept of geochemical facies. *Bull. Am. Ass. Petrol. Geol.*, 42: 387-430.
- Adams, J.A.S., Osmond, J.K. and Rodgers, J.J.W., 1959. The geochemistry of uranium and thorium. *Phys. Chem. Earth*, 3: 299-328.
- Anderton, R., Bridges, P.H., Leeder, M.R. and Sellwood, B.W., 1985. A dynamic stratigraphy of the British Isles. George Allen and Unwin, London, 301 pp.
- Aplin, A.C. and Macquaker, J.H.S., 1993. C-S-Fe geochemistry of some modern and ancient anoxic marine muds and mudstones. *Phil. Trans. R. Soc. Lond.*, 344: 89-100.
- Aplin, A.C., Bishop, A.N., Clayton, C.J., Kearsley, A.T., Mossman, J.R., Patience, R.L., Rees, A.W.G. and Rowland, S.J., 1992. A lamina-scale geochemical and sedimentological study of sediments from the Peru Margin (site 680, ODP leg 112). In: Summerhayes, C.P., Prell, W.L. and Emeis, K.C. (eds), *Upwelling Systems: Evolution Since the Early Miocene*. Geological Society Special Publication, 64, pp. 131-149.
- Arnosti, C. and Muller, P.J., 1987. Pyrolysis-GC characterization of whole rock and kerogen-concentrate samples of immature Jurassic source rocks from NW Germany. *Org. Geochem.*, 13: 505-513.
- Arpino, P.J., Ignatiadis, I. and De Rycke, G., 1987. Sulphur-containing polynuclear aromatic hydrocarbons from petroleum: Examination of their possible statistical formation in sediments. *J. Chrom.*, 390: 329-348.
- Astin, T.R., 1986. Septarian crack formation in carbonate concretions from shales and mudstones. *Clay Minerals*, 21: 617-631.
- Astin, T.R. and Scotchman, I.C., 1988. The diagenetic history of some septarian concretions from the Kimmeridge Clay, England. *Sedimentology*, 35: 349-368.
- Atkins, P.W., 1986. *Physical Chemistry*. Oxford Univ. Press, Oxford, 857 pp.

- Aizenschtat, Z., Stoler, A., Cohen, Y. and Nielsen, H., 1983. The geochemical sulphur enrichment of recent organic matter by polysulphides in the Solar Lake. In: Bjorøy, M. (ed), *Advances in Organic Geochemistry 1981*. Wiley, Chichester, pp. 279-288.
- Bada, J.L. and Lee, C., 1977. Decomposition and alteration of organic compounds dissolved in seawater. *Mar. Chem.*, 5: 523-534.
- Baldwin, B. and Butler, C.O., 1985. Compaction Curves. *Bull. Am. Ass. Petrol. Geol.*, 69: 622-626.
- Baskin, D.K. and Peters, K.E., 1992. Early generation characteristics of a sulphur-rich Monterey kerogen. *Am. Ass. Petrol. Geol.*, 76: 1-13.
- Baumgartner, L.P. and Rumble, D., 1988. Transport of stable isotopes: I: Development of a kinetic continuum theory for stable isotope transport. *Contrib. Mineral. Petrol.*, 94: 417-430.
- Behar, F. and Vandembroucke, M., 1986. Représentation chimique de la structure des kérogènes et des asphaltènes en fonction de leur origine et de leur degré d'évolution. *Rev. Inst. Fr. Pétr.*, 41: 173-188.
- Behar, F. and Vandembroucke, M., 1988. Characterisation and quantification of saturates trapped inside kerogen: Implications for pyrolysate composition. *Org. Geochem.*, 13: 927-938.
- Bein, A. and Nielsen, H., 1988. Sulphur diagenesis in freshwater lignites (Hula Basin, Israel): Implications for S-C relationships in organic sediments. *J. Geol. Soc. Lond.*, 145: 133-136.
- Bein, A., Almogi-Labin, A. and Sass, E., 1990. Sulfur sinks and organic carbon relationships in Cretaceous organic rich carbonates: Implications for evaluation of oxygen-poor depositional environments. *Am. J. Sci.*, 290: 882-911.
- Benzel, W.M. and Graf, D.L., 1984. Studies of smectite membrane behaviour: Importance of layer thickness and fabric in experiments at 20°C. *Geochim. Cosmochim. Acta*, 48: 1169-1188.
- Berner, R.A., 1964. Distribution and diagenesis of sulfur in some sediments from the Gulf of California. *Mar. Geol.*, 1: 117-140.
- Berner, R.A., 1967. Thermodynamic stability of sedimentary iron sulfides. *Am. J. Sci.*, 265: 773-785.
- Berner, R.A., 1968. Rate of concretion growth. *Geochim. Cosmochim. Acta*, 32: 447-483.
- Berner, R.A., 1970. Sedimentary pyrite formation. *Am. J. Sci.*, 268: 1-23.
- Berner, R.A., 1972. Sulphate reduction, pyrite formation and the oceanic sulphur budget. In: Dyrssen, D. and Jagner, D. (eds), *The Changing*

Chemistry of the Oceans. Almgvist and Wiksell, Nobel Symposium 20, pp. 347-361.

- Berner, R.A., 1980. Early Diagenesis: A Theoretical Approach. Princeton Univ. Press, Princeton, 241 pp.
- Berner, R.A., 1982. Burial of organic carbon and pyrite sulfur in the modern ocean: Its geochemical and environmental significance. *Am. J. Sci.*, 282: 451-473.
- Berner, R.A., 1984. Sedimentary pyrite formation: An update. *Geochim. Cosmochim. Acta*, 48: 605-615.
- Berner, R.A. and Raiswell, R., 1983. Burial of organic carbon and pyrite sulfur in sediments over Phanerozoic time: A new theory. *Geochim. Cosmochim. Acta*, 47: 855-862.
- Berner, R.A. and Raiswell, R., 1984. C/S method for distinguishing freshwater from marine sedimentary rocks. *Geology*, 12: 365-368.
- Berner, R.A. and Westrich, J.T., 1985. Bioturbation and the early diagenesis of carbon and sulfur. *Am. J. Sci.*, 285: 193-206.
- Bisat, W.S., 1934. *Anthracoceras* from the E2 zone of the Namurian. *Trans. Leeds Geol. Ass.*, 5: 112-117.
- Bloxham, T.W. and Thomas, R.L., 1969. Palaeontological and geochemical facies in the *Gastrioceras subcrenatum* Marine Band and associated rocks from the north crop of the South Wales coalfield. *Quat. J. Geol. Soc. Lond.*, 124: 239-281.
- Blumer, M., Mullin, M.M. and Thomas, D.W., 1964. Pristane in the marine environment. *Helgol. Wiss. Meeresunters*, 10: 187-201.
- Boles, J.R., Landis, C.A. and Dale, P., 1985. The Moeraki boulders-anatomy of some septarian concretions. *J. Sed. Petrol.*, 55: 398-406.
- Booker, K.M., 1926. The Carboniferous sequence of the Craven Lowlands south of the reef limestones of Cracoe. *Proc. Yorks. Geol. Soc.*, 20: 411-438.
- Boreham, C.J. and Powell, T.G., 1987. Sources and preservation of organic matter in the Cretaceous Toolebuc Formation, Eastern Australia. *Org. Geochem.*, 11: 433-449.
- Bott, M.P.H., 1987. Subsidence mechanisms of Carboniferous basins in Northern England. In: Miller, J., Adams, A.E. and Wright, V.P. (eds), *European Dinantian Environments*. Wiley, Chichester, pp. 21-31.
- Bottrell, S.H. and Miller, M.F., 1989. Analysis of reduced sulfur species in inclusion fluids. *Economic Geology*, 84: 940-945.

- Bottrell, S.H. and Moore, S.A., 1991. Carbon isotope analysis of catalyst deposits produced during the co-reforming of petroleum and coal-derived naphthas. *Fuel*, 70: 1111-1111.
- Bottrell, S.H. and Raiswell, R., 1989. Primary versus diagenetic origin of Blue Lias rhythms (Dorset, UK): Evidence from sulphur geochemistry. *Terra Nova*, 1: 451-456.
- Bottrell, S.H., Louie, P.K.K., Bartle, K.D., Taylor, N., Wallace, S., Kemp, W. and Steedman, W., 1990. Differentiation of forward and back reactions during co-processing of coal and petroleum by isotope mass balance analysis. *Fuel*, 69: 1332-1333.
- Bottrell, S. H., Banks, D., Bird, D. and Raiswell, R., 1991. A simple method for field determination of some reduced sulphur species in soil gases. *Environmental Technology*, 12: 393-398.
- Boudou, J-P., Pelet, R. and Letolle, R., 1984. A model for the diagenetic evolution of coaly sedimentary organic matter. *Geochim. Cosmochim. Acta*, 48: 1357-1362.
- Boudreau, B.P. and Westrich, J.T., 1984. The dependence of bacterial sulphate reduction on sulphate concentration in marine sediments. *Geochim. Cosmochim. Acta*, 48: 2503-2516.
- Bradley, C. and Schiller, D.J., 1986. Determination of sulfur compound distribution in petroleum by gas chromatography with a flame photometric detector. *Analytical Chemistry*, 58: 3017-3021.
- Brassell, S.C., Comet, P.A., Eglinton, G., Isaacson, P.J., McEvoy, J., Maxwell, J.R., Thomson, I.D., Tibbetts, P.J.C. and Volkman, J.K., 1980. The origin and fate of lipids in the Japan Trench. In: Douglas, A.G. and Maxwell, J.R. (eds), *Advances in Organic Geochemistry 1979*. Pergamon Press, Oxford, pp. 375-393.
- Brassell, S.C., Lewis, C.A., de Leeuw, J.W., de Lange, F. and Sinninghe Damsté, J.S., 1986. Isoprenoid thiophenes: Novel products of sediment diagenesis? *Nature*, 320: 160-162.
- Bray, E.E. and Evans, E.D., 1961. Distribution of n-paraffins as a clue to recognition of source beds. *Geochim. Cosmochim. Acta*, 22: 2-15.
- Briggs, D.E.G., Bottrell, S.H. and Raiswell, R., 1991. Pyritization of soft-bodied fossils: Beecher's Trilobite Bed, Upper Ordovician, New York State. *Geology*, 19: 1221-1224.
- Brooks, P.W., Maxwell, J.R. and Patience, R.L., 1978. Stereochemical relationships between phytol and phytanic acid, dihydrophytol and C<sub>18</sub> ketone in recent sediments. *Geochim. Cosmochim. Acta*, 42: 1175-1180.
- Burst, J.F., 1959. Clay mineral reactions during diagenesis. *Proc. 6th Nat. conf. Clays and Clay Minerals*. Pergamon, Oxford, pp. 327-331.



- Calcutt, R. and Boddy, R., 1983. *Statistics for Analytical Chemists*. Chapman and Hall, New York, 235 pp.
- Calvert, S.E. and Karlin, R.E., 1991. Relationships between sulphur, organic carbon and iron in the modern sediments of the Black Sea. *Geochim. Cosmochim. Acta*, 55: 2483-2490.
- Canfield, D.E., 1989a. Reactive Iron in marine sediments. *Geochim. Cosmochim. Acta*, 53: 619-632.
- Canfield, D.E., 1989b. Sulfate reduction and oxic respiration in marine sediments: Implications for organic carbon preservation in euxinic environments. *Deep-Sea Research*, 36: 121-138.
- Canfield, D.E. and Raiswell, R., 1991a. Pyrite formation and fossil preservation. In: Allison, P.A. and Briggs, D.E.G. (eds), *Taphonomy: Releasing the Data Locked in the Fossil Record*. Plenum, New York, pp. 337-387.
- Canfield, D.E. and Raiswell, R., 1991b. Carbonate precipitation and dissolution: Its relevance to fossil preservation. In: Allison, P.A. and Briggs, D.E.G. (eds), *Taphonomy: Releasing the Data Locked in the Fossil Record*. Plenum, New York, pp. 411-453.
- Canfield, D.E., Raiswell, R., Westrich, J.T., Reaves, C.M. and Berner, R.A., 1986. The use of chromium reduction in the analysis of reduced inorganic sulfur in sediments and shales. *Chemical Geology*, 54: 149-155.
- Canfield, D.E., Raiswell, R. and Bottrell, S.H., 1992. The reactivity of sedimentary iron minerals toward sulfide. *Am. J. Sci.*, 292: 659-683.
- Casagrande, D. and Siefert, K., 1977. Origins of sulfur in coal: Importance of the ester sulfate content of peat. *Science*, 19: 675-676.
- Casagrande, D., Idowu, G., Friedman, A., Rickert, P., Siefert, K. and Schlenz, D., 1979. H<sub>2</sub>S in coal precursors: Origins of organic sulphur in coal. *Nature*, 282: 599-600.
- Chambers, L.A. and Trudinger, P.A., 1978. Microbiological fractionation of stable sulfur isotopes: A review and critique. *J. Geomicrobiology*, 1: 249-293.
- Chambers, L.A., Trudinger, P.A., Smith, J.W. and Burns, M.S., 1976. A possible boundary condition in bacterial sulfur isotope fractionation. *Geochim. Cosmochim. Acta*, 40: 1191-1194.
- Chanton, J.P., Martens, C.S., Paull, C.K. and Coston, J.A., 1993. Sulfur isotope and porewater geochemistry of Florida escarpment seep sediments. *Geochim. Cosmochim. Acta*, 57: 1253-1266.
- Christensen, P.A., Hamnett, A., Hillman, A.R., Swann, M.J. and Higgins, S.J., 1992. Charge conduction in polybithiophene: An in situ Fourier-transform infrared study. *J. Chem. Soc. Faraday Trans.*, 88(4): 595-604.

- Claypool, G.E. and Kaplan, I.R., 1974. The origin and distribution of methane in marine sediments. In: Kaplan I.R. (ed), *Natural Gases in Marine Sediments*. Plenum Press, New York, pp. 99-139.
- Claypool, G.E., Holser, W.T., Kaplan, I.R., Sakai, H. and Zak, I., 1980. The age curves of sulfur and oxygen isotopes in marine sulfate and their mutual interpretation. *Chem. Geol.*, 28: 199-260.
- Clayton, C., 1991. Carbon isotope fractionation during natural gas generation from kerogen. *Mar. Petrol. Geol.*, 8: 233-240.
- Clayton, R.N., Friedman, I., Graf, D.L., Mayeda, T.K., Meents, W.F. and Shimp, N.F., 1966. The origin of saline formation waters I. Isotopic composition. *J. Geophys. Res.*, 71: 3869-3882.
- Coleman, M.L., 1980. Corrections for mass spectrometry analysis of sulphur dioxide. *Isotope Geology Unit, Stable Isotope Report*: 45.
- Coleman, M.L. and Raiswell, R., 1981. Carbon, oxygen and sulphur isotope variations in concretions from the Upper Lias of NE England. *Geochim. Cosmochim. Acta*, 45: 329-340.
- Coleman, M.L. and Raiswell, R., 1993. Microbial mineralization of organic matter: Mechanisms of self-organisation and inferred rates of precipitation of diagenetic minerals. *Phil. Trans. R. Soc. Lond.*, 344: 69-87.
- Coleman, M.L., Hedrick, D.B., Lovley, D.R., White, D.C. and Pye, K., 1993. Reduction of Fe(III) in sediments by sulphate-reducing bacteria. *Nature*, 361: 436-438.
- Collinson, J.D., 1988. Controls on Namurian sedimentation in the Central Province basins of Northern England. In: Besley, B.M. and Kelling, G. (eds), *Sedimentation in a Synorogenic Basin Complex: The Upper Carboniferous of Northwest Europe*. Blackie, London and Glasgow, pp. 85-101.
- Cope, J.C.W., 1974. New information on the Kimmeridge Clay of Yorkshire. *Proc. Geol. Ass.*, 85: 211-221.
- Cope, M.J., 1980. Physical and chemical properties of coalified and charcoalified phytoplasts from some British Mesozoic sediments; an organic geochemical approach to palaeobotany. In: Douglas, A.G. and Maxwell, J.R. (eds), *Advances in Organic Geochemistry 1979*. Pergamon Press, Oxford, pp. 663-677.
- Cotton, F.A. and Wilkinson, G., 1988. *Advanced Inorganic Chemistry*. Wiley-Interscience, New York, 1455 pp.
- Coveney, R.M.Jr., Watney, W.L. and Maples, C.G., 1991. Contrasting depositional models for Pennsylvanian black shale discerned from molybdenum abundances. *Geology*, 19: 147-150.

- Craig, H., 1957. Isotopic standards for carbon and oxygen isotope correction factors for mass-spectrometric analysis of carbon dioxide. *Geochim. Cosmochim. Acta*, 12: 133-149.
- Craig, H., 1965. The measurement of oxygen isotope paleotemperatures. *Proc. Conference on Stable Isotopes in Oceanographic Studies and Paleotemperatures*, pp. 3-24.
- Creaney, S. and Passey, Q.R., 1993. Recurring patterns of total organic carbon and source rock quality within a sequence stratigraphic framework. *Am. Assoc. Petrol. Geol.*, 77: 386-401.
- Curtis, C.D., 1977. Sedimentary geochemistry: Environment and processes dominated by involvement of an aqueous phase. *Phil. Trans. R. Soc. Lond.*, 286: 353-372.
- Curtis, C.D., 1980. Diagenetic alteration in black shales. *J. Geol. Soc. Lond.*, 137: 189-194.
- Curtis, C.D., 1983. Link between aluminium mobility and destruction of secondary porosity. *Am. Ass. Petrol. Geol.*, 67: 380-393.
- Curtis, C.D., 1987. Inorganic geochemistry and petroleum exploration. *Adv. Petrol. Geochem.*, 2: 91-139.
- Curtis, C.D., Coleman, M.L. and Love, L.G., 1986. Pore water evolution during sediment burial from isotopic and mineral chemistry of calcite, dolomite and siderite concretions. *Geochim. Cosmochim. Acta*, 50: 2321-2334.
- Dacey, J.W.H., King, G.M. and Wakeham, S.G., 1987. Factors controlling emission of dimethylsulphide from salt marshes. *Nature*, 330: 641-645.
- Dansgaard, W., 1964. Stable isotopes in precipitation. *Tellus*, 16: 463-468.
- de Graaf, W., Sinninghe Damsté, J.S. and de Leeuw, J.W., 1992. Laboratory simulation of natural sulphurization: I. Formation of monomeric and oligomeric isoprenoid polysulphides by low temperature reactions of inorganic polysulphides with phytol and phytadienes. *Geochim. Cosmochim. Acta*, 56: 4321-4328.
- de Haan, S.B., 1991. A review of the rate of pyrite oxidation in aqueous systems at low temperatures. *Earth Sci. Rev.*, 31: 1-10.
- de Leeuw, J.W. and Baas, M., 1986. Early stage diagenesis of steroids. In: Johns, R.B. (ed), *Biological Markers in the Sedimentary Record*. Elsevier, Amsterdam, pp. 101-123.
- Deer, W.A., Howie, R.A. and Zussman, J. 1985. *An Introduction to the Rock Forming Minerals*. Longman, Harlow, 528 pp.
- Deines, P., 1980. The isotopic composition of reduced organic carbon. In: Fritz, P. and Fontes, J.Ch., (eds), *Handbook of Environmental Isotope Geochemistry*. Elsevier, Amsterdam, 1A, pp. 329-406.

- Derenne, S., Largeau, C., Casadevall, E., Teglaar, E.W. and de Leeuw, J.W., 1988. Relationships between algal coals and resistant cell wall biopolymers of extant algae as revealed by Py-GC-MS. *Fuel Process. Tech.*, 20: 93-101.
- Derenne, S., Largeau, C., Casadevall, E., Berkaloff, C. and Rousseau, B., 1991. Chemical evidence of kerogen formation in source rocks and oil shales via selective preservation of thin resistant outer wall of microalgae: Origin of ultramarinae. *Geochim. Cosmochim. Acta*, 55: 1041-1050.
- Didyk, B.M., Simoneit, B.R.T., Brassell, S.C. and Eglinton, G., 1978. Organic geochemical indicators of palaeoenvironmental conditions of sedimentation. *Nature*, 272: 216-222.
- Dill, H. and Nielsen, H., 1986. Carbon-sulphur-iron-variations and sulphur isotope patterns of Silurian graptolite shales. *Sedimentology*, 33: 745-755.
- Dinur, D., Spiro, B. and Aizenshtat, Z., 1980. The distribution and isotopic composition of sulfur in organic-rich sedimentary rocks. *Chemical Geology*, 31: 37-51.
- Dowuona, G.N., Mermut, A.R. and Krouse, H.R., 1993. Stable isotope geochemistry of sulphate in relation to hydrogeology in Southern Saskatchewan, Canada. *Applied Geochemistry*, 8: 255-263.
- Drushel, H.V., 1969. Sulfur compound type distributions in petroleum using an in-line reactor or pyrolysis combined with gas chromatography and a microcoulometric sulfur detector. *Analytical Chemistry*, 41: 569-576.
- Durand, B., 1980. Sedimentary organic matter and kerogen. Definition and quantitative importance of kerogen. In: Durand, B. (ed), *Kerogen*. Technip, Paris, pp. 13-34.
- Durand, B. and Monin, J.C., 1980. Elemental analysis of kerogens (C, H, O, N, S, Fe). In: Durand, B. (ed), *Kerogen*. Technip, Paris, pp. 113-142.
- Durand, B., Espitalié, J., Nicaise, G. and Combaz, A., 1972. Etude de la matière organique insoluble des argiles du Toarcien du Bassin de Paris. *Rev. Inst. Fr. Pétr.*, 27: 865-884.
- Earp, J.R., Poole, E.G. and Whiteman, A.J., 1961. *Geology of the country around Clitheroe and Nelson*. HMSO, London, 346 pp.
- Eglinton, T.I., Sinninghe Damsté, J.S., Kohnen, M.E.L. and de Leeuw, J.W., 1990. Rapid estimation of the organic sulphur content of kerogens, coals and asphaltenes by pyrolysis-gas chromatography. *Fuel*, 69: 1394-1404.
- Elsgaard, L. and Jørgensen, B.B., 1992. Anoxic transformations of radiolabelled hydrogen sulfide in marine and freshwater sediments. *Geochim. Cosmochim. Acta*, 56: 2425-2435.

- Evans, I.J., 1989. Geochemical fluxes during shale diagenesis, an example from the Ordovician of Morocco. In: Miles, T. (ed), *Water-Rock Interaction*. Balkema, Rotterdam, pp. 219-222.
- Farrimond, P., Eglinton, G., Brassell, S.C. and Jenkyns, H.C., 1989. Toarcian anoxic event in Europe: An organic geochemical study. *Mar. Petrol. Geol.*, 6: 136-147.
- Feistner, K.W.A., 1989. Petrographic examination and reinterpretation of concretionary carbonate horizons from the Kimmeridge Clay, Dorset. *J. Geol. Soc. Lond.*, 146: 345-350.
- Ferdelman, T.G., Church T.M. and Luther III, G.W., 1991. Sulfur enrichment of humic substances in a Delaware salt marsh core. *Geochim. Cosmochim. Acta*, 55: 979-988.
- Fessenden, R.J. and Fessenden, J.S., 1986. *Organic Chemistry*. Brooks/Cole Publishing, Monterey, California, 1129 pp.
- Feux, A.N., 1977. The use of stable carbon isotopes in hydrocarbon exploration. *J. Geochem. Exploration*, 7:155-188.
- Fisher, I. St.J., 1986. Pyrite formation in bioturbated clays from the Jurassic of Britain. *Geochim. Cosmochim. Acta*, 50: 517-523.
- Fisher, I. St.J. and Hudson, J.D., 1987. Pyrite formation in Jurassic shales of contrasting biofacies. In: Brooks, J. and Fleet, A.J. (eds), *Marine Petroleum Source Rocks*. Geological Society Special Publication, 26: 69-78.
- Forbes, P.L., Ungerer, P.M., Kuhfuss, A.B., Rils, F. and Eggen, S., 1991. Compositional modelling of petroleum generation and expulsion: Trial application to a local mass balance in the Smorbukk Sor Field, Haltenbanken Area, Norway. *Bull. Am. Ass. Petrol. Geol.*, 75: 873-893.
- François, R., 1987. A study of sulphur enrichment in the humic fraction of marine sediments during early diagenesis. *Geochim. Cosmochim. Acta*, 51: 17-27.
- Franks, P.C., 1969. Nature, origin and significance of cone-in-cone structures in the Kiowa formation (early Cretaceous), North Central Kansas. *J. Sed. Petrol.*, 39: 1438-1454.
- Fredorak, P.M., 1990. Microbial metabolism of organosulfur compounds in petroleum. In: Orr, W.L. and White C.M. (eds), *Geochemistry of Sulphur in Fossil Fuels*. American Chemical Society, Washington D.C., pp. 93-112.
- Fry, B., Cox, J., Gest, H. and Hayes, J.M., 1986. Discrimination between 32-S and 34-S during bacterial metabolism of inorganic sulfur compounds. *J. Bact.*, 165: 328-330.
- Fukushima, K., Yasukawa, M., Muto, N., Uemura, H. and Ishiwatari, R., 1992. Formation of C<sub>20</sub> isoprenoid thiophenes in modern sediments. *Org. Geochem.*, 18: 83-91.

- Gad, M.A., Catt, J.A. and le Riche, H.H., 1969. Geochemistry of the Whitbian (Upper Lias) sediments of the Yorkshire coast. *Proc. Yorks. Geol. Soc.*, 37(1): 105-139.
- Gaffney, J.S., Premuzic, E.T. and Manowitz, B., 1980. Note on the usefulness of sulfur isotope ratios in crude oil correlations. *Geochim. Cosmochim. Acta*, 44: 135-139.
- Garrels, R.M. and Lerman, A., 1981. Phanerozoic cycles of sedimentary carbon and sulfur. *Proc. Nat. Acad. Sci. USA*, 78: 4652-4656.
- Gautier, D.L. and Claypool, G.E., 1984. Interpretation of methanic diagenesis in ancient sediments by analogy with processes in modern diagenetic environments. In: McDonald, D.A. and Surdam, R.C. (eds), *Clastic Diagenesis*. *Am. Ass. Petrol. Geol. Mem.*, 37: 434 pp.
- Gawthorpe, R.L., 1986. Sedimentation during carbonate ramp-to-slope evolution in a tectonically active area: Bowland Basin (Dinantian), Northern England. *Sedimentology*, 33: 185-206.
- Gawthorpe, R. L., 1987a. Burial dolomitization and porosity development in a mixed carbonate-clastic sequence: An example from the Bowland Basin, Northern England. *Sedimentology*, 34: 533-558.
- Gawthorpe, R.L., 1987b. Tectono-sedimentary evolution of the Bowland Basin, Northern England, during the Dinantian. *J. Geol. Soc. Lond.*, 144: 59-71.
- Gawthorpe, R.L. and Clemmey, H., 1985. Geometry of submarine slides in the Bowland Basin (Dinantian) and their relation to debris flows. *J. Geol. Soc. Lond.*, 142: 555-565.
- Gawthorpe, R.L., Gutteridge, P. and Leeder, M.R., 1989. Late Devonian and Dinantian basin evolution in Northern England and North Wales. In: Arthurton, R. and Gutteridge, P. (eds), *The Role of Tectonics in Devonian and Carboniferous Sedimentation in the British Isles*. *Yorks. Geol. Soc.*, Wigley, London, pp. 1-23.
- George, G.M. and Gorbaty, M.L., 1989. Sulphur K-edge X-ray absorption spectroscopy of petroleum asphaltenes and model compounds. *J. Am. Chem. Soc.*, 111: 3182-3186.
- Goldhaber, M.B., 1983. Experimental study of metastable sulfur oxyanion formation during pyrite oxidation at pH 6-9 and 30°C. *Am. J. Sci.*, 283: 193-217.
- Goldhaber, M.B. and Kaplan, I.R., 1974. The sulfur cycle. In: Goldberg, E.D. (ed), *The Sea*. Wiley-Interscience, New York, 5, pp. 569-655.
- Goldhaber, M.B. and Kaplan, I.R., 1980. Mechanism of sulphur incorporation and isotope fractionation during early diagenesis in sediments of the Gulf of California. *Mar. Chem.*, 9: 95-143.

- Goldhaber, M.B., Aller, R.C., Cochran, J.K., Rosenfeld, J.K., Martens, C.S. and Berner, R.A., 1977. Sulfate reduction, diffusion and bioturbation in Long Island Sound sediments: Report from the FOAM group. *Am. J. Sci.*, 277: 193-237.
- Goni, M. and Hedges, J.I., 1992. Lignin dimers: Structures, distribution and potential geochemical applications. *Geochem. Cosmochim. Acta*, 56: 4025-4043.
- Gossens, H., de Leeuw, J.W., Schenck, P.A. and Brassell, C.A., 1984. Tocopherols as likely precursors of pristane in ancient sediments and crude oils. *Nature*, 312: 440-442.
- Gough, M.A. and Rowland, S.J., 1990. Characterization of unresolved complex mixtures of hydrocarbons in petroleum. *Nature*, 344: 648-650.
- Gransch, J.A. and Posthuma, J., 1974. On the origin of sulphur in crudes. In: Tissot, B. and Bienner, F. (eds), *Advances in Organic Geochemistry 1973*. Technip., Paris, pp. 729-739.
- Grantham, P.J. and Wakefield, LL., 1988. Variations in the sterane carbon number distributions of marine source rock derived crude oils through geological time. *Org. Geochem.*, 12: 61-73.
- Greenwood, N.N. and Earnshaw, A., 1984. *Chemistry of the Elements*. Pergamon Press, Oxford, 1542 pp.
- Guadalupe, M.F.M., Castello Branco, V.A. and Schmid, J.C., 1991. Isolation of sulphides in oils. *Org. Geochem.*, 17: 355-361.
- Hackley, K.C. and Anderson, T.F., 1986. Sulfur isotopic variations in low-sulfur coals from the Rocky Mountain region. *Geochim. Cosmochim. Acta*, 50: 1703-1713.
- Hallam, A., 1966. Siderite and calcite-bearing concretionary nodules in the Lias of Yorkshire. *Geol. Mag.*, 104: 222-227.
- Hallam, A., 1967. The depth significance of shales with bituminous laminae. *Marine Geol.*, 5: 481-493.
- Hallberg, R.O., 1985. Computer simulation of sulfur isotope fractionation in a closed sulfuretum. *J. Geomicrobiology*, 4: 131-152.
- Hancock, N.J. and Taylor, A.M., 1978. Clay mineral diagenesis and oil migration in the Middle Jurassic Brent Sand Formation. *J. Geol. Soc. Lond.*, 135: 69-72.
- Harrison, A.G. and Thode, H.G., 1958. Mechanism of bacterial reduction of sulphate from isotope fractionation studies. *Trans. Faraday Soc.*, 54: 84-92.
- Hartman, B. and Hammond, D.E., 1981. The use of carbon and sulfur isotopes as correlation parameters for the source and identification of beach tar in

- the Southern Californian borderland. *Geochim. Cosmochim. Acta*, 45: 309-319.
- Hendy, C.H., 1971. The isotopic geochemistry of speleothems-I. The calculation of the effects of different modes of formation on the isotopic composition of speleothems and their applicability as paleoclimatic indicators. *Geochim. Cosmochim. Acta*, 35: 801-824.
- Henrichs, S.M. and Reeburgh, W.S., 1987. Anaerobic mineralization of marine sediment organic matter: Rates and the role of anaerobic processes in the oceanic carbon economy. *J. Geomicrobiology*, 5: 191-237.
- Hesselbo, S.P. and Palmer, T.J., 1992. Reworked early diagenetic concretions and the bioerosional origin of a regional discontinuity within British Jurassic marine mudstones. *Sedimentology*, 39: 1045-1065.
- Hirner, A.V. and Robinson, B.W., 1989. Stable isotope geochemistry of crude oils and of possible source rocks from New Zealand-2: Sulfur. *App. Geochem.*, 4: 121-130.
- Hirner, A.V., Graf, W., Treibs, R., Melzer, A.N. and Hahn-Weinheimer, P., 1984. Stable sulfur and nitrogen isotopic compositions of crude oil fractions from Southern Germany. *Geochim. Cosmochim. Acta*, 48: 2179-2186.
- Ho, T.Y., Rogers, M.A., Drushel, H.V. and Koch, C.B., 1974. Evolution of sulphur compounds in crude oils. *Bull. Am. Ass. Petrol. Geol.*, 58: 2238-2348.
- Ho, E.S., Meyers, P.A. and Mauk, J.L., 1989. Organic geochemical study of mineralization in the Keweenawan Nonesuch Formation at White Pine, Michigan. *Org. Geochem.*, 16: 229-234.
- Hoefs, J., 1980. *Stable Isotope Geochemistry* (2nd Edition). Springer-Verlag, New York. 241 pp.
- Holmes, J. and Bisat, W.S., 1925. Goniatite zones in the Keasden Beck area. *Naturalist*, 307-312.
- Holt, B.D., Kumar, R. and Cunningham, P.T., 1981. Oxygen-18 study of the aqueous phase oxidation of sulphur dioxide. *Atmospheric Environment*, 15: 557-566.
- Holt, B.D., Cunningham, P.T., Ehgelkemeir, A.G., Graczyk, D.G. and Kumar, R., 1983. Oxygen-18 study of non aqueous-phase oxidation of sulphur dioxide. *Atmospheric Environment*, 17: 625-632.
- Hood, A., Gutjahr, C.C.M. and Heacock, R.L., 1975. Organic metamorphism and the generation of petroleum. *Bull. Am. Ass. Petrol. Geol.*, 59: 986-996.
- Howarth, M.K., 1962. The Jet Rock series and the Alum Shale series of the Yorkshire coast. *Proc. Yorks. Geol. Soc.*, 33(4): 381-422.
- Howarth, R.W. and Jørgensen, B.B., 1984. Formation of  $^{35}\text{S}$ -labelled elemental sulfur and pyrite in coastal marine sediments (Limfjorden and Kysing



- Fjord, Denmark) during short-term  $^{35}\text{S-SO}_4^{-2}$  reduction measurements. *Geochim. Cosmochim. Acta*, 48: 1807-1818.
- Huang, W. and Meinschein, W.G., 1979. Sterols as ecological indicators. *Geochim. Cosmochim. Acta*, 43: 739-745.
- Huc, A.Y., 1980. Origin and formation of organic matter in recent sediments and its relation to kerogen. In: Durand, B. (ed), *Kerogen - Insoluble Organic Matter from Sedimentary Rocks*. Technip, Paris, pp. 445-472.
- Hudson, J.D., 1978. Concretions, isotopes and the diagenetic history of the Oxford Clay (Jurassic) of Central England. *Sedimentology*, 25: 339-370.
- Hudson, R.G.S., 1944. The faunal succession in the *Ct. nitidus* zone in the Mid Pennines. *Leeds Lit. Phil. Soc.*, 4: 233-242.
- Hudson, R.G.S., 1945. The goniatite zones of the Namurian. *Geol. Mag.*, 82: 1-9.
- Husain, S.A. and Krouse, H.R., 1978. Sulphur isotope effects during the reaction of sulphate with hydrogen sulphide. In: Robinson, B.W. (ed), *Stable Isotopes in the Earth Sciences*. Bull. Dept. Sci. Indus. Res., 220: 207-210.
- IEA Coal Research, 1989. *Reviews in coal science: The problems of sulphur*. Butterworths, London, 354 pp.
- Irwin, H., Curtis, C. and Coleman, M., 1977. Isotopic evidence for source of diagenetic carbonates formed during burial of organic-rich sediments. *Nature*, 269: 209-213.
- Ishiwatari, R. and Fukushima, K., 1979. Generation of unsaturated aromatic hydrocarbons by thermal alteration of a young kerogen. *Geochim. Cosmochim. Acta*, 43: 1343-1349.
- Iversen, N. and Jørgensen, B.B., 1985. Anaerobic methane oxidation rates at the sulphate-methane transition in marine sediments from Kattegat and Skagerrak (Denmark). *Limnol. Oceanogr.*, 30: 944-955.
- Jackson, M.J. and Raiswell, R., 1991. Sedimentology and carbon-sulphur geochemistry of the Velkerri Formation, a mid-Proterozoic potential oil source in Northern Australia. *Precambrian Research*, 54: 81-108.
- Jasper, J.P. and Gagosian, R.B., 1993. The relationship between sedimentary organic carbon isotopic composition and organic biomarker compound concentration. *Geochim. Cosmochim. Acta*, 57: 167-186.
- Jenkyns, H.C., 1988. The early Toarcian (Jurassic) anoxic event: Stratigraphic, sedimentary and geochemical evidence. *Am. J. Sci.*, 288: 101-151.
- Johnson, W.C. (ed), 1955. *Organic Reagents for Metals*. Hopkin and Williams, Chadwell Heath, 1, pp. 124-129.
- Jørgensen, B.B., 1977. The sulfur cycle of a coastal marine sediment (Limfjorden, Denmark). *Limnol. Oceanogr.*, 5: 814-832.

- Jørgensen, B.B., 1982. Mineralization of organic matter in the sea bed - the role of sulfate reduction. *Nature*, 296: 643-645.
- Jørgensen, B.B., 1983. Processes at the sediment-water interface. In: Bolin, B. and Cook, R.B. (eds), *The Major Biochemical Cycles and Their Interactions*. Wiley, New York, pp. 477-509.
- Kaplan, I.R. and Rittenberg, S.C., 1964. Microbiological fractionation of sulphur isotopes. *J. Gen. Microbiol.*, 34: 195-212.
- Katz, B.J., 1983. Limitation of Rock Eval pyrolysis for typing organic matter. *Org. Geochem.*, 4: 195-199.
- Kinney, I.W. and Cook, G.L., 1952. Identification of thiophene and benzene homologs. *Analytical Chemistry*, 24: 1391-1396.
- Kiyosu, Y. 1980. Chemical reduction and sulphur isotope effects of sulphate by organic matter under hydrothermal conditions. *Chem. Geol.*, 30: 47-56.
- Kiyosu, Y. and Krouse, H.R., 1990. The role of organic acid in the abiogenic reduction of sulphate and the sulphur isotope effect. *J. Geochem.* 24: 21-27.
- Knipe, R.J., 1992. Faulting processes and fault seal. In: Larsen, R.M., Brekke, H., Larsen, B.T. and Talleraas, E. (eds), *Structural and Tectonic Modelling and its Application to Petroleum Geology*. Elsevier, Amsterdam, NPF Special Publication, 1, pp. 325-342.
- Kohnen, M.E.L., Sinninghe Damsté, J.S., ten Haven, H.L. and de Leeuw, J.W., 1989. Early incorporation of polysulphides in sedimentary organic matter. *Nature*, 341: 640-641.
- Kohnen, M.E.L., Sinninghe Damsté, J.S., Kock-Van Dalen, A.C., ten Haven, H.L., Rullkoter, J. and de Leeuw, J.W., 1990. Origin and diagenetic transformation of C<sub>25</sub> and C<sub>30</sub> highly branched isoprenoid sulphur compounds: Further evidence for the formation of organically bound sulphur during early diagenesis. *Geochim. Cosmochim. Acta*, 54: 3053-3063.
- Kohnen, M.E.L., Sinninghe Damsté, J.S. and de Leeuw, J.W., 1991a. Biases from natural sulphurization in palaeoenvironmental reconstruction based on hydrocarbon biomarker distributions. *Nature*, 349: 775-778.
- Kohnen, M.E.L., Sinninghe Damsté, J.S., Kock-Van Dalen, A.C. and de Leeuw, J.W., 1991b. Di- or polysulphide-bound biomarkers in sulphur-rich geomacromolecules as revealed by selective chemolysis. *Geochim. Cosmochim. Acta*, 55: 1375-1394.
- Kohnen, M.E.L., Schouten, S., Sinninghe Damsté, J.S., de Leeuw, J.W., Merritt, D.A. and Hayes, J.M., 1992. Recognition of palaeobiochemicals by a combined molecular sulphur and isotope geochemical approach. *Science*, 236: 358-362.

- Krauskopf, K.B., 1985. Introduction to Geochemistry. McGraw-Hill, London, 617 pp.
- Krom, M.D. and Berner, R.A., 1983. A rapid method for the determination of organic and carbonate carbon in geological samples. *J. Sed. Petrol.*, 53: 660-663.
- Kroopnick, P. and Craig, H., 1972. Atmospheric oxygen: Isotopic composition and solubility fractionation. *Science*, 175: 54-55.
- Krouse, H.R., 1977. Sulfur isotope studies and their role in petroleum exploration. *J. Geochem. Explor.*, 7: 189-211.
- Krouse, H.R., Ritchie, R.G.S. and Roche, R.S., 1987. Sulphur isotope composition of H<sub>2</sub>S evolved during the non-isothermal pyrolysis of sulphur-containing materials. *J. Anal. App. Pyrol.*, 12: 19-29.
- Kusakabe, M., Rafter, T.A., Stout, J.D. and Collie, T.W., 1976. Sulphur isotopic variations in nature: 12. Isotopic ratios of sulphur extracted from some plants, soils and related materials. *N.Z. J. Sci.*, 19: 433-440.
- LaLonde, R.T., Ferrara, L.M. and Hayes, M.P., 1987. Low-temperature polysulfide reactions of conjugated ene carbonyls: A reaction model for the geologic origin of S-heterocycles. *Org. Geochem.*, 11: 563-571.
- Langmuir, D., 1978. Uranium solution-mineral equilibria at low temperatures with applications to sedimentary ore deposits. *Geochim. Cosmochim. Acta*, 42: 1753-1766.
- Largeau, C., Casadevall, E., Kadouri, A. and Metzger, P., 1984. Formation of *Botryococcus*-derived kerogens. Comparative study of immature torbanite and the extant algae *Botryococcus braunii*. In: Schenck, P.A. *et al.* (eds), *Advances in Organic Geochemistry 1983*. Pergamon Press, Oxford, pp. 327-332.
- Largeau, C., Derenne, S., Casadevall, E., Kadouri, A. and Sellier, N., 1986. Pyrolysis of immature torbanite and of the resistant biopolymer (PRB A) isolated from the extant algae *Botryococcus braunii*. Mechanism for the formation and structure of torbanite. *Org. Geochem.*, 10: 1023-1032.
- Law, G.A.D., 1992. The influence of lithology and kerogen composition on immature bitumen geochemistry. Ph.D. Thesis, NRG, Univ. Newcastle upon Tyne, 269 pp. (Unpubl.).
- Lawrence, J.R., Gieskes, J.M. and Anderson, T.F., 1976. Oxygen isotope material balance calculations Leg 35. In: *Initial of the Deep-Sea Drilling Project*, 35: 507-512.
- Leeder, M.R., 1988a. Devonian-Carboniferous river systems and sediment dispersal from the orogenic belts and cratons of NW Europe. In: Harris, A.L. and Fettes, D.J. (eds), *The Caledonian-Appalachian Orogen*. Geological Society Special Publication, 38, pp. 549-558.

- Leeder, M.R., 1988b. Recent developments in Carboniferous geology: A critical review with implications for the British Isles and NW Europe. *Proc. Geol. Ass.*, 99(2): 73-100.
- Leventhal, J.S., 1990. Organic matter and thermochemical sulfate reduction in the Viburnum trend, Southeast Missouri. *Economic Geology*, 85: 622-632.
- Leventhal, J.S. and Taylor, C., 1990. Comparison of methods to determine degree of pyritization. *Geochim. Cosmochim. Acta*, 54: 2621-2625.
- Lewis, C.L.E. and Moore, M.E., 1992. Apatite fission track analysis of four outcrop samples from Lancashire, Northwest England. *Geotrack Report #381*, for British Gas.
- Leythaeuser, D. and Schwarzkopf, T., 1986. The pristane/n-heptadecane ratio as an indicator for recognition of hydrocarbon migration effects. *Org. Geochem.*, 10: 191-197.
- Lippmann, F., 1955. Ton geoden und minerale des Barreme von Hoheneggelsen. *Geol. Rundschau*, 43: 475-503.
- Litke, R., Klussmann, U., Krooss, B. and Leythaeuser, D., 1991. Quantification of loss of calcite, pyrite and organic matter due to weathering of Toarcian black shales and effects on kerogen and bitumen characteristics. *Geochim. Cosmochim. Acta*, 55: 3369-3378.
- Lloyd, G.E., 1987. Atomic number and crystallographic contrast images with the SEM: A review of backscattered electron techniques. *Min. Mag.*, 51: 3-19.
- Lloyd, R.M., 1967. Oxygen-18 composition of ocean sulphate. *Science*, 156: 1228-1231.
- Lloyd, R.M., 1968. Oxygen isotope behaviour in the sulphate-water system. *J. Geophys. Res.*, 73: 6099-6209.
- Lord, C.J., 1982. A selective and precise method for pyrite determination in sedimentary materials. *J. Sed. Petrol.*, 52: 664-666.
- Loshner, A.J. and Kelts, K.R., 1989. Organic sulphur fixation in freshwater lake sediments and the implication for C/S ratios. *Terra Nova*, 1: 253-261.
- Lowson, R.T., 1982. Aqueous oxidation of pyrite by molecular oxygen. *Chem. Rev.*, 82: 461-497.
- Luther, G.W., Giblin, A.E. and Varsolona, R., 1985. Polarographic analysis of sulfur species in marine porewaters. *Limnol. Oceanogr.*, 30(4): 727-736.
- Machel, H.G., 1987. Some aspects of diagenetic sulphate-hydrocarbon redox reactions. In: Marshall, J.D. (ed), *Diagenesis of Sedimentary Sequences*. Geological Society Special Publication, 36: 15-28.

- Machel, H.G., 1992. Low-temperature and high-temperature origins of elemental sulfur in diagenetic environments. In: Wessel, G.R. and Wimberly, B.H. (eds), *Native Sulfur Developments in Geology and Exploration*. Society for Mining, Metallurgy and Exploration, Littleton, Colorado, pp. 3-22.
- MacKenzie, A.S., 1984. Applications of biological markers in petroleum geochemistry. In: Brooks, J. and Welte, D. (eds), *Advances in Petroleum Geochemistry - Volume 1*. Academic Press, London, pp. 115-214.
- MacKenzie, A.S., Brassell, S.C., Eglinton, G. and Maxwell J.R., 1982. Chemical fossils - the geological fates of steroids. *Science*, 217: 491-505.
- MacKenzie, W.S. and Guilford, C., 1980. *Atlas of Rock-Forming Minerals in Thin Section*. Longman, Harlow, 98 pp.
- Mango, F.D., 1983. The diagenesis of carbohydrates by hydrogen sulfide. *Geochim. Cosmochim. Acta*, 47: 1433-1441.
- Manheim, F.T., 1970. The diffusion of unconsolidated sediments. *Earth Planet. Sci. Letters*, 9: 307-309.
- Manowitz, B., Krouse, H.R., Barker, C. and Premuzik, E.T., 1990. Sulphur isotope data analysis of crude oils from the Bolivar coastal fields (Venezuela). In: Orr, W.L. and White C.M. (eds), 1990. *Geochemistry of Sulphur in Fossil Fuels*. American Chemical Society, Washington D.C., pp. 592-612.
- Margarlith, P., Silver, M. and Lundgren, D.G., 1966. Sulfur oxidation by the iron bacterium *Ferrobacillus ferrooxidans*. *J. Bacteriology*, 92: 1706-1709.
- Marshall, J.D., 1981. Zoned calcites in Jurassic ammonite chambers: Trace elements, isotopes and neomorphic origin. *Sedimentology*, 28: 867-887.
- Marshall, J.D., 1982. Isotopic composition of displacive fibrous calcite veins: Reversals in pore-water composition trends during burial diagenesis. *J. Sed. Petrol.*, 52: 0615 - 0630.
- Martin, T.H. and Hodgson, G.W., 1973. Geochemical origin of organic sulphur compounds: Reaction of Phenylalanine with elemental sulphur. *Chemical Geology*, 12: 189-208.
- Mayer, B., Fritz, P., Knief, K., Li, G., Fischer, M., Rehfuss, K-E. and Krouse, H.R., 1991. Evaluating pathways of sulphate between the atmosphere and hydrosphere using stable sulphur and oxygen isotope data. *Isotope Techniques in Water Resources Development*, IAEA, Vienna, pp. 3-17.
- Maynard, J.R., 1991. Upper Carboniferous marine transgressions and their deposits. Ph.D. Thesis, Univ. Leeds, 273 pp. (Unpubl.).
- Maynard, J.R., Wignall, P.B. and Varker, W.J., 1991. A 'hot' new shale facies from the Upper Carboniferous of Northern England. *J. Geol. Soc. Lond.*, 148: 805-808.

- McArthur, J.M., 1985. Francolite geochemistry-compositional controls during formation, diagenesis, metamorphism and weathering. *Geochim. Cosmochim. Acta*, 49: 23-35.
- Mello, M.R., Gaglianone, P.C., Brassell, S.C. and Maxwell, J.R., 1988. Geochemical and biological marker assessment of depositional environments using Brazilian offshore oils. *Mar. Petrol. Geol.*, 5: 205-223.
- Menzel, D.W., 1974. Primary productivity, dissolved and particulate organic matter and the sites of oxidation of organic matter. In: Goldberg E.D. (ed), *The Sea*. Wiley-Interscience, New York, 5, pp. 659-678.
- Middelburg, J.J., 1991. Organic carbon, sulphur and iron in recent semi-euxinic sediments of Kau Bay, Indonesia. *Geochim. Cosmochim. Acta*, 55: 815-828.
- Miles, J.A., 1989. *Illustrated Glossary of Petroleum Geochemistry*. Oxford Univ. Press, Oxford, 137 pp.
- Mizutani, Y. and Rafter, T.A., 1969a. Bacterial fractionation of oxygen isotopes in the reduction of sulphate and in the oxidation of sulphur. *N.Z. J. Sci.*, 12: 60-68.
- Mizutani, Y. and Rafter, T.A., 1969b. Oxygen isotopic fractionation in the bisulphate ion-water system. *N.Z. J. Sci.*, 12: 54-59.
- Moncaster, S.J. and Bottrell, S.H., 1991. Extraction of low-level sulphide from groundwaters for sulphur isotope analysis. *Chemical Geology (Isotope Geoscience Section)*, 94: 79-82.
- Moncaster, S.J., Bottrell, S.H., Tellam, J.H. and Lloyd, J.W., 1992. Sulphur isotope ratios as tracers of natural and anthropogenic sulphur in the Lincolnshire Limestone aquifer, Eastern England. In: Kharaka and Maest (eds), *Proc. 7th Int. Symp. Water-Rock Interaction*. Balkema, Rotterdam, pp. 813-816.
- Morris, K.A., 1979. A classification of Jurassic marine shale sequences: An example from the Toarcian (Lower Jurassic) of Great Britain. *Palaeogeography, Palaeoclimatology and Palaeoecology*, 26: 117-126.
- Morris, K.A., 1980. Comparison of major sequences of organic-rich mud deposition in the British Jurassic. *J. Geol. Soc. Lond.*, 137: 157-170.
- Morse, J.W., 1991. Oxidation kinetics of sedimentary pyrite in seawater. *Geochim. Cosmochim. Acta*, 55: 3665-3667.
- Morse, J.W. and Cornwell, J.C., 1987. Analysis and distribution of iron sulfide minerals in recent anoxic marine sediments. *Mar. Chem.*, 22: 55-69.
- Moseley, F., 1952. The Namurian of the Lancaster Fells. *Proc. Yorks. Geol. Soc.*, 109: 423-454.

- Moseley, F., 1956. The geology of the Keasden area, west of Settle, Yorkshire. Proc. Yorks. Geol. Soc., 30: 331-352.
- Mossmann, J-R., Aplin, A.C, Curtis, C.D. and Coleman, M.L., 1991. Geochemistry of inorganic and organic sulphur in organic-rich sediments from the Peru Margin. Geochim. Cosmochim. Acta, 55: 3581-3595.
- Mucci, A. and Edenborn, H.M., 1992. Influence of an organic-poor landslide deposit on the early diagenesis of iron and manganese in a coastal marine sediment. Geochim. Cosmochim. Acta, 56: 3909-3921.
- Myers, K.J. and Wignall, P.B., 1987. Understanding Jurassic organic-rich mudrocks-new concepts using gamma-ray spectrometry and palaeoecology: Examples from the Kimmeridge Clay of Dorset and the Jet Rock of Yorkshire. In: Leggett, J.K. and Zuffa, G.G. (eds), Marine Clastic Sedimentology. Graham and Trotman, London, pp. 172-189.
- Nakai, N. and Jensen, M.L., 1964. The kinetic isotope effect in the bacterial reduction and oxidation of sulphur. Geochim. Cosmochim. Acta, 28: 1893-1912.
- Nip, M., Tegelaar, E.W., de Leeuw, J.W., Schenck, P.A. and Holloway, P.J., 1986. A new non saponifiable highly aliphatic and resistant biopolymer in plant cuticles: Evidence from pyrolysis and  $^{13}\text{C}$ -NMR analysis of present day and fossil plants. Naturwissenschaften, 73: 579-585.
- Nip, M., de Leeuw, J.W., Schenck, P.A., Windig, W., Meuzelaar, H.L.C. and Crelling, J.C., 1989. A flash pyrolysis and petrographic study of cutinite from the Indiana paper coal. Geochim. Cosmochim. Acta, 53: 671-683.
- Nissenbaum, A. and Kaplan, I.R., 1972. Chemical and isotopic evidence for the *in situ* origin of marine humic substances. Limnol. Oceanogr., 17: 570-582.
- Nriagu, J.O. and Soon, Y.K., 1985. Distribution and isotopic composition of sulfur in lake sediments of Northern Ontario. Geochim. Cosmochim. Acta, 49: 823-834.
- Oderinde, R.A. and Olanipekun, E.O., 1991. Composition analysis of the oil component of the Nigerian bitumen. J. African Earth Sciences, 12: 483-487.
- Oertel, G. and Curtis, C.D., 1972. Clay-ironstone concretion preserving fabrics due to progressive compaction. Bull. Am. Geol. Soc., 83: 2597-2606.
- Ogura, K., 1990. Lipid compounds in lake sediments. Verh. Internat. Verein. Limnol., 24: 274-278.
- Ogura, K., Machinara, T. and Takada, H., 1990. Diagenesis of biomarkers in Biwa Lake sediments over 1 million years. Org. Geochem., 16: 805-813.
- Orr, W.L., 1982. Rate and mechanism of non-microbial sulphate reduction (abs). Geol. Soc. America Abstracts with Programs, 14: 580.

- Orr, W.L., 1986. Kerogen/asphaltene/sulphur relationships in sulphur-rich Monterey Oils. *Org. Geochem.*, 10: 499-516.
- Orr, W.L. and White, C.M. (eds), 1990. *Geochemistry of Sulphur in Fossil Fuels*. American Chemical Society, Washington D.C., 708 pp.
- Ouirisson, G., Albrecht, P. and Rhomer, M., 1979. The hopanoids - palaeochemistry and biochemistry of a group of natural products. *Pure and Applied Chemistry*, 51: 709-729.
- Padfield, T. and Gray, A., 1971. Major element rock analysis by x-ray fluorescence - a simple fusion method. *Bull. Philips Analytical Equipment* FS35.
- Pattrick, R.A.D. and Russell, M.J., 1989. Sulphur isotopic investigation of Lower Carboniferous vein deposits of the British Isles. *Mineral. Deposita*, 24: 148-153.
- Payzant, J.D., Montgomery, D.S. and Strausz, O.P., 1986. Sulfides in petroleum. *Org. Geochem.*, 9: 357-369.
- Payzant, J.D., Cyr, T.D., Montgomery, D.S. and Strausz, O.P., 1988. Studies on the structure of terpenoid sulphide type biological markers in petroleum. In: Yen, T.F. and Moldowan J.M. (eds), *Geochemical Biomarkers*. Harewood, England, pp. 133-147.
- Pedersen, T.F. and Calvert, S.E., 1990. Anoxia vs. productivity: What controls the formation of organic-carbon-rich sediments and sedimentary rocks? *Bull. Am. Ass. Petrol. Geol.*, 74: 454-466.
- Peters, K.E., 1986. Guidelines for evaluating petroleum source rock using programmed pyrolysis. *Bull. Am. Ass. Petrol. Geol.*, 70: 318-329.
- Pettijohn, J.F., 1975. *Sedimentary Rocks (3rd Edition)*. Harper and Row, New York, 628 pp.
- Philip, R.P. and Gilbert, T.D., 1985. Source rock and asphaltene biomarker characterization by pyrolysis-gas chromatography-mass spectrometry-multiple ion detection. *Geochem. Cosmochim. Acta*, 49: 1421-1432.
- Pirrie, D. and Marshall, J.D., 1991. Field relationships and stable isotope geochemistry of concretions from James Ross Island, Antarctica. *Sed. Geol.*, 71: 137-150.
- Pourbaix, M., 1960. *Atlas of Electrochemistry in Aqueous Solutions*. Pergamon Press, Oxford, pp. 656.
- Powell, T.G. and MacQueen, R.W., 1984. Precipitation of sulphide ores and organic matter: Sulphate reactions at Pine Point, Canada. *Science* 224: 63-66.



- Powell, T.G., Douglas, A.G. and Allan, J., 1976. Variations in the type and distribution of organic matter in some Carboniferous sediments from Northern England. *Chemical Geology*, 18: 137-148.
- Prahl, F.G., Bennett, J.T. and Carpenter, R., 1980. The early diagenesis of aliphatic hydrocarbons and organic matter in sedimentary particulates from Dabob Bay, Washington. *Geochim. Cosmochim. Acta*, 44: 1967-1976.
- Pratt, L.M., Summons, R.E. and Hieshima, G.B., 1991. Sterane and triterpane biomarkers in the Precambrian Nonesuch Formation, North American Midcontinent Rift. *Geochem. Cosmochim. Acta*, 55: 911-916.
- Purvis, K. and Wright, V.P., 1991. Calcretes related to phreatophytic vegetation from the Middle Triassic Otter Sandstone of Southwest England. *Sedimentology*, 38: 539-551.
- Pye, K., 1985. Electron microscopy analysis of zoned dolomites in the Jet Rock Formation (Lower Toarcian) of the Whitby area, U.K. *Geol. Mag.*, 122: 279-286.
- Pye, K. and Krinsley, D.H., 1986. Microfabric, mineralogy and early diagenetic history of the Whitby mudstone formation (Toarcian), Cleveland Basin, U.K. *Geological Magazine*, 123: 191-202.
- Pye, K. and Miller, J.A., 1990. Chemical and biochemical weathering of pyritic mudrocks in a shale embankment. *Quat. J. Eng. Geol.*, 23: 365-381.
- Pyzik, A.J. and Sommer, S.E., 1991. Sedimentary iron monosulfides: Kinetics and mechanism of formation. *Geochim. Cosmochim. Acta*, 45: 687-6948.
- Rabinovich, A.L. and Grinenko, V.A., 1979. Sulfate sulfur isotope ratios for USSR river water. *Trans. from Geokhimiya*, 3: 441-454.
- Rafter, T.A., 1967. A method for the extraction of oxygen and its quantitative conversion to carbon dioxide for isotope radiation measurements. *N.Z. J. Sci.*, 10: 493-510.
- Rafter, T.A. and Mizutani, Y., 1967. Preliminary results on oxygen isotopic variation in sulphates and the relationship to their environment and to their  $\delta^{34}\text{S}$  values. *N.Z. J. Sci.*, 10: 816-840.
- Raiswell, R., 1971. The growth of Cambrian and Liassic concretions. *Sedimentology*, 17: 147-171.
- Raiswell, R., 1976. The microbiological formation of carbonate concretions in the Upper Lias of NE England. *Chemical Geology*, 18: 227-244.
- Raiswell, R., 1987. Non-steady state microbiological diagenesis and the origin of concretions and nodular limestones. In: Marshall, J.D. (ed), *Diagenesis of Sedimentary Sequences*. Geological Society Special Publication, 36, pp. 41-54.

- Raiswell, R., 1992. The pyritisation of soft-bodied fossils. In: Kharaka, Y.K. and Maest, A.S. (eds), *Proc. 7th Int. Symp. Water-Rock Interaction*. Balkema, Rotterdam, pp. 301-304.
- Raiswell, R., 1993. Kinetic controls on depth variations in localised pyrite formation. *Chemical Geology*, 107: 467-469.
- Raiswell, R. and Al-Biatty, H.J., 1989. Depositional and diagenetic C-S-Fe signatures in early Palaeozoic normal marine shales. *Geochim. Cosmochim. Acta*, 53: 1147-1152.
- Raiswell, R. and Al-Biatty, H.J., 1992. Depositional and diagenetic C-S-Fe signatures and the potential of shales to generate metal-rich fluids. In: Schidlowski, M. *et al.* (eds), *Early Organic Evolution: Implications for Mineral and Energy Resources*. Springer-Verlag, Berlin Heidelberg, pp. 415-425.
- Raiswell, R. and Berner, R.A., 1985. Pyrite formation in euxinic and semi-euxinic sediments. *Am. J. Sci.*, 285: 710-724.
- Raiswell, R. and Berner, R.A., 1986. Pyrite and organic matter in Phanerozoic normal marine shales. *Geochim. Cosmochim. Acta*, 50: 1967-1976.
- Raiswell, R. and Berner, R.A., 1987. Organic carbon losses during burial and thermal maturation of normal marine shales. *Geology*, 15: 853-856.
- Raiswell, R. and Bottrell, S.H., 1991. The disposal of flue gas desulphurisation waste: Sulphur gas emissions and their control. *Environmental Chemistry and Health*, 13(2): 119-126.
- Raiswell, R., Buckley, F., Berner, R.A. and Anderson, T.F., 1988. Degree of pyritisation of iron as a palaeoenvironmental indicator of bottom-water oxygenation. *J. Sed. Petrol.*, 58: 812-819.
- Raiswell, R., Bottrell, S.H., Al-Biatty, H.J. and Tan, M. MD., 1993a. The influence of bottom water oxygenation and reactive iron content on sulfur incorporation into bitumens from Jurassic marine shales. *Am. J. Sci.*, 293: 569-596.
- Raiswell, R., Whaler, K., Dean, S., Coleman, M.L. and Briggs, D.E.G., 1993b. A simple three-dimensional model of diffusion-with-precipitation applied to localised pyrite formation in framboids, fossils and detrital iron minerals. *Mar. Geol.*, 113: 89-100.
- Raiswell, R., Canfield, D.E. and Berner, R.A., 1994. A comparison of iron extraction methods for the determination of degree of pyritisation and the recognition of iron-limited pyrite formation. *Chemical Geology*, 111: 101-110.
- Ramsbottom, W.H.C., 1973. Transgressions and regressions in the Dinantian: A new synthesis of British Dinantian stratigraphy. *Proc. Yorks. Geol. Soc.*, 39: 567-607.

- Ramsbottom, W.H.C., 1977. Major cycles of transgression and regression (mesothems) in the Namurian. *Proc. Yorks. Geol. Soc.*, 41: 261-291.
- Ramsbottom, W.H.C., Sabine, P.A., Dangerfield, J. and Sabine, P.W., 1981. Mudrocks in the Carboniferous of Britain. *Quat. J. Eng. Geol. Lond.*, 14, 27-262.
- Raynaud, J-F., Lugardon, B. and Lacrampe-Couloume, G., 1989. Lamellar structures and bacteria as main components of the amorphous matter of source rocks. *Bull. Centres. Rech.*, 13: 1-21.
- Rees, C.E., Jenkins, W.J. and Monster, J., 1978. The sulphur isotopic composition of ocean water sulphate. *Geochim. Cosmochim. Acta*, 42: 377-381.
- Redfield, A.C., 1942. The processes determining the concentration of oxygen, phosphate and other organic derivatives within the depth of the Atlantic Ocean. *Pap. Phys. Ocanogr. Meteorol.*, 9: 1-22
- Rickard, D.T., 1974. The kinetics and mechanism of the sulfidation of goethite. *Am. J. Sci.*, 274: 941-952.
- Rickard, D.T., 1975. Kinetics and mechanisms of pyrite formation at low temperatures. *Am. J. Sci.*, 275: 636-652.
- Rickard, D.T., 1989a. An apparatus for the study of fast precipitation kinetics. *Min. Mag.*, 50: 527-530.
- Rickard, D.T., 1989b. Experimental concentration-time curves for the iron (II) sulphide precipitation process in aqueous solutions and their interpretation. *Chem. Geol.*, 78: 315-324.
- Riley, J.T., Ruba, G.M. and Lee, C.C., 1990. Direct determination of total organic sulphur in coal. In: Orr, W.L. and White C.M. (eds), *Geochemistry of Sulphur in Fossil Fuels*. American Chemical Society, Washington D.C., pp. 231-240.
- Robin, P.L. and Rouxhet, P.G., 1978. Characterization of kerogens and study of their evolution by infrared spectroscopy: Carbonyl and carboxyl groups. *Geochem. Cosmochim. Acta*, 42: 1341-1349.
- Robinson, B.W. and Kusakabe, M., 1975. Quantitative preparation of sulfur dioxide, for  $^{34}\text{S}/^{32}\text{S}$  analyses, from sulfides by combustion with cuprous oxide. *Analytical Chemistry*, 47: 1179-1181.
- Robinson, B.W., Hirner, A.V. and Lyon, G.L., 1991. Stable carbon and sulfur isotope distributions of crude oil and source rock constituents from Burgan and Raudhatain oil fields (Kuwait). *Chemical Geology (Isotope Geoscience Section)*, 86: 295-306.
- Ronov, A.B., 1976. Global carbon geochemistry, volcanism carbonate accumulation and life. *Trans. from Geokhimiya*, 13(4): 172-195.

- Roy, A.B. and Trudinger, R.A., 1970. *The Biochemistry of Inorganic Compounds of Sulphur*. Cambridge Univ. Press, Cambridge, 400 pp.
- Rudd, J.W.M., Kelly, C.A. and Furutani, A., 1986. The role of sulfate reduction in long term accumulation of organic and inorganic sulfur in lake sediments. *Limnol. Oceanogr.*, 31(6): 1281-1291.
- Rukin, N., 1990. The diagenesis of the Shales-with-beef of the Lower Lias, West Dorset. Ph.D. Thesis, Univ. Liverpool (Unpubl.).
- Rullkötter, J., Aizenshtat, Z. and Spiro, B., 1984. Biological markers in bitumens and pyrolyzates of Upper Cretaceous bituminous chalks from the Ghareb Formation, Israel. *Geochim. Cosmochim. Acta*, 48: 151-157.
- Rullkötter, J. and Michaelis, W. (1990). The structure of kerogen and related materials. A review of recent and future trends. In: Durand, B. and Behar, F. (eds) *Advances in Organic Geochemistry 1989*. Pergamon Press, Oxford, pp. 829-852.
- Ryther, J.H., 1963. Geographic variations in productivity. In: Hill, M.N. (ed), *The Sea, Ideas and Observations in the Study of the Seas*. Wiley Interscience, New York, 2: 347-380.
- Sælen, G.S., 1994. Application of stable-isotope techniques to studies of belemnite rostra, organic matter and sedimentary pyrite: Interpreting environmental conditions during deposition of organic-rich shales. Ph.D. Thesis, Univ. Bergen (Unpubl.).
- Sandell, E.B., 1959. Colorimetric Determination of Traces of Metals. In: Clarke, B.L., Elving, P.J. and Kolthoff, I.M. (eds), *Chemical Analysis*. Wiley Interscience, New York, 3, pp. 536-543.
- Sass, E., Bein, A. and Almogi-Labin, A., 1991. Oxygen-isotope composition of diagenetic calcite in organic-rich rocks: Evidence for  $^{18}\text{O}$  depletion in marine anaerobic pore water. *Geology*, 19: 839-842.
- Schmid, J.C., Connan, J. and Albrecht, P., 1987. Occurrence and geochemical significance of long-chain dialkylthiacyclopentanes. *Nature*, 329: 54-56.
- Schou, L. and Myhr, M.B., 1988. Sulfur aromatic compounds as maturity parameters. *Org. Geochem.*, 13: 61-66.
- Scotchman, I.C., 1988. Diagenesis and primary migration in Upper Jurassic claystone source rocks in North Sea: Discussion. *Bull. Am. Ass. Petrol. Geol.*, 72: 1423-1425.
- Scotchman, I.C., 1991a. Kerogen facies and maturity of the Kimmeridge Clay formation in Southern and Eastern England. *Mar. Petrol. Geol.*, 8: 278-295.
- Scotchman, I.C., 1991b. The geochemistry of concretions from the Kimmeridge Clay formation of Southern and Eastern England. *Sedimentology*, 38: 79-106.

- Scotchman, I.C., 1993. Diagenetic pore fluid evolution in the Kimmeridge Clay formation: From concretions to sandstone cements. In: Manning, D.A.C., Hall, P.L. and Hughes, C.R. (eds.), *Geochemistry of Clay-Pore Fluid Interactions*. Chapman and Hall, London, pp. 127-159.
- Scrutton, C. (Ed), 1994. *Yorkshire Rocks and Landscape: A Field Guide*. Ellenbank Press, Maryport, Cumbria, 224 pp.
- Searl, A. and Fallick, A.E., 1990. Dinantian dolomites from East Fife: Hydrothermal overprinting of early mixing-zone stable isotopic and Fe/Mn compositions. *J. Geol. Soc. Lond.*, 147: 623-638.
- Seifert, W.K. and Moldowan, M., 1979. The effect of biodegradation on steranes and terpanes in crude oils. *Geochim. Cosmochim. Acta*, 43: 111-126.
- Seifert, W.K. and Moldowan, M., 1980. The effect of thermal stress on source-rock quality as measured by hopane stereochemistry. In: Douglas, A.D. and Maxwell, J.R. (eds), *Advances in Organic Geochemistry 1979*. Pergamon Press, Oxford, pp. 229-237.
- Seifert, W.K. and Moldowan, M., 1981. Palaeoreconstruction by biological markers. *Geochim. Cosmochim. Acta.*, 45: 783-794.
- Silfer, J.A., Engel, M.H., Macko, S.A. and Jumeau, E.J., 1991. Stable carbon isotope analysis of amino acid enantiomers by conventional isotope ratio mass spectrometry and combined gas chromatography/isotope ratio mass spectrometry. *Analytical Chemistry*, 63: 370-374.
- Sinninghe Damsté, J.S. and de Leeuw, J.W., 1989. Analysis, structure and geochemical significance of organically-bound sulphur in the geosphere: State of the art and future research. *Org. Geochem.*, 16: 1077-1101.
- Sinninghe Damsté, J.S. and de Leeuw, J.W., 1992. Organically bound sulphur in coal: A molecular approach. *Fuel Proc. Technol.*, 30: 109-178.
- Sinninghe Damsté, J.S. and Rijpstra, W.I.C., 1993. Identification of a novel C<sub>25</sub> highly branched isoprenoid thiophene in sediments. *Org. Geochem.*, 20: 327-331.
- Sinninghe Damsté, J.S., Rijpstra, W.I.C., de Leeuw, J.W. and Schenck, P.A., 1987. Origin of organic sulphur compounds and sulphur-containing high molecular weight substances in sediments and immature crude oils. *Org. Geochem.*, 13: 593-606.
- Sinninghe Damsté, J.S., Eglinton, T.I., de Leeuw, J.W. and Schenck, P.A., 1989a. Organic sulphur in macromolecular sedimentary organic matter: I. Structure and origin of sulphur-containing moieties in kerogen, asphaltenes and coal as revealed by flash pyrolysis. *Geochim. Cosmochim. Acta*, 53: 873-889.
- Sinninghe Damsté, J.S., Rijpstra, W.I.C., de Leeuw, J.W. and Schenck, P.A., 1989b. The occurrence and identification of series of organic sulphur compounds in oils and sediment extracts: II. Their presence in samples

from hypersaline and non-hypersaline palaeoenvironments and possible application as source, palaeoenvironmental and maturity indicators. *Geochim. Cosmochim. Acta*, 53: 1323-1341.

Sinninghe Damsté, J.S., Rijpstra, W.I.C., Kock-Van Dalen, A.C., de Leeuw, J.W. and Schenck, P.A., 1989c. Quenching of labile functionalised lipids by inorganic sulphur species: Evidence for the formation of sedimentary organic sulphur compounds at the early stages of diagenesis. *Geochim. Cosmochim. Acta*, 53: 1343-1355.

Sinninghe Damsté, J.S., Van Koert, E.R., Kock-Van Dalen, A.C., De Leeuw, J.W. and Schenck, P.A., 1989d. Characterisation of highly branched isoprenoid thiophenes occurring in sediments and immature crude oils. *Org. Geochem.*, 14: 555-567.

Sinninghe Damsté, J.S., Kohnen, M.E.L. and de Leeuw, J.W., 1990. Thiophene biomarkers for palaeoenvironmental assessment and molecular stratigraphy. *Nature*, 345: 609-611.

Skoog, D.A., West, D.M. and Holler, F.A., 1988. *Fundamentals of Analytical Chemistry*. Saunders College Publishing, London, 893 pp.

Slinger, F.C., 1936. Millstone grit and glacial geology of Caton Moor, near Lancaster. *Rep. Brit. Ass. Blackpool*, 1936: 345.

Smith, P.E., Farquhar, R.M. and Hancock, R.G., 1991. Direct radiometric age determination of carbonate diagenesis using U-Pb in secondary calcite. *Earth and Planetary Science Letters*, 105: 474-491.

Stark, J.G. and Wallace, H.G., 1986. *Chemistry Data Book*. John Murray, London, 112 pp.

Steger, H.F., 1977a. Determination of ferrous and ferric iron in samples of pyrrhotite, pyrite and chalcopyrite. *Talanta*, 24: 251-254.

Steger, H.F., 1977b. Determination of metal in the oxidation products of galena, sphalerite and chalcopyrite. *Talanta*, 24: 268-270.

Steger, H.F., 1979. Ferrous and ferric iron in the water-soluble oxidation products of iron-sulfide minerals. *Talanta*, 26: 455-460.

Steger, H.F. and Desjardins, L.E., 1977. Oxidation of sulfide minerals-III Determination of sulphate and thiosulphate in oxidised sulfide minerals. *Talanta*, 24: 673-679.

Stoneley, R., 1983. Fibrous calcite veins, overpressures and primary oil migration. *Bull. Am. Ass. Petrol. Geol.*, 67: 1427-1428.

Stookey, L.L., 1970. Ferrozine-a new spectrophotometric reagent for iron. *Analytical Chemistry*, 42: 779-781.

- Suess, E., 1970. Interaction of organic compounds with calcium carbonate-I. Association phenomena and geochemical implications. *Geochim. Cosmochim. Acta*, 34: 157-168.
- Suzuki, N. and Philp, R.P., 1990. Formation of melanoidins in the presence of H<sub>2</sub>S. *Org. Geochem.*, 15: 361-366.
- Sweeney, R.E. and Kaplan, I.R., 1973. Pyrite framboid formation: Laboratory synthesis and marine sediments. *Econ. Geol.*, 68: 618-634.
- Taar, W., 1921. Syngenetic origin of concretions in shale. *Bull. Am. Geol. Soc.*, 32: 373-384.
- Takahashi, M., Okazaki, R., Inamoto, N., Sugwara, T. and Iwamura, H., 1992. Spectroscopic detection and reactions of a thionitroso compound. *J. Am. Chem. Soc.*, 114: 1830-1837.
- Tan, M.T.D., 1985. Aspects of carbon, nitrogen, and sulphur diagenesis in sediments. Ph.D. Thesis, Univ. East Anglia, 292 pp. (Unpubl.).
- Tannenbaum, E. and Kaplan, I.R., 1985. Role of minerals in the thermal alteration of organic matter-I: Generation of gases and condensates under dry condition. *Geochim. Cosmochim. Acta*, 49: 2589-2604.
- Tarney, J. and Schreiber, B.C., 1976. Cone-in-cone and beef-in-shale textures from DSDP site 330, Falkland Plateau, South Atlantic. In: Barker, P.F. and Dalziel, I.W.D., *et al.*, (eds), Initial Reports of the Deep Sea Drilling Project. US Govt. Print. Office, Washington D.C., 36, pp. 865-870.
- Taylor, B.E., Wheeler, M.C. and Nordstrom, D.K., 1984. Stable isotope geochemistry of acid mine drainage: Experimental oxidation of pyrite. *Geochim. Cosmochim. Acta*, 48: 2669-2678.
- Taylor, H.P.Jr., 1974. The application of oxygen and hydrogen isotope studies to problems of hydrothermal alteration and ore deposition. *Econ. Geol.*, 69: 843-883.
- ten Haven, H.L. and Rullkötter, J., 1988. Pristane/phytane as environmental indicators. *Nature*, 333: 604.
- ten Haven, H.L., de Leeuw, J.W., Rullkötter, J. and Sinnighe Damsté, J.S., 1987. Restricted use of the pristane/phytane ratio as a palaeoenvironmental indicator. *Nature*, 330: 641-643.
- Tegelaar, E.W., de Leeuw, J.W., Derenne, S. and Largeau, C., 1989. A reappraisal of kerogen formation. *Geochim. Cosmochim. Acta*, 53: 3103-3106.
- Thode, H.G., 1991. Sulphur isotopes in nature and the environment: An overview. In: Krouse, H.R. and Ginenko, V.A. (eds), *Stable Isotopes - Natural and Anthropogenic Sulphur in the Environment*. *Scope* 43, pp. 1-26.

- Tissot, B.P. and Welte, D.H., 1984. *Petroleum Formation and Occurrence*, 2nd Edition. Springer-Verlag, Berlin, 246 pp.
- Tomkoeff, S., 1927. On the occurrence and mode of origin of certain kaolinite-bearing nodules in the Coal Measures. *Proc. Geol. Ass.*, 38: 518-547.
- Toran, L. and Harris, R.F., 1989. Interpretation of sulfur and oxygen isotopes in biological and abiological sulfide oxidation. *Geochim. Cosmochim. Acta*, 53: 2341 - 2348.
- Treibs, A., 1934. Chlorophyll und Haminderivate in bituminösen Gesteinen, Erdölen und Erdwaschen und Asphalten. *Ann. Chem.*, 510: 42-62.
- Trudinger, P.A., Chambers, L.A. and Smith, J.W., 1985. Low-temperature sulphate reduction: Biological versus abiological. *Can. J. Earth Sci.*, 22: 1910-1918.
- Tudge, A.P. and Thode, H.G., 1950. Thermodynamic properties of isotopic compounds of sulphur. *Can. J. Res.*, B28: 567-578.
- Tuttle, M.L., Rice, C.A. and Goldhaber, M.B., 1990. In: Orr, W.L. and White C.M. (eds), *Geochemistry of Sulphur in Fossil Fuels*. American Chemical Society, Washington D.C., pp. 114-148.
- Tyson, R.V. and Pearson, TH., 1991. Modern and ancient continental shelf anoxia: A Review. In: Tyson, R.V. and Pearson, TH. (eds), *Modern and Ancient Continental Shelf Anoxia*. *Geol. Soc. Spec. Pub.*, 58: 1-24.
- Urey, H.C., 1947. The thermodynamic properties of isotopic substances. *J. Chem. Soc.*, 562.
- Urmos, J., Sharma, S.K. and MacKenzie, F.T., 1991. Characterization of some biogenic carbonates with Raman spectroscopy. *Am. Mineral.*, 76: 641-646.
- Vairavamurthy, A. and Mopper, K., 1987. Geochemical formation of organosulphur compounds (thiols) by addition of H<sub>2</sub>S to sedimentary organic matter. *Nature*, 329: 623-625.
- Valeton, I., 1988. Verwitterung und Verwitterungslagerstätten. In: Füchtbauer, H. (ed), *Sedimente und Sedimentgesteine*. E. Schweizerbart, pp. 11-68.
- van Buchem, F.S.P., Melnyk, D.H. and McCave, I.N., 1992. Chemical cyclicity and correlation of Lower Lias mudstones using gamma ray logs, Yorkshire, UK. *J. Geol. Soc. Lond.*, 149: 991-1002.
- van Everdingen, R.O. and Krouse, H.R., 1985. Isotope composition of sulphates generated by bacterial and abiological oxidation. *Nature*, 315: 395-396.
- van Everdingen, R.O. and Krouse, H.R., 1988. Interpretation of isotopic compositions of dissolved sulphates in acid mine drainage. U.S. Bureau of Mines Circular 9183: *Mine drainage and surface mine reclamation*, pp. 147-156.



- van Krevelen, D.W., 1961. Coal. Elsevier, Amsterdam, 273 pp.
- van Krevelen, D.W., 1984. Organic geochemistry-old and new. *Org. Geochem.*, 6: 1-10.
- Veizer, J. and Hoefs, J., 1976. The nature of  $^{18}\text{O}/^{16}\text{O}$  and  $^{13}\text{C}/^{12}\text{C}$  secular trends in sedimentary carbonate rocks. *Geochim. Cosmochim. Acta*, 40: 1387 - 1395.
- Volkman, J.K., Alexander, R., Kagi, R.I. and Rullkötter, J., 1983. GC-MS characterisation of  $\text{C}_{27}$  and  $\text{C}_{28}$  triterpanes in sediments and petroleum. *Geochim. Cosmochim. Acta*, 47: 1033-1040.
- Wada, H. and Suzuki, K., 1983. Carbon isotope thermometry calibrated by dolomite-calcite solvus temperatures. *Geochim. Cosmochim. Acta*, 47: 697-706.
- Wall, D., 1965. Microplankton, pollen and spores from the Lower Jurassic in Britain. *Micropalaeontology*, 11: 151-190.
- Weeks, L.G., 1957. Origin of carbonate concretions in shales, Magdalena Valley, Columbia. *Bull. Am. Ass. Petrol. Geol.*, 67: 1427-1428.
- Welte, D.H., 1969. Organic geochemistry of carbon. Handbook of geochemistry. Springer-Verlag, Berlin.
- Welte, D.H. and Waples, D., 1973. Über die Bevorzugung geradzakliger n-alkane in Sedimentgesteinen. *Naturwissenschaften*, 60: 516-517.
- Wendorf, S.R. and Pratt, L.M., in press. Concentration and isotopic fractionation of sulfur compounds in sediments of the Santa Monica basin, offshore California. *Am. J. Sci.*
- Westgate, L.M. and Anderson, T.F., 1982. Extraction of various forms of sulfur from coal and shale for stable sulfur isotope analysis. *Analytical Chemistry*, 54: 2136-2139.
- Westgate, L.M. and Anderson, T.F., 1984. Isotopic evidence for the origin of sulfur in the Herrin (no. 6) coal member of Illinois. *Int. J. Coal Geology*, 4: 1-20.
- Westrich, J.T. and Berner, R.A., 1984. The role of sedimentary organic matter in bacterial sulfate reduction: The G model tested. *Limnol. Oceanogr.*, 29: 236-249.
- Whitten, D.G.A. and Brooks, J.R.V., 1987. The Penguin Dictionary of Geology. Penguin, Harmondsworth, 495 pp.
- Wicks, C.M., Herman, J.S. and Mills, A.L., 1991. Early diagenesis of sulfur in the sediments of lakes that receive acid mine drainage. *App. Geochem.*, 6: 213-224.

- Wiesenburg, D.A., Brooks, J.M. and Bernard, B.B., 1985. Biogenic hydrocarbon gases and sulfate reduction in the Orca Basin brine. *Geochim. Cosmochim. Acta*, 49: 2069-2080.
- Wigley, T.M.L., Plummer, L.N. and Pearson, F.J., 1978. Mass transfer and carbon isotope evolution in natural water systems. *Geochim. Cosmochim. Acta*, 42: 1117-1139.
- Wignall, P.B., 1991. Model for transgressive black shales? *Geology*, 19: 167-170.
- Wignall, P.B., 1994. *Black Shales*. Clarendon Press, Oxford, 124 pp.
- Wignall, P.B. and Hallam, A., 1991. Biofacies, stratigraphic distribution and depositional models of British onshore Jurassic black shales. In: Tyson, R.V. and Pearson, T.H. (eds), *Modern and Ancient Continental Shelf Anoxia*. *Geol. Soc. Spec. Pub.*, 58: 291-309.
- Wignall, P.B. and Maynard, J.R., 1993. The sequence stratigraphy of transgressive black shales. In: Katz, B.J. and Pratt, L.M. (eds), *Source Rocks in Sequence Stratigraphic Framework*. AAPG, *Studies in Geology*, 37.
- Wilkinson, M., Crowley, S.F. and Marshall, J.D., 1992. Model for the evolution of oxygen isotope ratios in the pore fluids of mudrocks during burial. *Mar. Petrol. Geol.*, 9: 98-105.
- Williams, N., 1978. Studies of the base metal sulfide deposits at McArthur River, Northern Territory, Australia: II. The sulfide-S and organic-C relationships of the concordant deposits and their significance. *Econ. Geol.*, 73: 1036-1056.
- Williams, P.F.V. and Douglas, A.G., 1981. The effects of lithologic variation on organic geochemistry in the Kimmeridge Clay of Britain. *Advances in Organic Geochemistry*, (1981): 568-575.
- Williamson, M.A. and Rimstidt, J.D., 1992. Correlation between structure and thermodynamic properties of aqueous sulfur species. *Geochim. Cosmochim. Acta*, 56: 3867-3880.
- Wilson, T.R.S., Thomson, J., Colley, S., Hydes, D.J. and Higgs, N.C., 1985. Early organic diagenesis: The significance of progressive subsurface oxidation fronts in pelagic sediments. *Geochim. Cosmochim. Acta*, 49: 811-822.
- Wilson, V., 1934. A synopsis of the Jurassic rocks of Yorkshire. *Proc. Geol. Ass.*, 45:(3) 248-291.
- Yardley, B.W.D. and Bottrell, S.H., 1992. Silica mobility and fluid movement during metamorphism of the Connemara shists, Ireland. *J. Met. Geol.*, 10: 453-464.
- Yen, T.F., 1974. A new structural model of oil shale kerogen. *Am. Chem. Soc.*, 19: 109-114.

- Zaback, D.A. and Pratt, L.M., 1992. Isotopic composition and speciation of sulfur in the Miocene Monterey Formation: Reevaluation of sulfur reactions during early diagenesis in marine environments. *Geochim. Cosmochim. Acta*, 56: 763-774.
- Zaback, D.A., Pratt, L.M. and Hayes, J.M., 1993. Transport and reduction of sulphate and immobilization of sulphide in marine black shales. *Geology*, 21: 141-144.
- Zheng, Y-F., 1992. Discussion on the use of  $\delta$ - $\Delta$  diagram in interpreting stable isotope data. *Eur. J. Mineral.*, 4: 635-643.
- Zilm, K.W., Pugmire, R.J., Larter, S.R., Allan, R.J. and Grant, D.M., 1981. Carbon-13 CP/MAS spectroscopy of coal macerals. *Fuel*, 60: 717.



0008-6223(94)00070-0

ISOTOPE FRACTIONATION IN THE  
SYNTHESIS OF FULLERENESK. M. THOMAS,\* J. M. LEWIS, S. H. BOTTRELL,<sup>1</sup> S. P. DEAN,<sup>1</sup> and J. FOULKES<sup>2</sup>

Northern Carbon Research Laboratories, Department of Chemistry, Bedson Building,

University of Newcastle upon Tyne, Newcastle upon Tyne, NE1 7RU, U.K.

<sup>1</sup>Department of Earth Sciences, University of Leeds, Leeds, LS2 9JT, U.K.<sup>2</sup>Alpherantz Research, PO Box 350, Burwell, Cambridge, CB5 0AX, U.K.

(Received 31 January 1994; accepted 25 April 1994)

**Abstract**—The synthesis of fullerenes by the direct current (DC) carbon arc evaporation method produces a number of different carbon materials. This investigation has involved the structural characterisation of the materials and the study of their isotopic composition. The cathode deposit was a highly ordered graphite with the basal planes oriented in the axial direction of the graphite rod. Raman microprobe spectroscopy, X-ray powder diffraction, and temperature programmed combustion measurements also showed that the material was heterogeneous. The structural characterisation results were consistent with the deposit being formed at progressively lower heat-treatment temperatures with increasing deposition. The fullerene soot was a very heterogeneous material with a large surface area. Isotope composition studies showed that the raw fullerene soot, fullerene depleted soot (toluene extract), C<sub>60</sub>, and C<sub>70</sub> were enriched in <sup>13</sup>C relative to the graphite anode, whereas the cathode deposit was depleted in <sup>13</sup>C. The measurements show that C<sub>60</sub> is richer in <sup>13</sup>C compared with both C<sub>70</sub> and the toluene-extracted soot. The implications regarding the mechanisms for the formation of fullerenes are discussed.

**Key Words**—Fullerene, graphite, isotope ratios, X-ray, Raman.

## 1. INTRODUCTION

The synthesis of fullerenes by the DC carbon arc evaporation method[1] and the chromatographic purification and proof of the structure[2] represented the major breakthroughs that allowed the development of research into the chemistry and physics of fullerenes. Despite its widespread use, there is still considerable controversy concerning the mechanism of fullerene formation and the precise nature and mechanism of the processes involved in the formation of fullerenes. Perhaps the most surprising aspect of the synthesis of fullerenes by the DC carbon arc evaporation process is that such a highly symmetrical molecule as C<sub>60</sub> results in high yields from the high-energy carbon arc plasma. The major problem with establishing the mechanism is that it is very difficult to carry out measurements on the species present in plasmas. Five main mechanisms for the formation of fullerenes have been proposed[3]. These mechanisms involve (a) the growth of open sheets of pentagons and hexagons[4], (b) fullerene growth by the addition of small carbon radicals to fullerenes in the range C<sub>30</sub>–C<sub>40</sub>[5], (c) the six-fold combination of naphthalenic C<sub>10</sub> units[6], (d) the growth of fullerenes starting with the combination of a C<sub>10</sub> unit with a C<sub>18</sub> ring[7], (e) the collapse of large carbon clusters to stable C<sub>60</sub> and C<sub>70</sub> structures[8]. The problem is to devise experiments that allow some of these mechanisms to be ruled out or, alternatively, for one of the mechanisms to be proved unequivocally.

The coaxial electrode DC carbon arc process is commonly employed to produce fullerene materials[9,10].

The chief advantage of this method is that, as the cathode is not consumed at all, only one moveable electrode is required and the system is self-aligning. During the process, a cathode deposit always progressively builds up. Under low anode evaporation rates, at optimal inert gas pressures, the cathode deposit has been shown to contain highly orientated nanotube structures[11], and this area continues to receive much attention. However, characterisation of the cathode deposit produced under high-power conditions optimised for fullerene synthesis has received little attention. In this paper the characterisation of the products of the DC carbon arc evaporation process were investigated with emphasis on the quantification of structural heterogeneity. Furthermore, the <sup>13</sup>C/<sup>12</sup>C isotope ratios of the materials were measured to assess any atomic mass related phenomena, such as diffusional effects that might yield further clues regarding the fullerene formation mechanism.

## 2. EXPERIMENTAL

## 2.1 Materials used

The fullerenes and cathode deposit were synthesised by the carbon arc evaporation of coaxially mounted, high-purity, graphite rods under DC power conditions (typically <30 V, >400 A) in ca. 100 torr of flowing helium. The arc is initiated by contact of the electrodes, and a fragile condensed deposit is quickly established on the cooler cathode that shrouds the tip of the anode. The contact zone quickly reaches a steady state, and around 15% of the evaporating anode mass is deposited on the cathode. This deposit has a shape reminiscent of a mushroom. Afterwards, the

\*Author to whom correspondence should be addressed.

soot is collected from the chamber and the cathode deposit is pulled off the cathode. There is never any fusion between cathode and deposit, and this may indicate that, even at the very highest carbon temperatures, there is no appreciable interfacial diffusion or cross bonding between carbon materials. Additionally, when the power is switched off there is never any black soot condensation on the inside of the cathode deposit, whereas the anode tip is always coated.

The raw fullerene soot was extracted with toluene with ca. 10 wt% fullerene yield. The composition of the extract was typically 4:1, C<sub>60</sub>:C<sub>70</sub>, with a small amount of higher fullerenes. Chromatographic procedures were used to separate pure (<99%) C<sub>60</sub> and C<sub>70</sub> (>92%).

### 2.2 Raman microprobe spectroscopy

The Raman spectra were recorded using a Spex 1401 double monochromator fitted with a Spectr Acq spectrometer computer control system. The Raman signal was detected using an RC31034A photomultiplier in conjunction with the Spectr Acq photon counting system. The Raman spectra were obtained using the 488 nm line of a Spectra Physics 2016 argon ion laser. The sample illumination and collection system was a BGSC microscope system fitted with a Nikon  $\times 40/0.9$  objective. The slit width used gave a spectral resolution of 8 cm<sup>-1</sup>. Spectra were recorded with 1 cm<sup>-1</sup> steps with 1 sec count times. In some cases where the spectra were weak or the background level high, multiple scans were used and the data averaged to improve the signal-to-noise ratio.

The Raman spectra were curve resolved using the computer software programme 'Origin' supplied by Microcal. This programme provided the Raman band width and intensity data.

### 2.3 X-ray diffraction

The X-ray diffraction profiles were recorded using a Phillips CW1774 X-ray diffractometer with CuK<sub>α</sub> radiation (1.54158 Å).

### 2.4 Surface area measurements

The total surface areas (TSA) of the carbons were determined from the adsorption isotherm for CO<sub>2</sub> at 273 K using a Micromeritics Digisorb 2600 instrument. An area of  $2 \times 10^{-19}$  m<sup>2</sup> was used for the area of a carbon dioxide molecule.

### 2.5 Thermogravimetric analysis-mass spectrometry (TG-MS)

The temperature-programmed combustion of the samples was carried out in a Thermal Sciences STA 780 thermogravimetric analysis-mass spectrometry system (TG-MS). The evolved gas profiles were measured by sampling directly 1 cm above the carbon sample being gasified, and a VG Quadrupole mass spectrometer was used for the gas analysis. The carbon sample (~5 mg) was heated at 15 K min<sup>-1</sup> in 20% oxygen/argon at a flow rate of 50 cm<sup>3</sup> min<sup>-1</sup>, and the sample gasified. The following *m/z* ratios were monitored throughout the course of the reaction: 28, 29, 30, 44,

45, 46. These correspond to the ions for CO and CO<sub>2</sub> and their <sup>13</sup>C and <sup>18</sup>O isotope components.

### 2.6 Isothermal reactivity studies

Isothermal reactivity studies were carried out in a Stanton Redcroft STA780 thermogravimetric analyser. Initially the sample (5 mg) was taken up to the reaction temperature (973 K) in argon with a flow rate 50 cm<sup>3</sup> min<sup>-1</sup> at a heating rate of 50 K min<sup>-1</sup>. After stabilization of the weight at 973 K, the gas was switched to air, and the sample gasified. The reactivities were calculated from the rate of gasification in the rectilinear region of the weight loss curve using the following equation:

$$R/\text{gg}^{-1} \text{ s}^{-1} = (1/w_0)(dw/dt),$$

where *w*<sub>0</sub> = initial weight, *R* = reactivity, and (*dw/dt*) = rate of gasification.

### 2.7 <sup>13</sup>C/<sup>12</sup>C Isotope ratio measurements

The small variations in the natural abundances of <sup>12</sup>C and <sup>13</sup>C are usually compared using the <sup>13</sup>C/<sup>12</sup>C ratio (*R<sub>x</sub>*) relative to an internationally accepted standard PDB (*R<sub>std</sub>*) using δ<sup>13</sup>C values expressed in parts per thousand, according to the following equation:

$$\delta^{13}\text{C} = \frac{(R_x - R_{std})}{R_{std}} \times 10^3.$$

The values quoted in the paper have been subtracted from that of the graphite rod used in order to ensure accurate direct comparisons.

The isotope ratio tracers have been used previously [12] to study the combustion of the components of heterogeneous carbonaceous materials. These measurements involve oxidation in the absence of gaseous molecular oxygen. Silica tubes were heated in air to 1123 K to remove all traces of adsorbed hydrocarbons and other species. Approximately 1–2 mg of powdered carbon sample was placed in a 6 mm o.d. thin-walled silica tube of volume approximately 10 cm<sup>3</sup>, together with an excess of CuO to oxidize the sample. Silver and copper wires were added to remove any oxides of sulphur or nitrogen present. This is of particular importance when impure carbonaceous materials are studied. The tube was heated to 383 K to ensure the sample was dry, and then it was evacuated, sealed, and heated to 1143 K for 12 h. After cooling, the carbon dioxide was purified cryogenically. The mass spectrometric measurements were carried out using a VG-SIRA-10 gas source isotope ratio instrument. The instrument had a dual inlet, 90° magnetic sector and triple collector configuration. The *m/z* 44, 45, and 46 ion beams were monitored simultaneously.

Both <sup>13</sup>C<sup>16</sup>C<sup>16</sup>O and <sup>12</sup>C<sup>16</sup>O<sup>17</sup>O contribute to the mass 45 peak. The contribution of <sup>12</sup>C<sup>16</sup>O<sup>17</sup>O to the mass 45 peak can be calculated using the intensity of the mass 46 peak, which is mainly <sup>12</sup>C<sup>16</sup>O<sup>18</sup>O, and the known <sup>17</sup>O/<sup>18</sup>O isotope ratio. The measurements on the carbon dioxide sample from the composites

were compared with the carbon dioxide produced by the combustion of an internal standard (National Bureau of Standards Oil Number 22 (-29.8% PDB)). Using the Australian National University (ANU) sucrose standard, a  $\delta^{13}\text{C}$  value of  $-10.43 \pm 0.05\%$  was obtained (cf. reported value of  $-10.42\%$ ). Twelve measurements were made alternately on the sample and the standard isotope reference carbon dioxide gas. The standard deviations for the measurements are always less than 0.1%.

The data for each series was referenced to the particular graphite rod used, thereby ensuring a true comparison of isotope ratios. Measurements of the isotope ratios for the graphite rods revealed only very small differences in isotopic composition between different rods.

### 3. RESULTS

The synthesis of fullerenes using the carbon arc evaporation produces a deposit on the cathode shaped like a 'mushroom,' as well as the raw fullerene soot. In order to understand the DC carbon arc synthesis of fullerenes the characterisation of all the products is required.

#### 3.1 Cathode deposit

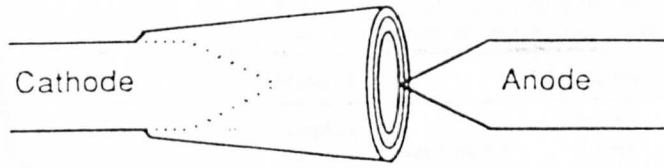
Figure 1a depicts the carbonaceous deposit on the cathode, and Fig. 1b shows an optical micrograph of a cross-section of cathode deposit. It is apparent that the deposit is highly anisotropic, with the basal planes aligned parallel to the axis of the graphite rod. The structure of the deposit was characterised by Raman microprobe spectroscopy and X-ray diffraction. Raman microprobe spectroscopy has high spatial resolution, and therefore it is capable of characterising structural differences in the deposit in relation to the radial and axial directions of the graphite rod. Raman spectroscopic characterisation data for the carbon materials produced in the carbon arc evaporation process are given in Table 1. Figure 2a shows the Raman spectra in the radial direction of the cathode deposit, and Fig. 2b shows the Raman spectra of the cathode deposit along the axis of the graphite rod. The first order phonon spectrum shows two main bands at  $\sim 1360\text{ cm}^{-1}$  (D band) and  $\sim 1580\text{ cm}^{-1}$  (G band), and a weak band at  $\sim 1620\text{ cm}^{-1}$  (D' band). The D and D' bands are associated with disorder in the carbons. The

D' band is more clearly observed in the spectra of the outside of the cathode deposit. The spectra show that the intensity ratio  $I_{\text{D}}/I_{\text{G}}$  decreases in moving radially from the outside to the inside of the deposit. The Raman spectrum of the inside is very similar to that of the graphite rod. The second order Raman spectra of the inside of the cathode deposit shows two main bands at  $\sim 2687$  and  $2733\text{ cm}^{-1}$ . The Raman spectrum of the outside of the cathode deposit shows a single band at  $\sim 2713\text{ cm}^{-1}$ , which presumably is comprised of two bands,  $2687$  and  $2733\text{ cm}^{-1}$ , observed for the inside of the deposit. Previous work [13] has shown that the band at  $\sim 2711\text{ cm}^{-1}$  becomes a doublet when the structure is ordered to the extent that the  $d_{002}$  X-ray diffraction spacing is less than  $0.338\text{ nm}$ . This agrees with the results presented here, since the  $d_{002}$  spacing for the inside and outside of the cathode deposit are  $0.3368$  and  $0.3411\text{ nm}$ , respectively. These spectra are consistent with the carbon structure being more ordered in the initial stages of the formation of the deposit where the heat treatment temperature is highest. The physical temperature distribution along the cathode carbon deposition interface is expected to be strongly affected by both the heat sinking effect of the cathode backing rod and black body radiation losses from the external surface of the mushroom-shaped deposit. For the latter case, thermal losses are expected to be of the order of kilowatts/cm<sup>2</sup> for the conditions employed. Furthermore, as the mushroom cathode deposit increases in length and hence external surface area, the heat sinking effect increases, and this is expected to lead to a progressive lowering of average interfacial deposition temperature. The structural variation of the carbon within the mushroom is thus expected to follow a complex pattern. In comparison, the Raman spectrum of the fullerene soot (Fig. 2c) is much broader, and is typical of a highly disordered carbon formed at relatively low temperature.

The X-ray diffraction data are given in Table 2. A comparison of the data for the cathode deposit with that of the graphite rod used shows some differences. The  $d_{002}$  value for the graphite rod was  $0.3357\text{ nm}$ . In comparison, the  $d_{002}$  values for the cathode deposit were  $0.3411$  and  $0.3368\text{ nm}$  for the outside and inside of the deposit, respectively. The  $I_{\text{D}}$  and  $I_{\text{G}}$  values for the inside and outside of the cathode deposit also showed differences. In particular, the  $I_{\text{G}}$  value for the graphite rod was larger than those for both the inside

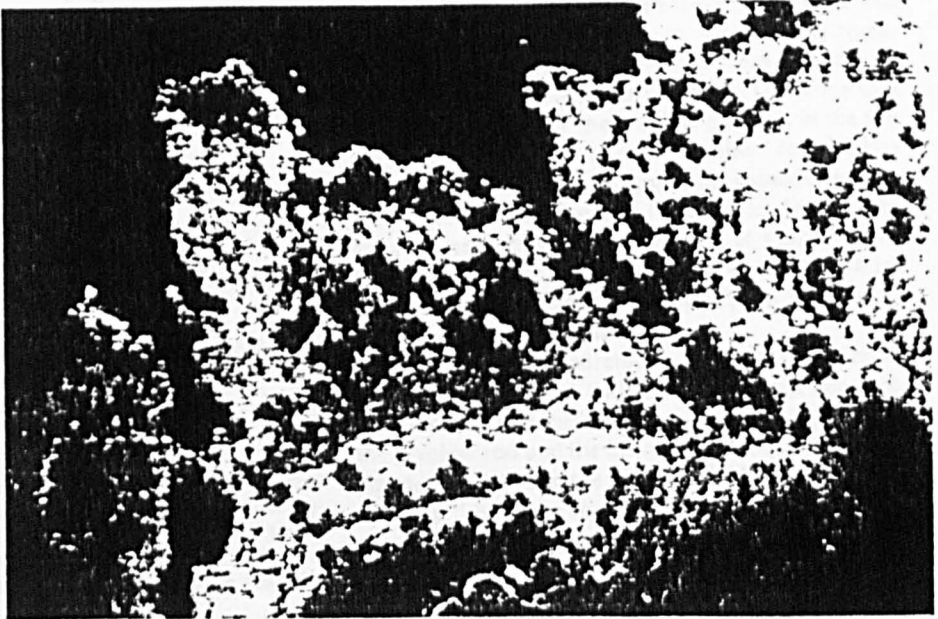
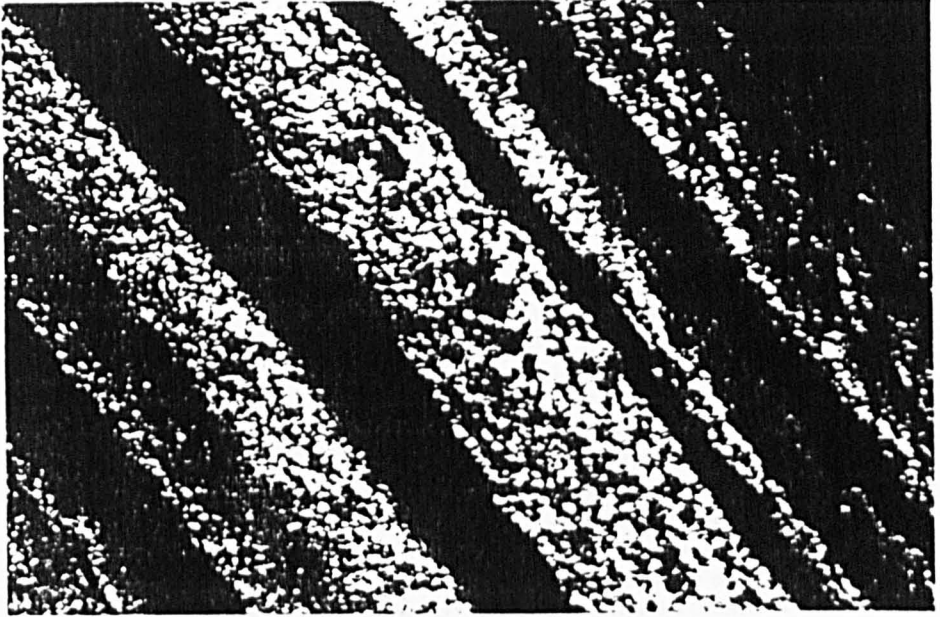
Table 1. Surface area and Raman spectroscopic data for the products of the carbon arc evaporation process for the synthesis of fullerenes

Carbon material	Surface area/ $\text{m}^2\text{ g}^{-1}$	G band/ $\text{cm}^{-1}$		D band ( $\text{cm}^{-1}$ )		$I_{\text{D}}/I_{\text{G}}$
		Position ( $\Delta\nu$ )	width	position ( $\Delta\nu$ )	Width ( $\Delta\nu_{\text{w}}$ )	
Graphite rod	<20	1578	20	1357	34	0.49
Cathode deposit (inside)	<20	1575	24	1354	36	0.27
Cathode deposit (outside)	<20	1578	22	1355	34	0.95
Fullerene soot	219	1597	74	1348	149	1.61
Fullerene soot (toluene-extracted)	220	—	—	—	—	—



(a)

(inside)

50  $\mu\text{m}$ 

(outside)

(b)

Fig. 1. (a) A schematic diagram of the cathode deposit. (b) Optical micrograph of the cross-section of the mushroom-shaped cathode deposit.



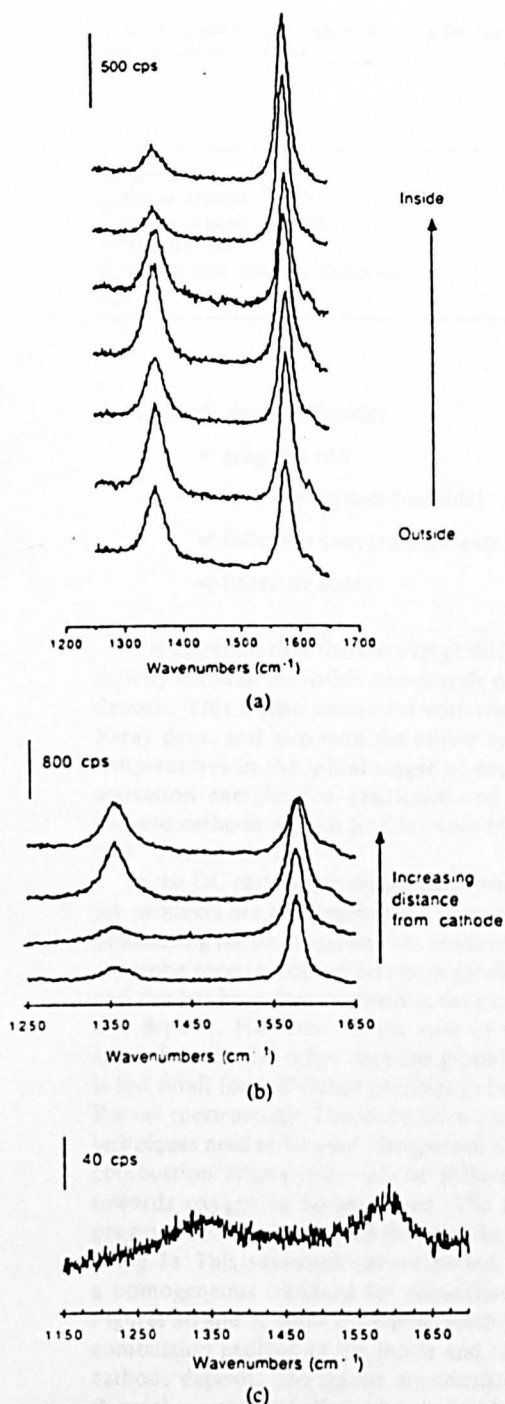


Fig. 2. Raman spectra of (a) the mushroom-shaped cathode deposit along the radial axis of the graphite rod (spatial separation  $\sim 500 \mu\text{m}$ ), (b) the cathode deposit in the direction of the axis of the rod (spatial separation  $2.5 \text{ mm}$ ), and (c) the fullerene soot. Spectra have been offset along the y axis for clarity.

and outside of the cathode deposit, with the former being slightly higher than the latter. However, the  $I_c$  values for both the inside and outside of the cathode deposit are consistent with a graphitic structure.

Table 2. X-ray diffraction data for the products of carbon arc evaporation process for the synthesis of fullerenes

Material	$d_{002}/\text{nm}$	$I_a/\text{nm}$	$I_c/\text{nm}$
Graphite rod	0.3357	44.15	26.58
Cathode deposit (inside)	0.3368	42.44	13.32
Cathode deposit (outside)	0.3411	22.79	11.92
Graphite in fullerene soot	0.3351	13.02	17.37

Larger differences are observed between the  $I_a$  values obtained for the inside and outside of the deposit. The former is very similar to that obtained for the graphite rod, whereas the latter is approximately half the value. These results are consistent with a higher heat-treatment temperature in the initial stages of carbon deposition on the cathode.

### 3.2 Fullerene soot

The X-ray diffraction profile of the fullerene soot contains a sharp  $d_{002}$  band superimposed on a broad background containing some weak peaks that extend to  $\sim 2\theta = 30^\circ$ . The  $I_c$  and  $d_{002}$  spacing data are consistent with a graphitic structure, but the intensity is much lower than for the graphite. These peaks arise from graphitic particles in the soot ( $\sim 10\%$  graphite). The general X-ray profile of the soot was similar to earlier published patterns of Scanlon[14], and Werner[15].

The origin of the graphite in the fullerene soot is of interest in relation to the mechanism of fullerene formation. The graphite rods used in the synthesis are composite materials produced from needle coke and coal tar pitch as binders. Hence, it is possible to envisage fragmentation of particles from the rod by breakage at the binder-filler interface. The X-ray  $d_{002}$  and  $I_c$  parameters for the graphite particles in the fullerene soot are similar to those obtained for graphite rod and, also, the initial stages of the cathode deposit. However, it is feasible that the particles form in the arc zone, especially as the anode runs at a much higher temperature than the cathode. Several workers[14,16] have suggested that the graphite particles can be formed in the gas phase.

Surface area measurements ( $\text{CO}_2$ , 273 K) showed that both the raw soot and fullerene-depleted soot (toluene extract) had surface areas  $\sim 220 \text{ m}^2\text{g}^{-1}$ , whereas the graphite rod and the inside and outside of the cathode deposit had surface areas  $< 20 \text{ m}^2\text{g}^{-1}$ . A value of  $267 \text{ m}^2\text{g}^{-1}$  has been reported by Werner *et al.*[15] for the raw soot, in good agreement with the present results.

### 3.3 Reactivity measurements

Isothermal combustion studies were used to characterise the gasification of the carbon materials produced in the carbon arc evaporation process, and the data are given in Table 3. The order of reactivity was as follows:



Table 3. Combustion reactivity data for the products of the carbon arc evaporation process for the synthesis of fullerenes

	Isothermal combustion reactivity at 973 K/gg <sup>-1</sup> s <sup>-1</sup>	Temperature-programmed combustion	
		T <sub>max</sub> /K	CO/CO <sub>2</sub>
Graphite rod	2.85 × 10 <sup>-4</sup>	1103	0.14
Cathode deposit (inside)	2.28 × 10 <sup>-4</sup>	1103	0.15
Cathode deposit (outside)	1.64 × 10 <sup>-3</sup>	963	0.34
Fullerene soot	4.55 × 10 <sup>-3</sup>	653,843,973	0.50
Fullerene soot (toluene extracted)	3.65 × 10 <sup>-3</sup>	653,813,973	0.32
C <sub>60</sub>	—	923	0.82

Cathode deposit (inside)

< graphite rod

≪ cathode deposit (outside)

< fullerene soot (toluene extracted)

< fullerene soot.

It is apparent that there are large differences in reactivity between the inside and outside of the cathode deposit. This is also consistent with the Raman and X-ray data, and also with the higher heat-treatment temperatures in the initial stages of deposition. The activation energies for gasification of the graphite rod and cathode deposit (inside) were 159 and 137 kJ mol<sup>-1</sup>, respectively.

In the DC carbon arc evaporation process, the major products are heterogeneous. Therefore, methods of assessing the heterogeneity are required. Raman microprobe spectroscopy offers high spatial resolution, and this has been demonstrated in the case of the cathode deposit. However, in the case of the fullerene soot, the material other than the graphite fragments is too small for individual particles to be selected for Raman spectroscopy. Therefore, other characterisation techniques need to be used. Temperature-programmed combustion allows materials of different reactivity towards oxygen to be identified. The temperature-programmed combustion of the graphite rod is shown in Fig. 3a. This is symmetrical as expected, and provides a homogeneous standard for comparison purposes. Figures 3b and 3c show the temperature-programmed combustion profiles of the inside and outside of the cathode deposit. The results are consistent with isothermal reactivity studies, with the inside of the cathode deposit being the least reactive. The symmetrical evolved gas profiles suggest that the sample taken from a small area on the inside of the deposit is reasonably homogeneous. In comparison, the temperature-programmed combustion profiles of the graphite rod are very similar. The outside of the cathode deposit is much more reactive, reaching a maximum rate of gasification at 963 K, and shows some evidence for heterogeneity, since the evolved gas profiles extend over a wider temperature range and appear to be composed of three peaks.

The temperature-programmed combustion profiles of C<sub>60</sub> are shown in Fig. 3d. This profile is fairly sym-

metric, indicating a high degree of purity. The onset of C<sub>60</sub> oxidation occurs at approximately 800 K, in agreement with the earlier measurements of Werner *et al.* [15]. The temperature-programmed combustion profiles for the C<sub>60</sub> + C<sub>70</sub> mixture showed a low temperature peak, which can be attributed to the volatilization of small amounts of solvent occluded in the sample.

The temperature-programmed combustion evolved gas profiles of the fullerene soot and the corresponding toluene-extracted material are very similar (see Figs. 3e and f). Both materials are very reactive and have complex combustion profiles due to their heterogeneity. A broadly similar CO<sub>2</sub> evolution profile for the raw soot has been reported previously by Werner *et al.* [15]. The CO and CO<sub>2</sub>-evolved gas profiles start at ~523 K and contain four main peaks. It is difficult to assign these peaks to specific components, since there are complex heat and mass transfer and structural effects. However, the highest temperature peak is approximately 80 K higher in temperature than the C<sub>60</sub> peak and approximately the same temperature as the outer cathode deposit. Graphite has been detected in the fullerene soot by X-ray diffraction techniques, and this may be the source of the high temperature peak. The other three peaks overlap to a large extent and arise from the gasification of the disordered carbon, which has a large surface area.

#### 3.4 Isotope fractionation

The results of the <sup>13</sup>C/<sup>12</sup>C isotope ratio studies are given in Table 4. The isotope fractionation process is expected to be very sensitive to variations in sample geometry and experimental conditions between individual runs. Therefore, each isotope ratio was referenced to the particular graphite rod used in the run. These results are unequivocal, with the cathode deposit having a lower <sup>13</sup>C/<sup>12</sup>C ratio than the graphite rod, whereas the C<sub>60</sub>, C<sub>70</sub>, raw fullerene soot and solvent-extracted fullerene soot ratios are higher than the graphite rod. Since all the species have exclusively carbon-carbon bonds, thermodynamic isotope discrimination effects are insignificant. Hence, only physical diffusional processes will discriminate between <sup>13</sup>C and <sup>12</sup>C, and since these effects are related to mass, only C<sub>n</sub> when n ≤ 3 will be involved. The heavier mass and lower diffusional velocity of <sup>13</sup>C containing C<sub>n</sub> species will have a slightly larger average residence

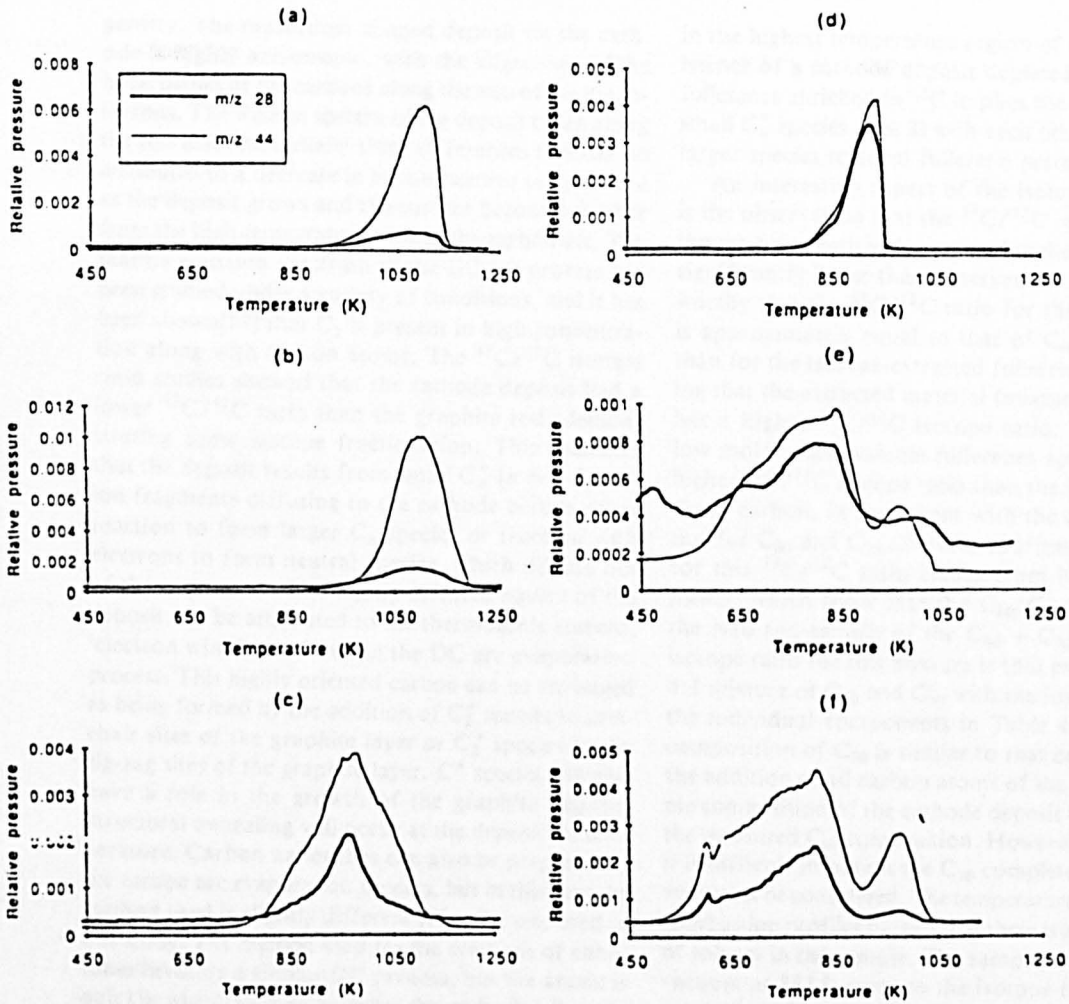


Fig. 3. Temperature programmed combustion profiles for (a) graphite rod, (b) cathode deposit (inside), (c) cathode deposit (outside), (d)  $C_{60}$ , (e) fullerene soot, and (f) fullerene soot (toluene-extracted).

time in the carbon arc plasma zone. This effect will only give rise to significant differences in the diffusion for  $C_n$  where  $n \leq 3$ . Hence, there is a greater probability of the larger  $C_n$  species formed in the hot part of

the carbon arc having been enriched in  $^{13}C$ . On this basis, the formation of  $^{13}C$ -enriched fullerene precursors and other components of fullerene soot requires synthesis of larger  $C_n$  species in the highest temperature part of the zone, which presumably forms fullerenes after diffusing out into the cooler regions of the reactor. However, the cathode deposit is formed by cation  $C_n^+$  species ( $n \leq 3$ ) depleted in  $^{13}C$  that have diffused out into a lower temperature region of the cathode, but deposition still occurs at temperatures in excess of 2273 K.

Table 4.  $^{13}C/^{12}C$  isotope ratios for the product of the carbon arc evaporation process for the synthesis of fullerenes

Series	$\Delta_{GR}$ $^{13}C$ (‰ PDB scale)
Series A	
Fullerene soot	$+1.14 \pm 0.15$
Series N13	
Cathode deposit (outside)	$-1.79 \pm 0.03$
Fullerene soot (toluene extracted)	$+0.60 \pm 0.03$
$C_{60}$	$+1.05 \pm 0.02$
Series N16	
Cathode deposit (1)	$-3.17 \pm 0.03$
Cathode deposit (2)	$-3.43 \pm 0.03$
$C_{60}$	$+1.08 \pm 0.12$
$C_{70}$	$+0.54 \pm 0.12$
$C_{60} + C_{70}$	$+0.96 \pm 0.12$

All measurements are referenced to the graphite rod used in the synthesis of the particular series of samples.

#### 4. DISCUSSION

The results reported in this paper cover the characterisation of all the carbon materials produced during the DC carbon arc evaporation process for the synthesis of fullerenes. The X-ray diffraction and Raman spectroscopic data for the cathode deposit show that it is graphitic, but not as well ordered as the graphite rod. The X-ray diffraction parameters vary across the radial direction, indicating structural hetero-

generality. The mushroom-shaped deposit on the cathode is highly anisotropic, with the alignment of the basal planes of the carbons along the axis of the graphite rods. The Raman spectra of the deposit taken along the rod axis and radially show differences that can be attributed to a decrease in heat-treatment temperature as the deposit grows and the surface becomes further from the high-temperature zone in the carbon arc. The plasma emission spectrum of the DC arc process has been studied under a variety of conditions, and it has been shown[17] that  $C_2$  is present in high concentration along with carbon atoms. The  $^{13}C/^{12}C$  isotope ratio studies showed that the cathode deposit had a lower  $^{13}C/^{12}C$  ratio than the graphite rod, demonstrating some isotope fractionation. This indicates that the deposit results from small  $C_n^+$  ( $n = 1-3$ ) cation fragments diffusing to the cathode before either reaction to form larger  $C_n$  species or reaction with electrons to form neutral species, which diffuse out of the carbon arc. The highly oriented nature of the deposit can be attributed to the thermoionic current, 'electron wind', produced in the DC arc evaporation process. This highly oriented carbon can be envisaged as being formed by the addition of  $C_2^+$  species to arm-chair sites of the graphite layer or  $C_3^+$  species to the zig-zag sites of the graphite layer.  $C^+$  species will also have a role in the growth of the graphite deposit. Structural annealing will occur at the deposition temperature. Carbon nanotubes can also be prepared by the carbon arc evaporation process, but in this case the method used is slightly different from the one used in this study. The method used for the synthesis of nanotubes involves a similar DC process, but the anode is quickly withdrawn away from the cathode after the arc has been established. In this case a low-density deposit results on the cathode, and the nanotubes with their axes oriented parallel to the rod axis are formed. For this process to work, the current must flow over the surface of the hexagonal carbon 'graphene' layers. This represents a similar orientation to that found in the mushroom-shaped cathode deposit formed in the synthesis of fullerenes. Thus, the orientation may be explained by the driving force of transfer of electrons along the direction of lowest electrical resistance (i.e., with the basal plane orientation along the direction of the current).

The fullerene soot is a highly disordered, high surface area material containing a variety of types of material. The sharp  $d_{002}$  peak superimposed on a broad background scattering extending from low scattering angles is due to graphite particles released or formed during the carbon arc evaporation process, since it has a similar  $d_{002}$  spacing and  $I_c$  values to that of the graphite rod. The presence of graphite has been confirmed by Raman microprobe spectroscopy. The raw fullerene soot probably contains less than 10% graphite particles. The  $^{13}C/^{12}C$  ratios for the  $C_{60}$ ,  $C_{70}$ , and fullerene soot are higher than for the graphite rod, indicating enrichment in  $^{13}C$ . The observation that all these species are enriched in  $^{13}C$  indicates they are produced by the same phenomenological process, and from intermediates that have a longer residence time

in the highest temperature region of the arc. The existence of a cathode deposit depleted in  $^{13}C$  and the fullerenes enriched in  $^{13}C$  implies the combination of small  $C_n^+$  species ( $n \leq 3$ ) with each other or with other larger species to form fullerene precursors.

An interesting aspect of the isotope ratio studies is the observation that the  $^{13}C/^{12}C$  ratio for  $C_{70}$ , although being enriched compared to the graphite rod, is significantly lower than observed for  $C_{60}$ . It is noteworthy that the  $^{13}C/^{12}C$  ratio for the fullerene soot is approximately equal to that of  $C_{60}$  and is higher than for the toluene-extracted fullerene soot, indicating that the extracted material (mixture of fullerenes) has a higher  $^{13}C/^{12}C$  isotope ratio. Therefore, the low molar mass soluble fullerenes appear to have a higher  $^{13}C/^{12}C$  isotope ratio than the insoluble disordered carbon, in agreement with the data on the ratios for  $C_{60}$  and  $C_{70}$ . Further confirmatory evidence for this  $^{13}C/^{12}C$  ratio comes from NMR measurements, which show that the  $C_{60}:C_{70}$  ratio is 4:1 in the N16 run sample of the  $C_{60} + C_{70}$  mixture. The isotope ratio for this mixture is that expected from a 4:1 mixture of  $C_{60}$  and  $C_{70}$  with the isotope ratios for the individual components in Table 4. The isotopic composition of  $C_{70}$  is similar to that calculated from the addition of 10 carbon atoms of the average isotopic composition of the cathode deposit to 60 atoms of the measured  $C_{60}$  composition. However, the fact that it is difficult to obtain the  $C_{70}$  completely free of solvent must be considered. The temperature-programmed combustion profiles suggest that there is a small amount of solvent in the sample. The sample was dried under vacuum at 383 K prior to the isotope ratio measurements in order to remove as much of the solvent as possible. The data in Table 4 allow an approximate mass balance to be carried out. We assume the carbon arc evaporation products to consist of cathode deposit (15%) and fullerene soot (85%) with the latter yielding 10% fullerenes divided in the  $C_{60}:C_{70}$  ratio of 4:1 and 10% graphite particles. It is apparent that there is an approximate mass balance in the isotope ratio measurements. Thus, account has been taken of all the carbon species produced during the carbon arc evaporation.

The mechanisms proposed for the formation have been discussed previously[3,18]. There are several possible explanations in terms of the formation mechanism for these observations of isotope fractionation within the fullerenes. These relate to the growth and reaction of fullerenes leading to the formation of high yields of  $C_{60}$  and  $C_{70}$ . Both the 'fullerene road' and the 'collapse of larger fullerene' mechanisms predict[3] higher yields of  $C_{60}$  relative to  $C_{70}$ . The isotope fractionation studies are consistent with the interconversion of fullerenes involving  $C_n$  species where  $n \leq 3$ .

Laser vapourisation of graphite shows three distinct regions[4,19] in the mass spectrum corresponding to different molar mass species.

1. Low molar mass species:  $C_n$  where  $n \leq 3$  with high intensities for  $C_2$  and  $C_3$ . These species are responsible for the isotope fractionation.



- Intermediate molar mass species:  $C_n$  where  $8 < n < 28$  with slightly higher intensities for  $C_{11}$ ,  $C_{15}$ ,  $C_{19}$ ,  $C_{23}$  species.
- Fullerenes:  $C_n$  where  $n \geq 32$  and unusually high intensities for  $C_{60}$  and, to a lesser extent,  $C_{70}$ .

When considering the mechanism for the formation of fullerenes, the following facts need to be considered[19].

- Isotope distribution studies show[19-22] that the growth process leading to fullerenes involves individual carbon atoms.
- Cationic species appear to play an important role in the growth process[23].
- The coalescence of cationic carbon ring species produces fullerenes in ion/molecule reactions. There is a size-selective growth process[24,25].
- Optimum fullerene yields occur over a narrow range of reaction conditions.
- If reactive gases,  $H_2$ [26-28] and  $Cl_2$ [29] are added to the helium under the DC carbon arc process, in some cases polyynes and polynuclear aromatics containing five-membered rings are produced, depending on the gas. These are possible intermediates in the synthesis of fullerenes.

A reaction scheme for the formation of graphite and fullerene soot in the DC carbon arc evaporation based on the results obtained in this study and given in the literature is shown in Fig. 4. The low molar mass  $C_n^+$  species ( $n \leq 3$ ) can diffuse rapidly to the cathode,

react with other carbon species, or react with electrons to become a neutral species. The  $^{12}C$  species have a lower diffusion time and higher diffusion velocity, thereby leading to increased amounts of  $^{12}C$  relative to  $^{13}C$  in the cathode deposit. The  $^{13}C$  species will have a greater probability of reacting with other carbon species, thereby increasing the diffusion time, or of reacting with electrons present in the plasma arc to form neutral species. The neutral species diffuse rapidly out of the arc to react with other species, forming raw fullerene soot. The isotope fractionation within the fullerene materials ( $C_{60}$ ,  $C_{70}$ , etc.) is related to the probability of the  $C_n^+$  where  $n = 1-3$  becoming enriched in  $^{13}C$ . Clearly, the extent of  $^{13}C$  enrichment will be in the order  $C_1^+ > C_2^+ > C_3^+$ , etc. The fullerene growth mechanism relies on the reaction of these small carbon species. It is more likely that the higher molar mass species will have been formed from larger amounts of  $C_2$  and  $C_3$  species, which have lower levels of enrichment in  $^{13}C$  than the  $C_1$  species. Hence, the levels of enrichment of  $^{13}C$  in the fullerenes will decrease with increasing molar mass, and this has been observed in this study.

Recent work has shown that fullerenes can be synthesised from the pyrolysis of naphthalene at  $1000^\circ C$ [30]. This suggests that  $C_{60}$  formation can be ascribed from the combination of  $C_{10}$  species at low temperatures, compared with the carbon arc process. Therefore, reactions in the lower temperature regions of the carbon arc reactor to form fullerenes are possible. These larger fullerene precursor species are formed from the small  $C_n$  species produced in the carbon arc. The observation that the structure of the

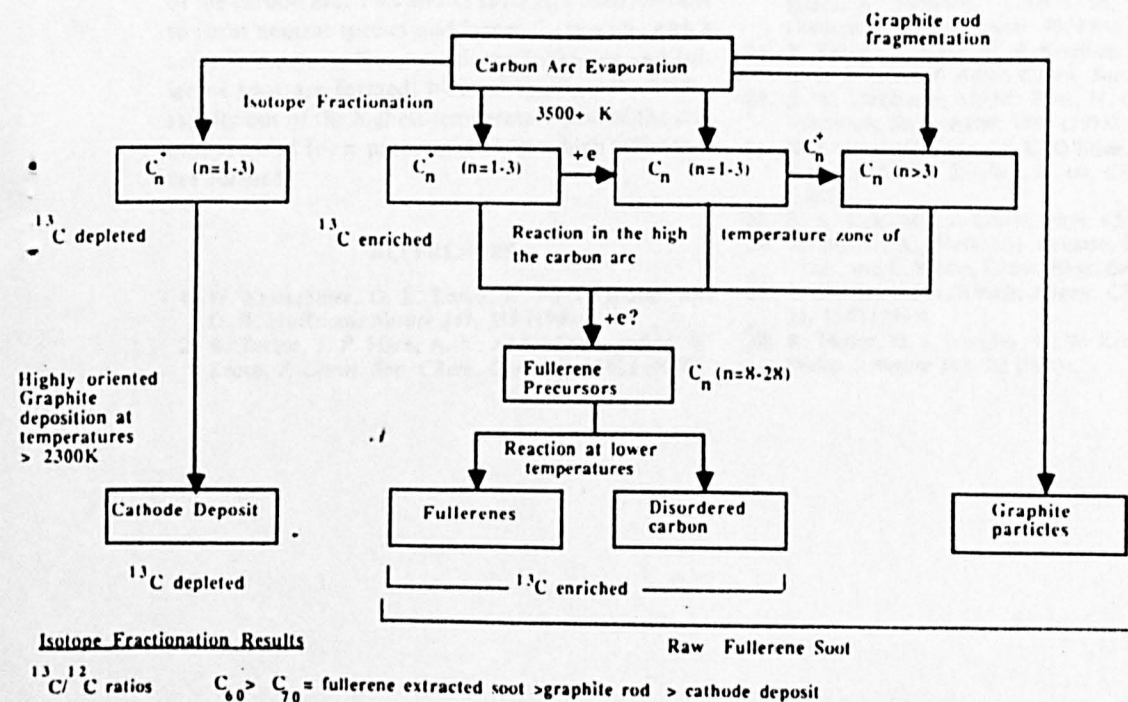


Fig. 4. A schematic diagram of the formation of fullerenes, graphites, and disordered carbons in the carbon arc evaporation process.

extracted fullerene soot changes on heat treatment supports the view that carbon vapour reacts in the lower temperature regions to form raw fullerene soot (fullerenes and disordered carbon).

### 5. CONCLUSIONS

The synthesis of fullerenes using the carbon arc evaporation method involves a complex series of physical and chemical processes. The results show that highly symmetric fullerenes ( $C_{60}$ , etc.) and a highly ordered graphite deposit on the cathode are produced in high yields, which is surprising, bearing in mind the extremely high energies involved in producing and condensing the carbon vapour. The carbon deposit on the cathode is highly oriented. The alignment of the basal planes of the deposit along the axis of the graphite rod is thought to be related to the flow of electrons in relation to the direction of minimum electrical resistance of the graphite basal plane layers. In comparison, the fullerene soot is a very heterogeneous, high surface area material, which contains a small amount of graphite, probably due to fragmentation of the graphite rod during the carbon arc evaporation. Isotope fractionation occurs during the carbon arc evaporation process. The cathode deposit is depleted in  $^{13}C$  relative to the graphite rod, whereas  $C_{60}$ ,  $C_{70}$ , and the solvent-extracted fullerene soot and fullerene soot are enriched in  $^{13}C$ . The results suggest that the cathode deposit is formed from small  $C_n^+$  species ( $n \leq 3$ ), which have a higher probability of diffusing to the cathode before reaction. The carbon species ( $C_n^+$  where  $n \leq 3$ ) containing  $^{13}C$  are slower diffusing compared with the corresponding  $^{12}C$  species, and hence have a higher residence time in the hottest zone of the carbon arc. This allows sufficient reaction time to form neutral species and larger  $C_n$  species, which are intermediates from which the fullerenes and fullerene soot are formed. Neutral species will diffuse rapidly out of the highest-temperature part of the carbon arc and form precursors from which fullerenes are formed.

### REFERENCES

1. W. Kratschmer, D. L. Lamb, K. Fostiropoulos, and D. R. Huffman, *Nature* 347, 354 (1990).
2. R. Taylor, J. P. Hare, A. K. Abdul-Sada, and H. W. Kroto, *J. Chem. Soc. Chem. Commun.*, 1423 (1990).
3. R. F. Curl, *Nature* 363, 14 (1993).
4. R. E. Smalley, *Accts. Chem. Res.* 25, 98 (1992).
5. J. R. Heath, In *Fullerenes: Synthesis, Properties and Chemistry of Large Carbon Clusters* (Edited by G. S. Hammond and V. J. Kuck), pp. 1-23. American Chemical Society, Washington, DC (1991).
6. A. Goeres and E. Sedlmayr, *Chem. Phys. Lett.* 184, 310 (1991).
7. T. Wakabayashi and Y. Achiba, *Chem. Phys. Lett.* 190, 465 (1992).
8. G. van Heiden, N. G. Gotts, and M. T. Bowers, *Nature* 363, 60 (1993).
9. Y. Saito, M. Inagaki, H. Shinohara, H. Nagashima, M. Ohkohchi, and Y. Ando, *Chem. Phys. Lett.* 200, 643 (1992).
10. A. Mittelbach, W. Honle, H. G. von Schnering, J. Carlsson, R. Janiak, and H. Quast, *Angew. Chem. Int. Ed. Eng.* 31, 1640 (1992).
11. T. W. Ebbesen and P. M. Ajayan, *Nature* 358, 220 (1992).
12. K. M. Thomas, F. Dillon, S. Bottrell, P. K. K. Louie, and K. D. Bartle, *Carbon* 31, 273 (1993).
13. P. Lespade, A. Marchand, M. Couzi, and F. Cruege, *Carbon* 22, 375 (1984).
14. J. C. Scanlon and L. B. Ebert, *J. Phys. Chem.* 97, 7138 (1993).
15. H. Werner, D. Hersin, J. Blocker, B. Henschke, and U. Tegtmeier, *Chem. Phys. Lett.* 194, 62 (1992).
16. L. S. K. Pang, M. A. Wilson, G. H. Taylor, J. Fitzgerald, and L. Brunckhorst, *Carbon* 30, 1130 (1992).
17. T. W. Ebbesen, H. Hiura, J. Fujita, Y. Ochiai, S. Matsui, and K. Tanigaki, *Chem. Phys. Lett.* 209, 83 (1993).
18. H. Schwarz, *Angew. Chem. Int. Ed. Eng.* 32, 1412 (1993).
19. S. W. McElvany, M. R. Ross, and J. H. Callahan, *Acc. Chem. Res.* 25, 162 (1992).
20. J. M. Hawkins, A. Meyer, S. Loren, and R. Nunlist, *J. Am. Chem. Soc.* 113, 9394 (1992).
21. T. W. Ebbesen, J. Tabuchi, and K. Tanagaki, *Chem. Phys. Lett.* 191, 336 (1992).
22. G. J. Meijer and D. S. Bethune, *J. Chem. Phys.* 93, 7800 (1990).
23. R. F. Bunshah, S. Jou, S. Prakash, H. J. Doerr, L. Issacs, A. Wehosig, C. Yeretizian, H. Cynn, and F. Diederich, *J. Phys. Chem.* 96, 6866 (1992).
24. Y. Rubin, M. Kahr, C. B. Knobler, F. Diederich, and C. L. Wilkins, *J. Amer. Chem. Soc.* 113, 495 (1991).
25. S. W. McElvany, M. M. Ross, N. C. Goroff, and F. Diederich, *Science* 259, 1594 (1993).
26. R. J. Heath, Q. Zhang, S. C. O'Brien, R. F. Curl, H. W. Kroto, and R. E. Smalley, *J. Am. Chem. Soc.* 109, 359 (1987).
27. E. A. Rohlfung, *J. Chem. Phys.* 93, 285 (1990).
28. M. Broyer, A. Goeres, M. Pellarin, E. Sedlmayr, J. L. Vialle, and L. Wöste, *Chem. Phys. Lett.* 198, 128 (1992).
29. T. Grosser and A. Hirsch, *Angew. Chem. Int. Ed. Eng.* 32, 1340 (1993).
30. R. Taylor, G. J. Langley, H. W. Kroto, and D. R. M. Walton, *Nature* 366, 23 (1993).

# A simple three-dimensional model of diffusion-with-precipitation applied to localised pyrite formation in framboids, fossils and detrital iron minerals

R. Raiswell<sup>a</sup>, K. Whaler<sup>a</sup>, S. Dean<sup>a</sup>, M.L. Coleman<sup>b</sup> and D.E.G. Briggs<sup>c</sup>

<sup>a</sup>Department of Earth Sciences, Leeds University, Leeds, LS2 9JT, UK

<sup>b</sup>Postgraduate Research Institute for Sedimentology, University of Reading, Reading, RG6 2AB, UK  
and BP Research and Engineering Centre, Chertsey Road, Sunbury-on-Thames, Middlesex, TW16 7LN, UK

<sup>c</sup>Department of Geology, Bristol University, Bristol, BS8 1RJ, UK

(Received and accepted May 5, 1993)

## ABSTRACT

Raiswell, R., Whaler, K., Dean, S., Coleman, M.L. and Briggs, D.E.G., 1993. A simple three-dimensional model of diffusion-with-precipitation applied to localised pyrite formation in framboids, fossils and detrital iron minerals. In: R.J. Parkes, P. Westbrook and J.W. de Leeuw (Editors), *Marine Sediments, Burial, Pore Water Chemistry, Microbiology and Diagenesis*. *Mar. Geol.*, 113: 89–100.

A three-dimensional diffusion-with-precipitation model is constructed to estimate radial variations in the amounts of pyrite which precipitate where a spherical mass of organic matter, producing H<sub>2</sub>S by sulphate reduction, is enveloped in a dissolved-iron bearing porewater. The model indicates that higher rates of sulphate reduction (more readily metabolisable organic matter), and larger organic masses, require increasingly high dissolved iron concentrations in order to confine pyrite (or iron sulphide) precipitation to the decay site. The maximum size sphere of exceedingly metabolisable organic matter (equivalent to fresh planktonic material) which can be pyritised is about 50 µm radius, where decay occurs in porewaters with typical dissolved iron levels. This radius is close to the maximum radius of framboidal pyrite, the formation of which could involve model-type processes. Fossil carcasses, although mainly composed of less readily metabolisable organic matter, may be orders of magnitude larger and the model demonstrates that their pyritisation requires unusually high porewater dissolved iron concentrations. These inferred chemical conditions are consistent with sedimentological observations of pyritisation in Beecher's Trilobite Bed (New York State). At greater depths within the sediment, pyritisation is controlled by the kinetics of iron mineral reactivity towards H<sub>2</sub>S. Sediments vary widely in their exposure times to H<sub>2</sub>S which can range at least from 50 to > 10<sup>6</sup> years. At low exposure times only iron oxides are pyritised, whereas at high exposure times even the most refractory iron silicates can become pyritised.

## Introduction

Pyrite is unusual in exhibiting a wide variety of aggregated forms over scales which range from the microscopic (e.g. framboids, clusters) to the macroscopic (e.g. pyritised faecal pellets and burrows, pyritised fossils and pyrite concretions and lenses). This wealth of detail has generally discouraged any search for a common pattern to these phenomena, although the detail itself must reflect subtle variations in diagenetic conditions. Thus an understanding of the controls of localised pyrite formation might be of considerable palaeoenvironmental

value. One promising approach (Canfield and Raiswell, 1991) recognised that the associations between pyrite and organic matter differ mainly in the position of pyrite precipitation with respect to the boundary layer between the organic matter decay site and the enveloping sediment.

Canfield and Raiswell (1991) used a simple diffusion-plus-precipitation model derived by Helfferich and Katchalsky (1970) to show how the location (and extent) of pyrite precipitation depends on porewater composition and the rate of sulphate reduction at the decay site. This model has been used to explain the pyritisation of soft-



bodied fossils (Briggs et al., 1991; Raiswell, 1992) and the formation of pyrite zones at the margins of carbonate concretions (Coleman and Raiswell, in press).

The model of Helfferich and Katchalsky (1970) envisages two infinite reservoirs which contain solutions of dissolved sulphide (representing organic matter decaying by sulphate reduction) and dissolved ferrous iron (representing porewaters in the surrounding sediments). The reservoirs are joined by a permeable plug along which the solutes diffuse, react and precipitate. The locus of precipitation is controlled principally by the ratio of the reservoir concentrations of dissolved sulphide and iron, such that an increase in the ratio drives precipitation towards the lower concentration reservoir. The model is idealised in a number of respects, the most serious limitation perhaps being its 1-D nature.

Here we derive a 3-D model (see Appendix), assuming that a spherical organic matter decay site (Fig. 1) is completely buried in a sediment with iron-rich porewater. The model is quantified by expressions which show the rate of precipitation ( $j$ ) as a function of radial distance ( $r$ ) from the centre of the decay site, and the position of the precipitation maxima ( $R_{j\max}$ ). In conjunction with modern sediment data these results can be used to provide fresh insights into localised pyritisation as framboids, the pyritisation of soft-bodied organisms, and the replacement of detrital iron phases by pyrite.

#### Evidence from modern anoxic sediments

Pyrite forms in anoxic marine sediments by reaction between detrital iron minerals and the  $H_2S$  generated by sulphate-reducing bacteria (Goldhaber and Kaplan, 1974). In marine sediments iron and sea water sulphate are normally present in abundance and pyrite formation is apparently limited by the concentration of metabolisable organic carbon (Berner, 1970, 1984).

A common misconception is that sediments supporting rapid rates of sulphate reduction (tens to hundreds of mmol/litre per year), such as are typical of continental margin sediments are necessarily rich in dissolved sulphide. Although this is often

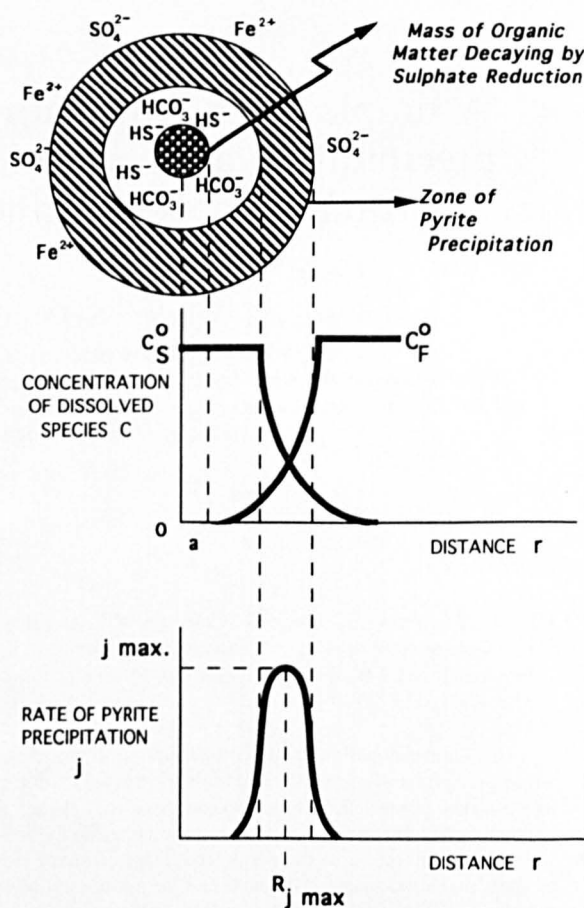
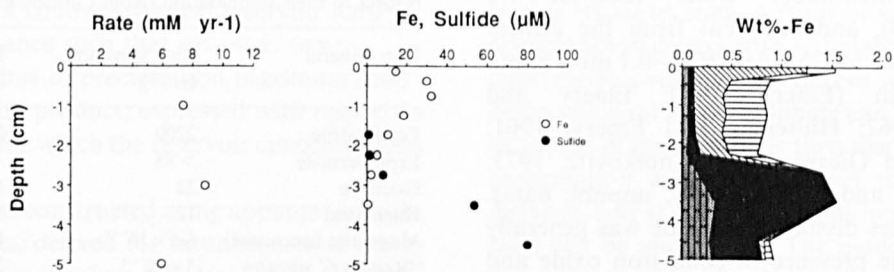


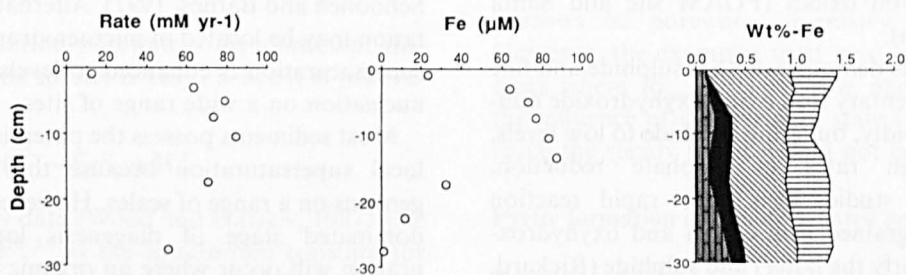
Fig. 1. A spherical mass of organic matter (radius  $a$ ) decaying by sulphate reduction maintains a steady state concentration  $C_S^0$  of dissolved sulphide which diffuses into pore waters containing a dissolved iron concentration  $C_F^0$ .

the case, some sediments with active sulphate reduction never accumulate dissolved sulphide (an example is the Mississippi Delta; Canfield, 1989). In addition, in most continental margin sediments supporting sulphate reduction, the most rapid rates (which are usually found within several centimetres of the sediment surface) are rarely associated with elevated levels of dissolved sulphide (Canfield and Raiswell, 1991; Fossing, 1990). This is illustrated by the relationships between sulphate reduction rates, sediment pore-water chemistry, and solid phase iron speciation in three contrasting marine sediments (Fig. 2). Three sites are considered; the well studied FOAM site in Long Island Sound (Goldhaber et al., 1977; Aller 1980a,b;

### Santa Barbara Basin



### Sta 18



### FOAM

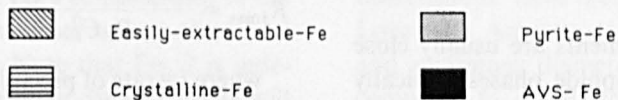
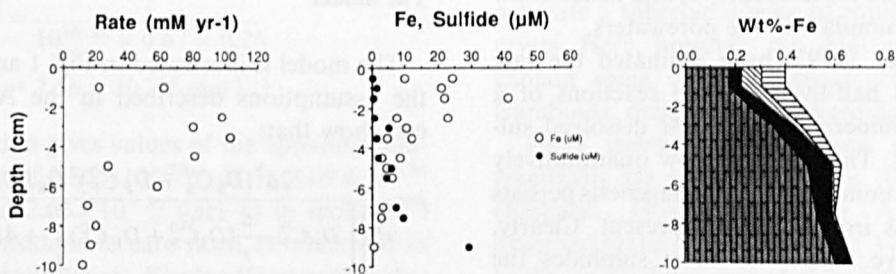


Fig. 2. Sulphate reduction rates, porewater dissolved iron and sulphide concentrations, and solid phase iron speciation for sediments from FOAM (Long Island Sound), Sta 18 (Mississippi Delta) and the Santa Barbara Basin, *AVS-Fe* represents all acid-volatile sulphide, easily-extractable Fe represents mainly lepidocrocite and ferrihydrite, and crystalline Fe represents goethite and haematite. From Canfield and Raiswell (1991).



Krishnawami et al., 1984; Berner and Westrich, 1985); a rapidly depositing sediment from the subaqueous Mississippi Delta (Station 18; Canfield, 1989), and sediment from the central depression in the low-oxygen (0.05–0.1 ml/l) Santa Barbara Basin (Emery, 1960; Emery and Hülseman, 1962; Hülseman and Emery, 1961; Sholkovitz and Gieskes, 1971; Sholkovitz, 1973; D.A. Canfield and C.E. Reimers, unpubl. data). At all three sites dissolved sulphide was generally very low in the presence of solid iron oxide and oxyhydroxide mineral phases, regardless of sulphate reduction rate. Significantly, the depth at which sulphide accumulation begins in sediment porewaters almost coincides with that where the formation of iron sulphide minerals has exhausted solid phase iron oxides (FOAM site and Santa Barbara Basin).

These results demonstrate that sulphide and fine grained sedimentary iron oxide/oxyhydroxide minerals react rapidly, buffering sulphide to low levels, even at high rates of sulphate reduction. Experimental studies also show rapid reaction between fine-grained iron oxides and oxyhydroxides (particularly the latter) and sulphide (Rickard, 1974; Pyzik and Sommer, 1981; Canfield, 1989). The iron-containing minerals that remain, typically accounting for a majority of the iron in the sediment (Canfield, 1988) include silicates and minor iron oxides (e.g. magnetite and iron-containing spinels) which are far less reactive, and hence allow sulphide to accumulate in the porewaters.

Canfield et al. (1992) have estimated the rate constants (and half-lives) for the reactions of a range of iron minerals with 1 mM dissolved sulphide (Table 1). These values show quantitatively how the iron-dominated stage of diagenesis persists only as long as iron oxides are present. Clearly, once these have reacted to form sulphides the residual iron phases (mainly silicates) react too slowly to prevent the change to dissolved sulphide-dominated porewaters.

Both porewater environments are usually close to saturation with iron sulphide phases, typically mackinawite (Canfield and Raiswell, 1991). In these circumstances the locations of pyrite (or iron sulphide) precipitation may be controlled by the availability of suitable nucleation sites (see

TABLE 1

Rate constants and half-lives of sedimentary iron minerals with respect to their sulphidation (from Canfield et al., 1992)

Iron mineral	Rate constant (yr <sup>-1</sup> )	Half-life
Ferrihydrite	2200	2.8 hours
Lepidocrocite	> 85	< 3 days
Goethite	22	11.5 days
Haematite	12	31 days
Magnetite (uncoated)	6.6 × 10 <sup>-3</sup>	105 days
"Reactive" silicates	3 × 10 <sup>-3</sup>	230 years
Sheet silicates	8.2 × 10 <sup>-6</sup>	84,000 years
Ilmenite, garnets, Augite, amphibole	<< 8.2 × 10 <sup>-6</sup>	>> 84,000 years

Schoonen and Barnes, 1991). Alternatively precipitation may be located in microenvironments where supersaturation is enhanced to levels which allow nucleation on a wide range of sites.

Most sediments possess the potential to generate local supersaturation because they are heterogeneous on a range of scales. However, in the iron-dominated stage of diagenesis local supersaturation will occur where an organic matter decay site generates dissolved sulphide, whereas in the sulphide-dominated stage local supersaturation will occur (but only on a microscopic scale) where unreacted detrital iron phases are available.

### The model

The model is illustrated in Fig. 1 and, subject to the assumptions described in the Appendix, we can show that:

$$j = \frac{2a^2(D_S C_S^0 + D_F C_F^0)^2 D_S D_F K}{r^4 \left\{ \left[ D_F C_F^0 - \frac{a}{r} (D_S C_S^0 + D_F C_F^0) \right]^2 + 4D_S D_F K \right\}^{3/2}} \quad (1)$$

$$R_{j\max} = \frac{a(D_S C_S^0 + D_F C_F^0)}{D_F C_F^0} \quad (2)$$

where  $j$  = rate of precipitation (moles cm<sup>-3</sup> yr<sup>-1</sup>) at a distance  $r$  (cm), where  $a < r < \infty$

$D_S, D_F$  = diffusion coefficients for dissolved sulphide and dissolved iron, respectively (cm<sup>2</sup> yr<sup>-1</sup>)

$C_S^0, C_F^0$  = reservoir concentrations of dissolved

sulphide and dissolved iron respectively (moles  $\text{cm}^{-3}$ )

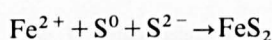
$a$  = radius of central spherical reservoir (cm)

$r$  = any distance such that  $a < r < \infty$  (cm)

$R_{j_{\max}}$  = radius of precipitation maximum (cm)

$K$  = solubility product, expressed with respect to those species for which the reservoir concentrations are defined.

The model is constructed using apparent equilibrium constants, derived for saturation state calculations in sea water (see Boudreau and Canfield, 1988). Goldhaber and Kaplan (1974) define the ion activity product of pyrite from:



$$K = 2.4 \times 10^{-28} \text{ moles}^2 \text{ litres}^{-2}$$

In most marine porewaters the dominant dissolved sulphide species is  $\text{HS}^-$ , hence it is preferable to write:



Free energy data (Wood and Garrels, 1987) give a value of  $10^{16.35}$  as the equilibrium constant for this reaction. The activity coefficients for  $\text{HS}^-$  and  $\text{Fe}^{2+}$  in sea water are 0.67 and 0.26 (see Boudreau and Canfield, 1988), so an apparent solubility product for pyrite can be expressed (in concentration units) as

$$\frac{[\text{Fe}^{2+}][\text{HS}^-]}{[\text{H}^+]} = \frac{1}{10^{16.35} \times 0.67 \times 0.26}$$

$$= 2.56 \times 10^{-16} \text{ mol l}^{-1}$$

This equation gives values of the apparent solubility product of  $2.56 \times 10^{-29}$  ( $p\text{H}$  7),  $8.09 \times 10^{-30}$  ( $p\text{H}$  7.5) and  $2.56 \times 10^{-30}$  ( $p\text{H}$  8) in  $\text{mol cm}^{-3}$ . However, considerable care must be exercised in choosing an appropriate  $K$  value (for example due to the possible involvement of different FeS precursors) and in some cases it may be preferable to use empirical values based on observations of natural or experimental systems. Note that Eq. 2 is independent of  $K$  and the examples discussed here will use only this result. Values of  $D_s$  and  $D_F$  for sea water are 376 and 149  $\text{cm}^2 \text{ yr}^{-1}$ , respectively (Boudreau and Canfield, 1988).

Initially the model assumes that sulphide diffuses

away from a spherical organic matter decay site, and reacts with dissolved iron to precipitate pyrite. In this transient state, a front of sulphide (whose concentration decays with radial distance from the concretion) continues to diffuse away from the decay site until all the sulphide can be precipitated as pyrite. A steady state is then reached and pyrite precipitation will continue over the same radial distance, and at the same site, as long as the steady state can be maintained. The model allows  $j$  (the rate of pyrite precipitation) to be calculated, at a steady state, as a function of radial distance from the centre of the spherical decay site.

Near-steady state conditions are often reached in modern sediments (e.g. Berner, 1980), and appear also to hold in modelling the influence of burrows on porewater chemistry (Aller, 1977). However, the examples used here are confined to cases where  $R_{j_{\max}}$  is close to  $a$ , and hence where the influence of the transient state (or a failure to reach the steady state) should not be significant.

### Pyrite formation in iron-dominated porewaters

#### *Framboidal pyrite*

Framboidal pyrite has been the subject of numerous investigations (e.g., Love and Amstutz, 1966; Rickard, 1970) aimed mainly at identifying the physical and chemical conditions needed to generate a spheroidal mass of equigranular microcrystals. Here, however, we shall attempt only to explain some of the external characteristics of framboids; their size and spheroidicity.

There seems to be common agreement that framboids are rarely more than 100  $\mu\text{m}$  diameter (Rickard, 1970). Love and Amstutz (1966) observed maximum diameters of 34  $\mu\text{m}$ , compared to 40  $\mu\text{m}$  by Raybould (1973), 100  $\mu\text{m}$  (Massaad, 1974) and 60  $\mu\text{m}$  (Al-Biatty, 1990). Rather fewer observations have been made of sphericity but Love and Amstutz (1966) show that maximum and minimum diameters are in the ratio 1.2:1, compared to <1.3:1 for the samples measured by Al-Biatty (1990).

Rickard (1970) discussed possible reasons for the nearly-spherical form of framboidal pyrite, which he attributed to the infilling of organic

globules by pyrite. However, framboids are frequently the earliest and most rapidly formed pyrite phase in a sediment, as can be demonstrated texturally and isotopically (e.g., Raiswell, 1982). In fact sulphur isotope values usually indicate formation from porewaters which were not sulphate-depleted and were therefore close enough to the sediment/water interface to maintain free diffusive connections to the overlying sea water. Porewaters close to the sediment/water interface are usually iron-dominated (see earlier) and thus local supersaturation could be created where organic matter decay generated  $H_2S$ . The resulting vacuoles of organic matter and  $H_2S$  could produce the iron sulphide spheres which Sweeney and Kaplan (1973) found to be precursor framboids (but see Butler and Rickard, in prep.). Surface tension forces would keep the vacuoles spherical, provided the organic matter was partially or wholly fluid (and immiscible with water). The case where framboids are located at organic matter decay sites can be modelled as below; it may not be the only mechanism for the formation of framboids.

In this case the diffusion-plus-precipitation model envisages a spherical mass of organic matter (radius  $a$ ) immersed in an iron-dominated porewater. The model does not unfortunately cover the case where precipitation occurs in the organic matter (the region 0 to  $a$ ) but the probable circumstances in which this could occur can be predicted using Eq. 2. Clearly  $Rj_{max}$  approaches  $a$  for  $C_S^0/C_F^0 < 1$ ; that is iron-rich porewaters are required to prevent diffusive loss of dissolved sulphide and thus confine pyrite formation to the decay site. An arbitrary but realistic choice for  $C_S^0/C_F^0$  might be 0.1. Note that the expression for  $Rj_{max}$  is independent of  $K$  so model predictions are here independent of the nature of the iron sulphide phase which is first formed.

The next step is to estimate the value of  $C_S^0$  that is likely to exist in the vicinity of organic matter decaying by sulphate reduction at a rate  $R$  (moles  $cm^{-3} yr^{-1}$ ).

Dissolved sulphide will be produced at a rate of  $4/3\pi a^3 R$  moles  $yr^{-1}$  and its flux through any surface radius  $r$  ( $\geq a$ ) is therefore:

$$\text{Flux} = \frac{4/3\pi a^3 R}{4\pi r^2} = \frac{a^3 R}{3r^2} \text{ moles } cm^{-2} yr^{-1}$$

Using Fick's Law,

$$\frac{a^3 R}{3r^2} = -D_s \frac{dc}{dr}$$

where  $c$  = concentration of dissolved sulphide

$$\int dc = \int dr \left( -\frac{a^3 R}{3D_s r^2} \right)$$

Integrating with respect to  $c$  and using  $c \rightarrow 0$  when  $r = \infty$  gives:

$$c = \frac{a^3 R}{3D_s r}$$

So when  $r = a$ ,  $c = C_S^0$ :

$$C_S^0 = \frac{a^3 R}{3D_s a} = \frac{a^2 R}{1128} \text{ moles } cm^{-3} \quad (3)$$

Now  $R$  must be expressed in terms of  $k$ , the first order rate constant for organic matter decay by sulphate reduction. Berner (1964) gives:

$$R = -LkG \text{ moles } cm^{-3} yr^{-1} \quad (4)$$

where  $L = 1/2$  (the stoichiometric coefficient relating the number of moles of dissolved sulphide produced from one mole of organic matter) and  $G$  is the concentration of metabolisable organic matter. For a spherical mass of organic matter, density  $\rho$  ( $1.1 \text{ g } cm^{-3}$ ).

$$G = \rho/30 \text{ moles } cm^{-3}$$

Hence substituting into Eq. 4 gives:

$$R = -0.018k \quad (5)$$

The minus sign simply indicates a decay process, and substituting Eq. 5 into Eq. 3 therefore gives:

$$C_S^0 = 1.6 \times 10^{-5} a^2 k \text{ moles } cm^{-3} \quad (6)$$

Equation 6 is plotted in Fig. 3, assuming a range of  $a$  from  $10 \mu m$  to  $1 \text{ m}$ . However, it was assumed earlier that  $C_S^0/C_F^0 < 0.1$  is required to localise pyrite formation at the decay site. Furthermore observations of modern anoxic sediments suggest that  $C_F^0$  rarely exceeds  $10^{-4} \text{ moles } l^{-1}$  (see Fig. 2), thus  $C_S^0$  must be  $< 10^{-8} \text{ moles } cm^{-3}$  in order that pyrite formation occurs at the decay site.

Estimates for the rate constants of organic matter decay by sulphate reduction were summa-



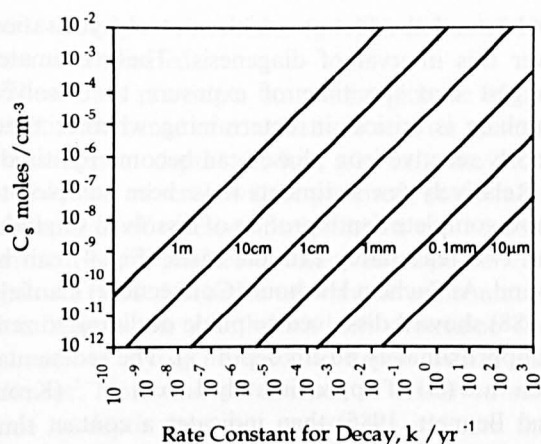


Fig. 3. Relationship between reservoir concentration of dissolved sulphide ( $C_S^0$ ) at the decay site and organic matter rate constant ( $k$ ), for organic masses of different radii.  $C_S^0 < 10^{-8}$  moles  $\text{cm}^{-3}$  is required for pyritisation of the organic mass (see text).

risied by Middelburg (1989). Highest recorded  $k$  values are  $> 10 \text{ yr}^{-1}$  in laboratory experiments or 1 to  $0.1 \text{ yr}^{-1}$  in sediments (based on  $^{35}\text{S}$  measurements). Since the sediment data are averaged over depth intervals we may assume that laboratory  $k$  values on materials such as plankton represent realistic estimates of transient, very highly metabolisable material. With  $k = 10 \text{ yr}^{-1}$  values of  $C_S^0 < 10^{-8}$  moles  $\text{cm}^{-3}$  can only be obtained for organic spheres with radii less than about  $50 \mu\text{m}$  (Fig. 3). This value is close to the typical maximum size of framboidal pyrite; larger organic masses of this readily metabolisable organic matter would lose too much dissolved sulphide to their surroundings unless unusually high porewater iron concentrations were present.

Inevitably this type of modelling is subject to errors. For example, increasing the assumed  $C_S^0/C_F^0$  (or decreasing  $k$ ) by an order of magnitude produces a  $10^{0.5}$  increase in the maximum possible sphere radius. The assumptions are also idealised and may be unrealistic in some cases (see Appendix). Thus larger spheres of organic matter may decay only at the surface, rather than uniformly throughout their volume. Furthermore the model gives no indication as to how the internal microcrystalline structure of framboidal pyrite originates and there may in addition be other mechanisms of framboid formation. However, if

the mechanisms envisaged here are correct, then the maximum size of framboids provides a measure of the maximum concentrations of dissolved iron which occurred during early diagenesis. It would be possible to test this hypothesis on modern sediments, and thus calibrate maximum framboid size as a paleoenvironmental indicator.

#### *The pyritisation of soft-bodied fossils*

Although pyrite occurs in most marine sediments as a framboidal phase, it is also commonly associated with fossils. However, these are usually the remains of biomineralised or at least refractory tissues, and only rarely does pyrite contribute significantly to the preservation of more metabolisable soft-tissues. Two such occurrences have been documented, Beecher's Trilobite Bed (Ordovician, New York State) and the Hunsrückschiefer (Devonian, western Germany), both of which are characterised by preservation of delicate, readily metabolisable material. In Beecher's Bed the fauna is dominated by trilobites, but a much wider range of taxa are preserved in the Hunsrückschiefer including trilobites, cephalopods, ctenophores and fishes. The pyritisation of these organisms has been studied by Briggs et al. (1991, in press). The diffusion-plus-precipitation model can also be used to identify the chemical conditions required for this unusual style of preservation.

Even where the assumption of spherical geometry is unrealistic for these organisms, the equations will provide an indication of the conditions necessary for the pyritisation to occur. Thus the scarcity of soft part pyritisation can be predicted (Fig. 3) by the same constraints outlined above ( $C_S^0/C_F^0 < 0.1$ ,  $C_F^0$  normally less than  $10^{-7}$  moles  $\text{cm}^{-3}$ ). Rate constants ( $k$ ) for the decay of organism soft-parts are probably similar to the most rapid values observed in modern sediments ( $1$  to  $0.1 \text{ yr}^{-1}$ ). Soft parts with these  $k$  values, and radii of  $0.1$ – $1.0 \text{ cm}$  are capable of producing high porewater dissolved sulphide concentrations ( $> 10^{-7}$  moles  $\text{cm}^{-3}$ , see Fig. 3). Localised pyrite formation then requires much higher concentrations of dissolved iron ( $> 10^{-6}$  moles  $\text{cm}^{-3}$ , since  $C_S^0/C_F^0 < 0.1$ ) than are commonly observed (see earlier). We therefore attribute preservation to

a combination of physical and chemical conditions which produced rapid burial to shallow depths (to avoid scavenging benthos) and a high porewater dissolved iron.

The sedimentology and chemistry of Beecher's Bed is consistent with these criteria. The trilobites were buried by a single influx of sediment forming a bed about 4 cm thick, and apparently represent a mass mortality (Cisne, 1973). The surrounding sediments contain low concentrations of organic carbon (0.02–0.2%), and are also low in pyrite sulphur (typically less than 2%). These observations suggest that sulphate reduction occurred only to a limited extent outside the decaying organism. Crucially, however, the sediments still contain high concentrations of HCl-extractable iron (1.4–2.7%), which is potentially reactive towards  $H_2S$  (Berner, 1970). These chemical data suggest that sulphate reduction in the enclosing sediments was suppressed (due to low concentrations of organic matter) and there was, as a result, an unusually intense phase of iron reduction (possibly mediated by sulphate reducing bacteria; see Coleman et al., 1993) which provided iron-dominated porewaters. These porewaters were effective at trapping sulphide at the decay site, and enabling soft part preservation to occur. In other circumstances (where organic carbon concentrations were higher, or reactive iron contents lower, as in Fig. 2) porewater dissolved iron concentrations would have been too low for readily metabolisable material to be pyritised (Briggs et al., 1991).

#### Pyrite formation in sulphide-dominated porewaters

In sulphide-dominated porewaters deeper in the sediment, the kinetics of iron mineral reactivity towards dissolved sulphide play a crucial role in dictating where localised pyrite formation occurs. Once iron oxides have been exhausted, the residual iron phases are only reactive towards  $H_2S$  over relatively long periods (Table 1). Reaction rates depend on factors such as sulphide concentration, and the concentrations of iron minerals and their specific surface area. The estimates in Table 1 use an arbitrary dissolved sulphide concentration of 1 mM for comparison, but they can still be used to

understand the factors which control pyritisation over this interval of diagenesis. These estimates suggest that the time of exposure to dissolved sulphide is critical in determining whether these poorly reactive iron phases can become pyritised.

Relatively few sediments have been sampled to show complete depth profiles of dissolved sulphide, but two reasonably extreme cases (Fig. 4) can be found. At Sachem Harbour (Connecticut) Canfield (1988) showed dissolved sulphide declining to zero at approximately 80 cm depth ( $\chi$ ). The sedimentation rate ( $\omega$ ) of approximately  $1.5 \text{ cm yr}^{-1}$  (Krom and Bennett, 1985) then indicates a contact time for dissolved sulphide ( $\chi/\omega$ ) of approximately 50 years. The other extreme is illustrated in the Peru Margin (Mossman et al., 1991) where dissolved sulphide persists over depths of approximately 75 m and sedimentation rates were 20–50 m per  $10^6$

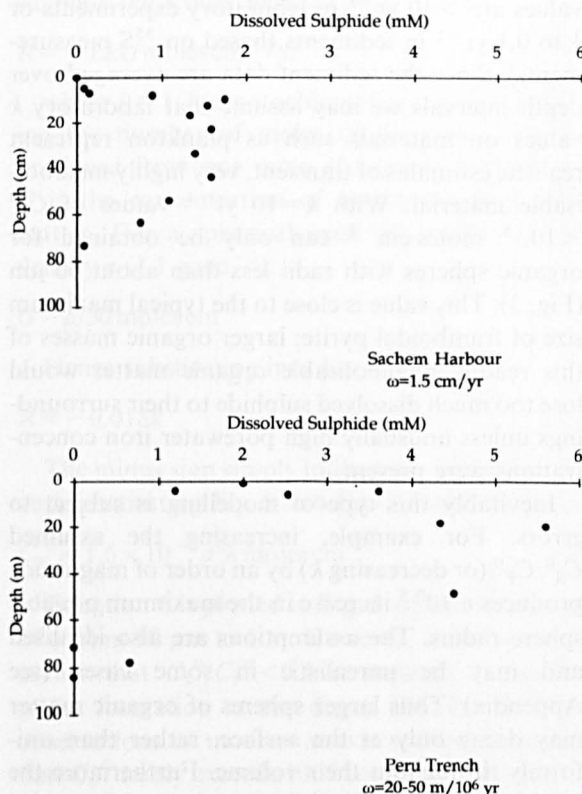


Fig. 4. Profiles of dissolved sulphide with depth. Data at Sachem Head Harbour from Canfield (1988) with depth in centimetres; data from Peru Trench from Mossman et al. (1991) with depth in metres.

years. Clearly contact times ( $\chi/\omega$ ) in excess of  $10^6$  years are indicated.

These data provide a tantalising glimpse of the potential influence of contact time on iron mineral pyritisation at depth. At low  $\chi/\omega$  only the most reactive iron minerals will be pyritised; at the most extreme  $\chi/\omega$  all reactive iron minerals can become pyritised. More profiles of dissolved sulphide with depth are needed in order to evaluate environmental influences on  $\chi/\omega$ , which will determine the amounts of pyrite formed at depth within the sediment. Note that an absence of dissolved sulphide at depth does not necessarily indicate the absence of pyrite formation, since rates of sulphate reduction may in some circumstances be slow enough that even poorly-reactive iron silicates are efficient at buffering sulphide to negligible levels (see Parkes et al., 1990).

At these depths, the reactivity of the residual silicate phases is comparable to that of accompanying organic matter. Thus sulphur incorporation into organic matter is contemporaneous with silicate pyritisation and this is reflected in the similarity between the isotopic values of late stage pyrite and of sulphur bearing bitumens in the Jet Rock (Lower Jurassic, England). These data (Raiswell et al., 1993) demonstrate a new role for sulphur isotope studies in timing sulphur reactions at depth, and in assessing the relative reactivities of iron minerals and organic matter in sulphide dominated porewaters.

## Conclusions

A 3-D diffusion-with-precipitation model can be used to predict the location and extent of pyrite precipitation when a spherical mass of organic matter, producing  $H_2S$  by sulphate reduction, is surrounded by porewaters containing dissolved iron. The locus of the precipitation maxima  $R_{j_{max}}$  is a simple function of  $C_S^0$  (the concentration of dissolved sulphide at the decay site) and  $C_F^0$  (the concentration of dissolved iron in the porewaters), such that precipitation occurs closer to the decay site as  $C_F^0$  increasingly exceeds  $C_S^0$ . Since  $R_{j_{max}}$  is independent of  $K$ , the solubility product, it is possible to make some model predictions without knowing whether pyrite precipitation took place

directly or indirectly, via an iron sulphide precursor.

Model values of  $C_S^0$  can be estimated from a knowledge of the rate constant for organic matter decaying by sulphate reduction and  $C_F^0$  can be inferred from studies of modern anoxic sediments. The model demonstrates that the size of the spherical organic mass and its rate of decomposition determine whether organic matter pyritisation can occur. Fresh planktonic organic matter decays so rapidly that typical porewater iron concentrations ( $<100 \mu m$ ) are only able to pyritise this material in spheres of radii  $>50 \mu m$ . The scarcity of framboids with radii  $<50 \mu m$  suggests that framboidal pyrite may originate by the rapid pyritisation of an organic precursor.

The preservation of soft tissue by pyritisation is also uncommon. Here the model suggests that organisms composed of readily metabolisable organic matter can only become pyritised where porewaters are unusually rich in dissolved iron. An examination of the sediments in Beecher's Trilobite Bed indicates that an intense phase of iron rich porewaters could have been responsible for trilobite soft part pyritisation.

Once reactive iron oxides have been consumed to form pyrite, the remaining iron minerals have extremely long half-lives with respect to sulphidation. The amount of localised pyrite formation therefore depends on the contact time with dissolved sulphide, which can be estimated as  $\chi/\omega$ , where  $\chi$  is the sediment depth over which dissolved sulphide occurs and  $\omega$  is the mean rate of deposition. Contact times vary between 50 to at least  $10^6$  years.

## Acknowledgements

The NERC funded sulphur isotope studies at Leeds through GR3/7839 (RR), also the Beecher's Bed and Hunsrückschiefer studies at Bristol through GR9/13 and GR9/518 (DEGB and RR).

## Appendix

This model is a modification of the 1-D treatment of diffusion-plus-precipitation by Helfferich and Katchalsky (1970). It can be used to show where mineral precipitation occurs when



a spherical reservoir (containing a solution of a reactant A) is immersed in an infinite reservoir (of another reactant B). The model is idealised in the following respects, whose validity needs to be established for any particular case.

(1) The two reservoirs, as a result of the processes acting therein, are maintained at constant concentrations. Each reservoir initially contains only one reactant, which is uniformly dispersed.

(2) Mass transfer between the reservoirs occurs only by diffusion. The system is isothermal and there is no convection, or osmotic flow.

(3) Reactants A and B are either non-electrolytes, or there are no electrostatic interactions between the diffusing ions.

(4) Reaction between A and B is instantaneous and reversible, resulting in the precipitate AB when the solubility product ( $K$ ) is exceeded.

(5) The concentrations of A and B (assumed to be equal to the activities) in equilibrium with the precipitate are given by  $C_A C_B = K$ .

(6) The rate of precipitation is controlled exclusively by the diffusion supply of A and B, thus equilibrium is attained instantaneously and there is no supersaturation.

(7) The infinite reservoir remains permeable at all times and precipitation does not impede diffusion.

(8) The diffusion coefficients are independent of concentration.

Under these conditions the system can be expected to reach a steady state, shown in Fig. 1, which can be defined in terms of the reservoir concentrations  $C_A^0$  and  $C_B^0$ .

In the region of reaction:

$$\frac{\partial C_A}{\partial t} = -\text{div } \underline{J}_A - j$$

$$\frac{\partial C_B}{\partial t} = -\text{div } \underline{J}_B - j$$

where  $j$  is the rate of precipitation of AB (in units of moles per unit volume per unit time) at a distance  $r$  from the centre of the spherical reservoir:

$$\text{div } \underline{J} = \frac{1}{r^2} \frac{\partial}{\partial r} (r^2 J)$$

where  $J$  is the radial component of  $\underline{J}$ .

Then the diffusion equations are:

$$\frac{\partial C_A}{\partial t} = D_A \nabla^2 C_A - j$$

$$\frac{\partial C_B}{\partial t} = D_B \nabla^2 C_B - j$$

where  $\nabla^2$  is the Laplacian.

Now  $C_A = C_A(r, t)$  so

$$\nabla^2 C_A = \frac{1}{r^2} \frac{\partial}{\partial r} \left( r^2 \frac{\partial C_A}{\partial r} \right)$$

and similarly for B.

The equations give:

$$\frac{\partial C_A}{\partial t} = \frac{D_A}{r^2} \frac{\partial}{\partial r} \left( r^2 \frac{\partial C_A}{\partial r} \right) - j$$

$$\frac{\partial C_B}{\partial t} = \frac{D_B}{r^2} \frac{\partial}{\partial r} \left( r^2 \frac{\partial C_B}{\partial r} \right) - j$$

where

$$\underline{J}_A = -D_A \frac{\partial C_A}{\partial r}$$

$$\underline{J}_B = -D_B \frac{\partial C_B}{\partial r}$$

In the steady state

$$\frac{\partial C_A}{\partial t} = \frac{\partial C_B}{\partial t} = 0$$

and

$$\frac{\partial}{\partial r} = \frac{d}{dr}$$

Therefore

$$\frac{D_A}{r^2} \frac{d}{dr} \left( r^2 \frac{dC_A}{dr} \right) = j$$

$$\frac{D_B}{r^2} \frac{d}{dr} \left( r^2 \frac{dC_B}{dr} \right) = j$$

By subtraction

$$\frac{D_A}{r^2} \frac{d}{dr} \left( r^2 \frac{dC_A}{dr} \right) - \frac{D_B}{r^2} \frac{d}{dr} \left( r^2 \frac{dC_B}{dr} \right) = 0. \quad (3)$$

This is the radial part of Laplace's equation where

$$\frac{1}{Rr^2} \frac{d}{dr} \left( r^2 \frac{dR}{dr} \right) - l(l+1) = 0.$$

for  $R = D_A C_A - D_B C_B$  with  $l=0$  the solutions are:

$$R \propto \frac{1}{r^{l+1}}, \quad r^l$$

Therefore

$$D_A C_A - D_B C_B = \frac{c}{r} - d; \quad (4)$$

where  $c$  and  $d$  are constants whose values are determined by the boundary conditions which are

$$r = a, \quad C_A = C_A^0 \quad \text{and} \quad C_B = 0$$

$$r \rightarrow \infty, \quad C_A = 0 \quad \text{and} \quad C_B = C_B^0$$

where  $a$  is the radius of the central reservoir and

$$C_A C_B \leq K \quad \text{and} \quad 0 < r < \infty.$$

At  $r = a$  Eq. 4 gives

$$D_A C_A^0 = \frac{c}{a} - d \quad (5)$$

and as  $r \rightarrow \infty$

$$-D_B C_B^0 = -d. \quad (6)$$

Subtracting Eqs. 5 and 6 gives:

$$D_A C_A^0 + D_B C_B^0 = \frac{c}{a}$$

or

$$c = a(D_A C_A^0 + D_B C_B^0) \quad (7)$$

and from equation (6)

$$d = D_B C_B^0. \quad (8)$$

Thus Eqs. 7 and 8 define  $c$  and  $d$  in terms of model parameters.

Returning to Eq. 4 and substituting  $C_B = \frac{K}{C_A}$

$$D_A C_A^2 - \left(\frac{c}{r} - d\right) C_A - D_B K = 0$$

Solutions of this quadratic can be found by reference to

$$ax^2 + bx + c = 0$$

$$x = \frac{-b \pm \sqrt{b^2 - 4ac}}{2a}$$

Thus

$$C_A = \frac{\left(\frac{c}{r} - d\right) \pm \sqrt{\left(\frac{c}{r} - d\right)^2 + 4D_A D_B K}}{2D_A}$$

The numerator must be positive, so taking the plus sign gives the solution gives

$$C_A = \frac{\left(\frac{c}{r} - d\right) + \sqrt{\left(\frac{c}{r} - d\right)^2 + 4D_A D_B K}}{2D_A} \quad (9)$$

and similarly

$$C_B = \frac{-\left(\frac{c}{r} - d\right) + \sqrt{\left(\frac{c}{r} - d\right)^2 + 4D_A D_B K}}{2D_B} \quad (10)$$

Now  $j$  can be calculated from either Eq. 1 or 2 by substituting from either Eq. 9 or 10

$$j = \frac{D_B}{r^2} \frac{d}{dr} \left( r^2 \frac{dC_B}{dr} \right)$$

$$= \frac{1}{r^2} \frac{d}{dr} \left[ \frac{cr^2}{2r^2} \left\{ 1 + \frac{\left(\frac{c}{r} - d\right)}{\sqrt{\left(\frac{c}{r} - d\right)^2 + 4D_A D_B K}} \right\} \right]$$

$$j = \frac{c}{2r^2} \frac{d}{dr} \left\{ 1 + \frac{\left(\frac{c}{r} - d\right)}{\sqrt{\left(\frac{c}{r} - d\right)^2 + 4D_A D_B K}} \right\}$$

$$j = \frac{c}{2r^2} \left\{ \frac{\frac{c}{r^2}}{\sqrt{\left(\frac{c}{r} - d\right)^2 + 4D_A D_B K}} + \frac{\left(\frac{c}{r} - d\right) \left(-\frac{1}{r}\right) 2 \left(\frac{c}{r} - d\right) \left(\frac{c}{r^2}\right)}{\left[\left(\frac{c}{r} - d\right)^2 + 4D_A D_B K\right]^{3/2}} \right\}$$

which simplifies to

$$j = \frac{2c^2 D_A D_B K}{r^4 \left[\left(\frac{c}{r} - d\right)^2 + 4D_A D_B K\right]^{3/2}}$$

Now substitute for  $c$  and  $d$  from Eqs. 7 and 8

$$j = \frac{2a^2 (D_A C_A^0 + D_B C_B^0)^2 D_A D_B K}{r^4 \left\{ \left[ D_B C_B^0 - \frac{a}{r} (D_A C_A^0 + D_B C_B^0) \right]^2 + 4D_A D_B K \right\}^{3/2}} \quad (11)$$

The maximum of  $j$  occurs when  $c/r = d$

Let the distance  $r$  be  $R_{j\max}$ . Then

$$R_{j\max} = \frac{c}{d} = \frac{a(D_A C_A^0 + D_B C_B^0)}{D_B C_B^0}$$

## References

- Al-Biatty, H.J., 1990. Aspects of carbon-sulphur-iron geochemistry and diagenesis. Ph.D. Thesis, Univ. Leeds, 428 pp. (Unpubl.)
- Aller, R.C., 1977. The influence of macrobenthos on chemical digenesis of marine sediments. Ph.D. Thesis, Yale Univ., 600 pp. (Unpubl.)
- Aller, R.C., 1980a. Diagenetic processes near the sediment-water interface of Long Island Sound. I. Decomposition and nutrient element geochemistry. *Adv. Geophysics*, 22: 237-350.
- Aller, R.C., 1980b. Diagenetic processes near the sediment-water interface of Long Island Sound. II. Fe and Mn. *Adv. Geophysics*, 22: 351-415.
- Berner, R.A., 1964. Distribution and diagenesis of sulfur in some sediments from the Gulf of California. *Mar. Geol.*, 1: 117-140.
- Berner, R.A., 1970. Sedimentary pyrite formation. *Am. J. Sci.*, 268: 1-23.
- Berner, R.A., 1980. *Early Diagenesis: A Theoretical Approach*. Princeton Univ. Press, Princeton, 241 pp.
- Berner, R.A., 1984. Sedimentary pyrite formation: An update. *Geochim. Cosmochim. Acta*, 48: 605-615.
- Berner, R.A. and Westrich, J.T., 1985. Bioturbation and the early diagenesis of carbon and sulfur. *Am. J. Sci.*, 285: 193-206.
- Boudreau, B.P. and Canfield, D.E., 1988. A provisional diagenetic model for pH in anoxic porewaters. *J. Mar. Res.*, 46: 429-455.



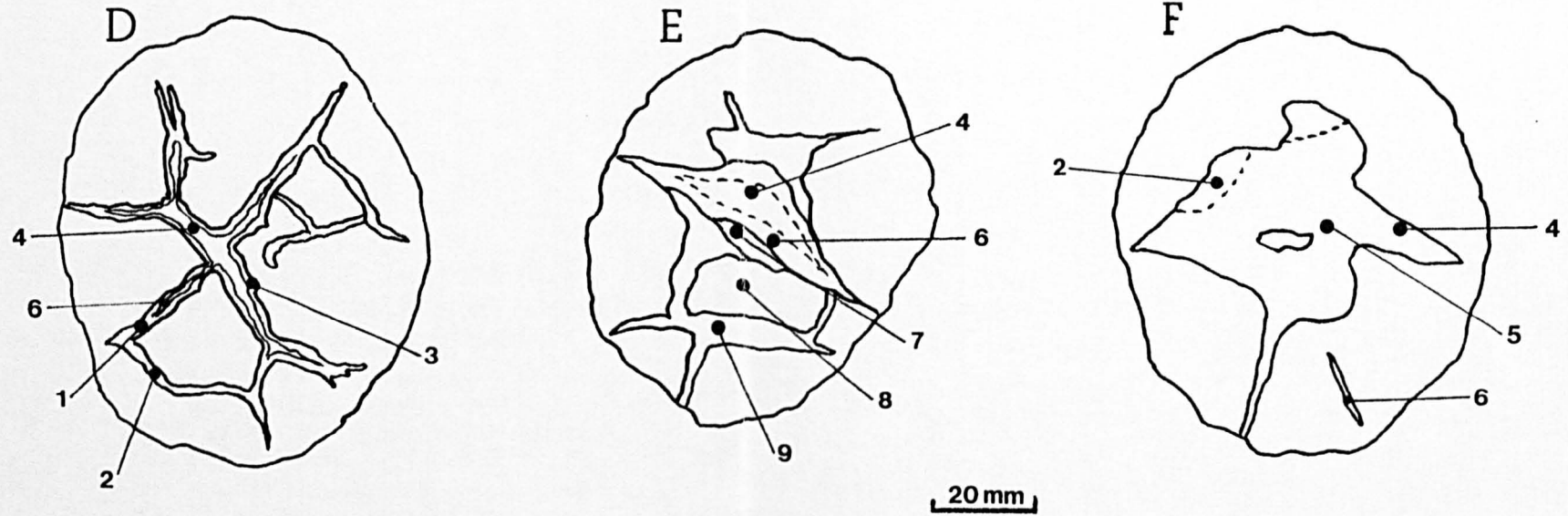
- Briggs, D.E.G., Bottrell, S.H. and Raiswell, R., 1991. Pyritization of soft-bodied fossils: Beecher's Trilobite Bed, Upper Ordovician, New York State. *Geology*, 19: 1221-1224.
- Briggs, D.E.G., Raiswell, R., Bottrell, S.H., Hatfield, D. and Bartels, C., in press. Sulphur isotopes and the pyritisation of exceptionally preserved fossils from the Lower Devonian Hunsrück Slate of Germany. *Bull. Geol. Soc. Am.*
- Butler, I. and Rickard, D.T., in prep. Inorganic self-ordering in pyrite framboids.
- Canfield, D.E., 1988. Sulfate reduction and the diagenesis of iron in anoxic marine sediments. Ph.D. Thesis, Yale Univ., 248 pp. (unpubl.).
- Canfield, D.E., 1989. Reactive iron in marine sediments. *Geochim. Cosmochim. Acta*, 53: 619-632.
- Canfield, D.E. and Raiswell, R., 1991. Pyrite formation and fossil preservation. In: P.A. Allison and D.E.G. Briggs (Editors), *Taphonomy: Releasing the Data Locked in the Fossil Record*. Plenum, New York, pp. 337-387.
- Canfield, D.E., Raiswell, R. and Bottrell, S.H., 1992. The reactivity of sedimentary iron minerals toward sulfide. *Am. J. Sci.*, 292: 659-683.
- Cisne, J.L., 1973. Beecher's Trilobite Bed revisited: Ecology of an Ordovician deepwater fauna. *Postilla*, 160, 25 pp.
- Coleman, M.L., Hedrick, D.B., Lovely, D.R., White, D.C. and Pye, K., 1993. Reduction of Fe(III) in sediments by sulphate-reducing bacteria. *Nature*, 261: 436-438.
- Coleman, M.L. and Raiswell, R., in prep. Sources of carbonate and origins of zonation in pyritiferous carbonate concretions. *Am. J. Sci.*
- Emery, K.O., 1960. *The Sea off Southern California: A Modern Habitat of Petroleum*. Wiley, New York, 366 pp.
- Emery, K.O. and Hülsemann, J., 1962. The relationship of sediments, life and water in a marine basin. *Deep-Sea Res.*, 8: 165-180.
- Fossing, H., 1990. Sulphate reduction in shelf sediments in the upwelling region off central Peru. *Cont. Shelf Res.*, 10: 355-367.
- Goldhaber, M.B. and Kaplan, I.R., 1974. The sulfur cycle. In: E.D. Goldberg (Editor), *The Sea*. Wiley-Interscience, New York, 5, pp. 569-655.
- Goldhaber, M.B., Aller, R.C., Cochran, J.K., Rosenfeld, J.K., Martens, C.S. and Berner, R.A., 1977. Sulfate reduction, diffusion and bioturbation in Long Island sound sediments: Report of the FOAM group. *Am. J. Sci.*, 277: 193-237.
- Helferich, F. and Katchalsky, A., 1970. A simple model of diffusion with precipitation. *J. Phys. Chem.*, 74: 306-314.
- Hülsemann, J. and Emery, K.O., 1961. Stratification in Recent sediments of Santa Barbara as controlled by organisms and water character. *J. Geol.*, 69: 279-290.
- Krishnaswami, S., Monaghan, M.C., Westrich, J.T. and Turekian, K.K., 1984. Chronologies of sedimentary processes in sediments of the FOAM site, Long Island Sound, Connecticut. *Am. J. Sci.*, 284: 706-733.
- Krom, M.D. and Bennett, J.T., 1985. Sources, deposition rates and decomposition of organic carbon in recent sediments of Sachem Head Harbour, Long Island Sound. *Estuarine Coastal Mar. Sci.*, 21: 323-336.
- Love, L.G. and Amstutz, G.C., 1966. Review of microscopic pyrite from the Devonian Chattanooga Shale and Rammelsberg Banderz. *Fortschr. Mineral.*, 43: 273-309.
- Massaad, M., 1974. Framboidal pyrite in concretions. *Mineral. Deposita*, 9: 87-89.
- Middelburg, J.J., 1989. A simple rate model for organic matter decomposition in marine sediments. *Geochim. Cosmochim. Acta*, 53: 1577-1581.
- Mossman, J.R., Aplin, A., Curtis, C.D. and Coleman, M.L., 1991. Geochemistry of inorganic and organic sulphur in organic-rich sediments from the Peru Margin. *Geochim. Cosmochim. Acta*, 53: 3581-3595.
- Parke, R.J., Cragg, B.A., Fry, J.C., Herbert, R.A. and Wimpenny, J.W.T., 1990. Bacterial biomass and activity in deep sediment layers from the Peru margin. *Philos. Trans. R. Soc. London*, A331: 139-153.
- Pyzik, A.J. and Sommer, S.E., 1981. Sedimentary iron monosulfides: Kinetics and mechanism of formation. *Geochim. Cosmochim. Acta*, 45: 687-698.
- Raiswell, R., 1982. Pyrite texture, isotopic composition and the availability of iron. *Am. J. Sci.*, 282: 1244-1263.
- Raiswell, R., 1992. The pyritisation of soft-bodied fossils. In: Y.K. Kharaka and A.S. Maest (Editors), *Proc. 7th Int. Symp. Water-Rock Interaction*. Balkema, Rotterdam, pp. 301-304.
- Raiswell, R., Bottrell, S.H., Al-Biatty, H.J. and Tan, M.Md., 1993. The influence of bottom water oxygenation and reactive iron content on sulfur incorporation into bitumens from Jurassic marine shales. *Am. J. Sci.*, 293.
- Raybould, J.G., 1973. Framboidal pyrite associated with lead-zinc mineralisation in mid-Wales. *Lithos*, 6: 175-182.
- Rickard, D.T., 1970. The origin of framboids. *Lithos*, 3: 269-293.
- Rickard, D.T., 1974. Kinetics and mechanism of the sulfidation of goethite. *Am. J. Sci.*, 274: 941-952.
- Schoonen, M.A.A. and Barnes, H.L., 1991. Reactions forming pyrite and marcasite from solution. I Nucleation of FeS<sub>2</sub> below 100°C. *Geochim. Cosmochim. Acta*, 55: 1495-1504.
- Sholkovitz, E., 1973. Interstitial water chemistry of the Santa Barbara basin sediments. *Geochim. Cosmochim. Acta*, 37: 2043-2073.
- Sholkovitz, E. and Gieskes, J.M., 1971. A physical study of the flushing of the Santa Barbara basin sediments. *Limnol. Oceanogr.*, 16: 479-489.
- Sweeney, R.E. and Kaplan, I.R., 1973. Pyrite framboid formation: Laboratory synthesis and marine sediments. *Econ. Geol.*, 68: 618-634.
- Wood, T.L. and Garrels, R.M., 1987. *Thermodynamic Values at Low Temperature for Natural Inorganic Materials*. Oxford Univ. Press, Oxford, 242 pp.

## **Enclosure 3**

**Simon Dean  
Ph.D Thesis 1994**

**A study of the organic and inorganic  
geochemistry of sulphur in shales**

Enclosure 3



Distribution of sample points taken from slices of concretions D, E and F.

## **Enclosure 1**

**Simon Dean  
Ph.D Thesis 1994**

**A study of the organic and inorganic  
geochemistry of sulphur in shales**





The distribution of septarian concretions in the Lowgill stream section of the Caton Shales.



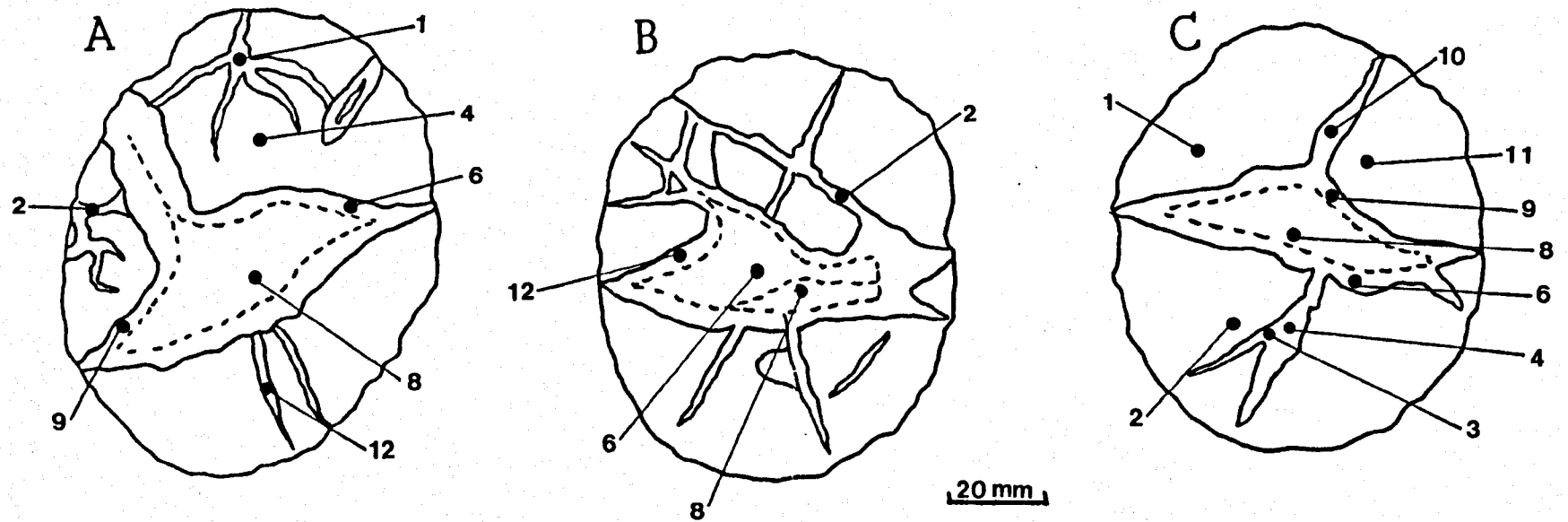
A cross section (parallel to bedding) of a typical septarian concretion from the Caton shales. Note the dark bituminous material in the centre of the slab.

## Enclosure 2

Simon Dean  
Ph.D Thesis 1994

A study of the organic and inorganic  
geochemistry of sulphur in shales

Enclosure 2



Distribution of sample points taken from slices of concretions A, B and C.